

Projeto Jupiter Team Project Pacífico

Team 133 Project Technical Report to the 2024 Spaceport America Cup

Juliana M. Carloni¹, Alison V. S. R. de Sousa², Amanda C. Catarino³, Antonio O. P. da Cruz⁴, Arthur M. Barboza⁵, Arthur S. de Almeida^{1,2}, Beatriz N. Silva², Branco F. Peixoto⁶, Breno M. Braga⁶, Caio C. G. Ribeiro^{1,2,4}, Caio de P. Colnago², Cauê R. Brondi², Cintia N. Ueda^{4,6}, Claudio L. C. da Silva⁷, Daniel A. B. Gontijo⁵, Danilo S. Santos⁴, Davi M. Laurino⁶, David K. Takeda⁴, Enzo Gevartosky⁵, Felipe C. I. Fonseca⁵, Felipe E. Schwarz⁴, Felipe F. Baptista^{1,6}, Felipe H. M. dos Santos⁶, Felipe M. de Carvalho⁸, Felipe S. Semerdjian^{1,5}, Francisco A. Villaza⁸, Gabriel P. R. Scavone⁴, Guilherme A. L. L. de Torres⁸, Gustavo A. C. S. R. Alves⁸, Gustavo H. Martins⁶, Gustavo K. P. e Costa², Hua H. Cao⁶, Igor B. Amaral⁸, Isabela C. M. Barbosa², João P. S. Nonato², Juli de A. Mavigno⁴, Julia M. C. de C. Paes⁵, Juliana M. Carloni⁹, Leonardo T. Valente⁸, Leonardo U. de Souza⁴, Léo C. Cymbalista⁸, Livia M. C. Silva³, Luana G. da Silva³, Lucas L. de Alcantara⁸, Lucas W. Jiajun⁶, Luisa do P. G. Pinto³, Luíza T. de Oliveira², Marcelo F. de Santana³, Maria C. C. Felipe⁶, Maria E. S. Silva⁶, Mateus C. A. da Silveira⁸, Mateus T. Pimenta⁸, Micael N. O. Souza⁷, Matheus T. de Andrade², Nicole V. Durand^{1,7}, Noelia Q. Condori⁵, Orlando R. S. dos S. Filho², Paloma G. da Silva⁷, Pedro H. F. Balduci^{4,6}, Pedro P. S. Coelho², Pedro P. de Souza⁴, Ricardo de Á. Mesquita⁵, Samuel N. de M. Santos^{3,8}, Soitiro Oura², Suellen de G. Camilo^{3,4}, Thais S. Melo^{1,8}, Ulysses L. Alves³, Vitor C. Souza⁵, Vitor H. Gushiken⁴, Vitor V. L. Pereira⁶, Willian de O. Silva², Yasmin F. Barnes³
Escola Politécnica of University of São Paulo, São Paulo, SP, 05508-010

Pacífico is a rocket developed by Projeto Jupiter for entry in the 10,000 ft apogee with SRAD solid propulsion system category at the 2024 Spaceport America Cup. The Pacífico rocket is propelled by a SRAD N2400 solid motor, Mandioca, and has a dual-event reefing recovery system. The embedded 3U cubesat-shaped payload is an experiment regarding attitude determination, robotics and image capturing and has a total mass of 8.8 lb. The rocket also transmits some collected flight data via telemetry system.

Nomenclature

A	=	ballistic factor
A_f	=	fin's side surface area
A_t	=	nozzle throat area
AR	=	aspect ratio
A_{ref}	=	reference area
b	=	semi-span
$BATES$	=	ballistic test and evaluation system
$CATO$	=	catastrophic outcome
$COTS$	=	commercial off-the-shelf
C_{D0}	=	drag coefficient for the nominal area
C_D	=	drag coefficient
C_f	=	thrust coefficient
$(C_{N_\alpha})_0$	=	normal force coefficient derivative for a 2 dimensional fin
$(C_{N_\alpha})_1$	=	normal force coefficient derivative for a 3 dimensional fin
C_r	=	root chord

¹Team Leader, 2231, Av. Professor Mello Moraes - Butantã, São Paulo - SP

²Electronic Systems, 2231, Av. Professor Mello Moraes - Butantã, São Paulo - SP

³Marketing, 2231, Av. Professor Mello Moraes - Butantã, São Paulo - SP

⁴Recovery Systems, 2231, Av. Professor Mello Moraes - Butantã, São Paulo - SP

⁵Payload Systems, 2231, Av. Professor Mello Moraes - Butantã, São Paulo - SP

⁶Aerodynamics and Structures Systems, 2231, Av. Professor Mello Moraes - Butantã, São Paulo - SP

⁷Finances, 2231, Av. Professor Mello Moraes - Butantã, São Paulo - SP

⁸Propulsion Systems, 2231, Av. Professor Mello Moraes - Butantã, São Paulo - SP

⁹Team Leader, 2231, Av. Professor Mello Moraes - Butantã, São Paulo - SP

C_t	=	tip chord
C_X	=	opening force coefficient
D_O	=	nominal diameter
D_R	=	reefed diameter
d	=	reference length or rocket's diameter
$EEPROM$	=	electrically erasable programmable read-only memory
$EPDM$	=	ethylene propylene diene monomer
F_D	=	drag force
F_X	=	parachute opening force
g	=	gravity
G	=	shear modulus
h_i	=	specific enthalpy
KNO_3	=	potassium nitrate
L	=	grain length
L_{ref}	=	reference length
L_B	=	bridle's length
M	=	mach number
\dot{m}	=	mass flow
$MEOP$	=	maximum expected operating pressure
N	=	number of fins
P or p_{atm}	=	atmospheric pressure
PCB	=	printed circuit board
P_i	=	i's pressure
P_c	=	combustion chamber pressure
P_e	=	nozzle outlet pressure
R	=	ideal gas constant divided by gas molar mass
r	=	grain port radius
\dot{r}	=	regression rate
r_t	=	rocket's radius
s	=	fin span
S	=	surface area
s_i	=	specific entropy at i-th iteration
S_m	=	rocket's static margin
$SRAD$	=	student researched and developed
t	=	thickness
T	=	temperature
v	=	specific volume
V	=	volume
V_c	=	combustion chamber free volume
v_0	=	rocket's freestream speed
v_s	=	speed of sound
x_i	=	vapor quality at i-th iteration
\bar{Y}_t	=	mean aerodynamic chord
α_c	=	opening angle for the circular-arc shaped tail
α_t	=	opening angle for the conical shaped tail
β	=	$\sqrt{ M^2 - 1 }$
γ or k	=	isentropic coefficient (C_p/C_v)
δ	=	fins dihedral angle
η_{cf}	=	thrust coefficient efficiency
λ	=	taper ratio
ρ	=	specific mass
ω	=	angular velocity

I. Introduction

Projeto Jupiter is an undergraduate student-run rocket design group from the University of São Paulo, established in 2015. The group has provided all its students an opportunity to develop, build, and work on aerospace projects. Such initiative was only possible with the support of teachers, researchers, and technicians in addition to the students' willingness. Throughout all processes of conception, parameters' definition, calculation, simulation, manufacturing, and launching of the team's rockets, Projeto Jupiter has always aimed to improve its members' abilities on working as a team, acquiring theoretical and technical knowledge, as well as communicating and solving projects' problems.

The group participates in competitions, organizes its own test launches and takes part in events such as industrial fairs, STEM conferences and charity events. Over the years, Projeto Jupiter has participated in several competitions, both nationally and internationally, proving its worth and achieving:

- First participation in IREC 2015 (Jupiter I);
- 24th place overall in IREC 2016 (Nabo I);
- 34th place overall and 4th category award place in SA Cup 2017 (Imperius);
- Overall winner in COBRUF 2017 (Imperius);
- Successful rocket launch and operations at USP campus - Pirassununga in 2018 (Euporia I);
- Successful rocket launch and operations at USP campus - Pirassununga in 2019 (Caldene);
- 77th place overall and 8th category award place in SA Cup 2019 (Callisto);
- 2nd place overall and 2nd category award place in LASC 2019 (Valetudo);
- Successful rocket launch and operations at USP campus - Pirassununga in 2020 (Temisto);
- 1st place overall, 1st place in the category award and Winner of the Award for Technical Excellence in LASC Online 2020 (Europa);
- 1st place overall, 1st place in the category award in LASC Online 2021 (Juno);
- 1st place overall, 1st place in the category award in LASC 2022 (Juno II);
- Successful rocket launch and operations at USP campus - Pirassununga in 2023 (Nyx);
- 51th place overall and 5th category award place in SA Cup 2023 (Juno III);
- 11th place overall and 1st category award place in LASC 2023 (Ganimedes);
- Successful rocket launch and operations at USP campus - Pirassununga in 2024 (Trix);

A. Stakeholders

In order to justify our project, the team's stakeholders take a crucial part in the team's motivation and ability to keep doing what we love: building rockets. Brazil is a country with a huge potential for economic and technological development in the aerospace sector, however, there are still many barriers along the process: lack of public policy and incentives for educators, researchers, companies, and students, amplified by modern problems like scientific and historical negligence.

Although the current scenario does not appear to be favorable, Projeto Jupiter stands still in its mission to spread science and knowledge across Brazil. Based on that, our main stakeholders are:

- **Team's students:** our initiative creates space for our members to grow and to learn new abilities which can provide great opportunities for them in the future, in addition to the joy of applying engineering in an exciting and complex problem;
- **Students and people external to the team:** people who can be inspired by our work and motivated to apply engineering concepts;
- **Our institution:** Projeto Jupiter places the name of the University of São Paulo among the greatest in national and international academic scenarios;
- **Our sponsors:** a symbiotic relationship is established, as their support to our rockets' development results in us spreading their brands around the community as part of innovative engineering initiatives such as experimental rocketry;
- **Our country:** being one of the Brazilian teams competing in the international rocketry scenario and showing the world that Brazilian's engineering is capable of great results despite the teams' limited economic resources.

B. Team Structure

Projeto Jupiter has 92 members that integrate the team's structure. These members come from various institutes of the University of São Paulo: engineering, physics, astronomy, mathematics, business, audiovisual, among others. Projeto Jupiter is organized in seven major groups, which are composed of five technical — Aerodynamics, Electronic

Systems, Payload, Propulsion, and Recovery — and two administrative ones — Finance and Marketing. Two internal committees are also part of the team’s organization: Human Resources and Safety Commissions. Each member takes part in one of these groups and may take part in any of the internal committees.

As a team, communication is crucial, thus a strong integration between all areas inside Projeto Jupiter’s structure (Fig. 1) is continuously guaranteed. Projeto Jupiter has one captain and each of its groups and committees has one leader. Professor Bruno Souza Carmo, full professor and researcher at the University of São Paulo, completes the team as its tutor.

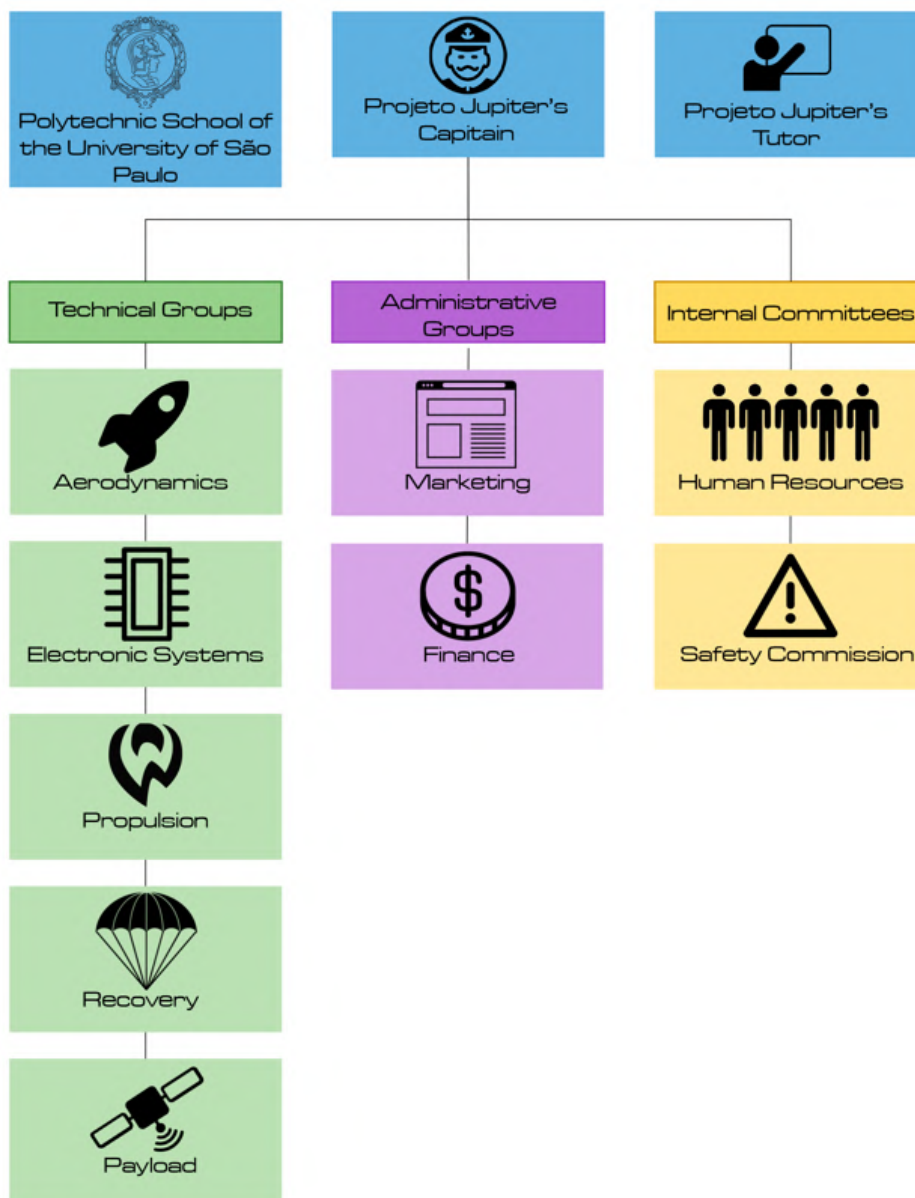


Fig. 1 Team’s organization chart.

Projeto Jupiter’s most important assets are its members. For this reason, it aims to cultivate a friendly and democratic workplace. With that in mind, each member has the freedom to develop individual tasks and contribute to the team as a whole, giving opinions always equally valued among the other members. This fact enriches the human relations inside the team and allows all members to participate in meaningful decisions and get experience during this process. Furthermore, weekly meetings are held so that these goals can be achieved: group, senior member, committee, and team

meetings occur periodically for updates, project progress sharing, members task assignments, and integration with other components of the team's structure.

C. Team Management Strategies

Communication and transparency are critical to team efficiency and workflow. To achieve this, various tools are used for management strategy. For primary online communication between members, messages are exchanged in chat groups on WhatsApp and there is a monthly newsletter named *The Jupiter Times*, which is written by different members every month. Since 2020, the team has successfully used Discord as communication software. In addition to weekly meetings held in person or via Google Meets as needed, these online tools have been very useful for sharing information.

The team uses *Autodesk Fusion 360* for creating 3D models of each of the rocket's components and for the final assembly. As this is online software, members can work on our project at the same time and enhance the collaborative construction of the rocket. All members have access to the models, which is a great way for members to understand the rocket's structure and to better comprehend the rocket's components and subsystems.

All of Projeto Jupiter's bibliography, references, and member-produced data are stored and shared through *Google Drive*. Calculations, desired parameters, reference papers and books, test documentation, meeting records, and previous rocket projects can be widely accessed by all members. *Microsoft Excel* spreadsheets are also utilized for task checklists, member activity and frequency control and for parameter calculations from given or desired parameter inputs.

Projeto Jupiter's journey to participate in the 2024 SA Cup began a long time ago. Since the team's participation in last year's edition (SA Cup 2023), members have been working on improving its systems to launch a rocket in Las Cruces once more. Given this context, for the Spaceport America Cup 2024, Projeto Jupiter is launching Pacifico, an innovative project with significant improvements over its predecessors. However, due to the need to transport the rocket from São Paulo, Brazil, to the competition site, there are limitations on what can be produced at the team's university and what needs to be completed in Las Cruces. Besides solving logistic issues, the team corrected mistakes made during SA Cup 2023. Although it was considered a good launch, as the rocket reached an apogee near to the simulated one and had a single-event recovery, several technical issues required attention. For example, some parts had their design changed so that the rocket assembly could be faster and less complex, as will be detailed in the next sections.

II. System architecture overview

Pacifico is divided into five main subsystems: Aerodynamics and Structures, Electronic Systems, Payload, Propulsion and Recovery. Each one corresponds to a technical group within the project. These subsystems are then organized into 3 sections: motor and fins' module, upper frame, and nosecone. The propulsion subsystem is found in the motor and fins module, which contains the combustion chamber and the nozzle. The motor is a solid KNSB class N called Mandioca. This structure will be used in the forthcoming launch and is being developed and tested by the Propulsion team through theoretical and semi-empirical methods. In the rocket's upper frame, one finds three naturally highly integrated modules, which are developed by the Electronic Systems, Recovery, and Payload teams. More specifically, the Electronic Systems team is responsible for the rocket's telemetry and for embedding the detection systems for the parachute events, which are triggered through adequate signaling to the Recovery Subsystems. The Payload team is responsible for researching and developing the scientific experiment placed inside the aircraft, Pacifico, studying the attitude of the rocket during its flight. Pacifico's Recovery consists of a dual-event reefing system, which is deployed via a 90 g CO₂ parachute ejection system. Finally, there is the nosecone, designed by the Aerodynamics and Structures subsystem, which is responsible for ensuring a stable flight and a lightweight and drag-optimised external fuselage of the rocket. Inside the nosecone stays the avionics bay, responsible for the main parachute ejection and disreefing.

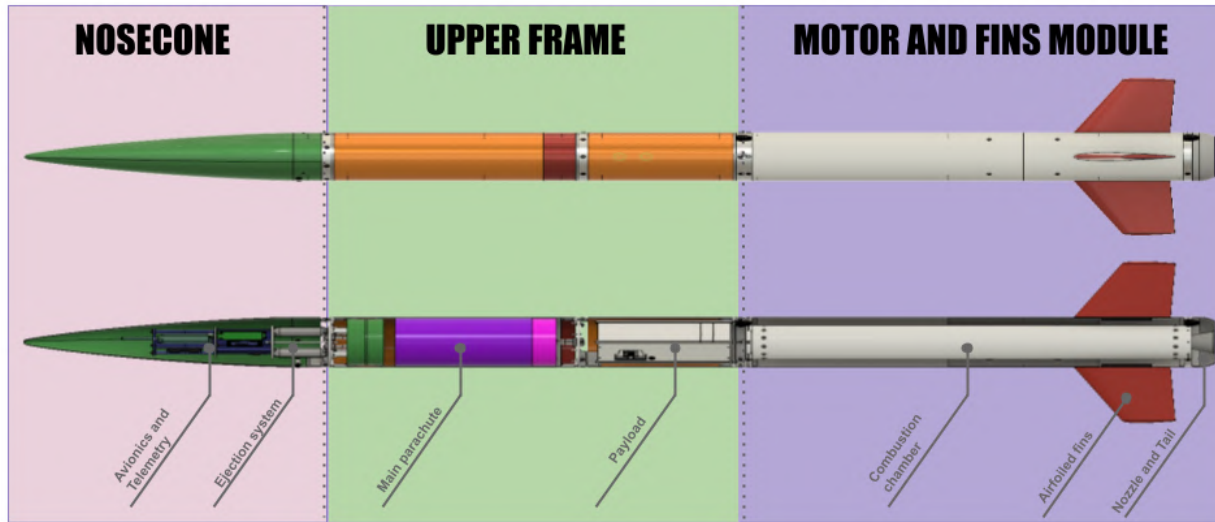


Fig. 2 Pacifico's architecture overview.

A. Propulsion Subsystem

1. Motor Overview

Mandioca uses 5 BATES grains of KNSB 65-35 as the propellant, mainly due to the simplicity and safety of its manufacturing process and the ease of acquisition of raw material. Extensive studies done on top of the composition's thermodynamic properties and burn rate, such as those available in Nakka's Experimental Rocketry Web Site[1], also contributed to the propellant's choice.

The grain inhibition is made with poliaramyd laminated at the external face of the grains with epoxy resin. The fiber was chosen due to its flame resistance, and the resin, due to its reliability in keeping the poliaramyd attached to the grain, in spite of having an exothermic cure reaction.

The motor structure consists of a 6101 aluminum casing, which has a wall thickness of 5.6 mm (0.22 in). On each end, there are twelve holes in order to place screws designed to couple the bulkhead and the nozzle to the casing, as well as eight M5 threads that attach a connector which sustains the tail. The alloy was picked since it was the only aluminum alloy found commercially available in the required dimensions. A fiber glass sheet, which was reinforced with epoxy resin was also employed as a liner to thermally insulate the combustion chamber and prevent the aluminum from losing any structural reliability due to thermal issues. Due to its low coefficient of thermal conductivity and ablative properties, heat transfer rates are low enough to guarantee that the aluminum will not reach temperatures near its melting point.

The nozzle was machined from SAE 1020 steel, enjoying a throat diameter of 22.8 mm (0.90 in) and expansion ratio of 8.13. The bulkhead is made from 6351 aluminum and has eight M5 threads designed to sustain screws which couple the motor to the rocket structure. Both of those alloys were chosen due to thermal and mechanical properties. A model of the Mandioca motor is shown in Fig. 3 and it's design data summarizes in Table 1.

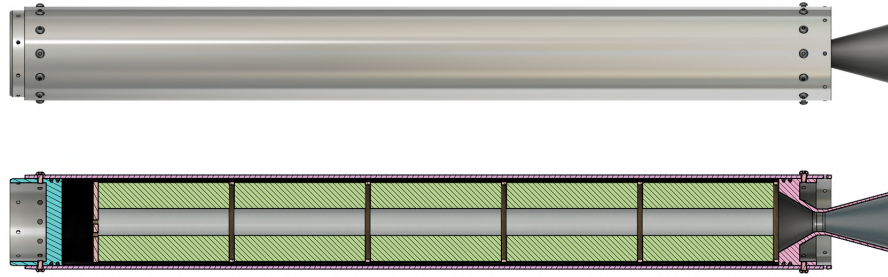


Fig. 3 Motor Overview.

Table 1 Mandioca's general and structural parameters

(a) Mandioca's general parameters

General		
Specification	Data	Unit
Oxidizer	KNO ₃	-
Fuel	Sorbitol	-
Empty mass	16.7	lb
Propellant mass	17.9	lb
Loaded mass	34.4	lb
Burn time	4.3	s
Total Impulse	2408	lbf·s
Specific Impulse	135	s
Max. Thrust	1098.6	lbf
Average Thrust	543.4	lbf
Ave. chamber pressure (est.)	601.5	psi
Max. chamber pressure (est.)	1160.3	psi
Characteristic Velocity	2680.5	ft/s

(b) Mandioca's structural parameters

Structural			
Component	Specification	Data	Unit
Nozzle	Material	SAE 1020 steel	-
	Throat Diameter	0.898	in
	Exit Diameter	2.559	in
	Expansion Ratio	8.13	-
	Divergence Angle	15°	-
Casing	Material	Al 6101	-
	External Diameter	4.469	in
	Thickness	0.22	in
	Length	37.8	in
Bulkhead	Material	Al 6351	-

Both the motor structure as well as the propellant have been fully designed and manufactured by the team students.

2. Structural analysis

In order to evaluate the motor's safety and allow for optimization, structural analyses were performed, both analytically and by the finite element method. Regarding factors of safety, the team considered 221 MPa as the yield point of Al 6101, value obtained from the alloy certificate of the batch of material. Using a script in Desmos Software, several types of motor failure were analysed, considering the bolt in shear.

Possible failures analysed were bolt shear, bolt tear-out, bearing failure, casing tensile and Von Mises yield failures. Through this analysis, the team got 2.2 as the lowest safety factor value factor concerning the different modes of failure. The value refers to bearing failure in the holes made for the screws to pass through. To calculate the SF for the different failure criteria, the following table was constructed:

Table 2 Mandioca's structural analytics methods

Type of failures	Equations		Results
Bolt Shear	$\sigma_{bs} = \frac{D_{ic}^2 MEOP}{N d_{pmin}^2}$	$FS_{bs} = \frac{0.75 UTS}{\sigma_{bs}}$	Fs= 3
Bolt tear-out	$\sigma_{to} = \frac{F_{bolt}}{E_{min} 2 t}$	$FS_{to} = \frac{SS}{\sigma_{to}}$	Fs= 9.9
Bearing	$\sigma_b = \frac{F_{bolt}}{d_{bmj} t}$	$FS_b = \frac{BYS}{\sigma_b}$	Fs= 2.2
Casing tensile	$\sigma_t = \frac{\pi D_{ic}^2 MEOP}{4[(D_{oc}-t)\pi - N d_{bmj}]t}$	$FS_t = \frac{YS}{\sigma_t}$	Fs= 4.9
Casing Von Mises	$\sigma_{vm} = \frac{\sqrt{(\sigma_1 - \sigma_2)^2 + (\sigma_2 - \sigma_3)^2 + (\sigma_3 - \sigma_4)^2}}{2}$	$FS_{vm} = \frac{YS}{\sigma_{vm}}$	Fs= 4.65

For the finite element analysis, the Von Mises yield criterion was adopted, which is based on the study of distortion energy. When compared to other analysis methods such as Tresca's, it returns results that tend to better match empirically obtained data.

By applying the criterion cited above in *ANSYS Mechanical*, with the appropriate boundary conditions, the highest Von Mises stress obtained was 96.4 MPa. With this we arrive, through the ratio of yield stress to Von Mises stress, at a safety factor of 2.48.

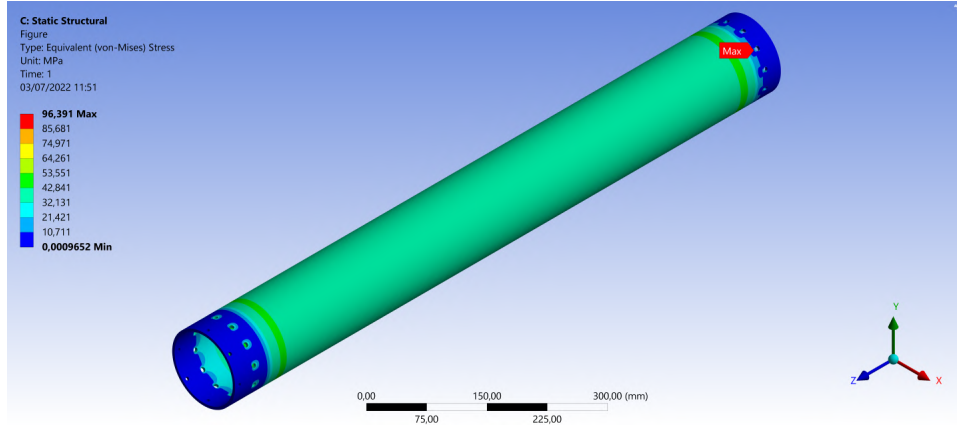


Fig. 4 Von Mises stress analysis of Mandioca's casing by FEA method.

3. Ballistics Simulations

It is rather important to predict the motor's burn characteristics (e.g. thrust and pressure curves) and critical parameters (e.g. maximum thrust and pressure) before it is actually manufactured, since the team must know if the designed motor is capable of achieving the desired results while the critical parameters are below their structural threshold for safety. Therefore, with this concept in mind, the team developed an internal software called *SolidPy* (available on GitHub [2] under MIT License) which computes the burn characteristics and critical parameters from physical models based on literature review. Furthermore, *SolidPy* can also process empirical thrust data obtained from static-fires and evaluate its main parameters, such as burn time, specific impulse and nozzle efficiency, so as to get the most from the static-fire tests.

Following similar methods from literature, *SolidPy*'s thermodynamic model assumes a unidirectional and isentropic flow from the combustion chamber to the nozzle exit. Differential calculus techniques used to describe the flow also assume that it is continuous. Hence, the core of the burn simulation is computed from an ordinary differential equation that relates the chamber pressure with the grain burn rate. This differential equation is derived from mass conservation laws in fluid mechanics:

$$\frac{\forall_0}{RT_0} \frac{dP_0}{dt} = A_b a P_0^n (\rho_g - \rho_0) - P_0 A_t \sqrt{\frac{k}{RT_0}} \left(\frac{2}{k+1} \right)^{\frac{k+1}{2(k-1)}} \quad (1)$$

Moreover, the software also allows solving for customised core geometries such as star and finocyl, through the employment of fast marching numerical methods. For this motor, we choose a BATES cylindrical port, which has a more neutral and predictable burn area as it regresses. In order to guarantee the results liability, Mandioca was simulated in OpenMotor and the performance was cross-checked between both softwares.

The results of Mandioca motor simulation produced by SolidPy are shown in Fig. 5.

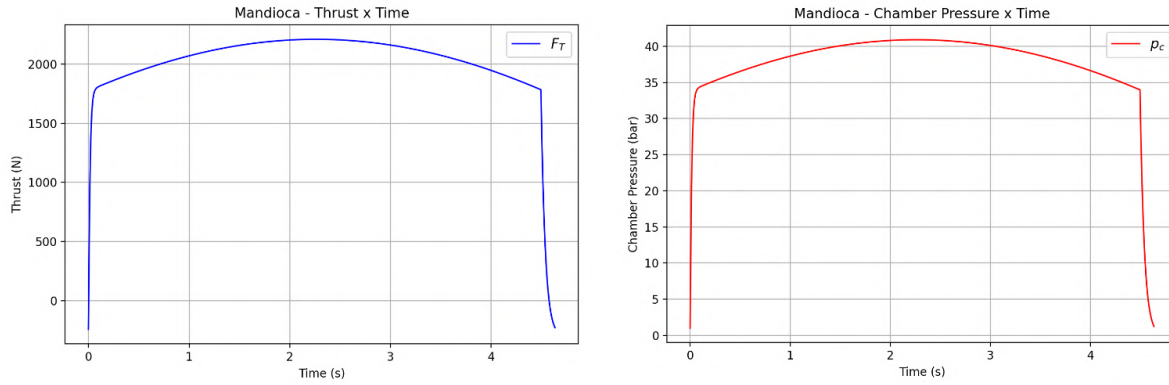


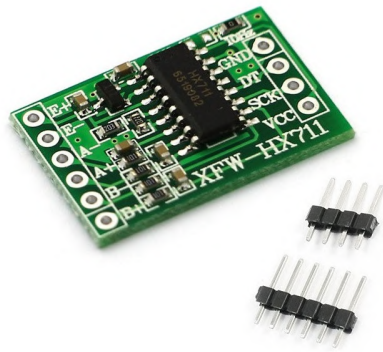
Fig. 5 SolidPy graphs simulating Mandioca's thrust and chamber pressure.

4. Test System

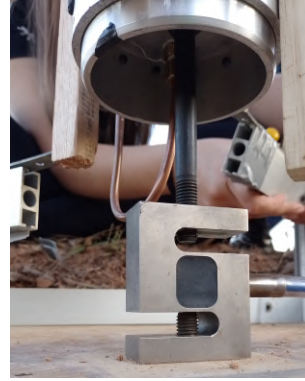
The test system's main goal is to enable the execution of the motor static fire test safely while collecting the motor's thrust data. In order to achieve it, the telemetry system sends the operator's signal to the ignition system and also transmits the data collected by the instrumentation system. All the processes are managed by a Raspberry Pi 4 model B.

- **Instrumentation System**

The instrumentation system has two main goals: register on-site thrust data from the motor and send it to the telemetry system. The former part is composed of the sensor, which is a S-type load cell paired with an HX711 module to measure the motor's thrust, and an Arduino Uno, which is used to process the data and send it to the RaspberryPi via USB serial communication (Fig. 6). In parallel to the thrust reading, there is also a pressure transducer that could work as an extra measure so as to verify each other, as the thrust curve should resemble the pressure curve and vice versa. As shown in Fig. 7, the pressure transducer is connected to the same Arduino Uno via a converter circuit that would allow the exit of 4-20 mA from the transducer to be read by an analog pin in the Arduino as tension ranging from 0 to 5 V. Subsequently, the information is acquired by the Arduino as bits, then it is also sent to the RaspberryPi with serial communication so that a CSV file may be created with both measurements, separated as (time, thrust, pressure).



(a) HX711 module.



(b) Load cell.

Fig. 6 Instruments for thrust gathering.



(a) Pressure Transducer.



(b) Converter module.

Fig. 7 Instruments for pressure gathering

- Ignition System** The ignition system consists of a circuit that works in a two-step activation: *arm*, which triggers the siren, and *ignite*, which allows the electric current to activate the igniter. The ignite signal is only allowed to be high if the arm signal is already high. Additionally, a manual switch is used to energize the circuit, creating an extra layer of protection for the operator. The circuit uses a logic signal from the Raspberry Pi's GPIOs to activate a P-channel MOSFET transistor. When *arm* is activated, the arm MOSFET allows the current to flow to the siren and to the ignition circuit. Then, when energized, the ignition circuit works similarly to the arm circuit, with the difference that it activates an e-match instead of the siren.
- Telemetry System** Regarding telemetry, in order to transmit data reliably, a TCP/IP communication protocol was adopted, primarily due to its simple implementation and effectiveness in delivering ordered data. To implement this physically, the system relies on the use of two 20 dBi directional parabolic antennas with an extendable range well beyond the required safety radius (shown in Fig. 8). Both antennas are connected to routers, with one of them simultaneously connected via an Ethernet cable to the instrumentation microcontroller. This allows the data collected by the microcontroller to be sent to the other end of the channel.



(a) Router.



(b) Antenna.

Fig. 8 Telemetry Hardware.

Once effective communication is established, the individual responsible for operating the computer can use a graphical interface software developed by the team. They are able to initiate the two-step ignition command, as well as monitor real-time thrust data through graphs. This setup allows for every personnel involved in the operation to be outside the 500 ft safety radius recommended by Tripoli Safety Code for class N motors, from the moment of arming onwards.

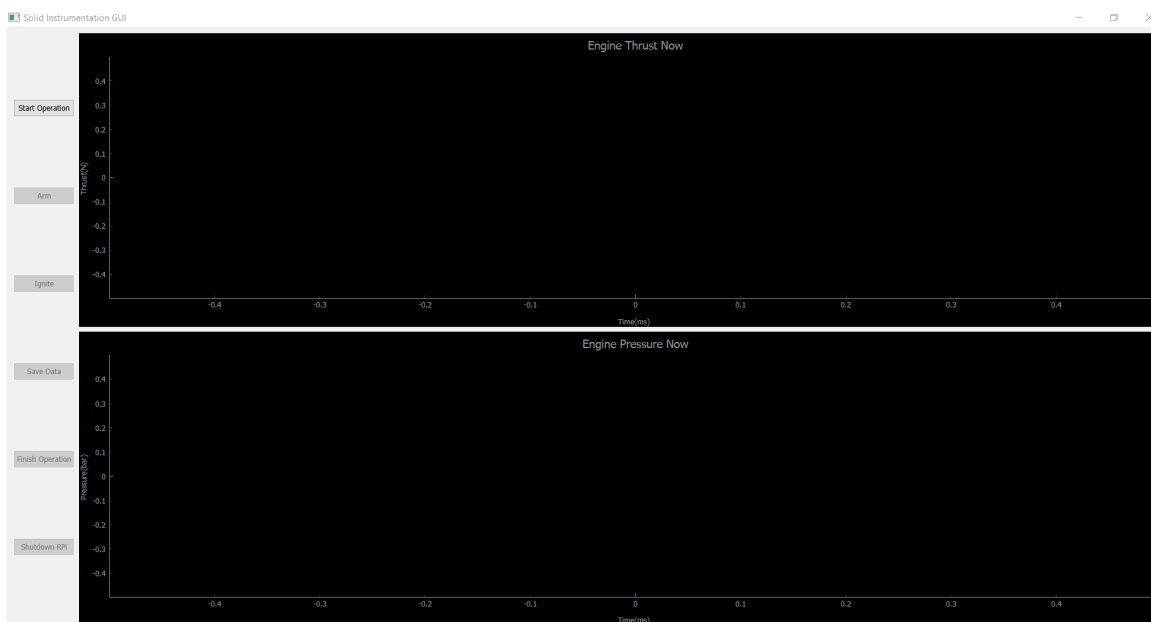


Fig. 9 Graphical Interface.

At the end of the test, the motor's thrust curve is obtained through the CSV file, which enables the plot of a graph. For instance, Fig. 10 shows the raw data from our latest static fire test. Admittedly, the raw data still requires a treatment owing to the change in mass whilst the propellant burns, as demonstrated by Fig. 11. Nonetheless, the raw curve is still an important piece of information as it ends in a value of roughly -7.8 kg which is expected since there was around 7.9 kg of propellant. Hence, it already suggests that the measurement is reliable and no significant flaws happened during the data acquisition of the load cell.

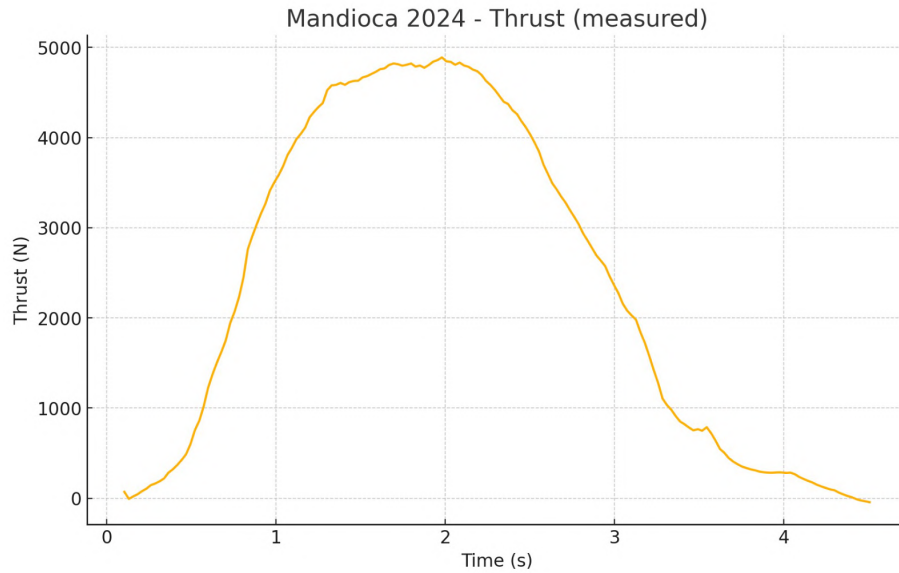


Fig. 10 Mandioca's thrust curve from static hot-fire test.

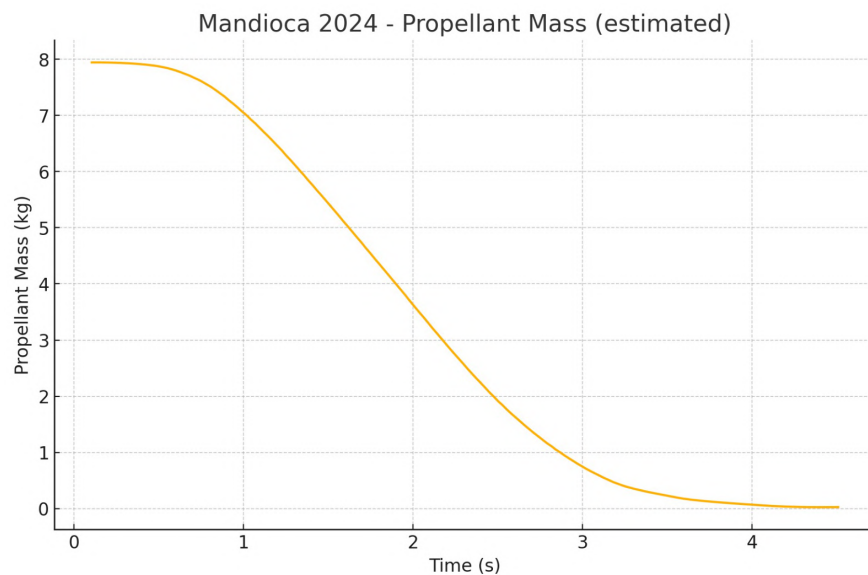


Fig. 11 Mandioca's mass variation curve.

Subsequently, as far as pressure is concerned, the resulting curve is shown in Fig. 12. and it is possible to see the resemblance to the thrust curve, thus giving a positive indication that the curve is reliable.

In this iteration of Mandioca our propellant manufacturing methodology has been altered, which led to a variation in this year's thrust curve. When analysing the graph, it is noticeable that there is a delay between ignition and maximum thrust, which is common in KNSB motors. With the propellant methodology changes, a steadier burn rate, as well as a shorter burn time was achieved, thus leading to a bigger total impulse of about 10700 Ns.

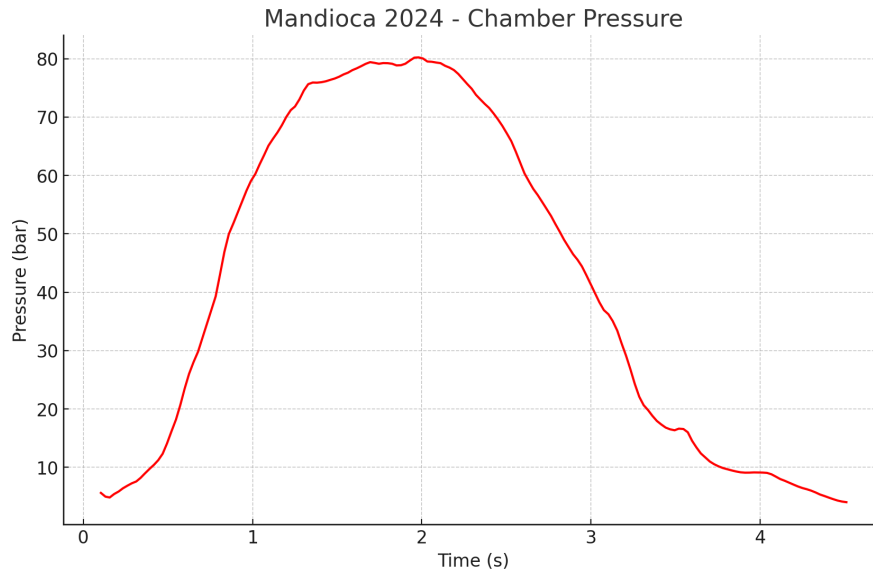


Fig. 12 Mandioca's pressure curve.

Some of the problems with large KNSB motors involve the grain's structural integrity, such as possible fractures and voids in its composition, leading to a rather "mountainous" looking curve. Another possible problem we have faced in the past is moisture, which leads to a long delay between ignition and peak in thrust as well as an increase of total burn time, due to its . All of those problems were avoided with the new manufacturing processes, as the graph became smoother and with a shorter total burn time in comparison to former versions of the motor. Another concern that was resolved and was deemed a big upgrade with propellant changes is out-of-rail velocity, which reached a value of 23.1m/s(75.6ft/s), meaning the rocket is within the acceptable standards.

B. Aerodynamics and Structures Subsystem

1. Base Structure

The aerodynamic and structural characteristics of a rocket are fundamental to achieving efficient and safe performance, and the optimization of these aspects aims to provide the foundation upon which all other subsystems are assembled and integrated to achieve a common goal: successfully launching and recovering the rocket.

In order to achieve efficiency and precision in this sophisticated project, it is necessary to employ enhanced and standardized manufacturing techniques – to produce lightweight and durable components – , complex numerical simulations to obtain precise data at low costs, and to make some topological improvements to the rocket's geometry in order to optimize flight performance.

For Pacífico, a modular structure was adopted, utilizing fiberglass tubes, aluminum coupling discs - bonded to the tubes with an epoxy based glue (hardener HW 5802 BR and HW 5800-1 BR, provided by Huntsman) -, truncated airfoil-shaped fins based on the NACA0012 airfoil, a Von-Kármán shaped nose cone and a circular spherical segment tail made of fiberglass laminated with epoxy resin.

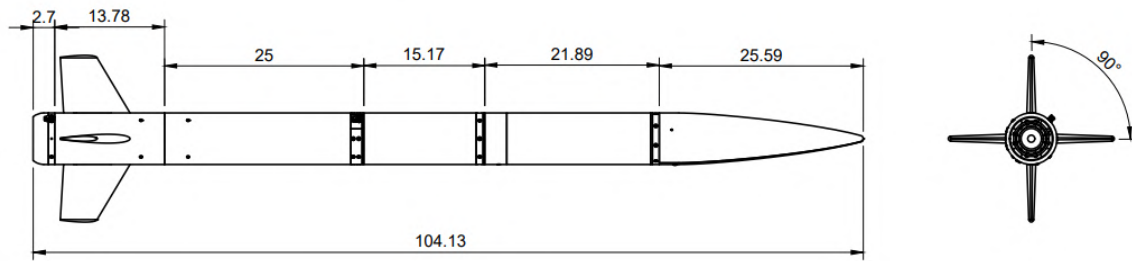


Fig. 13 Pacifico's dimensions in inches.

2. Modular division and Rocket Assembly

Pacifico was designed for easy assembly and handling, which are essential characteristics for rockets that must be transported over long distances and are usually assembled and disassembled several times before launch. This was possible by adopting a modular division, which allows the team to compartmentalize all the subsystems and assemble each pair of modules separately. An overview of the dimensions and inner connections of the modules are presented on Fig. 13, with a data summary on Table 4.

A second important characteristic is the adoption of standardized coupling disks. Almost all the coupling disks have the same design, facilitating their manufacture. The exceptions is the motor-airframe coupling disc, which can vary if the rocket comes to be launched at other times with a different motor. In the table below there is an overview of the current used coupling discs.

Table 3 Pacifico's coupling discs

Couplings	Material	Mass (g)	Volume (mm³)
Standard Female	Aluminum alloy 6351	319,868	79966,927
Motor/airframe bulkhead	Aluminum alloy 6351	530,689	1,97E+05
Centralizer	Aluminum alloy 6351	831,507	3,08E+05
Standard Male	Aluminum alloy 6351	548g	1.37E+05

At the intersection between the motor and the fuselage a female connection disc was adapted – adding one more row of bolt holes in the geometry –, so it could connect the chamber to the upper frame of the rocket. Another special disc is the motor centralizer, located at the bottom of the rocket. This centralizer was designed to hold the motor in place and to sustain the force applied to the nozzle due to combustion, ensuring a concentric alignment of the motor with the fuselage. The fiberglass tail and one of the two carbon fiber rail buttons are also attached to the centralizer. The second rail button is attached to the coupling that connects motor and payload tubes, as shown in Fig. 13 .

Table 4 Pacifico's characteristics summary.

Lengths	in	mm
Diameter	6.43	163.40
Overall length	104.13	2644.83
Nosecone	25.59	650
Recovery systems	20.85	528.49
Motor tube	23.37	593.5
Payload systems	14.09	357.95
Fin can	13.78	350
Tail	1.33	33.66

Masses	kg	lb
Vehicle mass	30.16	66.49
Propellant's mass	7.98	17.6
Payload's mass	4	8.82
Loaded mass	38.26	84.35

Part	Characteristic	
Nosecone shape	Von Kármán	
Tube's material	Glass fiber	
Fin's shape	Trapezoidal	
Airfoil's shape	Truncated NACA0012	
Tail shape	Spherical segment	
Number of fins	4	
Number of rail buttons	2	
First rail button	63.30	Positions measured from the nosecone (in)
Center of Mass	65.66	
Center of Pressure	85.27	
Second rail button	101.80	

3. Nosecone

With the intent of minimizing aerodynamic drag force, a *Haack* series with shape parameter (C) equal to 0 was chosen for Pacifico's nosecone. According to [3], the *Haack* series with $C = 0$, also known as the *Von Kármán* ogive, has superior aerodynamic performance at a transonic regime ($0.8 \leq Ma \leq 1.0$) and below, which are the predicted regime for Pacifico's flight. The nosecone's surface is described by Eq. (2), with a fineness ratio of 3.59 and a bluntness ratio of 0.12.

$$\theta = \cos^{-1} \left(1 - \frac{2x}{L} \right) \quad y = \frac{R \sqrt{\theta - \frac{\sin(2\theta)}{2} + C \sin^3 \theta}}{\sqrt{\pi}} \quad (2)$$

Its manufacture was carried out using a PLA-printed plug for mold construction, which was laminated over this plug. The ogive itself was laminated in this mold and is composed of a fiberglass-reinforced epoxy structure. A female coupling disc is bonded to its bottom, allowing an efficient coupling with the recovery subsystem. Inside the nosecone, the reefing cutter is placed. This device is responsible for releasing the reefed parachute and allowing it to reach its full diameter as referred to in the recovery section. The manufacturing process of the nosecone is described in Appendix B.

4. Tail

For the choice of tail's shape, in addition to the conducted CFD study (which will be shown later in section 8.a), the following points were also taken into consideration. The following "Drag of Conical and Circular-arc Boattail Afterbodies at Mach Numbers from 0.6 to 1.3" NACA research memorandum [?] was extensively used to base the decisions regarding the conical and spherical boattail conformations and their attributes.

For both shapes, those parameters were the tail base diameter : maximum tail diameter ratio (db/dm) and the opening angle α T, as represented in Fig. 16. Also, the total length of the boattail was fixed as that which aligned with the nozzle, so as to avoid unnecessary discussions and manufacturing, transportation, and gas exhaustion issues. That meant that tail length was considerably limited, which translates to greater ratios db/dm being desirable, given that, for the same α T and curvature (conical or circular), a shorter tail can only have such a small ratio. Careful consideration and analysis of the main information source suggested that the key to an optimal bottail shape was to determine the

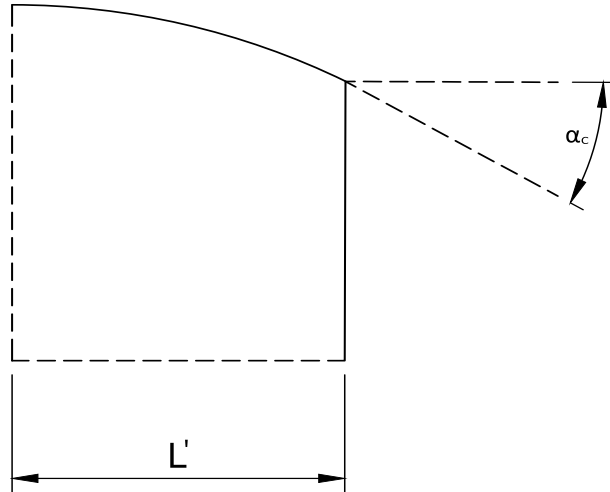


Fig. 14 Relevant Parameters of Circular-arc shape

suitable maximum angle αT and minimum db/dm ratio (while considering the limited boattail length), since these factors are easily associated with reduced drag. Thus, our limiting factor was the instability that appears at exaggerated values of αT and db/dm .

Some considerations to keep in mind: flight behavior at speeds of 0.6 to 0.9 Mach was given greater weight during analysis, since this range is closer to expected flight speeds; similarly, total drag was prioritized during analysis because the final rocket shape varied little compared to the memorandum's body shape except for the fins and because boattail-only drag was not elucidating for the analysis of db/dm , since it tends to 0 whenever db/dm tends to 1, which is far from true for the total-drag coefficient.

First, any angle above 30° made the flow separate over the entire length of the afterbody, according to the memorandum, so all values above 30° were outright discarded. Second, it was noticed that the gas's trajectory out of the engine varied negligibly when angles varied between 5° to 16° and separation flow began to become noticeable at 16° . Thus $\alpha T = 16^\circ$ became the limiting factor for experimentation and our lead when comparing shapes for the boattail and the ratio db/dm .

The Fig. 15 and Fig. 16 shows the relationship between different ratios, angles, and tails shapes, and their impact on drag, according to NACA [?].

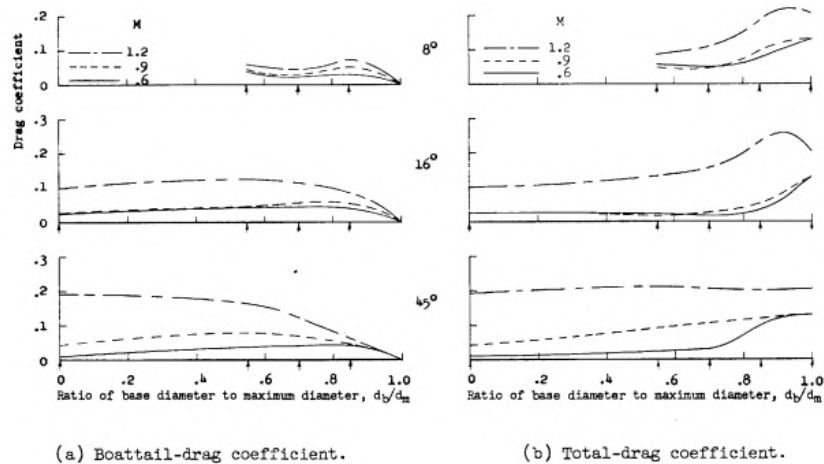


Fig. 15 Variation of boattail drag coefficients with ratio of base diameter to maximum diameter for circular-arc afterbodies.

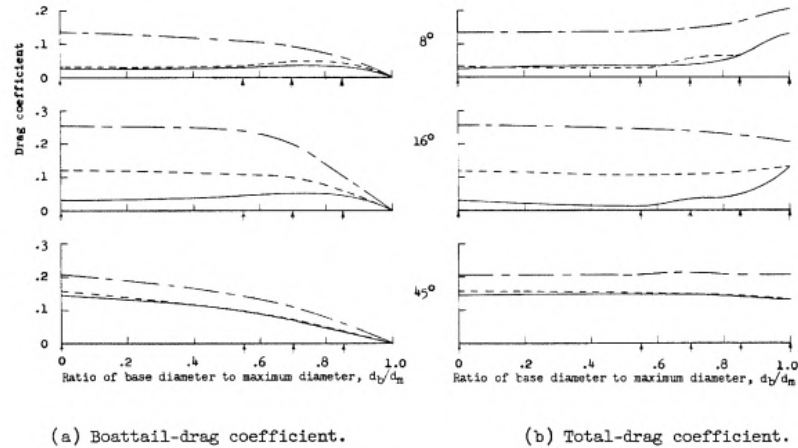


Fig. 16 Variation of boattail and total drag coefficients with ratio of base diameter to maximum diameter for conical afterbodies.

It is quite clear that, for the studied speed range, the circular-arc boat tail has considerably smaller total drag for the 16° angle, which guides the choice for this shape. That decided, it is easily noticeable that there are practically no changes in total drag between ratios 0.55, 0.70, and 0.85 for the circular shape across the considered speeds. Thus, taking into account the limited length for the boat tail, the 0.85 ratio boat tail was chosen. After the design of the rocket, the length available for the tail was 50mm, which justifies this choice for the boattail dimension, as initially stated.

Therefore, the final boattail has a length of 50mm, ratio $d_b/d_m = 0.85$, angle $\alpha_T = 16^\circ$, and maximum diameter equal to that of the rocket body (163.4mm).

In the CFD topic, analyses conducted through simulation comparing the two formats will be presented.

The fiberglass tail is manufactured using a 3D printed ABS mold to define its shape. The layup schedule comprises 8 layers of 200gsm (6oz/sqyd) BID E-glass plies across the internal part of the mold. The plies are oriented in a quasi-isotropic manner, with odd plies at 45° and even plies at $0^\circ/90^\circ$ angles. Huntsman's LY1563/HY2963 system serves as the matrix material. Consolidation of the plies is achieved using a vacuum bag method throughout the entire tail.



Fig. 17 Fiberglass tail curing in the vacuum bag.

5. Fins

The fins have a major impact on a rocket's stability, building a stabilizing force for the angles of attack and assuring a safe flight. For the Pacífico project, the fins were engineered to maximize performance while ensuring structural integrity and safety. This was achieved through several modifications to the fin design, including the truncation of the aerodynamic front section, utilization of a trapezoidal shape, and optimization of the area for maximum lift-to-drag ratio. The fins are composed of a carbon fiber plate covered with a ABS 3D-printed airfoil that provides the desired shape to the assembly. Pacífico has four fins that are attached to the motor fuselage tube using epoxy resin Fig. 18 presents the fin design and Table 7 its dimensions.

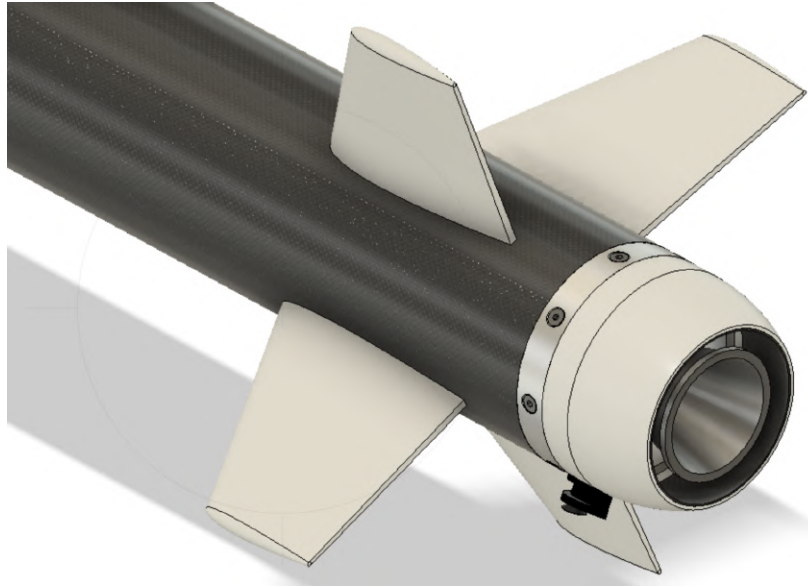
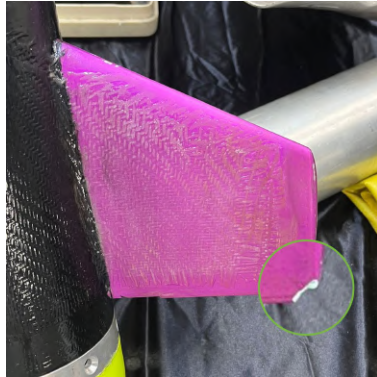


Fig. 18 CAD model of the fins attached to the fin body tube.

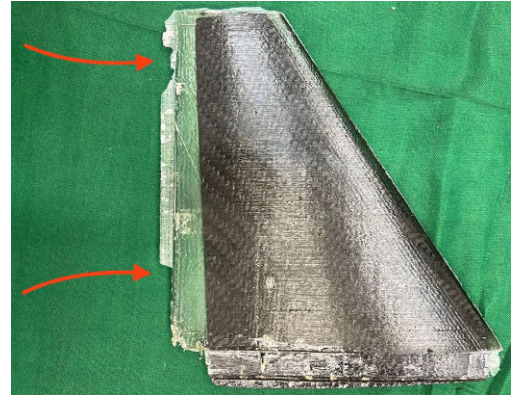
a) Airfoil section

The NACA0012 airfoil was chosen as the front section profile due to its high lift-over-drag value and to the large number of studies made on this shape in the literature. A more efficient shape enhances performance by promoting a greater lift for smaller angles of attack, a decrease in induced drag and a more efficient dynamic response, as described in Ref. [4].

Furthermore, the trailing edge of an airfoil is usually prone to chipping (Fig. 19), difficult to manufacture, and demands extra care when handling. In order to solve this problem, research was conducted, firstly analysing the literature[5–7] and, subsequently, conducting CFD simulations in Ansys Fluent on profiles truncated at 60%, 80% and 90% in order to validate the design.



(a) PLA fin airfoil profile.



(b) Resin fin airfoil profile.

Fig. 19 Damaged trailing edges.

Through this research, it was concluded that a truncation of 90% - i.e. eliminating the last 10% of the airfoil with a straight cut -, as shown in Fig. 20, does not significantly impact the lift and drag coefficients. Figure 21 shows the difference between a standard *NACA0012*, a truncated *NACA0012* and a flat surface fin. Table 5 shows the drag and lift coefficient of each simulated profile and Table 6 shows the ratio between lift and drag coefficients for each profile and angle of attack and also the average difference between the truncated profiles and the standard profile.

The truncated airfoil, given its minimal impact on the aerodynamics coefficients, renders a small decrease in the airfoil lift-over drag ratio, whilst eliminating the chipping prone section.

More information is available in Table V.

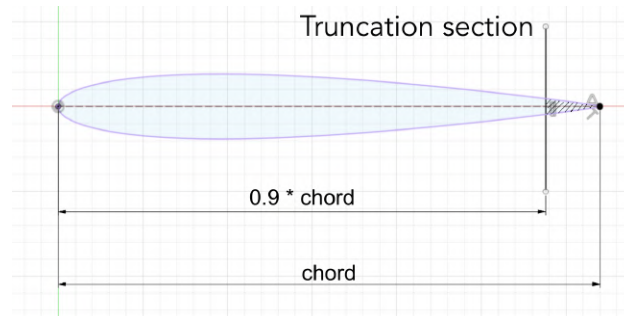


Fig. 20 Truncation schematics.

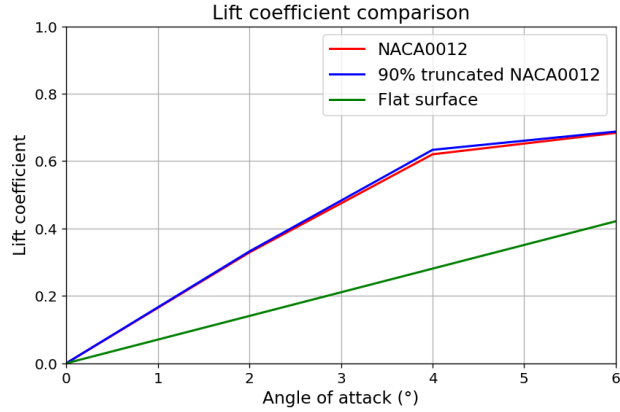


Fig. 21 Lift coefficient x α comparison between flat surface airfoil, standard NACA0012 and the 90% truncated NACA0012.

Table 5 Drag and lift coefficient extracted from CFD simulations.

α	NACA0012		NACA0012 90%		NACA0012 80%		NACA0012 60%	
	Cd	Cl	Cd	Cl	Cd	Cl	Cd	Cl
0	0.0103	-0.0002	0.0120	0.0002	0.0156	0.0006	0.0246	0.0001
2	0.0109	0.3289	0.0127	0.3320	0.0157	0.2968	0.0253	0.2282
4	0.0197	0.6203	0.0217	0.6335	0.0240	0.5958	0.0287	0.4697
6	0.0463	0.6838	0.0475	0.6877	0.0493	0.6889	0.0475	0.6158

Table 6 Cl over Cd ratio for the different profiles and relative difference from the standard profile.

α	NACA0012	NACA0012 90%		NACA0012 80%		NACA0012 60%	
0	0.0	0.0	0	0.0	0	0.0	0
2	30.1	26.1	-13.23%	18.9	-37.17%	9.0	-69.98%
4	31.5	29.1	-7.48%	24.8	-21.30%	16.4	-48.04%
6	14.8	14.5	-2.07%	14.0	-5.49%	13.0	-12.30%
Average	19.1	17.4	-5.70%	14.42	-15.99%	9.59	-32.58%

b) Trapezoidal shape

The trapezoidal shape was chosen for the fins. Although theoretically, the most aerodynamic fin shape is elliptical, simulations showed that the drag variation with the angle of attack of the rocket is considerably smaller with the trapezoidal shape than it is with the elliptical shape, as described in Ref. [8]. Coupled with the fact that they are easier to manufacture, trapezoidal fins were chosen to be used in Pacifico. Fig. 22 illustrates the concept behind this construction with the carbon-fibre core in contrast with the PETG aerofoil left transparent for mere illustration purposes.

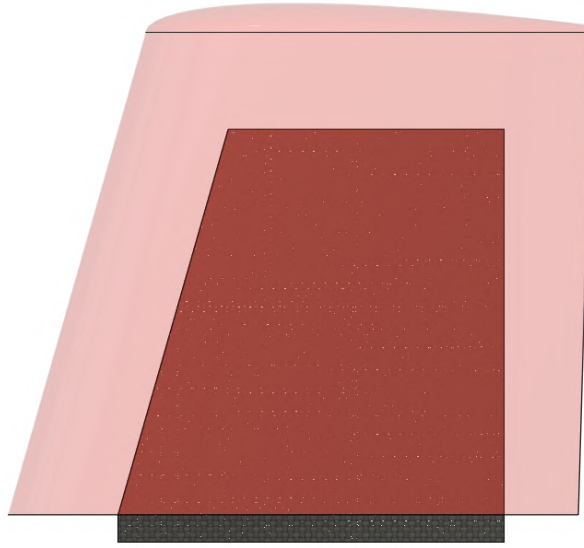


Fig. 22 Out of scale illustration of Pacífico's fins.

c) Area optimization

The dimensions of the fins were optimized using a merit function that is dependent on the static margin of the rocket. In this way, it is possible to correlate the root chord, tip chord, and span of the fins with desired values of the static margin.

The merit function is as follows:

$$M = \frac{e^{-\left(\frac{Sm-2}{0.4}\right)^2}}{A_f} \quad (3)$$

The function works so that the closer the static margin is to the desired static margin (which in this case is 2) and the lower the value of the area, the higher the value of M. The smaller the area of the fins, the smaller the drag forces; whilst if you lower the area too much, the static margin will not be a tolerant value. Thus, this analysis allows the determination of the possible optimized dimensions for the fins by encountering the highest possible value of M for reasonable fin parameters.

The function was implemented inside *RocketPy*, a rocket flight simulator that will be described in flight simulation subsubsection II.B.8. The obtained results are displayed in Table 7.

Table 7 Pacífico's fins size parameters.

	mm	in
Number of fins	4	
Span	180	6.89
Root Chord	230	9.05
Tip Chord	180	7.08

d) Flutter

Flutter is the phenomenon of excessive vibration on the fins caused by several different factors: pitching, yaw, and roll moment; drag forces; wind forces; elastic and mechanical properties of the fin's material and so on. In fact, fluttering

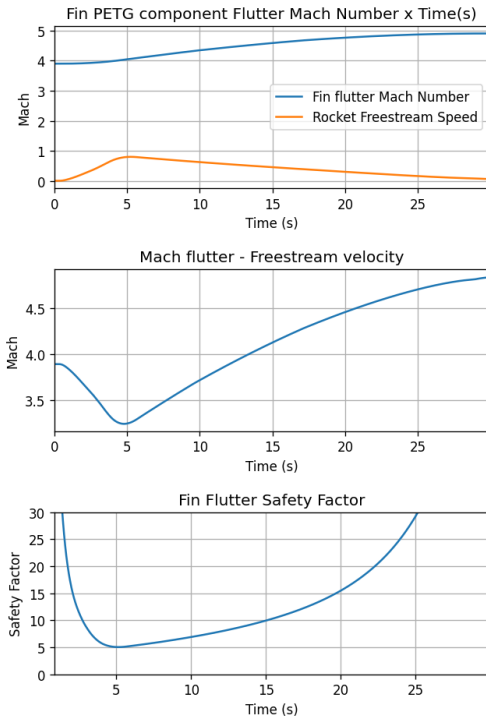
is a complex topic of study, but there is a simple and important equation that aids the analysis: the fluttering boundary equation, which gives the limit speed to prevent the fluttering (further than that limit, there is a high chance that the fins will break due to this phenomenon). The equation can be found at Ref. [9] and is reproduced below:

$$v_f = v_s \cdot \sqrt{\frac{G}{\frac{1,337 \cdot (AR)^3 \cdot P \cdot (\lambda + 1)}{2 \cdot (AR + 2) \cdot \left(\frac{t}{c_r}\right)^3}}} \quad (4)$$

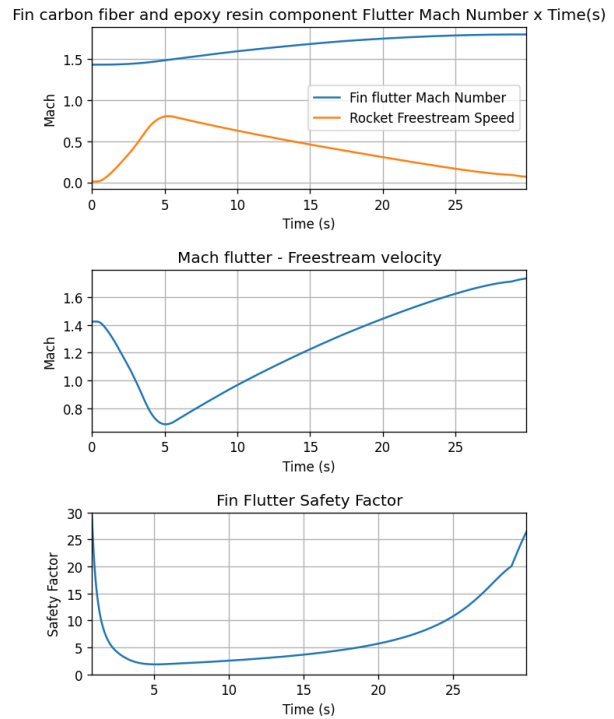
The value of v_f varies at every moment due to the constant changes in height and temperature conditions. Thus, the best way to analyse the situation is by considering the flutter speed at the height at which the rocket speed is maximum. If at that condition the flutter limit speed is not exceeded, it is safe to consider that the fins will not suffer fluttering.

The data relating to the maximum rocket speed and the height in which this speed was reached were calculated using *RocketPy*. The data obtained were: $v_{max} \approx 902$ ft/s, at a height of 2188 feet. Both the PETG ($\approx 2.9 \cdot 10^5$ psi) and epoxy resin ($\approx 1.59 \cdot 10^6$ psi) shear modulus G were considered in order to guarantee that neither of the fin's components would be unsafe.

Applying the mentioned values in Eq. (4), Pacífico's fins showed to be safe from fluttering.



(a) PETG flutter analysis.



(b) Epoxy resin and carbon fiber flutter analysis.

e) Predicted manufacture

Envisioning a lightweight and rigid fin, a carbon fiber laminated plate was chosen as a core for its structure. Then it will be covered with a piece of 3D printed ABS to give the desired airfoil shape and finally unified with specific adhesives (Ly 1564 + Aradur 2963 and AW 5800 provided by Huntsman).

6. Structural Analysis

a) General Considerations

Coupling disks, tubes and bolts are some of Pacífico's main tools for connecting its different parts and modules. Therefore, in order to guarantee Pacífico's structural integrity, these parts need to be simulated to ensure safety and

efficiency. With this objective in mind, computational structural simulations were performed using software from ANSYS Mechanical package.

The approach adopted was to identify the most critically loaded parts, simulate them and expand their results to other less critically loaded cases. Aiming to identify these most critically loaded parts, the following criteria were used:

- **Type of load:** There are two key instants of flight in which the highest loads are applied on the rocket. One of them happens when motor thrust is at its peak, during motor-propelled flight. The other occurs when the recuperation system is activated after the apogee is reached. Therefore, critically loaded parts were identified separately in these two moments.
- **Geometry:** Pacífico is composed of several parts with different geometries and structural behaviours. Therefore, one of each main geometry's components with important structural functions was simulated (tubes, male disks, female disks and U bolts).
- **Load value:** In each group of parts with similar geometries, the one with the highest load values was adopted as critical.

Through these criteria, parts classified as critically loaded ones were the payload module's bottom male and female disks, the motor's tube, and the bottom U bolt, as shown in ??.

Overall, the loads considered were the inertial load (mass being accelerated), the motor thrust and the specific loads of each part. These boundary conditions data (maximum motor thrust and acceleration) were obtained from RocketPy – Projeto Jupiter's flight simulation software. Additionally, the parachute opening force and the motor's internal pressure were estimated by the recuperation and propulsion areas. All the safety factors obtained concern the aluminium alloy's yield stress.

b) Male Coupling Disks

When studying the coupling disks of the rocket, there is a necessity for structural analysis due to the various forces exerted on them. The most critical load for this part happens at maximum thrust, where acceleration is the greatest. Given the symmetrical nature of this structure along the main axis, we chose to divide it into four parts, a modeling approach facilitated by Ansys Mechanical. This allowed us to generate a finer mesh, particularly in crucial regions such as the holes. By distributing the load proportionally across the segments of the analyzed structure, the software replicates the behavior across all other segments, thus reconstructing precise results. As can be seen in Fig. 24.

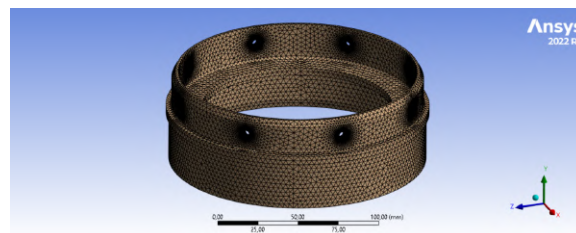


Fig. 24 Simulation Mesh.

After meshing and establishing a coordinate reference, locations for force application and fixed supports were determined. The chosen fixed supports were the sides of the disk, bonded to the tubes. This condition implies no movement, indicating no relative motion with respect to the tube.

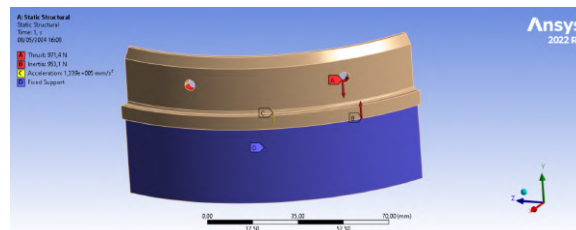
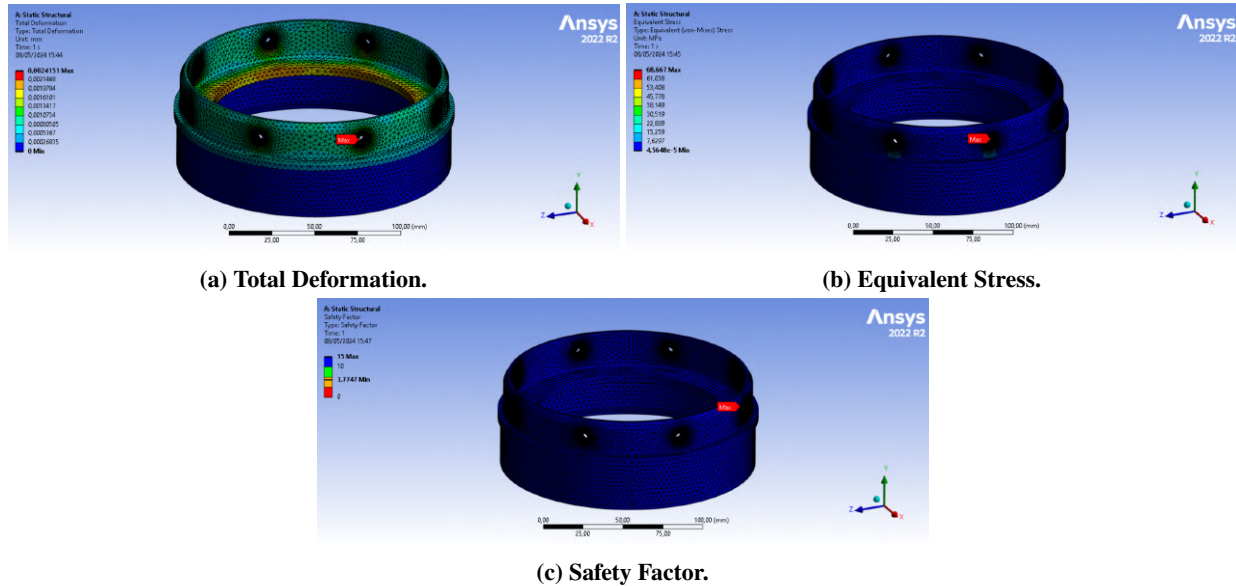
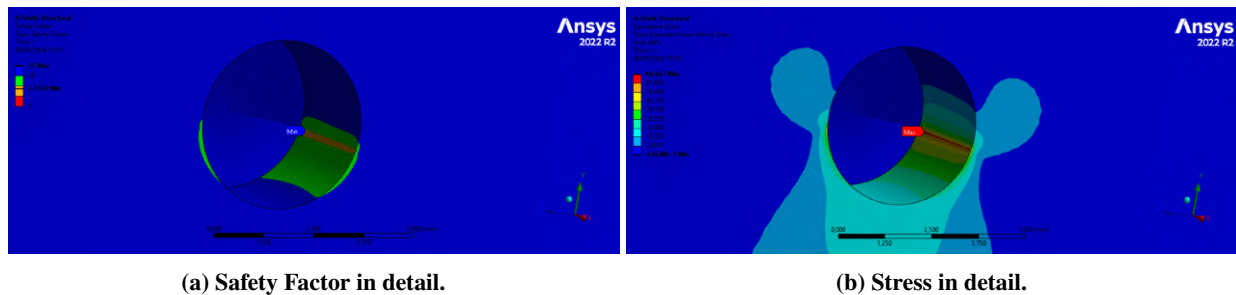


Fig. 25 Simulation Model.

Afterwards, forces are applied based on the methodology described at the beginning of the section, two forces are considered, the value of the inertial weight, 953.1N and 971.4N of thrust, all according to the coordinate system defined. The thrust force is directly applied to the holes, simulating force transmission through the screws. Finally, the inertial force of the upper frame is applied to a small support at the outer edge of the disk, where the tube is supported and bonded.



The results of considered boundary conditions in the geometry are the following, as displayed in 26a and 26b, regarding the deformation and stress that this piece endures during flight. Also, the minimum safety factor for this structure, with the simulation of several mesh points, decreased and converged to a factor around 3.77. As expected, the main concentration of stress was in the middle of the holes, due to the shear force of the screws.



c) Female Coupling Disk

The female coupling disks are modeled very similarly to the male disks, with only changes in the locations where forces are applied. Employing the same symmetry strategy, the structure was divided into eight parts, and the forces were distributed proportionally, as illustrated in 28. The results obtained with this model yielded an acceptable minimum safety factor for the part, ensuring the safety of the most critical female coupling disk in this project, located just above the payload module. Consequently, it can be inferred that other similar disks in less critical situations are also secured.

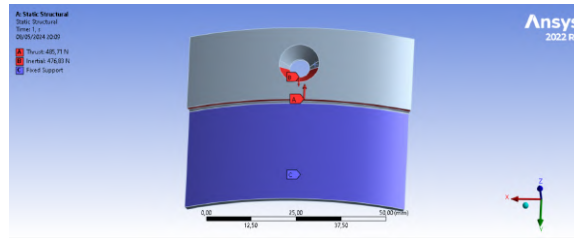
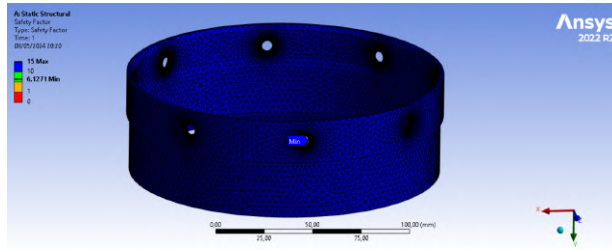
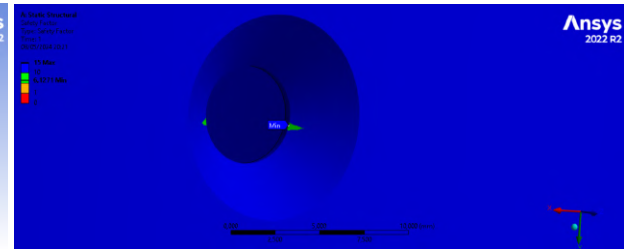


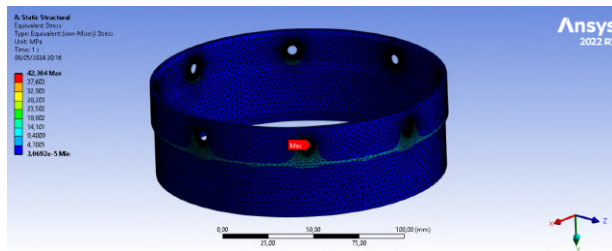
Fig. 28 Simulation Model.



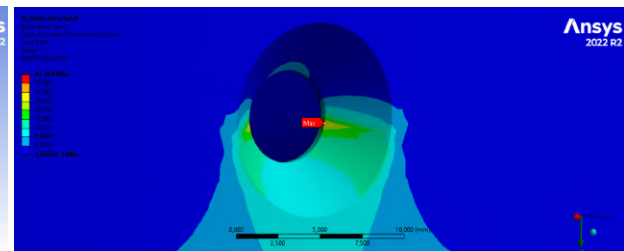
(a) Safety factor.



(b) Safety factor in detail.



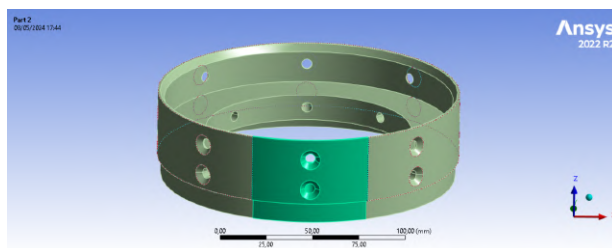
(a) Equivalent Stress.



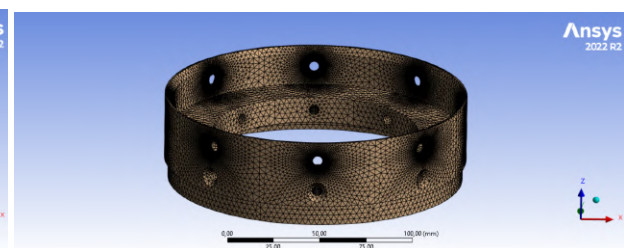
(b) Equivalent Stress in detail.

d) Female Disk of Propulsion Module

The female disk of the propulsion module stands out as a unique coupling component in the rocket, requiring more attention. It sustains the heaviest load during motor burn, and is responsible for transmitting all thrust to the upper frame and resisting resulting inertial forces. Additionally, its configuration with two lines of screws necessitates a slightly adapted model. To address this, the structure was partitioned into eight axisymmetric sections, enhancing the simulation's precision.



(a) Geometry of the structure.



(b) Simulation Mesh.

For this simulation, a thrust force of 485.71 N was applied to the upper segment of the lower holes of the disk, while an inertial load of 476.83 N was applied to the lower segment of the upper holes. The support was positioned at the lower part of the bottom holes, as this is where the main bolts attach to the bulkhead. All forces mentioned are already proportionally divided among the segment of the structure being analyzed.

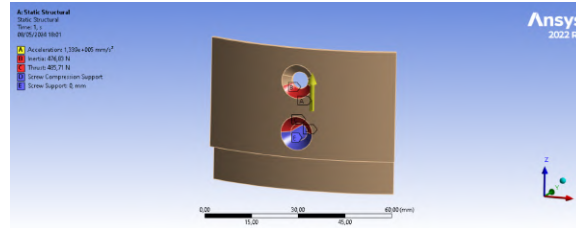


Fig. 32 Simulation Model.

The minimum safety factor converged to approximately 4.89, ensuring the structural integrity of the disk. The minimum safety factor and maximum stress are presented in figures Fig. 34 and Fig. 33a respectively.

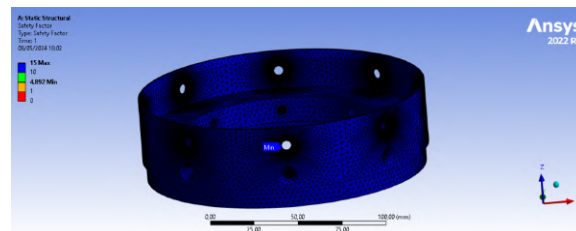
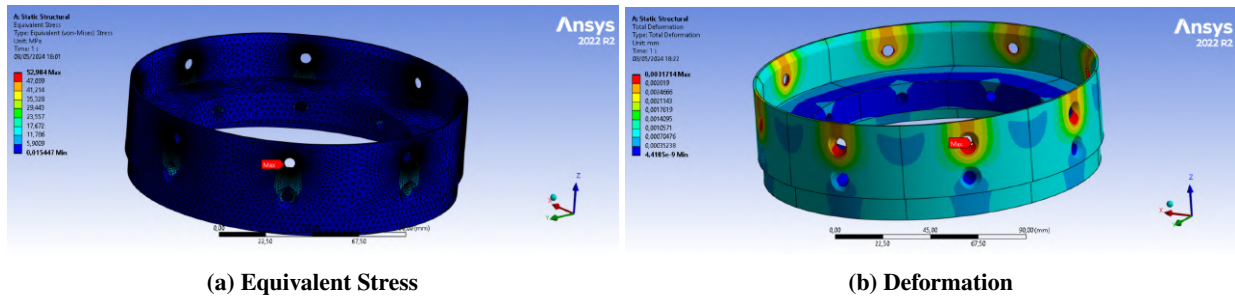
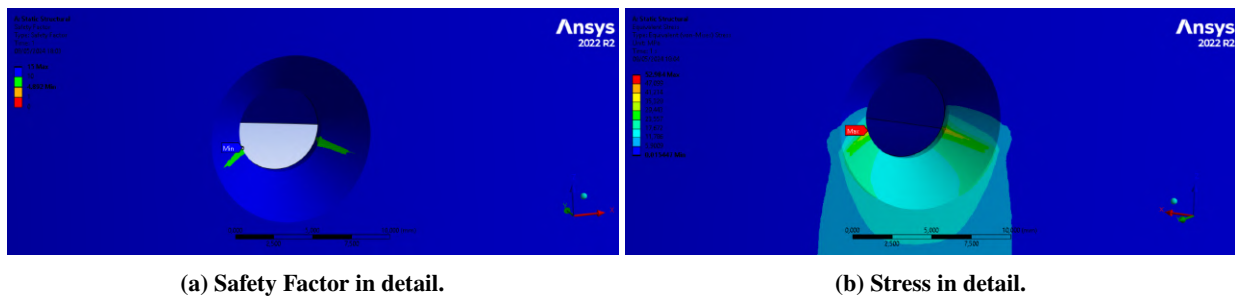


Fig. 34 Safety Factor.



e) U Bolt

The U-Bolt is a crucial component responsible for holding up the rocket and preventing it from free falling after the deployment and disreefing of the parachute. The model was made by separating parts of geometry and making finer meshes in different ways where the stress is applied. At the moment the force of disreefing is 2022N. Twenty points were used in the simulation and a safety factor of around 18.01 was obtained, which represents a reliable safety value.

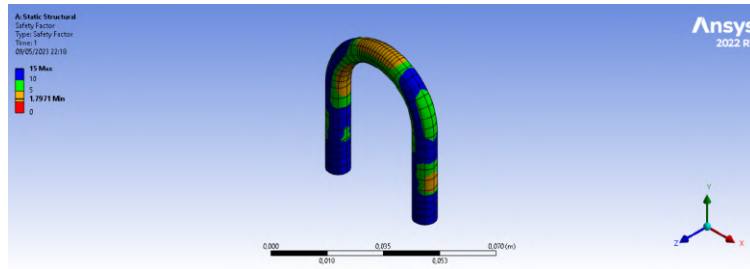


Fig. 36 U-Bolt Safety Factor.

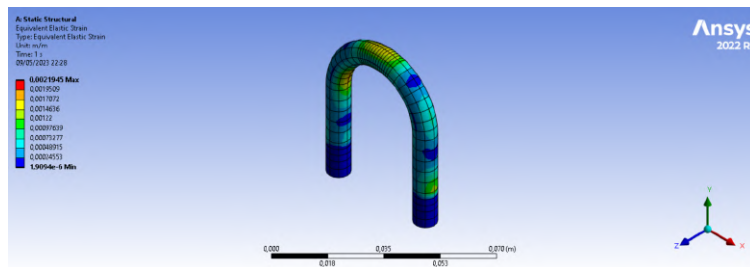


Fig. 37 U-Bolt Strain.

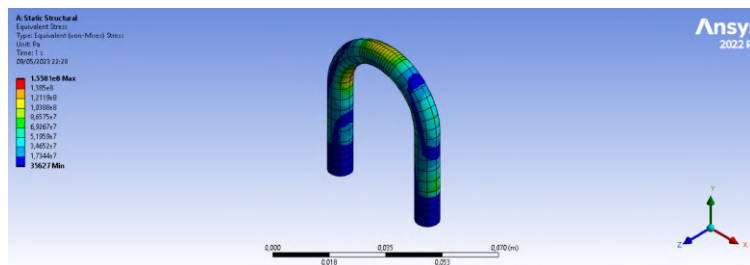


Fig. 38 U-Bolt Stress.

7. CFD Analysis

a) Tail

It is well known that the tail plays an important role in the rocket, especially when it comes to reducing the total drag force. But deciding the tail shape that will yield the best results for the rocket structure is a difficult task. After consulting Refs. [10], [11] and [12], two tail shapes that satisfy both the conditions of being easy to manufacture and that yield satisfactory results were found: the conical shape and the spherical shape.

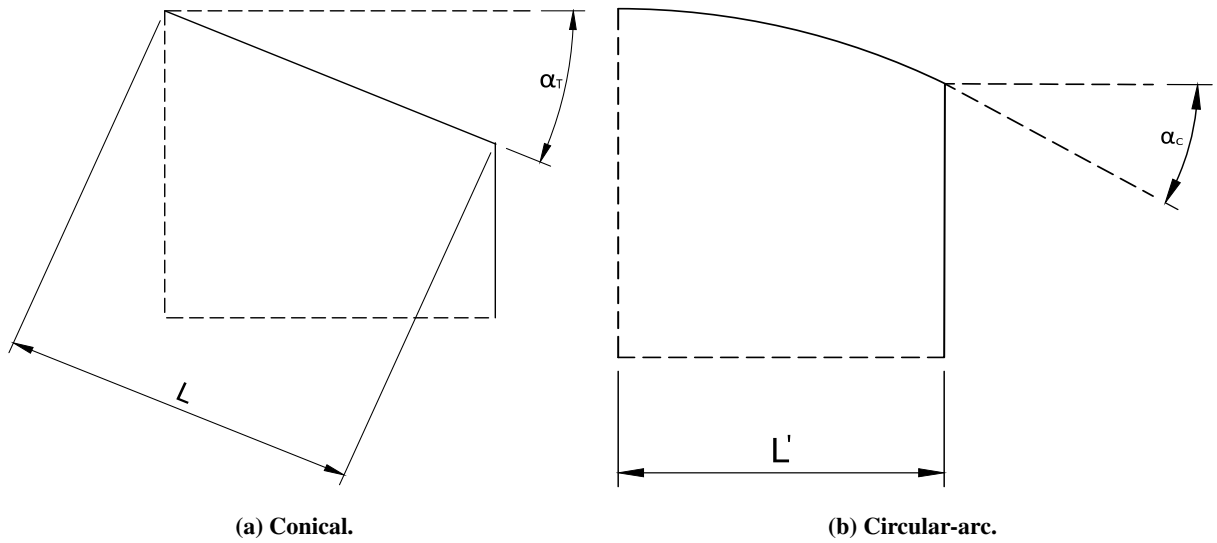


Fig. 39 Tail shapes studied and relevant parameters.

Once those tail shapes were chosen, the second thing decided was the parameters to be varied for each type of tail in order to study their influences on the drag forces. For the conical shape, those parameters were the total length L and the opening angle α_T , as represented in the Fig. 39a. For the circular-arc shape, they were the total horizontal length L' and the angle α_C (represented in Fig. 39b).

After varying the parameters and doing numerous 2D CFD simulations, some special cases with satisfactory drag values were found. These cases are represented in the tables below.

Table 8 Best results for the simulations of the circular-arc shape.

$L' (mm)$	α_C (degrees)	Total drag (N)
18	15	203.84
24	15	208.51
20	25	199.83
20	27	199.75

Table 9 Best results for the simulations of the conical shape.

$L (mm)$	α_T (degrees)	Total drag (N)
20	10	221.12
20	13	214.39
20	16	205.84
20	19	208.90

Considering that 2D CFD simulations without a tail have provided a total drag of approximately $250 N$, these tables confirm the expectations that the tail significantly reduces the drag. Comparing the data presented in the two tables, it is viable to affirm that the circular-arc shape shows better results. Once more, 2D CFD simulations were made varying both L' and α_C for the circular-arc shape.

Table 10 Results obtained by studying only the influence of the tail's horizontal length (L').

$L' (mm)$	α_C (degrees)	Drag on tail (N)	Total drag (N)
30	27 (fixed)	60.67	228.75
35		51.39	215.30
40		40.54	174.43
45		37.73	173.49
50		36.10	171.86

Table 11 Results obtained by studying only the influence of the tail's defined angle (α_C).

$L' (mm)$	α_C (degrees)	Drag on tail (N)	Total drag (N)
50 (fixed)	25	37.40	173.07
	26	36.37	172.09
	27	36.10	171.86
	28	35.27	171.05
	29	34.31	170.12

To clarify the final choice, some remarks should be made. Firstly, it was observed that the drag would decrease for values higher than $50mm$ of horizontal length. However, after considering analytical calculations of the ejection of the gases from the motor's nozzle, horizontal lengths bigger than $50mm$ would possibly be a threat to the tail integrity. Therefore, $50mm$ was chosen as the tail's length, once it presented the best drag and a minimum safety margin of $10mm$ between the tail's edge and the projection of the exhaust gases from the motor.

A second remark is that, aiming to keep the margin of $10mm$, the angle α_C was kept at 27 degrees, since it was the biggest angle where the safety margin was met. Moreover, larger angles than 27 had no significant advantages in terms of drag reduction. With the safety margin met, there was enough space for an carbon fiber layer, as shown in Fig. 40.

**Fig. 40 Final tail projected. The settled parameters were $L' = 50mm$ and $\alpha_C = 27$ degrees.**

b) Drag curve

Pacífico's drag curves were estimated using the RASAero II software to provide the drag curves for further flight analysis. To generate the curve, all the parameters of the rocket's components were provided to the software to generate it. The result in drag for the motor powered can be seen in Fig. 41.

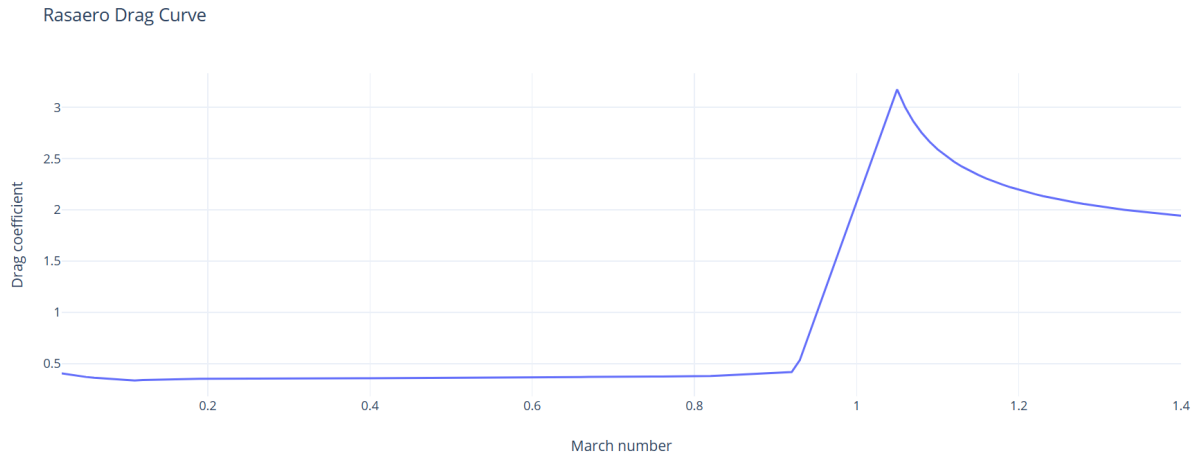


Fig. 41 Pacifico's drag curve.

8. Flight Analysis

Projeto Jupiter has developed its own software of flight analysis and simulation named *RocketPy*, which features motion capabilities of 6 degrees of freedom and wind data imported from NOMADS (NOAA – National Oceanic and Atmospheric Administration Operational Archive and Distribution System) and ECMWF (European Centre for Medium-Range Weather Forecasts), allowing the team to simulate realistic flight trajectories over different wind scenarios.

Furthermore, the software is equipped with tools to make accurate evaluations of the variation of mass throughout the flight, and it is able to import aerodynamics characteristics calculated by CFD as well. The information extracted from these characteristics is used to evaluate how the static margin varies through the flight and predict how the different forces will act as the mass and moment of inertia change. By combining all those data, *RocketPy* makes a trustworthy trajectory estimation. The detailed flight simulation performed in *RocketPy* can be found in Appendix G.

a) Trajectory simulation

The team adopted a standard simulation to evaluate flight parameters such as static margin and stability response, but the predicted flight parameters such as apogee, out-of-rail velocity, and impact point were estimated using a Monte Carlo method.

The atmospheric conditions used were based on ECMWF Forecasts at the competition launch site. This data was used as input for the Monte Carlo dispersion analysis. Figure 42 shows the wind profile and other important information about the atmospheric model considered in the standard simulation on competition site. However, for this simulation, specific recommended surface atmospheric conditions were also used, considering a constant wind speed of 6.69 ft/s (22 ft/s) heading 135.00°. Figure 43 shows the considered constant wind profile.

Lastly, it is important to register that the launch rail considered is the 5.18 m (17 ft) long provided by ESRA and it is located at latitude 32.990254° and longitude -106.974998°, which means that Pacifico's launch was simulated at the Spaceport America Launch site. At these coordinates, the altitude above sea level is approximately 1400 m (4593 ft).

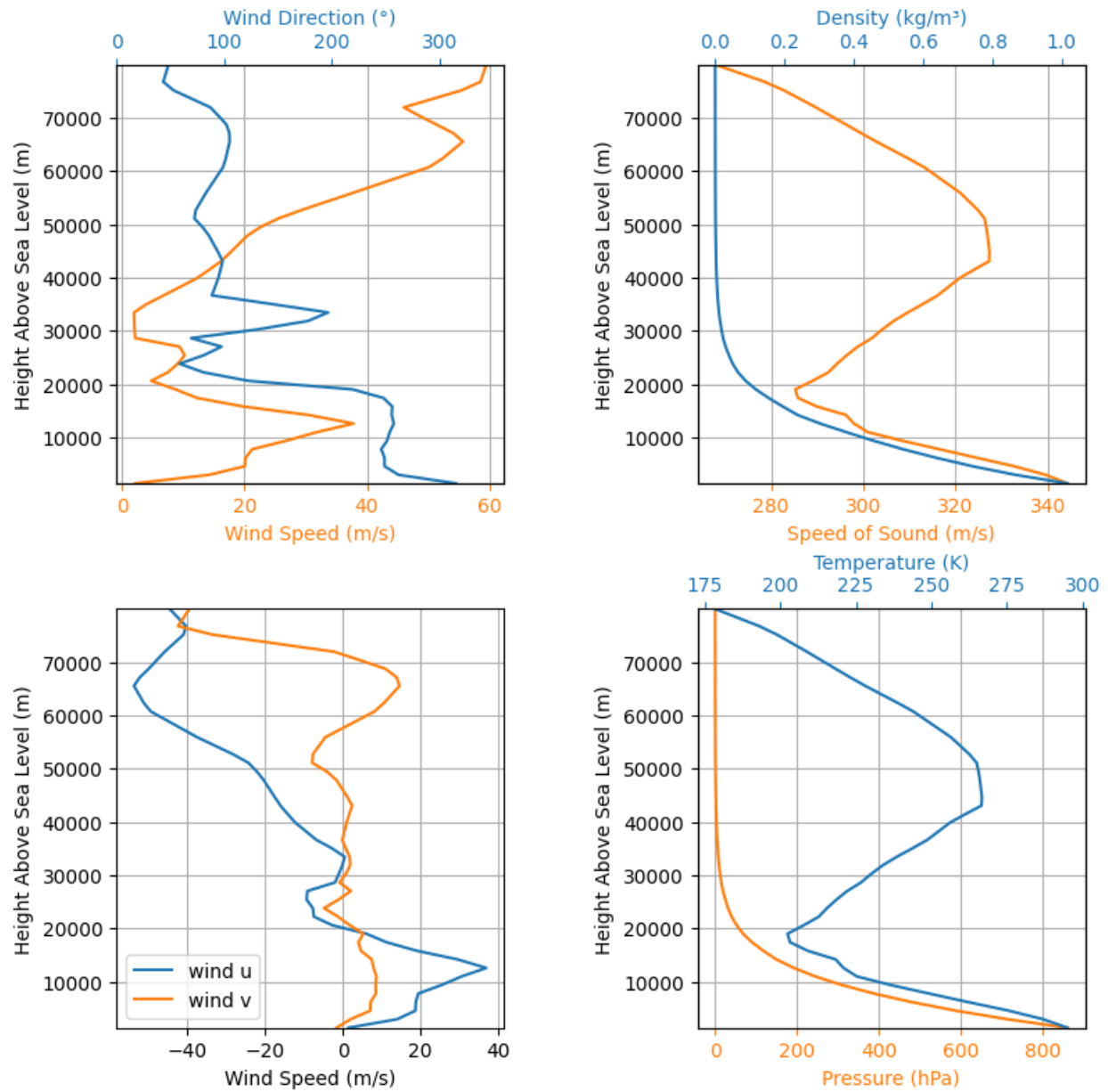


Fig. 42 Wind Profile.

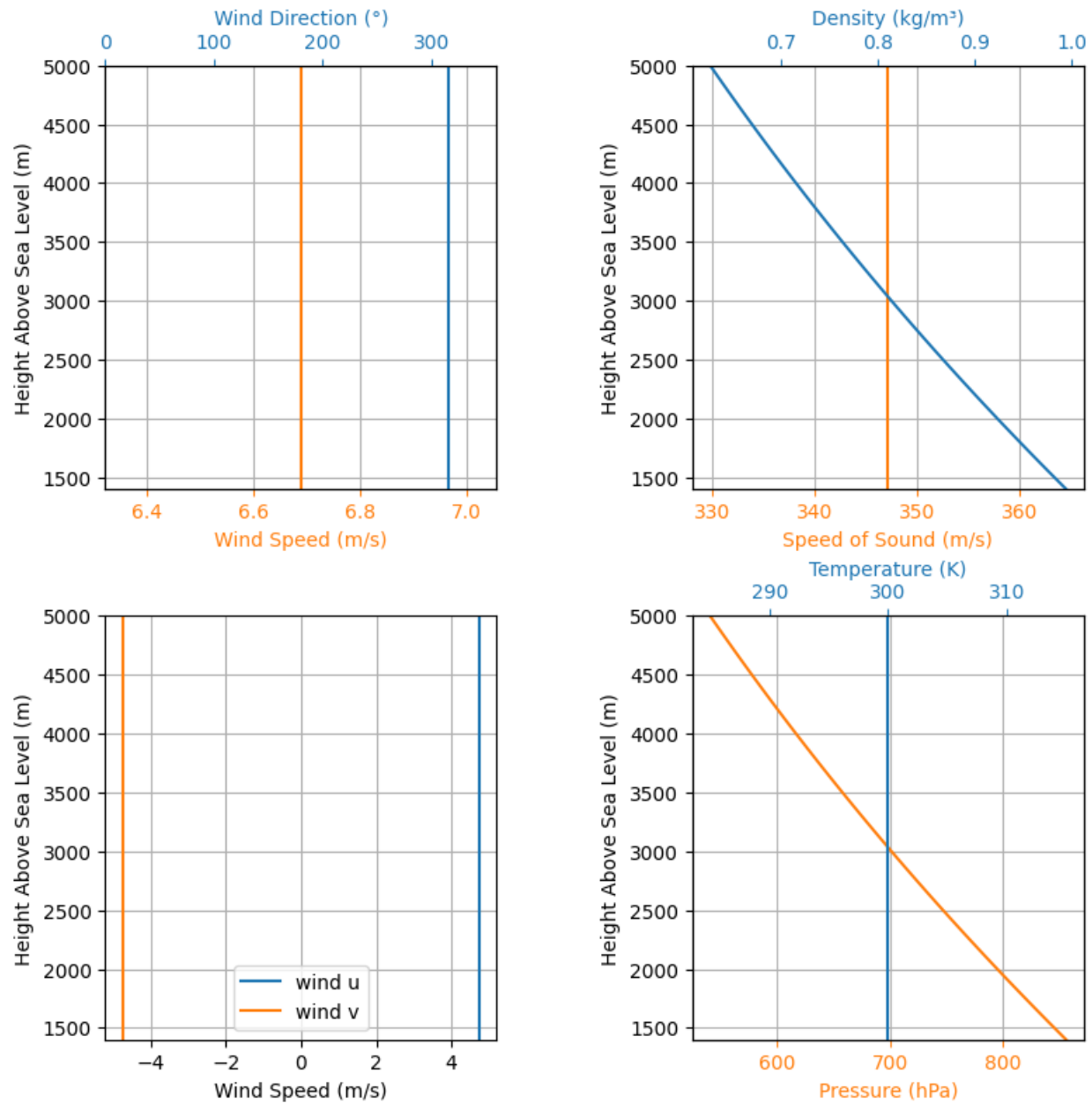


Fig. 43 Constant Wind Profile.

After defining the recommended environmental conditions, the motor, rocket and parachute information were used as inputs by the simulator. Regarding the motor, its thrust curve, the propellant mass and geometrical parameters are the most important data. All details about Pacifico's motor, named Mandioca, are presented in the propulsion section of this document. For the parachute, its C_{DS} (main nominal drag coefficient times its area) and opening delay are the most relevant input data. When it comes to determining the correct instant for the parachute deployment, *RocketPy* uses the avionics code (*SisRec*) that is actually embedded on the rocket – see Table V. Finally, the simulator will use as inputs many of the rocket's geometric, inertial and aerodynamic parameters.

With all the necessary information given, a simulation of the rocket can be obtained. A three-dimensional trajectory graph and a plethora of information about the rocket flight performance can be analysed. Considering a launch situation where the rail is oriented to an azimuth of 0° and an inclination angle of 84° , Pacifico has a predicted apogee of 3043 m (9983ft) (above aground level–AGL), reaching a maximum speed of 262.9 m s^{-1} (862 ft/s) at 3.62 s after ignition, with

a maximum Mach number of 0.761, taking into account the variation of the speed of sound with the change in altitude. It also has a maximum acceleration of 132.6 m/s^2 (435 ft/s^2) at 2.02 s, which divided by the local gravity acceleration can be represented as 13.5g.

Fig. 44a shows the predicted rocket trajectory from the flight simulation of Pacifico, considering that both parachute phases work nominally. In Fig. 44b, a total recovery failure scenario (ballistic) is presented. More information on these two flight simulations can be seen at Table 12. Pacifico's vertical speed and acceleration can be seen on Fig. 45 and the resultant drag load on Fig. 46.

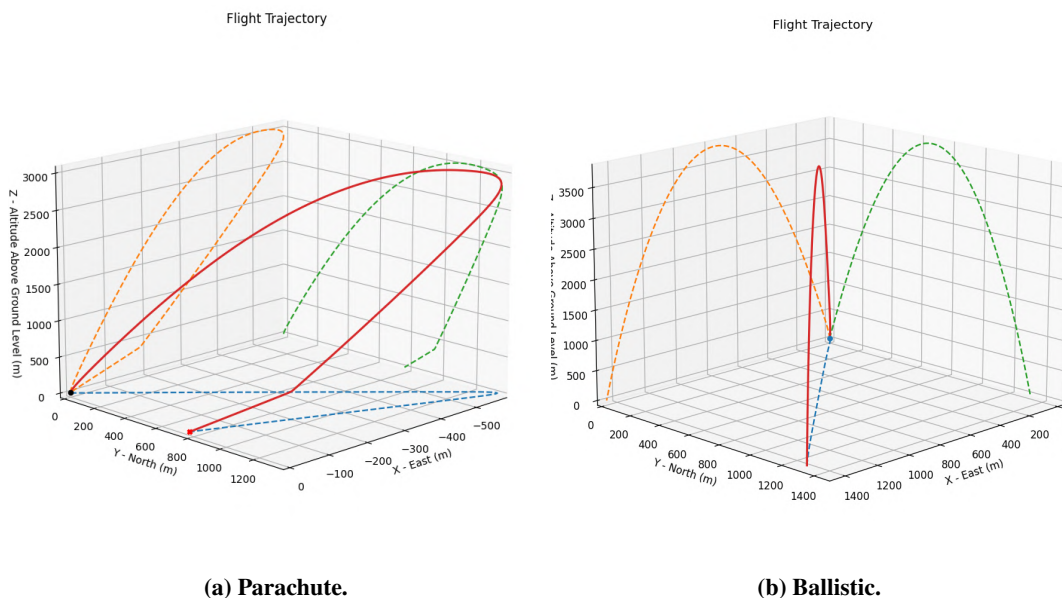


Fig. 44 Pacifico's predicted flight trajectory.

Table 12 Flight Events Data.

Flight Events Data					
Event	SI	Imperial Units	Event	SI	Imperial Units
Initial Static Margin	2.157c	2.157c	Freestream speed at apogee	50.506m/s	165.7ft/s
Static Margin at burnout	2.799c	2.799c	Time of disreefing	120.67	120.67s
Launch Rail Departure Velocity	23.074m/s	75.70ft/s	Altitude of disreefing	385.36m	1264.3ft
Time of burnout	4.3s	4.3s	Freestream speed at disreefing	26.69m/s	87.56ft/s
Altitude at burnout	621.8m	2040ft	Time of impact	159.72s	159.72s
Time of apogee	25.62s	25.62s	Impact Vertical Velocity	-9.53m/s	-31.26ft/s
Altitude at apogee	3043m	9983ft			

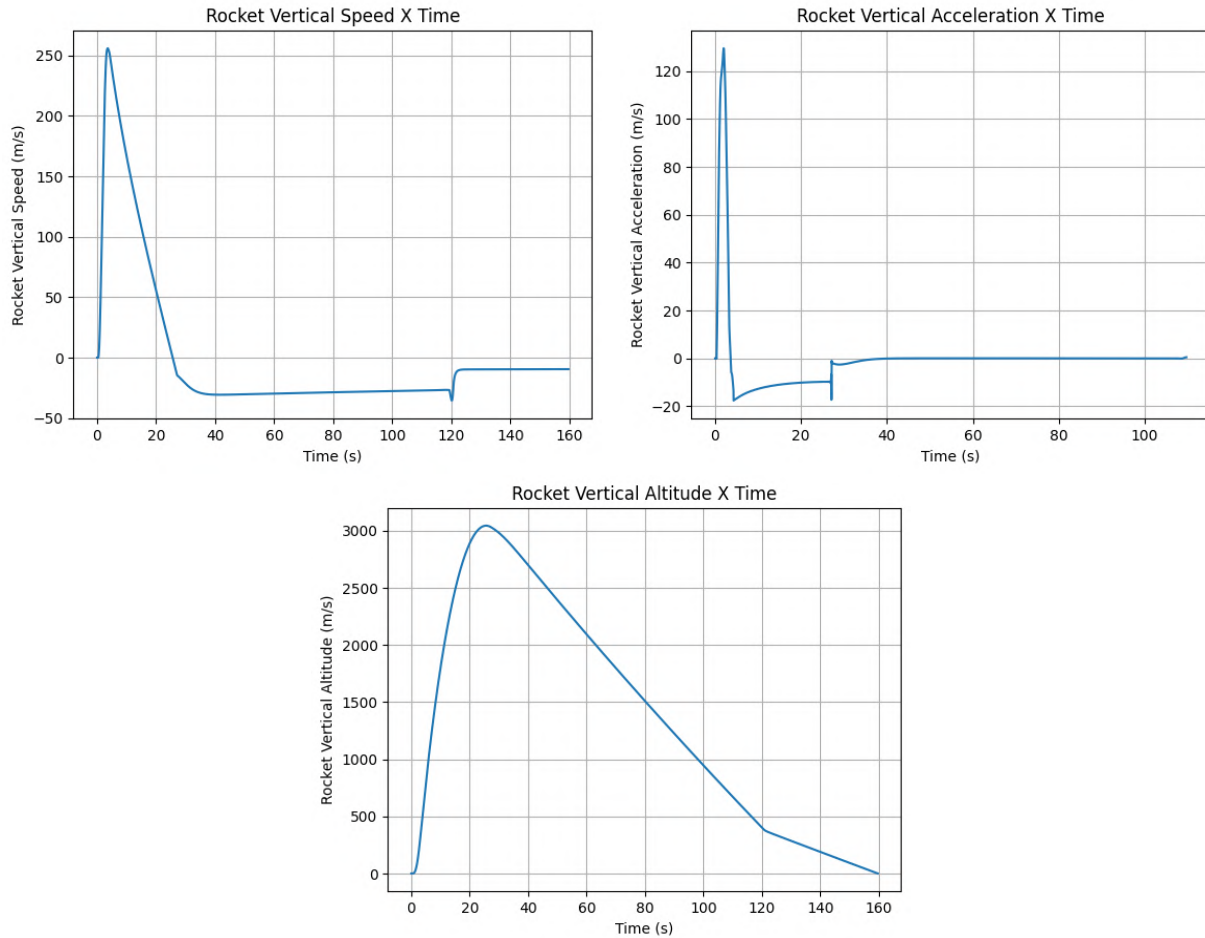


Fig. 45 Linear Kinematics results for the Pacifico flight simulation.

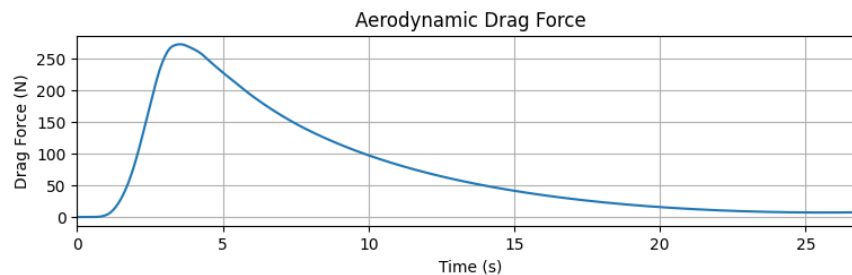


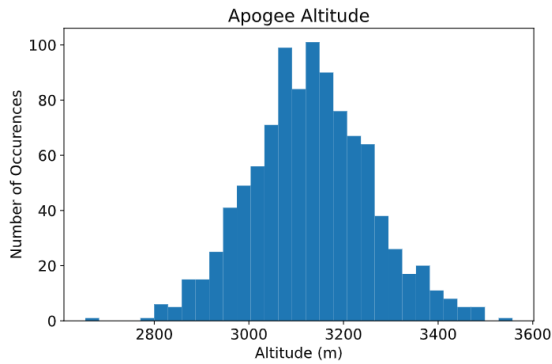
Fig. 46 Drag forces under Pacifico's fuselage.

b) Apogee and out of rail velocity analysis using Monte Carlo

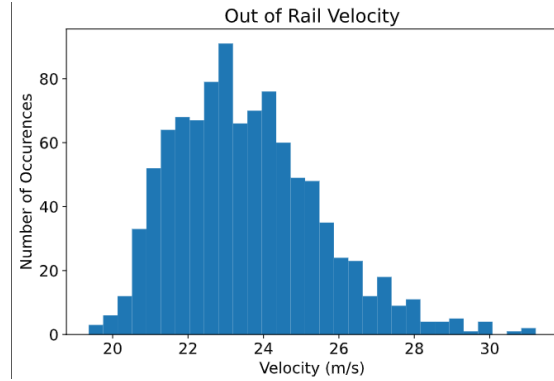
To evaluate the predicted apogee and the out of rail velocity of the rocket, a dispersion analysis using the Monte Carlo method was performed. All the input parameters, such as components lengths, masses, aerodynamic properties, environment characteristics, and the engine total impulse and burn time were varied.

Fig. 47.

In the presented simulations, the apogee reached a mean value of 3130 m (10269 ft) with a standard deviation of 126.26 m (415 ft), and the out of rail mean velocity was 23.6 m s^{-1} (77.4 ft/s) with a standard deviation of 1.94 m s^{-1} (6.36 ft/s).



(a) Pacifico's reached apogee dispersion.



(b) Pacifico's out of rail velocity dispersion.

Fig. 47 Pacifico's apogee and out of rail velocity dispersion.

c) Aerodynamic stability

The capability of a rocket to stay in its trajectory independently of external forces is defined as its aerodynamic stability. A good way to measure this is by analyzing the rocket's static margin.

Utilizing *RocketPy*, several different analyses regarding the static margin of the rocket were made. Firstly, a graph showing the change in the overall static margin of the rocket throughout time was created (Fig. 48). The cause of this change is the burning of the rocket propellant, which causes a variation in the position of the rocket's center of mass, thus a change in the static margin.

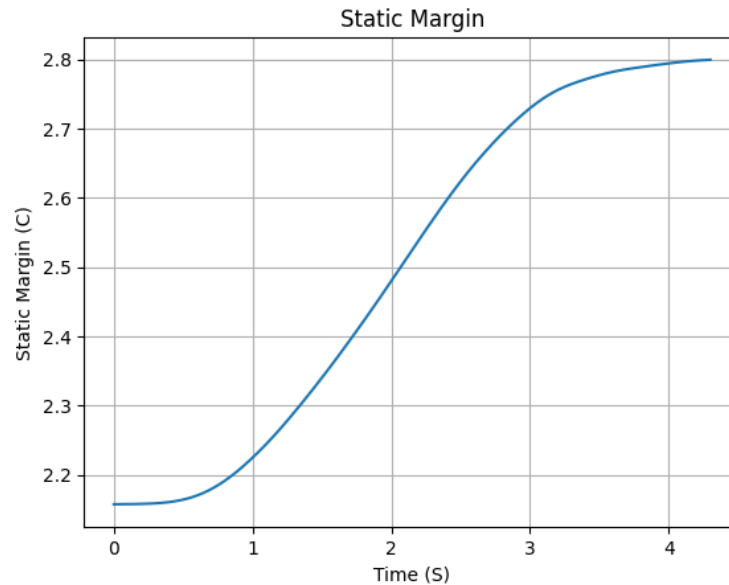


Fig. 48 Static margin by time.

C. Recovery Subsystems

The recovery system's main goal is to safely return the rocket to the ground, avoiding damage to its subsystems and guaranteeing the safety of spectators. The required dual-stage recovery is achieved through the reefing of a single main parachute, which is quarter-spherical.

This parachute configuration began development by the team in 2019, before the Covid-19 pandemic, because it was a new challenge for the team and innovation that members were interested in testing. Additionally, the need for a single

recovery module and single parachute was seen as an advantage when compared to the team's previous drogue-main recovery. Since then, the team's reefing design has been refined and it has flown in the 2022 Latin American Space Challenge, in which Projeto Jupiter achieved its first nominal recovery with the rocket Juno II, and in the 2023 Spaceport America Cup, with partial success due to the tangling of the parachute's suspension lines, a problem which has since been fixed. Given this context, the team chose to use a reefed parachute for Pacifico again due to: team members' familiarity with this recovery configuration, including its assembly and manufacturing; reefing's innovative nature; the need for only one recovery module and ejection system; and the team's previous success with this dual-event approach.

The ejection of the parachute is achieved through a redundant CO₂ based ejection system, which is pyrotechnically activated. A similar system has been used by the team in former launches, notably in the 2019 and 2023 Spaceport America Cup. It has since been altered to reduce the length of the recovery module, optimize its pressurization, and improve assembly. This iteration of the team's ejection system design was used in the 2022 Latin American Space Challenge, in the team's independent launch in March of 2023, and the 2023 Spaceport America Cup, performing successful ejections in all three flights. As a result, the team considers the system reliable for use in Pacifico. In addition to the ejection system, parachute deployment is aided by a ringsail pilot chute and a deployment bag, which also protects the canopy from the ejection charges.

Furthermore, to prevent the recovery module from opening before the rocket's apogee, which would lead to the opening of the chute at excessively high speeds, damaging it and the rocket, the team decided to use shear pins as a locking mechanism, securing the sliding coupler to the fuselage. The pins are designed to withstand the separation forces caused by drag during free flight and rupture with the pressurization forces from ejection, allowing the sliding coupler to move freely. Regarding the parachutes, the pilot chute helps to optimize the ejection while the reefed main one decelerates the rocket to a initial speed of 72.2 fps and later to 30.4 fps. Finally, to recover the rocket once it lands, the team will use both the GPS coordinates transmitted by the telemetry system, and the dispersion prediction, obtained via trajectory simulation.

The single recovery module is located between the avionics bay, located inside the nosecone, and the payload bay, as shown in section II. In the following sections, this report will go into more detail about each of the components of the recovery module shown from left to right.

1. Ejection System

a) Parachute Connection

The connections between the main parachute's shock cords and the payload bay, as well as between the chute and the avionics bay, are achieved through U-Bolts. Each of these bolts is fixed to 1/4" thick 5052 H34 aluminum bulkheads on each end of the module. Both the U-bolts and bulkheads were simulated on Ansys Static Structural to guarantee they can withstand the main chute's disreefing force of 200 lbf on the fore section of the rocket (nosecone, avionics bay and ejection system) and 489 lbf on the aft section (payload bay and motor) with a minimum safety factor of 2. For more details regarding the calculations done to obtain these forces, and the simulations, see Appendix G and Appendix H, respectively.

The shock cords are made out of tubular polyester webbing, rated to withstand 3300lbf of traction, providing a safety factor of 6.7. Additionally, a swivel link is used to avoid the effects of line torsion. It is attached between the U-bolt on the bulkhead between the recovery and payload modules and the confluence point of the nosecone and rocket's shock cords.

b) Locking mechanism

The locking mechanism is responsible for guaranteeing that the recovery module will not open until the rocket reaches apogee. To achieve this, the team is using 4 M2 Nylon 66 screws as shear pins that screw together the coupler and the fuselage of the recovery module, thus maintaining it closed. We chose this system because of its simplicity when assembling the module, and it has already been validated to not break in flight in the latest self-operated flight done by the team in February of 2024.

When enough shear force is applied to the pins, they break, allowing the module to open. To select the appropriate pin resistance, we calculate the maximum separation force experienced by the sliding coupler. This force can either be caused by drag experienced by the rocket or by handling the rocket on the ground, in which case the calculated force is the same as the fore section's (nosecone, avionics bay, ejection system and recovery module) weight. Once both forces are calculated, a shear pin layout is selected to withstand the greater of the two values. The layout is then ground tested

with weights, to verify that it can indeed support the expected load and also. Ejection tests are also executed to verify that the shear pins break with the ejection forces without compromising the parachute's deployment. The maximum separation forces caused by drag and handling are expected to be 7.5 lbf and 13,5 lbf respectively, which lead the team to base the layout on the handling force.

c) CO₂ powered ejection system

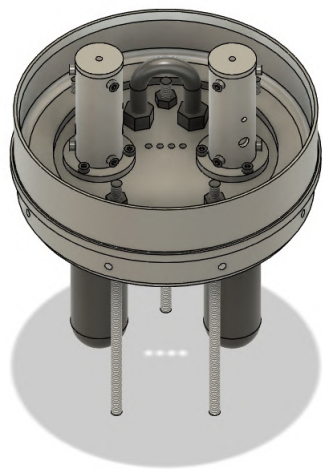
The team originally chose to develop a CO₂ based ejection system due to its better performance, safety, and minimal damage potential when compared to fully pyrotechnic systems. Additionally, the team's previously mentioned experience with this system, which has already been successfully used in three previous rocket flights (Juno II, Juno III and Nyx), guarantees our familiarity with it, as well as its reliability.

Additionally, the manufacturing of its parts is done by team members in-house, rather than by a third-party company, allowing more control over tolerances and fits. As a result, the team does not have to bear the often high cost of ordering machined parts nor trust companies' ability to manufacture parts in the required time frame. Not only that, but members can now repair the ejection system parts on their own when they get worn out after multiple tests and can guarantee that all parts fit the established quality standards, without having to rely on external providers. Since the team started manufacturing these parts on its own, testing results improved, as can be seen in Appendix B.

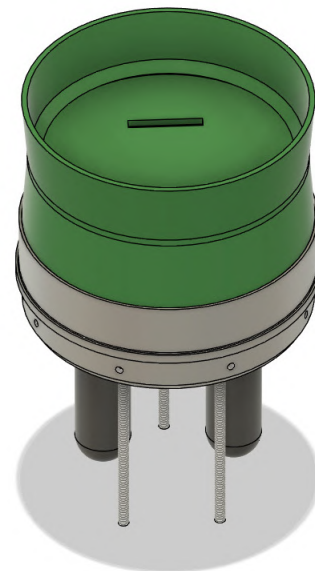
In this context, the 45g CO₂ charge, as well as the 0.024 oz black powder activation charge, used in each ejection unit were chosen empirically, which is detailed in Appendix B.

Similarly to the locking mechanism, the team's ejection system is both mechanically and electronically redundant. In this regard, both of the ejection system units have a black powder chamber with two e-matches, and each of them is connected to a different altimeter, so that either of them is capable of opening both cartridges. At the rocket's detected apogee, each one of the altimeters, one COTS and another SRAD, activates one e-match in each chamber, igniting the black powder in the chamber. When the black powder ignites, the awl is propelled down and breaches the CO₂ cartridge's seal. This process repeats itself in both SRAD ejection system units, pressurising the module and pushing against the 3D-printed piston, the deployment bag, and the coupling tube with the nosecone away from the main body of the rocket. As a result, the pilot and main parachutes are ejected at a distance of 6 calibers.

The 3D-printed PETG piston that covers the ejection system and locking mechanism, separating them from the parachute is essential to the adequate execution of the ejection. Initially, this piece was designed as a means of protecting the deployment bag, main parachute, and pilot chute from the occasional damages that may occur as may occur as a result of the black powder explosions related to these systems. Despite serving its original intent, further testing revealed it is a crucial component in the ejection system because it pushes the chute and optimises the pressurisation caused by the released gas.



(a) Ejection system without the piston.



(b) Ejection system covered by the piston.

Fig. 49 Illustrations of the Ejection system and PETG cover position.

The team has already used this PETG piston in several launches, in the Juno III rocket, some changes were implemented to improve and increase the reliability of the cover that will also be present in Pacifico. These modifications consist of shortening the cover length and adding a slight angle to its base to add a second point of contact between the cover and the fuselage, avoiding axial misalignment and guaranteeing a more swift ejection. As can be seen in Fig. 49b, the cover's design allows better stability during the ejection, since it has two points of contact with the module. This way, the cover's velocity remains parallel to the module and offers less resistance in movement.

As a safety measure, an aluminum disk was added to keep the CO₂ in place in case the threads holding them onto the ejection system fail or one gets loose during flight. The disk is kept in place by three threaded rods secured to the ejection system base disk and also doubles as the base for the avionics bay.

d) Rigging

The parachute is linked to both the fore (nosecone to sliding coupler) and the aft (sliding coupler to boat tail) sections of the rocket in a "Y" configuration, with a 1.5ft section connected to the parachute with a quick link, where the line cutters used for disreefing the chute are located. Below that, the shock cords split in two, one 7.6 ft long leading to the fore section, where the wiring for the cutters is located, and one 14 ft long, passing through the ejection piston and leading to the aft section. In the latter there's an appropriately rated swivel link to avoid twisting of the shock cords. The shock cords are made out of tubular polyester rated up to 3350 lbf are attached to u-bolts on either sections of the rocket with appropriately rated quick links.

The parachute is kept inside an SRAD Kevlar deployment bag to protect it from the ejection gases and to keep the lines from tangling. After ejection, a ring sail pilot chute is responsible for pulling the deployment bag with the main inside, weighing 2.87lb. In the configuration shown in Fig. 50, the effects of snatch forces are reduced and, thus, a "canopy first deployment" is avoided, which could muddle the main's deployment. For the same reason, the parachute is placed canopy first inside the deployment bag.

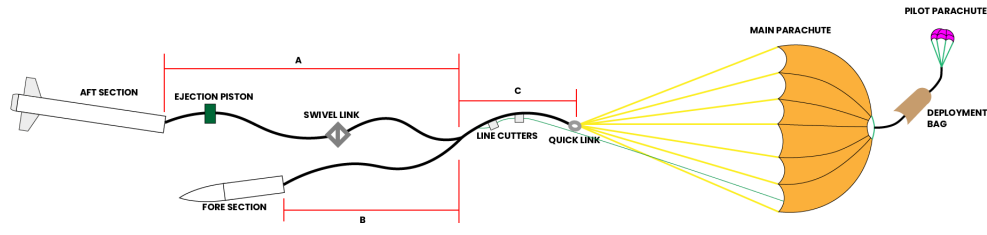


Fig. 50 Schematic illustration of rigging, in which $A = 14$ ft, $B = 7.6$ ft and $C = 1.5$ ft.

2. Parachutes

a) Pilot chute

The calculations relative to the pilot chute's dimensions were done using a spreadsheet based on the methods established by E. G. Ewing [13] and by T. W. Knacke [14].

In our calculations, the rocket velocity at the apogee was less than 150 KEAS. Using the parameters shown in Fig. 51, the drag area ratio of 0.03 between the main and pilot chute was applied, and a 2.3 ft^2 pilot chute drag area was obtained. The pilot chute used in Latin American Space Challenge (LASC) 2022 and in the 2023 Spaceport America Cup has a similar area, therefore, the team decided to use the same chute in the recovery of Pacifico, as it has a similar enough drag force and has already been tested in flight, guaranteeing reliability.

TABLE 6-5. Pilot and Main Parachute Drag-Area Ratios.

Deployment velocity, KEAS	Pilot-to-main-parachute drag-area ratio
< 150	0.03
150 to 250	0.02
> 250	0.005

Fig. 51 Reference table for the drag area ratio between main and pilot chute.

b) Main parachute

The main parachute is a quarter spherical chute with a drag coefficient of $C_d = 0.92$. This is the second highest drag coefficient listed in the literature according to Knacke [14], an attribute that guided the team's choice of using this model, considering the high rocket mass and low terminal velocity. Despite the choice of a high drag model, the parachute's final diameter was $D_o = 9,87 \text{ ft}$.

Furthermore, the team calculated the opening forces that will act on the U-Bolts and disk assemblies when the parachute opens and disreefs via the Pflanz method [14]. In both inflation events, the opening forces were calculated for the fore and aft sections of the rocket separately.

Table 13 Main parachute's data summarized. For the reefed main parachute, the terminal velocity is the same as the velocity at disreefing.

	REEFED MAIN PARACHUTE	DISREEFED MAIN PARACHUTE
Drag Area ($C_D S$) [ft^2]	9.484	70.515
Deployment Force on Fore Section [lbf]	163	201
Deployment Force on Aft Section [lbf]	270	489
Deployment Velocity [ft/s]	180	72.2
Terminal Velocity [ft/s]	72.2	30.5

c) Manufacturing

The main and pilot chutes were similarly manufactured by the team. Both of them are separated into gores to evenly disperse the drag force between the multiple seams and fabric pieces. The main and pilot parachutes were designed to have 16 and gores, respectively. The decision on the number of gores for the main parachute was based on the team's experience in the 2022 Latin American Space Challenge and in the 2023 SA Cup. For the 2022 competition, the team manufactured a 20-gore quarter-spherical chute with a similar diameter. However, the high number of gores led to an overly complex and long manufacturing process. Furthermore, exchanging experiences with other teams, the team concluded that 20 gores was excessive considering the seams' resistance to the opening force. For the Juno III rocket, a 16-gore chute was made, and it proved itself as an adequate number of gores. Hence the chute being made for Pacifico also has 16 gores.

After laser-cutting the gore patterns, generated by the team, each pair of gores was sewn with polyamide line according to the diagram represented in Fig. 52. The paracords were sewn to the canopy at the skirt, starting at a height of $0.33 ft$ from the base. To determine the suspension line length, the ratio $le = 1.15D_o$ was used as determined in Knacke [14], and $0.66 ft$ was added to account for the sewing process in both ends of the kevlar suspension lines. The shock cords and the bridle are made of tubular polyester and the attachment points are also sewn with polyamide thread.

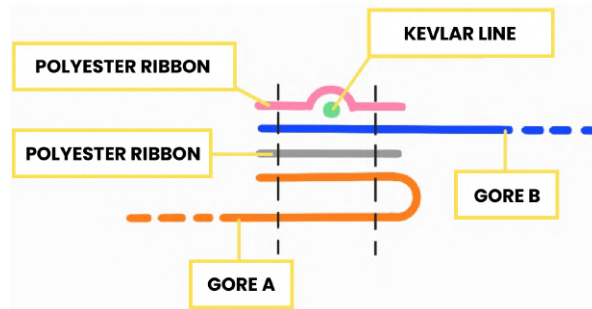


Fig. 52 This fold was used between each pair of gores, using an additional fabric to increase the seam's resistance.

3. Reefing and reefing-cutter device

The reefing of the main parachute is achieved by passing a reefing line through 16 reefing rings sewn at the center of each gore, in a configuration known as mid-gore reefing.

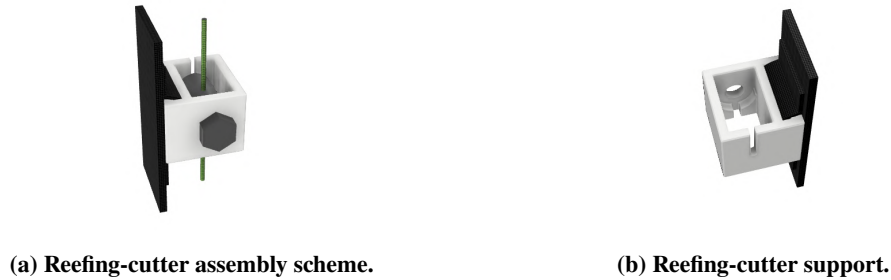


Fig. 54 Different views of the reefing cutter system.

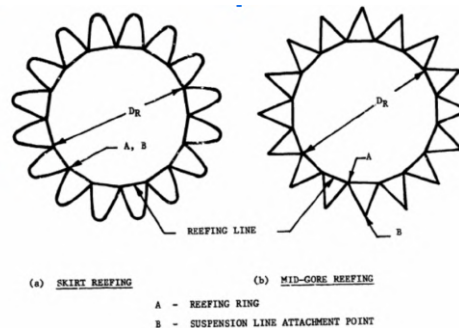


Fig. 53 Schematic drawing comparing skirt with mid-gore reefing retrieved from Knacke [14]

This reefing configuration is an improvement of the skirt-reefing method, which was chosen because the opening force during the reefed stage is distributed between the seams between gores and the seams of the reefing rings. In other words, the mid-gore reefing uses twice the number of resistance points in the canopy, as can be seen in Fig. 53. As a result, a more uniform and stable drag is created.

One of the ends of the reefing line stays at the canopy and has a metal loop through which the other end can be threaded to form a lasso. The free end is then pulled until it reaches the shock cords, where it passes through two redundant line cutters, and is tied with a knot below them. As a result, the created lasso can restrict the inflation of the main parachute, keeping it reefed. To achieve the desired effect, the length of the line must be dimensioned to get a precise reefed diameter of 4.3 ft .

The second recovery event is the disreefing of the main parachute. This is achieved through the use of two redundant pyrotechnic line cutters, which are familiar to the team and have been validated in flight (2022 Latin American Space Challenge and 2023 Spaceport America Cup). The line cutters are sewn to the riser, and not to the canopy, for two main reasons: to prevent the gas discharge from the powder combustion from damaging the parachute, which could lead to tears during flight and deployment. The black powder chambers are attached to the riser, as shown in Fig. 54a, with a 3D-printed PETG case and a polyester strap. This attachment method was chosen to keep the forces that act on the riser from acting on the cutters. The line cutters work by burning up the paracord core that runs through it. When the black powder is ignited, the core yarns melt and due to the gas discharge and tension in the line, they rupture. When the reefing line is cut, the main parachute opens to its maximum area.

As seen in Fig. 54b, a slit was added to the right side of the cases to allow the passage of the e-matches' leads, which streamlines assembly since the chambers may be worked on separately, with e-matches, paracord, and black powder, and attached afterwards.

D. Avionics and Telemetry Subsystems

1. Subsystem overview

The Electronic Systems team area in Projeto Jupiter is responsible for developing the Avionics Subsystem and the Telemetry Subsystem. In previous rockets designed by the team, those systems were dispersed through several modules. For instance, in the 2023 Spaceport America Cup, the Telemetry Subsystem was fitted into the Payload's module, and

the Avionics Bay was divided into Apogee Detection System and Disreefing Altitude Detection System, located in modules below the parachute and inside the nosecone, respectively.

For the *Pacifico* rocket, however, the entirety of the Subsystems is confined inside the nosecone, which facilitates assembly of the module and the overall organization of the team. In Fig. 55 one can see the entire Electronic Systems Module, composed of the Avionics Bay and the Telemetry Bay.



Fig. 55 Schematic view of the Electronic Systems in the nosecone.

Both aforementioned systems are comprised of a COTS solution and a custom *SRAD* PCB. Since the previous Spaceport America Cup edition, the team has been able to design, manufacture and flight-test new *SRAD* boards for its systems. Both of them are microcontrolled PCBs, based on STM32 chips. The new version of the barometric altimeter was named *Apogeotico v2* and the novel telemetry PCB was given the name *Telemetrico v1*. In Fig. 56 it is possible to observe a block diagram of the entirety of the Electronic Systems and their connections to the Recovery Subsystem.

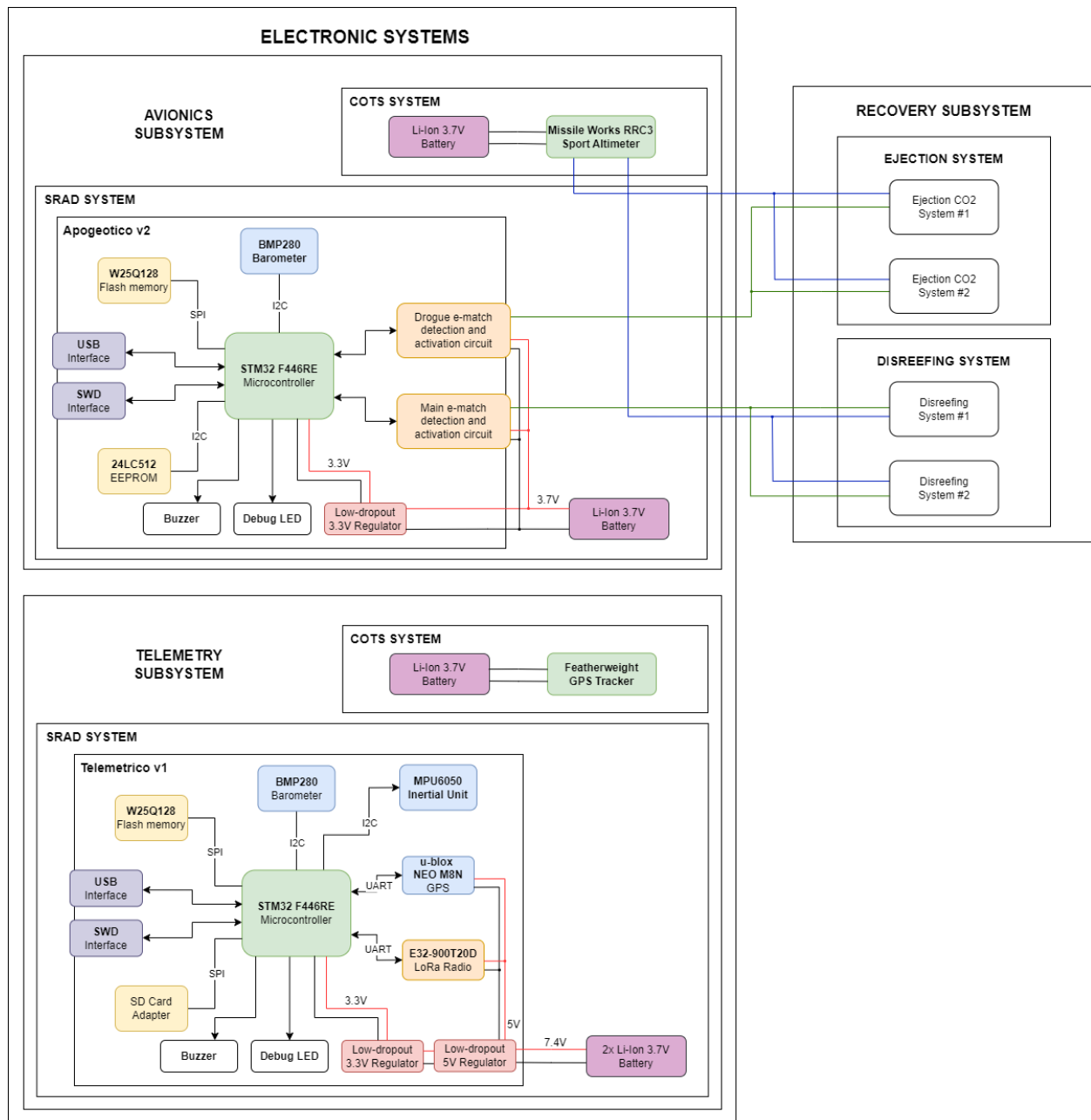


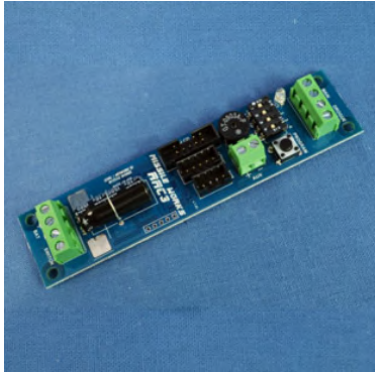
Fig. 56 Block diagram of the entire system.

2. Event Detection Systems

The *Pacifico* rocket employs two altimeters for apogee detection, ensuring redundancy and enhancing reliability to detect critical flight moments, such as apogee and disreefing altitude. The primary altimeter system utilized is the *Missile Works RRC3 Altimeter COTS* system, while the secondary altimeter system is a custom *SRAD* board. Both are described more thoroughly in the subsections ahead. To provide the equalization of the air pressure inside the electronics bay and the air pressure outside the rocket required by these barometric altimeters, there are three equally spaced static pressure ports on the nosecone's surface.

a) Primary system

The primary detection system for the apogee is a *RRC3 "Sport" Altimeter* [15] by *Missile Works* as shown in Fig. 57a. It is powered by a single 3.7 V lithium-ion battery. Several tests have been conducted in order to test whether the battery was sufficient to activate the required number of e-matches. The altimeter will be powered on before takeoff by a key-switch positioned on the rocket's fuselage, like the one in Fig. 57b. It is worth noting that the team opted to utilize the RRC3 altimeter due to its ease of programming, which offers a convenient feature for configuring its settings, as well as its reliability.



(a) Missile Work's RRC3 "Sport" Altimeter



(b) Key-switch for activation

Fig. 57 Primary system components.

b) Secondary system

The secondary flight event detection system is an *SRAD* system comprised of the microcontroller STM32 F446RE from STMicroelectronics, a pressure sensor (BMP280), an EEPROM (24LC512), a flash memory device (W25Q128JVS) and other circuitry, all integrated using a custom PCB called *Apogeotico v2*. The microcontroller runs a detection software developed by the team and named *SisRec*. For more information on the tests conducted on this system, refer to Appendix B. Additionally, the system activation on the launch rail occurs in a similar way as the primary system, counting on an independent key-switch and independent battery.

- *Software (Sisrec)*

To be able to detect flight events accurately, a software was implemented to run on the embedded microcontroller. Given the complexity of the actual dynamics of the system and the difficulty of getting precise altitude data from the pressure data (due to dynamic effects and sensor noise), an adaptive approach was taken for the data filtering and pressure measures were directly used for both filtering and detection.

The filtering stage is an Adaptive Line Enhancer based on an Normalized Least Mean Squares (NLMS) adaptive filter. It consists of an NLMS adaptive filter, utilizing the pressure signal as the reference ($d(i)$) and employing the same signal as input, albeit delayed by a number of samples.

In this way, the algorithm estimates a discrete system model (in this case a Finite Impulse Response filter), which is used to estimate the current pressure value from past ones and, thus, under some conditions, filtering out the non-deterministic components of the signal. In order to detect the apogee the algorithm relies on the fact that near the trajectory's highest point the rocket's velocities are reduced (i.e. without the motor operating) and, thus, the trajectory near this point can be approximated fairly well as parabolic.

The detection is done by creating a reference parabola and performing a quadratic regression with a fixed minimum position of this parabola. Two parameters are defined for the regression: one that relates to the acceleration experienced near the apogee, and other that indicates the extent to which the filtered pressure data can be approximated by a parabolic curve. By comparing these two parameters to predefined thresholds, it is possible to determine whether the apogee has been reached or not.

It is important to note that these two thresholds are determined using rocket trajectory data from statistical

simulations, which take into account both the barometer noise and the variability of the flights. Furthermore, optimizations are made to get a probability of detection failure less than 10^{-6} and to meet the specified mean and uncertainty values for the parachute deployment times.

To detect the disreefing altitude, a straightforward method can be used due to the low-noise nature of the filtered signal. The method involves simply checking whether the filtered pressure signal has surpassed a predetermined disreefing pressure threshold, indicating that the rocket reached that point. Simulations of the described algorithm can be found in Appendix G.

During the time remaining between the filter and state update and the next pressure data reading, the system writes the current pressure value measured by the BMP280 in the onboard redundant memory circuits. The software is structured so that it can assume five states: "Initial", "Launch Detect", "Apogee Detect", "Disreefing Altitude", "Post Processing" and "Final". At each cycle an update routine is called, which receives the pressure as input and updates the state and the filter coefficients accordingly. A description of these states is given below:

- 1) **Initial:** state in which the system is set at initialization. In this state, the data buffers are guaranteed to be initialized with an initial value and are not updated.
- 2) **Launch Detect:** state in which a pressure threshold is set for the system to identify if takeoff occurred. This pressure threshold depends on the launch site and must be verified before every launch.
- 3) **Apogee Detect:** state in which the system is processing the data to detect the apogee event, which will cause it to transition to the "Disreefing Altitude" state. This transition triggers the activation of the parachute deployment signal.
- 4) **Disreefing Altitude:** state in which the system is processing the data to detect the disreefing event, which will cause it to transition to the "Post Processing" state and finally to the "Final" state. This transition triggers the parachute disreefing.
- 5) **Post Processing:** state in which the pressure curve recorded on the memory is processed to detect the apogee pressure and estimate the apogee altitude, after which the system transits to the "Final" state.
- 6) **Final:** state in which the system stays after the apogee altitude calculation. In this state the buzzer beeps the apogee altitude's digits continuously.

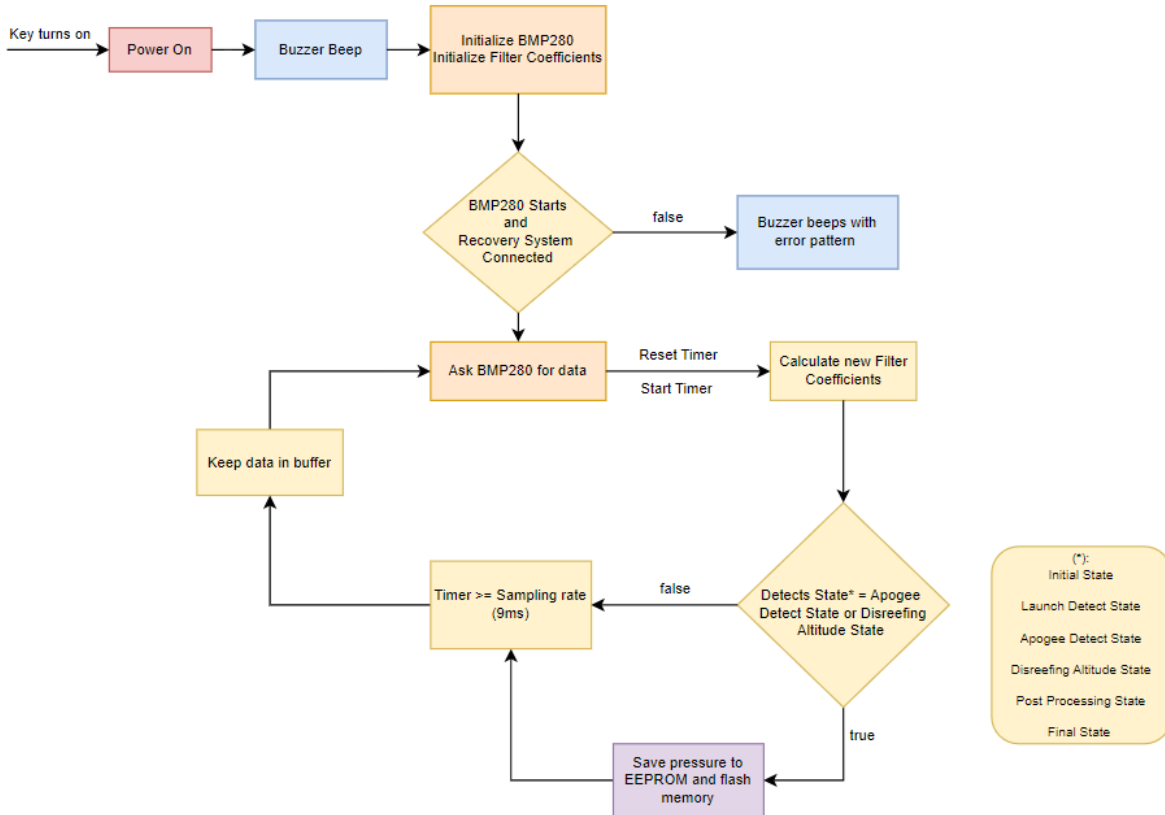


Fig. 58 Flowchart of the code that runs in *Apogeotico v2*

- **Hardware**

Apogeotico v2 is the Electronics Subsystems' *SRAD* altimeter for apogee and parachute disreefing detection. The system's core is an F446RE microcontroller, manufactured by STMicroelectronics, and a BMP280 sensor, both of which are placed on a single PCB along with the rest of the circuitry, all described in more detail below. The single-board design was chosen for its simplicity, cost-effectiveness and interchangeability with COTS altimeters, which the team has also used at times when fitting the boards into the modules' internal structures.

- **STM32F446RE:** it is an Arm Cortex-M4 microcontroller, responsible for reading and filtering out the data from the BMP280 sensor with an adaptive filtering algorithm for precise apogee and disreefing detection, sending signals to the power circuits for parachute event triggering (described below). The F4 was chosen for its processing power, necessary for the floating-point calculations to take place in a reasonable time frame, considering the necessity of sampling the pressure data quickly. On the Apogéotico's PCB there are pin headers for communication on both the Arm SWD protocol, used to program the F4, and the UART protocol, useful for reading data when testing the systems, running simulations, and recovering flight information. The F4 is powered either by the output of the 3.3V voltage regulator (also described below) or by USB power if the SWD or UART pins are connected to an external board;
- **BMP280:** the Bosch BMP280 is a barometer which communicates with the microcontroller through I2C serial communication, providing the necessary pressure data for altitude estimation. It is also capable of acquiring temperature data. For this novel board, the barometer was soldered directly on the board, without the need of a commercial module, which enhances the physical resistance of the board and its durability;
- **Buzzer circuit:** the buzzer is connected to one of the F4's GPIO pins and is used as an indicator for several relevant points of information to ensure that the whole system is functional before flight, such as proper connection of the BMP280 sensor and the detection of adequate connection between the Avionics Subsystems and the Recovery Subsystems. It is crucial to convey information on the current status of the

system in a non-visual way, to make sure the operator can listen to the beeps when the rocket is already on the launch rail;

- **E-Match activation circuits:** a custom circuitry was developed to ensure activation of the e-matches, at the moments determined by the microcontroller. Since the chip is not able to supply enough current to activate the e-matches, an N-Channel MOSFET is used to drive power directly from the battery to the e-matches;
- **E-Match detection circuits:** the parachute events are triggered by e-matches connected to the power circuits. The detection circuits are used to inform the operator about whether a connection to the e-matches has been made, with a specific buzzer sound sequence indicating the status of the connection;
- **Power circuits:** The circuit is powered by a Lithium-Ion battery. By using a high power battery, it is possible to ensure that the e-matches will be activated simultaneously and reliably. Furthermore, a Low Dropout (LDO) voltage regulator is used, to adjust the input voltage of 3.7V to the 3.3V required to power the chip. With this circuitry it was possible to reduce the quantity of batteries required in the *SRAD* system;
- **EEPROM and flash memory:** both the EEPROM and the flash memory store flight information regarding the pressure data measured by the BMP280, which is especially important when embedding redundant altimeter systems - having the flight data, it is possible to determine which of the systems worked properly, validating and supporting the teams' development activities and assisting in the identification of errors for future improvement. Having two memory devices recording the same data is important for redundancy, guaranteeing data storage in a secondary source in case the primary system fails.
- **Micro USB:** The Micro USB connector in this *SRAD* Circuit Board is used for programming and serial interface debugging, facilitating the Apogeoítico's operation.

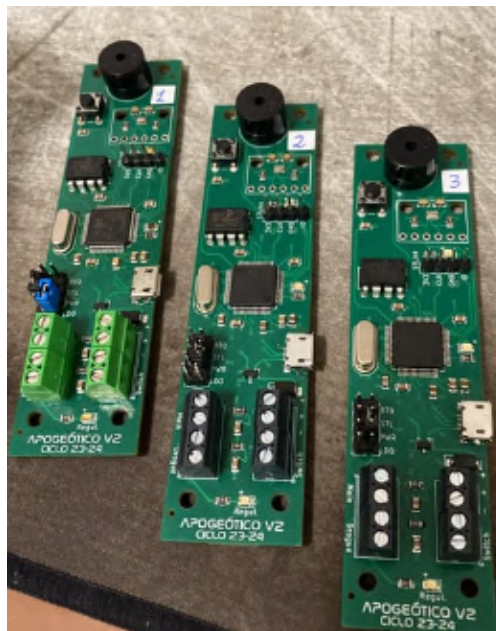


Fig. 59 SRAD altimeters *Apogeoítico v2* manufactured by the team

3. Telemetry subsystem

The Telemetry subsystem is composed of *SRAD* and *COTS* boards, which are both located within the Electronics Systems module in the nosecone. The first has the function of obtaining, transmitting and recording data related to rocket flight, such as acceleration, angular velocity, pressure, temperature and geolocation whereas the latter only transmits GPS data to a ground station. The data in the *SRAD* system known as *Telemetrício v1* is recorded in two ways: by micro SD card and by flash memory. The *SRAD* telemetry transmitter sends the collected data wirelessly from the rocket to the ground receiver. On the ground, the receiver captures the transmitted data and relays it to a computer. This computer is equipped with a graphical interface that allows for real-time visualization of the data. The received

data is then processed and displayed in the graphical interface, enabling easy monitoring and analysis of the rocket's parameters. The COTS transmitter sends data to a COTS ground station connected via Bluetooth to a team member's phone where GPS data can be acquired.

- *SRAD Telemetry Hardware*

Telemetrico v1 is the Eletronics Subsystem *SRAD* telemetry board for data acquisition and a system located on the rocket that transmits the data. The system consists in:

- **STM32F446RE:** Microcontroller manufactured by STMicroelectronics, use for reading the sensors data and transmission
- **SX1276 915MHz E32-900T20D Wireless LoRa Module:** Used for communication between microcontrollers over long distances
- **BMP280:** Barometer which communicates with the microcontroller through I2C serial communication, providing the necessary pressure data
- **MPU-6050:** Contains an accelerometer and a MEMS-type gyroscope on a single chip. There are 3 axes for the accelerometer and 3 axes for the gyroscope, with a total of 6 degrees of freedom (6DOF)
- **U-blox NEO-M8N GPS:** Was chosen because of the high maximum navigation update rate of 10Hz, the greater availability
- **Memory circuit:** Winbond W25Q128 flash memory and in a micro SD card, for redundancy purposes. The choice of the W25Q128 flash memory for data storage in the telemetry system was based on some factors. Firstly, the team had prior experience with this particular flash memory and had already tested and programmed it successfully, which reduced development time. Besides, the W25Q128 flash memory offers a storage capacity of 128 Mbit, equivalent to 16MB. This larger capacity ensures that there is enough space available for storing the obtained sensor flight data, without the risk of running out of storage space.
- **Buzzer Circuit:** The buzzer used as an indicator for several points of information to ensure that the whole system is functional before flights
- **Micro USB:** The Micro USB in this SRAD Circuit Board is used for programming and serial interface



Fig. 60 SRAD Telemetry system *Telemetrico v1* manufactured by the team.

The second system is the receiver, comprised of an E32-900T20D LoRa transceiver, but with STM32F103C8T6 microcontroller (Bluepill), used for data acquisition system and for visualization in the Graphic Interface. Furthermore, GPS data is used to facilitate the Recovery Team's work and data such as acceleration, angular velocity and pressure are used to compare the real flight with the simulations and improve the models adopted by the team.

The transmitter is powered by two 3.7V Lithium-ion batteries in series due to the fact that the minimum required voltage for some modules to operate is approximately 5V. By connecting the batteries in series, the total voltage output reaches around 7.4V, which ensures that the voltage requirement is met. Additionally, the overall discharge current of the transmitter is approximately 200mA, which allows for reliable operation throughout the time of service, which ranges approximately 3 hours and 40 minutes

- *Transmitter characteristics*

The transmission module will be the LoRa E32-900T20D by Ebyte with the following characteristics:

- Output power: +20 dBm;
- Operation frequency: 862 ~ 931 MHz;
- Transmission rate: up to 19.2 kbit/s.

The transmission device is a small omnidirectional 50 Ω antenna by *Linx Technologies*.

- *Receiver characteristics*

The reception module will be composed of a COTS RFID microstrip antenna with the following characteristics:

Table 14 Ground antenna characteristics.

Nominal Frequency	902 - 928 MHz
Gain	7.5 dBi
Polarization	Right Hand Circular Polarized (RHCP)
Impedance	50 Ω
Half Power Beamwidth–HPBW (Elevation)	72°
Half Power Beamwidth–HPBW (Azimuth)	77°
Output connector	Female SMA

- *COTS GPS Transmitter*

The COTS GPS system is based on the Featherweight GPS Tracker solution, composed of a transmitter located within the rocket and a receiver ground station. The transmitter uses LoRa transmission protocol at 915MHz band and a u-blox NEO-M8 GPS to obtain geopositioning data.

- *Telemetry Onboard Software*

The telemetry onboard software is the program that runs in *Telemetrico v1*, during the flight. It orchestrates communication between the STM32F446RE chip with BMP280 and MPU-6050 to get the sensor array data and the u-blox NEO-M8N to get the GPS data. The software also manipulates these data to store in the SD card using FAT file system and in the Flash memory using the Little File System, which ensures data redundancy in case of an unexpected restart.

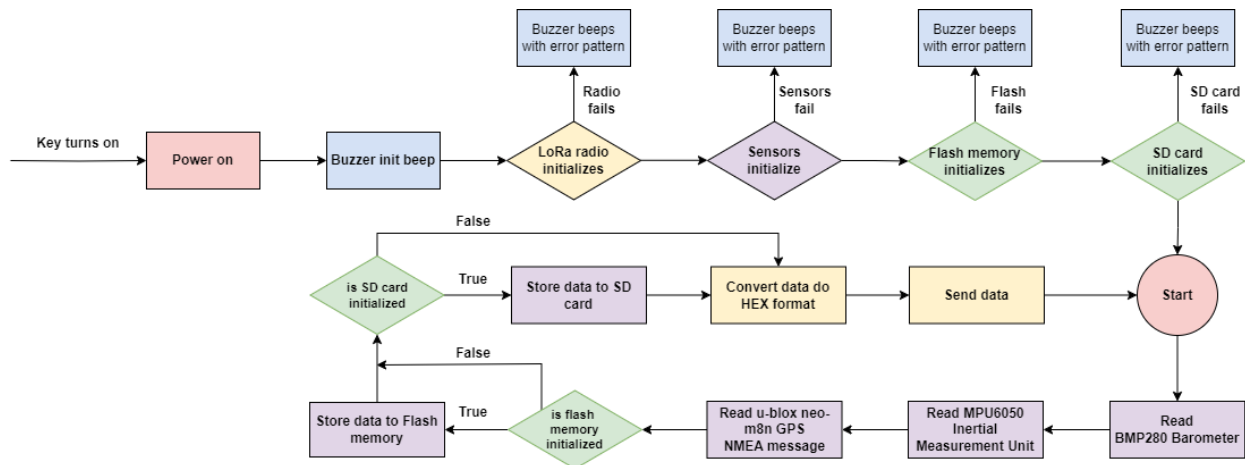


Fig. 61 Telemetry onboard software flowchart.

- *Telemetry Receiver Hardware and Software*

A Graphical User Interface (GUI) has been developed for real-time monitoring of the flight data. The GUI operates by receiving binary data from the telemetry transmitter on the rocket, which transmits to a ground receiver. The ground receiver, composed of a board with an SD card reader, a Bluepill board (STM32F103C8T6), and an Ebyte E32-900T20D module, sends the received data to a computer using USB.

Due to the Bluepill's limitations, it receives the data in hexadecimal format, saves it on the SD card, and then sends it to a computer using serial communication via USB. This ensures compatibility with the Bluepill's processing capabilities.

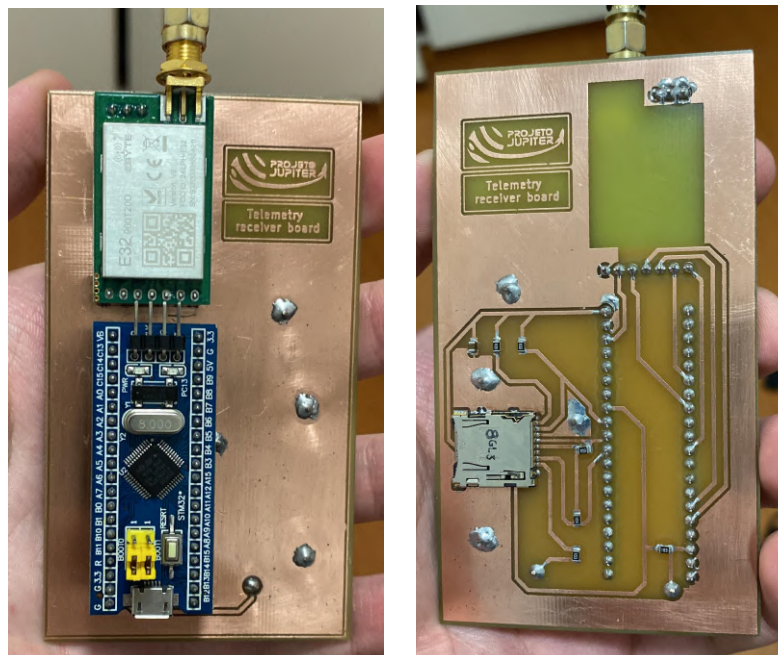


Fig. 62 SRAD Telemetry Receiver manufactured by the team.

On the computer, a Python program receives the data via serial communication, saves it in a log file, and sends JSON packets to the GUI via an open WebSocket connection. The WebSocket enables multiple devices on the same network to run the GUI simultaneously.

The computer system utilizes the Electron framework alongside the React library to render the GUI, in which the received data is displayed as graphs that are updated in real-time. Users can save and view the data on the same interface, allowing for later analysis. The graphs provide a visual representation of the rocket's parameters, enabling visualization of the launch status (whether it is nominal or has failures). The data retrieved from the GUI can also be utilized to improve later simulations and rocket projects. Additionally, in the GUI, if a user clicks on a location, a link to Google Maps with the coordinates is automatically copied to the computer's clipboard, facilitating easy retrieval.



Fig. 63 Telemetry Graphical User Interface.

4. Structure

Compared to previous rockets, innovative changes have been implemented in the module's structure with the goal of reducing the number of parts. This simplifies assembly and also facilitates handling in case any alterations, for example minor changes in wiring or circuits, are required during the rocket's assembly procedure.

The main goal was to develop a modular structure that allows each redundant system to be independently replaced with minimal disassembly. Additionally, it needed to be rigid and strong enough to withstand the accelerations of the normal flight and ideally be able to survive the impact in case of a failure in parachute deployment. This led to the creation of a triangular structure, comprised of three 3D-printed vertical walls that can be removed independently. The walls are attached to the base disk through three threaded rods, which also keep the walls under compression along the vertical axis, avoiding the failure of the 3D-printed parts along the layer lines.

The most remarkable innovation is that each redundant system can be assembled on its own wall and can be removed entirely after loosening three nuts, which allows the rapid replacement of a subsystem with minimal tools and in a short amount of time. Also, this retains the versatility of the structure for future applications, since the layout of a wall can be changed to permit the use of different components without altering the way it interfaces with the others, thereby keeping the system retrocompatible.

The base of the structure consists of an aluminum disk with three equidistant threaded rods fixed to it. Then each of the 3D-printed walls, made out of PETG, slide around one of the threaded rods in a way that when all three of them

are assembled, they cannot swivel and are fully constrained. This material and layout were chosen due to their high impact-resistance relative to the weight, which is optimal for protecting the electronic components inside the nosecone.

The *RRC3* commercial altimeter is screwed to its own wall, alongside a 3.7V lithium-ion battery as a power source. The non-conductive nature of the PETG makes it unnecessary to have any sort of isolating material between the altimeter and the structure. The same goes to the *SRAD* altimeter, and the *Featherweight* commercial GPS Tracker, each on its wall alongside its correspondent Li-Ion battery. The boards and battery holders are secured into the walls using thermal inserts, which enables screws to be attached to the 3D-printed pieces.



Fig. 64 Avionics module with the altimeters and the Featherweight GPS Tracker.

Atop the aforementioned triangular structure, another 3D-printed module was designed to house the novel telemetry *SRAD* board. It is similarly supported by an aluminium disc and secured using three threaded rods equally spaced, each with nuts on both ends.

The 3D-printed parts contain a custom vertical wall, which allows the telemetry board to be attached on one of the sides, and the double battery holder to be attached to the other, which is an optimal design to use the module's space more efficiently. A top disc is also mounted to the structure, with the purpose of allowing the threaded rods to be screwed and locked, and also to provide protection to the telemetry board in case of any impact coming from the top of the nosecone.



Fig. 65 Telemetry module with *SRAD* telemetry board and two Li-Ion batteries.

E. Payload

F. Introduction and our Mission

In this Technical Report, we will clarify the role of the payload in the context of the Projeto Jupiter team for the 2024's SACUP, characterizing the technical aspects of the payload project, its integration process and the data that we are anticipating. Following this topic, we will explain the function of the payload in our project, detailing how it was designed, the component selection process, and how it consolidates itself with the rest of the rocket.

When delving into the intricacies of a rocket launch, one of the paramount factors dictating the trajectory is its orientation, often referred to as attitude. Determining the rocket's attitude involves various techniques, ranging from camera systems to onboard sensors. Among these sensors, a basic approach entails utilizing gyroscopic sensors to track rotation matrices from the initial position. However, a significant challenge lies in mitigating the compounded errors stemming from gyroscopic drift. To address this, accelerometers are employed in conjunction with a complementary filter to compensate for these errors, albeit unable to fully estimate sensor orientation. To overcome this limitation, magnetometer data is integrated to achieve comprehensive attitude estimation and completing the sensor fusion algorithm.

This year's mission, shown in Figure 66 is named T.I.L.T.A.D.O. which is an acronym for The Image Levelling Tracker and Attitude Determination Operator. It involves the application of our engineering knowledge to create an experiment that will enable the capture of images that keep the horizon aligned regardless of the orientation of the rocket. This is possible due to the use of two rotatable cameras equipped with fisheye lenses that provide analog-like stability to the images captured thereby. The stability of the cameras is provided by stepper motors guided by sensors that measure the rocket's attitude. The data captured by the sensors is then used to determine the appropriate angle to maintain the alignment during the whole flight.

Additionally, through the construction of such a system, we aim to capture clear and stable imagery of Pacifico's entire flight, being able to provide valuable content to our Marketing segment and for analysis goals.



Fig. 66 3D Rendering of T.I.L.T.A.D.O.

G. Structure

1. External Structure

Due to the advantages offered by the cubesat form factor and the fact that the rocket's diameter offers enough space to fit this structure inside it, this payload is housed inside a 3U cubesat which was entirely designed and manufactured by Projeto Jupiter's members. With its base measuring 100x100 mm and its height measuring 300 mm, it has a total mass of 8.8 lb when also considering the components inside and the boilerplate, which weighs less than 2.2 lb. The

cubesat frame is built in Aluminum 6061 alloy, an easy to machine and corrosion resistant material, and consists of only four detachable parts, thus making it an easy-to-assemble structure. It also has two non-structural acrylic side walls to facilitate the visualization of internal components.

2. Internal Structure

For the cubesat's internal structure, threaded brass standoffs are used to separate each subsystem. This method allows both the internal and external structures to be separately assembled, thus facilitating access to handling and assembly of individual components.

Each custom designed shelf is made of 2 mm Aluminum 1100 alloy and was water-jet cut.

3. Camera Positioning System

In order to capture only the horizon and not the inside of the rocket's fuselage, the wide angle field of view cameras used in this experiment must be coplanar to the rocket's outside structure. Nonetheless, by placing the cameras on a fixed position and fulfilling the aforementioned requirements, the experiment would exceed the 100x100x300 mm maximum dimensions thus losing its cubesat compliance. Therefore, a custom SRAD mechanism that pulls and pushes the cameras forwards and backwards had to be developed.

This system uses two redundant sets of pinions and racks actuated by NEMA 17 stepper motors, as shown in Figure 67. Two extra stepper motors are used to rotate the cameras in order to maintain the initial angle. As the activation of this push-pull mechanism is done right after the integration of the cubesat to the rocket and not during launch, the rocket dynamics during flight is not critical to the desired functioning of this subsystem.

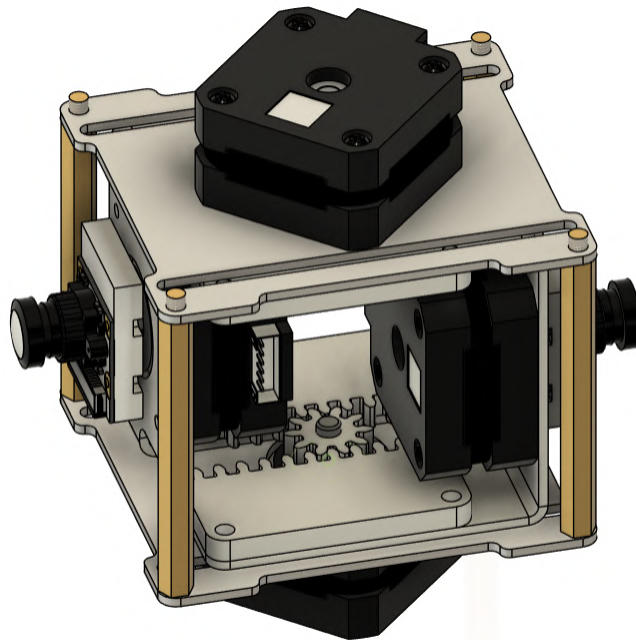


Fig. 67 3D Rendering of the Camera Positioning Mechanism

4. Integration with the rocket

Finally, it is worth mentioning that this non-deployable payload is integrated to the rocket by screwing the cubesat to the rocket coupler using one M5 screw on each of the four cubesat rails.

H. Electronics

Considering the development of a payload optimised for the proposed task, the following components were carefully chosen during the mission design process. A variety of factors, including cost, weight, size, performance, among others, were crucially considered to ensure that the system captures images with the desired quality.

The 5MP OV5647 200° wide angle camera for Raspberry Pi was chosen due to its small size, adequate video quality, 200° angle recording and its compatibility with the Raspberry Pi Zero 2W, which was chosen to control the camera and store the recording in a Kingston Canvas Select Plus 32Gb MicroSD. Each one of the two cameras require their own microcontroller and external memory. In order to improve the system's response time, the attitude estimation algorithm will be running from an additional Raspberry Pi Pico, with data collected from the MPU9250 9-axis inertial sensor. This model of sensor was chosen because it allows a complete attitude estimation of the rocket during flight. Additionally, the A4988 is a physical stepper driver that facilitates communication between the microcontroller and the NEMA 17 17hs08-1004s stepper motor, and allows for configuration of microsteps. The experiment uses four of these motors, two to push the cameras closer to the rocket's tube and two to rotate the cameras according to the estimated attitude.

Finally, out of the 8 18650 Li-Ion batteries, 3 are used as power supply for the Raspberry Pi Zero 2W and Pico, 4 of them are needed to reach the 12V required by the motors, and because mechanical components tend to drain a lot of current, these batteries will be separate from the ones used for the microcontrollers, which also helps in adding weight to the system. The last battery goes towards powering another PCB, unrelated to the experiment, that will be mounted on our structure and requires its own power supply.

I. Software Implementation

Our team has developed custom C++ and python software alongside available modified libraries to be run on the Raspberry Pi Pico and Raspberry Pi Zero. The flight computers carry out various functions, including video capturing, datalogging, attitude determination and also the step determination. Raspberry Pi Zeros handle video capture and data storage, utilizing Raspberry Pi Python libraries. The Pico interfaces with the MPU for data acquisition and controls stepper motors for camera movement, including translation and rotation.

1. Attitude determination algorithm

The payload's attitude determination algorithm relies on the Madgwick Orientation Filter, pioneered by Sebastian Madgwick [16]. This sophisticated filter harnesses data from the MPU to calculate a quaternion representation of the system's current 3D orientation. The algorithm fuses data from the accelerometer, gyroscope, and magnetometer to derive orientation. Notably, it incorporates gyroscope drift compensation and corrects for electromagnetic field distortion. Once the orientation quaternion is computed, extracting the rocket's Euler angles becomes straightforward.

2. Step calculation

Utilizing Euler angles enables the derivation of a 3D rotation matrix representing the orientation relative to the initial 3x3 identity matrix. The 3D orientation matrix is obtained through the sequential multiplication of individual matrices, each corresponding to rotation about the yaw (θ), pitch (ψ), and roll (ϕ) angles, as depicted below:

$$\begin{bmatrix} \cos(\theta)\cos(\psi) & \cos(\theta)\sin(\psi)\sin(\phi) - \sin(\theta)\cos(\phi) & \cos(\theta)\sin(\psi)\cos(\phi) + \sin(\theta)\sin(\phi) \\ \sin(\theta)\cos(\psi) & \sin(\theta)\sin(\psi)\sin(\phi) + \cos(\theta)\cos(\phi) & \sin(\theta)\sin(\psi)\cos(\phi) - \cos(\theta)\sin(\phi) \\ -\sin(\psi) & \cos(\psi)\sin(\phi) & \cos(\psi)\cos(\phi) \end{bmatrix}$$

From the values of the matrix above, it is possible to derive the tilt relative to the z axis which is then used to define the appropriate position of the steppers motors. This process is done by mapping the values of tilt to a specific position of the motors, with the objective of counteracting the effect of the orientation of the rocket on the image alignment.

III. Mission Concept of Operations Overview

The rocket's assembly procedure is described in Appendix E. After crew confirmation checks, an activation signal will fire an e-match rigged with the ignition charge, therefore initiating the combustion reaction. With the initial thrust, begins the liftoff.

During the initial 4.3 seconds of flight, the rocket will be propelled by the motor until all the propellant is burned. At this point, the motor is shut down and the rocket is in free flight.

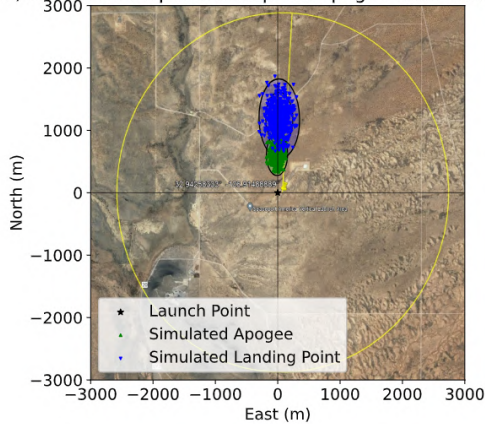
After the free flight, a signal from the electronic systems is sent to activate the parachutes' ejection system, starting the Reefed Deployment phase. In this phase, the rocket reaches a terminal velocity of 22 m/s (72.2 ft/s).

The next event will be the disreefing. This phase starts when, at the altitude of 400 m (1312.3 ft), the redundant detection systems for the disreefing send a signal to the reefing cutter, triggering the e-matches and cutting the reefing line and allowing disreefing. In this phase, the rocket reaches a terminal velocity of 9.3 m/s (30.5 ft/s) until ground.

The dispersion simulation was plotted by a code in Python developed by Projeto Jupiter and now maintained and developed by its on team, called RocketPy. Using environment conditions and rocket data, the flight was simulated 3000 times each to evaluate where the apogee and the rocket's landing point are most likely to be located. As observed in Fig. 68, the green ellipses represent the apogee dispersion and the blue ellipses represent the landing dispersion.

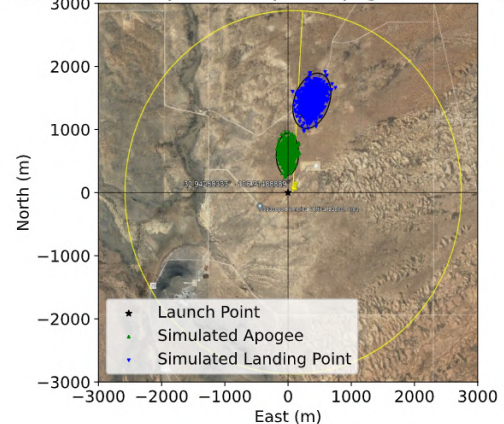
After the confirmation of landing, the ground recovery team will have the authorization to start searching for the rocket. Based on its trajectory and the dispersion simulation, the team will have a prediction of where it is. The ground recovery team will also have GPS data from our telemetry system, indicating Pacifico's location. Fig. 69 shows a phase chart summarizing the mission flight.

1 σ , 2 σ and 3 σ Dispersion Ellipses: Apogee and Lading Points



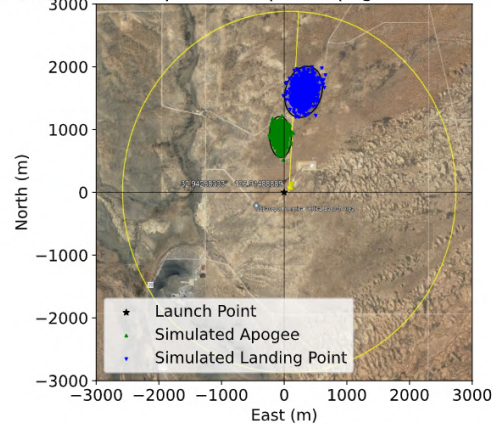
(a) Ballistic scenario.

1 σ , 2 σ and 3 σ Dispersion Ellipses: Apogee and Lading Points



(b) Reefed scenario.

1 σ , 2 σ and 3 σ Dispersion Ellipses: Apogee and Lading Points



(c) Disreefing scenario.

Fig. 68 Pacifico's dispersion simulations.

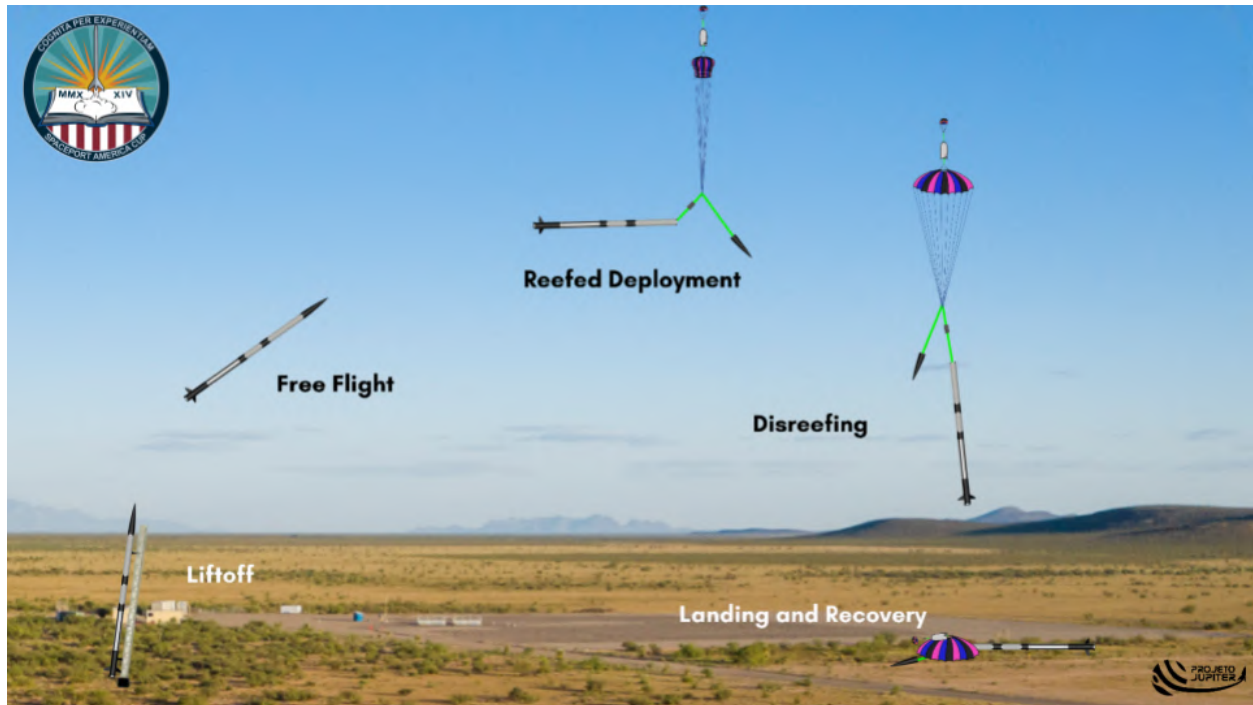


Fig. 69 Mission Concept Operations flowchart and its phases.

IV. Conclusions and Lessons Learned

Pacifico was a challenging project for Projeto Jupiter and members were faced with many new challenges. Its development began in 2023 and was intended to bring innovation to team's rocket design process and to some technical areas, especially the Recovery, Avionics and Payload areas.

After our launch in the SA Cup 2023, with a partially successful flight and 2nd place in the Jim Furfaro Award for Technical Excellence, our team was even more motivated to continue our hard work towards our main goal of representing Brazilian engineering excellence and aerospace potential. Hence the decision to bring an innovative project to the biggest rocketry competition in the world was taken. Working on a project for such a great competition was a new challenge for most of the members, for whom it is the first opportunity to experience first-hand a full on-site Spaceport America Cup. For this reason, Pacifico played a significant role in fostering the growth and development of the entire group. Better analysis methods were applied, such as student-developed numerical simulations and calculations in addition to software based on finite elements method. These tools not only completed, developed, and improved the understanding of the rocket's behaviour, but also helped the team comprehend the data collected from tests. With that, our team developed skills that, linked to the possibility of manufacturing and testing our systems, made our rocket a truly engineering project, from beginning to end. In this way, our team was able to make decisions and explain them more easily, in addition to better analyzing successful and unsuccessful tests.

The 2024 SA Cup offered the team an opportunity to solidify the resulting work and present it to other rocket teams and enthusiasts. Such an event is notorious for qualifying the presented work, thus allowing the team to improve each subsystem. Nevertheless, as mentioned before, the 2024 SA Cup will be the first contact of many Projeto Jupiter's members with an international competition, providing a complete experience regarding the rocketry community.

The best lesson Projeto Jupiter has learned from Pacifico was how fierce and determined its own team is, and how well-motivated members can move barriers towards a common goal. The crew worked as hard as it could and managed to finish and improve the previous project from the 2023 LASC. The group was also faced with many setbacks and difficulties as an international team and yet the team has persevered. Although it is not possible for all members to go to the site, Pacifico is a project that was an immeasurable effort of all people who make this project live.

The main achievement of this effort is the unified team and excited new members that can now identify themselves as part of Projeto Jupiter. This conclusion reinforces the team motto: "Projeto Jupiter is a project about people". As a team, we hope to keep growing as we have done during previous launches and during the SA Cup preparation. As a

project, we look forward to launching Pacifico in the 2024 SA Cup.

A. Aerodynamics and Structures managing view

Although Pacifico's aerodynamic and structural design has similarities to Juno III's, some innovations were implemented in this new project. The intermodular connection system remains the same as in the Juno III and the fuselage, despite being based on the same principles, relied on an optimized manufacturing process and new techniques to guarantee quality and mechanical resistance. There were also many learnings in the field of composite materials, where new techniques were implemented, guaranteeing the expected geometry and light weight, through a challenging process.

During Pacifico's project, the Aerodynamics and Structures team had the main objective of optimizing the manufacturing process of the aerodynamic surfaces, while also developing and increasingly specializing the team in numerical simulations.

B. Electronics systems managing view

For the launch of *Pacifico* in the 2024 SA Cup, the Electronics Systems team set out and strived to have all avionics systems working as expected. This critical task required meticulous planning of activities, rigorous testing of circuits and structures, and the expertise of experienced team members. However, the team also welcomed new members who had recently joined the group, recognizing the importance of knowledge transfer and fostering a collaborative environment.

Also, the Electronics Systems team had the opportunity to test their systems in February using the rocket Trix, developed by Projeto Jupiter. This flight test was crucial as several changes had been made to the avionics systems since the previous year, especially to the SRAD altimeter hardware and the novel SRAD telemetry PCB. The flight motivated the team to make some improvements to the 2024 SA Cup, in order to storage flight data more effectively, by enabling memory redundancy on the altimeter board, and to make our structures more robust. In addition, some design changes were made to the telemetry user interface, in order to enhance data display in a simple and elegant way.

C. Payload managing view

The Payload team's main goal was to develop a mechanical method to stabilize cameras during launch, thus maintaining the captured horizon leveled at all times.

During the development of T.I.L.T.A.D.O., the team had contact with many challenges and issues and had to take advantage of the vast expertise of its members to successfully design, manufacture and test each subsystem. For this reason, different sensor data processing algorithms and techniques, which were new to the team, were studied. Additionally, the team had to get familiar with all the components used, such as the Raspberry Pi Zero and Pico microcontrollers, the IMU sensor, the omnidirectional camera, and the stepper motor. On top of that, systems such as the camera alignment mechanism that had already been tested on other launches were able to get adapted and improved for this experiment.

In conclusion, the Payload project leads to the development of a multidisciplinary work, which assisted in the improvement of the abilities of the members. It was also possible to develop important multidisciplinary knowledge, including electronics design, image processing, and flight performance.

D. Propulsion managing view

In this mission project, the propulsion team decided to keep the same motor used in the Juno III rocket. The main improvements was aiming to refine propellant manufacturing, with the changes mainly focused on the KNSB melting method and grain mold design. These improvements should continue to be used in futures motors and the design mold improvement may allow future tests of different ports.

E. Recovery systems managing view

In Pacifico's project, the Recovery team set out to optimize methods and procedures in order to facilitate assembly and make the operation of the subsystem more reliable, avoiding significant changes in the ejection system. Consequently, the quarter spherical parachute, reefing system and CO₂ ejection system have been more extensively tested to understand and improve assembly and maintenance methods to ensure proper deployment. In these regards, the parachute and ejection system are very similar to last years launch, with small modifications to adress the problems found.

The only significant change is in the locking mechanism, which has since been changed from a pyrotechnic line cutter locking system to a more common shear pin method. This alteration has significantly simplified assembly and has been validated in many ground tests and a self operated flight in February 2024. Additionally, new testing methods have been developed for adequate parachute testing, such as a rig for drag tests in pickup trucks.

The ejection and disreefing systems are considered already validated because they were successfully employed in the team's two previous launches: Juno II on LASC 2022 and Nyx in March 2023, a test rocket, which are considered in-flight tested, while the shear pin locking mechanism has successfully flown in Trix in February 2024.

V. Appendix

Appendix A

System Weights, Measures, and Performance Data

BASIC ROCKET INFORMATION

Number of stages:

1

Vehicle length:

104.13 in

Airframe diameter:

6.43 in

Number of fins:

4

Fin span:

6.89 in

Fin tip:

7.08 in

Fin root chord:

9.05 in

Fin thickness:

1.09 in

Vehicle weight:

66.58 lb

Propellant weight:

17.9 lb

Empty motor case/structure weight:

16.7 lb

Payload weight:

9 lb

Liftoff weight:

84.48 lb

Center of pressure:

22.48 in

Center of gravity:

36.34 in

PROPULSION INFORMATION

Motor type:

SRAD

Motor letter classification:

N

Average thrust (N):

2417.25 N (543.43 lbf)

Total impulse (Ns):

10712.89 Ns (2408 lbf.s)

Motor burn time:

4.3 s

PREDICTED FLIGHT DATA

Launch rail length:

17 ft

Liftoff thrust-weight ratio (X:1):

9.671

Rail departure velocity:

75.7 ft/s

Minimum static margin:

2.157 c

Maximum acceleration (G):

13.52

Maximum velocity:

862.5 ft/s

Fin flutter velocity:

1761.78 ft/s

Target:

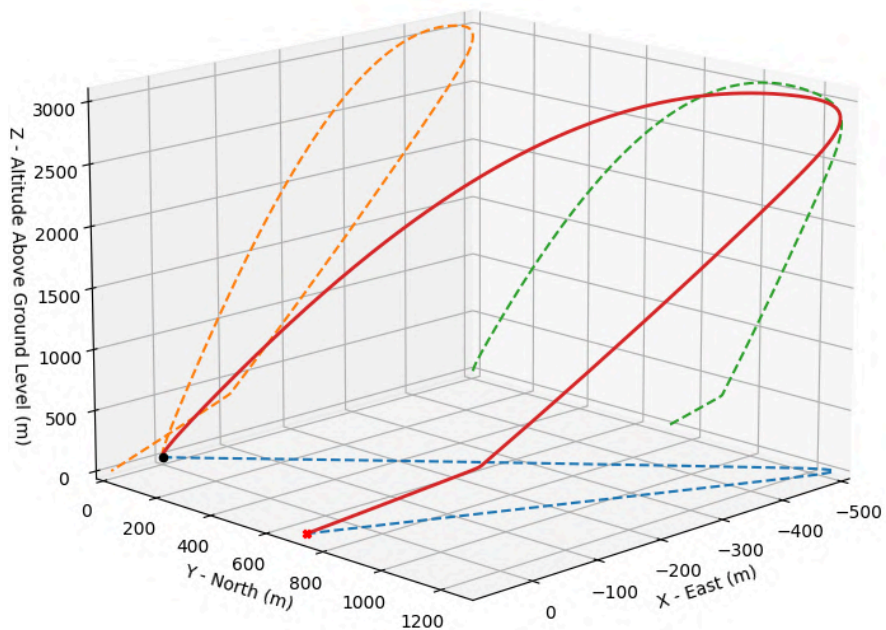
10000 ft

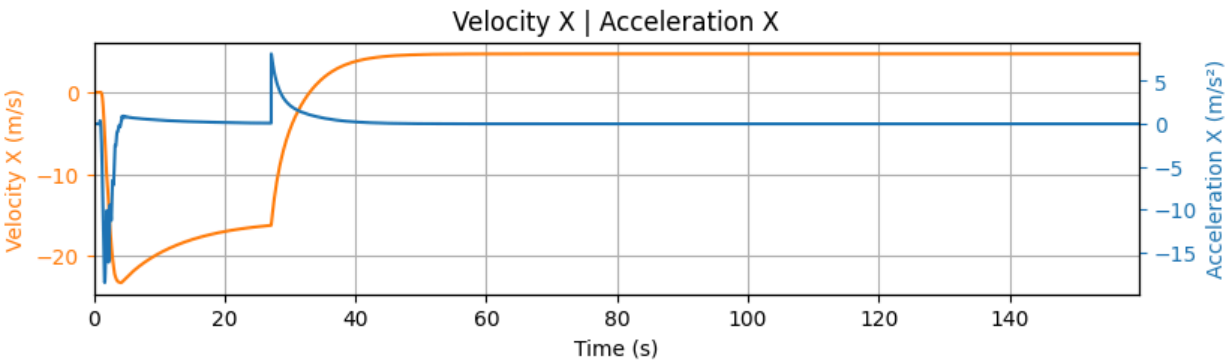
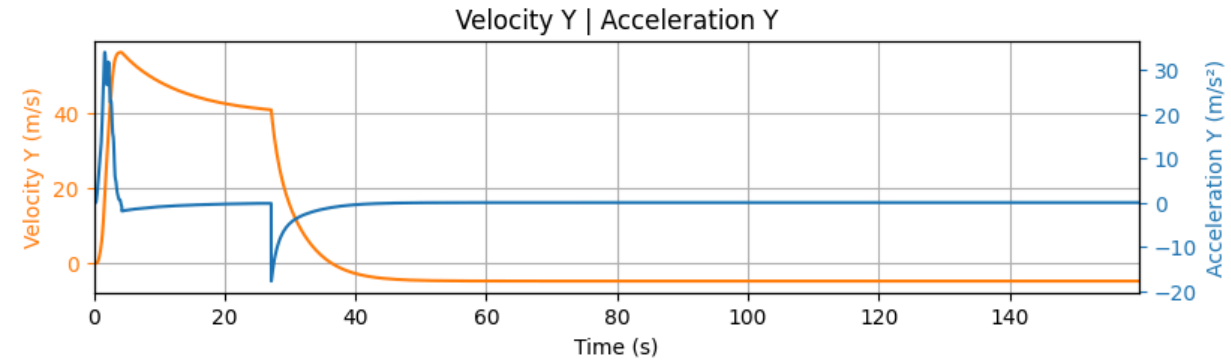
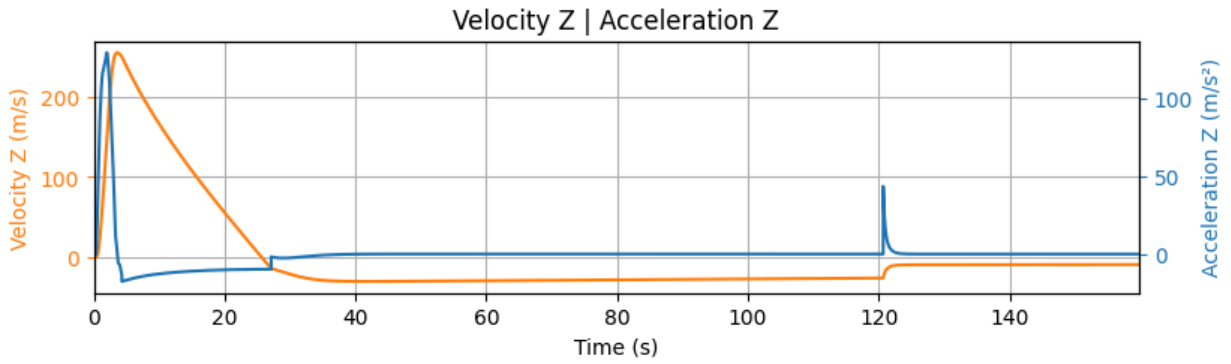
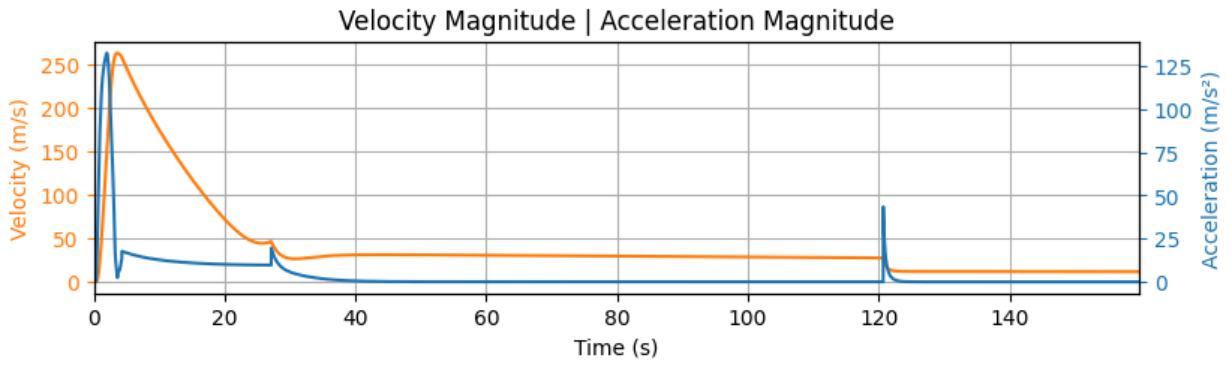
Predicted apogee:

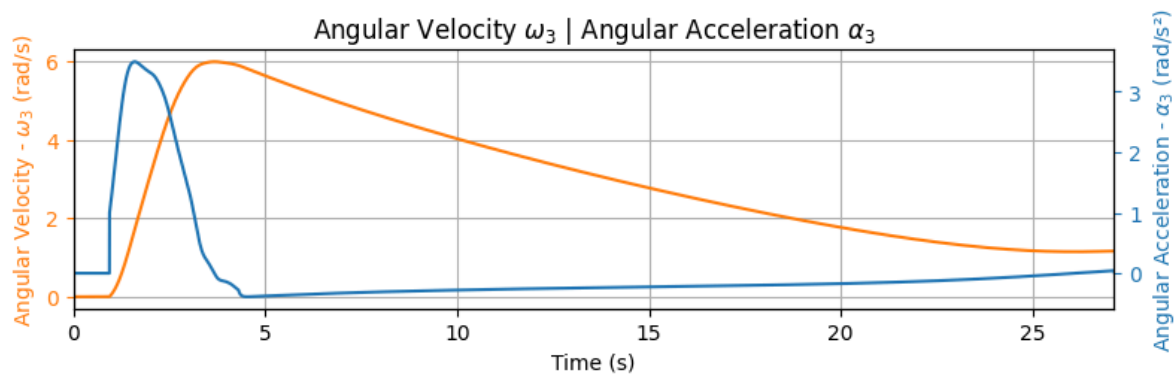
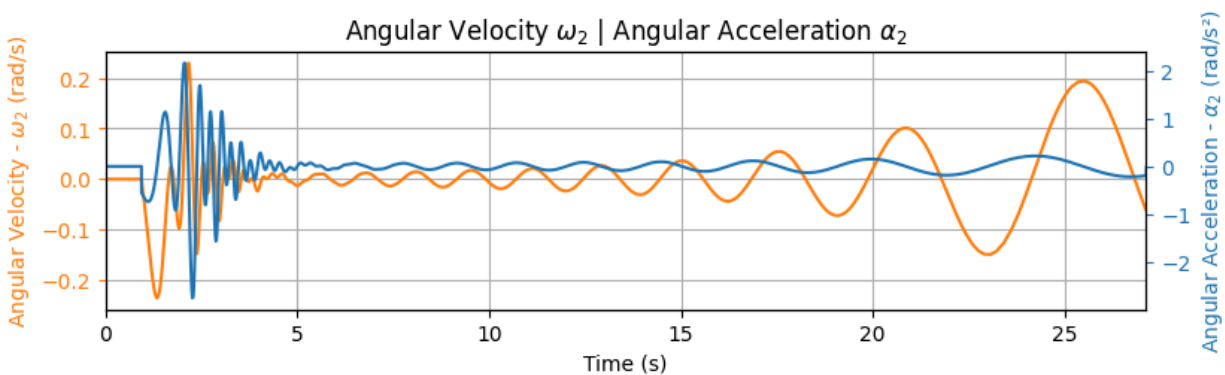
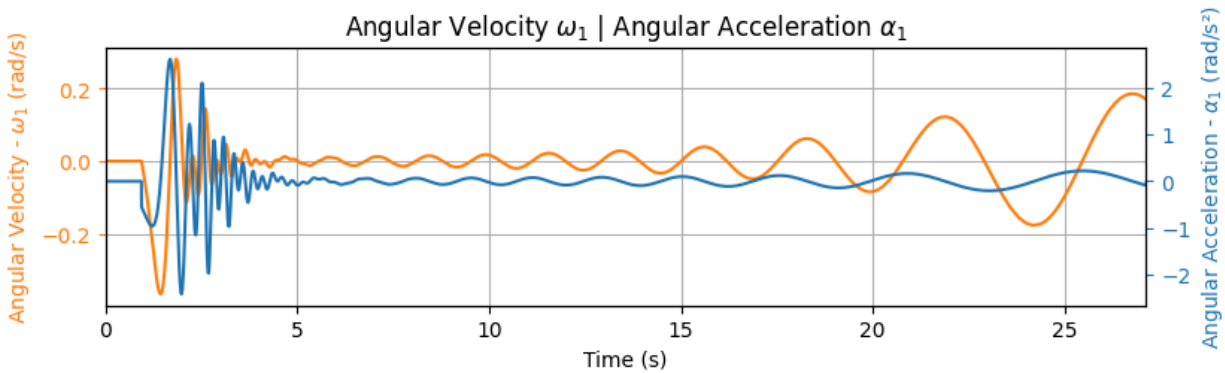
9985 ft

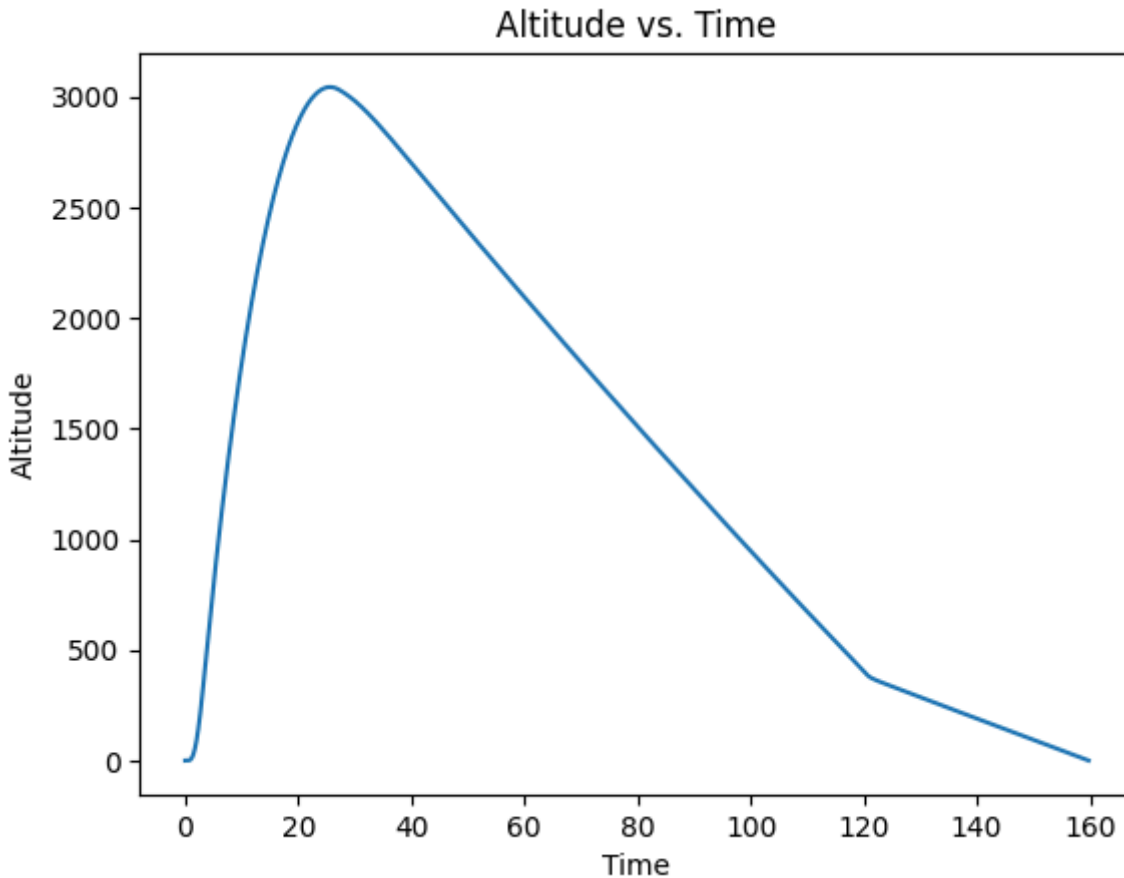
FLIGHT PROFILE GRAPH

Flight Trajectory









RECOVERY INFORMATION

COTS Altimeter:

Missileworks RRC3

Redundant altimeter:

SRAD

Drogue primary charge:

45g of CO₂

Drogue backup deployment charge:

45g of CO₂

Drogue deployment altitude:

9947 ft

Drogue descent rate:

72.2 ft/s

Main primary charge:

1g of black powder

Main backup deployment charge:

1g of black powder

Main deployment altitude:

1400 ft

Main descent rate:

30.5 ft/s

Shock cords:

One with 7.6 ft long leading to the fore section, where the wiring for the cutters is located, and one 14 ft long, passing through the ejection piston and leading to the aft section. The shock cords are made out of tubular polyester rated up to 3350 lbf are attached to u-bolts on either sections of the rocket with appropriately rated quick links.

Mechanical links:

Swivel link between the bottom section and the parachute

Parachute quick link

U-bolt on the aft section of the rocket and one on the fore section of the rocket

Appendix B

Project Test Reports

I. Recovery System Testing

A. CO₂ Ejection system tests

The team's SRAD CO₂ ejection system has been used many rockets: Juno II, launched at the 2022 Latin American Space Challenge, Nyx, which is the team's test rocket launched in March 2023, Juno III, launched at the 2023 Spaceport America Cup, Ganimedes, which had an attempted launch in the 2023 Latin American Space Challenge and Trix, another test rocket in February 2024. In the first three launches mentioned, the system worked as expected and parachute ejection was successful. In Trix's launch, the only one with shear pins, the COTS avionics system failed to detect apogee and the ejection system wasn't triggered, but the shear pins kept the rocket whole during the whole flight

Additionally, the team considers that the results of the previous ejection system tests made for said rockets are applicable for Pacifico, being sufficient to ensure the system's functionality. Specifically, the tests done for Ganimedes, which has the same module dimensions as Pacifico, as well as the same deployment bag and parachute type. An ejection test is considered successful when the mass ejected reaches a distance of 6 times the rocket's diameter from the module, according to Knacke [14]. In Pacifico case, this distance is equivalent to 38 inches.

Below is a detailed list of all the relevant ejection system tests done using Juno II, Juno III, Nyx, Ganimedes and Trix, all of them available on this link.

- 07/27/2022 - Juno II - Horizontal ejection system testing: 90g of CO₂ in a 5" diameter module

Assembly and activation of a single ejection system, with two 45g CO₂ cartridges inside the recovery module of the team's rocket, which has a 5 inch diameter. The module was placed on a table horizontally, in a height high enough so that the drag with the ground would not affect the test conclusions. As portrayed in Fig. 70, it was sufficient to eject the parachute from the module.



Fig. 70 Horizontal ejection system testing: 90g of CO₂ in a 5" diameter module.

- 08/03/2022 - Juno II - Vertical ejection system testing: 90g of CO₂ in a 5" diameter module

Assembly and activation of a single ejection system, with two 45g CO₂ cartridges inside the recovery module of the team's rocket, which has a 5 inch diameter. The module was placed on the ground vertically, and was sufficient to eject the parachute from the module, as well as the shock cords. This test was made the day before Juno II's successful launching on 08/04/2022.

- 02/22/2023 - Nyx - Vertical ejection system test: 50g of CO₂ in a 4.2" diameter module

Assembly and activation of the ejection system, with two 25g CO₂ cartridges inside the recovery module of the team's rocket, which has a 4.2 inch diameter. The module was placed on the ground vertically, and was sufficient

to eject the parachute from the module.



Fig. 71 Vertical ejection system testing: 50g of CO₂ in a 4.2" diameter module.

- 03/01/2023 - Nyx - Vertical ejection system test: 50g of CO₂ in a 4.2" diameter module

Assembly and activation of the ejection system, with two 25g CO₂ cartridge inside the recovery module of the team's rocket, which has a 4.2 inch diameter. The module was placed on the ground vertically, and was sufficient to eject the parachute from the module.



Fig. 72 Vertical ejection system testing: 50g of CO₂ in a 4.2" diameter module.

- 03/03/2023 - Nyx - Vertical ejection system test, integrated with avionics: 50g of CO₂ in a 4.2" diameter module

Just like the latter, the test requires the assembly and activation of the ejection system, with two 25g CO₂ cartridges inside the recovery module of the team's rocket, which has a 4.2" diameter. The module was placed on the ground vertically, and was sufficient to eject the parachute from the module. The main difference of this test from the previous one is that the ejection's activation is triggered by the SRAD altimeters on ground test mode, which causes a gap between the triggering and the activation of the system.



Fig. 73 Vertical ejection system testing: 50g of CO₂ with SRAD altimeters on ground test mode.

- 06/17/2023 - Juno III - Ejection system isolated test: 45g of CO₂

This is a test to verify with more detail the CO₂ ejection system. It's possible to observe the firing of the black powder and the seal being breached by the awl.



Fig. 74 Vertical ejection system testing: 50g of CO₂ with SRAD altimeters on ground test mode.

- 06/17/2023 - Juno III - Vertical ejection system test: 90g of CO₂ in a 5.2" diameter module

This is the last ejection test before the flight in the 2023 Spaceport America Cup. This ejection was triggered manually with a battery. The parachute was ejected successfully.



Fig. 75 Vertical ejection system testing: 50g of CO₂ with SRAD altimeters on ground test mode.

- 08/22/2023 - Ganimedes - Vertical ejection system test: 50g of CO₂ in a 6.3" diameter module

This is the first complete ejection test on a 6.3" airframe, with 50g of CO₂. This load of CO₂ was sufficient to eject the parachute completely. This ejection was triggered manually with a battery. Pacificos recovery module volume is very similar to this and will be using 90g of CO₂.



Fig. 76 Vertical ejection system testing: 50g of CO₂ with SRAD altimeters on ground test mode.

- 08/22/2023 - Ganimedes - Vertical ejection system test, integrated with avionics: 66g of CO₂ in a 6.3" diameter module

This is another vertical ejection test, but this time with the CO₂ charge that the rocket was supposed to fly with. The parachute was ejected completely.



Fig. 77 Vertical ejection system testing: 50g of CO₂ with SRAD altimeters on ground test mode.

- 10/21/2023 - Trix - Vertical ejection system test: 50g of CO₂ in a 4.2" diameter module with 3 M2 shear pins

This is the first ejection test with nylon shear pins. The module volume is equivalent to the one on the Nyx rocket. This test (and the following ones for this rocket) are the first experiences of the team with shear pins, with resounding success, since they sheared in every test.



Fig. 78 Vertical ejection system testing: 50g of CO₂ with SRAD altimeters on ground test mode.

- 11/28/2023 - Trix - Vertical ejection system testing, integrated with avionics: 50g of CO₂ in a 4.2" diameter module with 3 M2 shear pins

This is the first test with shear pins and avionics together, being thoroughly successful.



Fig. 79 Vertical ejection system testing: 50g of CO₂ with SRAD altimeters on ground test mode.

- 12/1/2023 - Trix - Vertical ejection system test: 25g of CO₂ in a 4.2" diameter module with 3 M2 shear pins

This test was done to verify if the 50g charge was indeed redundant. With the 25g charge it was more than sufficient to break the pins and fully eject the parachute.



Fig. 80 Vertical ejection system testing: 50g of CO₂ with SRAD altimeters on ground test mode.

- 02/16/2024 - Trix - Vertical ejection system testing, integrated with avionics: 25g of CO₂ in a 4.2" diameter module with 3 M2 shear pins
Another redundancy test, this time integrated with avionics to verify repeatability of the ejection. The test was once again successful.

B. Recovery System Electronics

1. SRAD Altimeter Flight Test

The SRAD altimeter was flight-tested on two separate occasions: first on March 4th, 2023, during the launch of Nyx and then again on June 26th, 2023, during the launch of the Juno III. On both occasions, the system successfully executed parachute ejection and disreefing operations. For the mini rocket Nyx, for instance, the parachute was successfully ejected at apogee and the rocket was recovered with no substantial damage, as seen in Fig. 81.



Fig. 81 Recovery of Nyx, with the parachute opened.

During Juno III's flight, the system successfully stored the pressure curve on the EEPROM, as depicted on Fig. 82. The data stored was obtained from the on-board BMP280 sensor used for apogee detection.

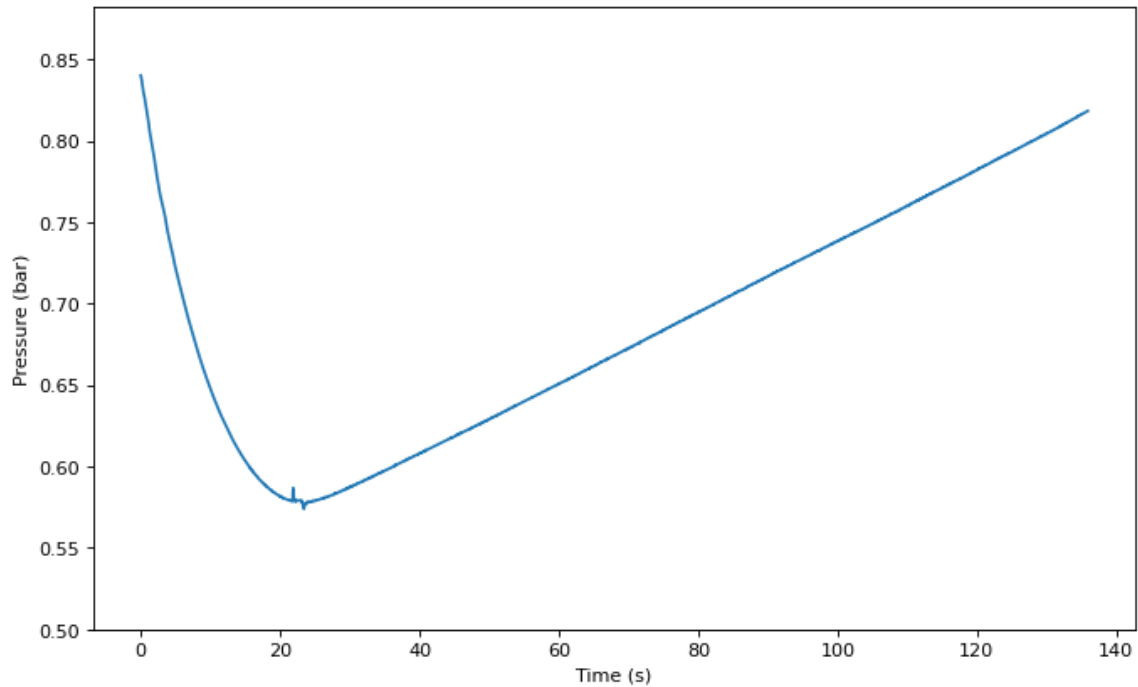


Fig. 82 Flight states stored in the onboard EEPROM.

2. SRAD Altimeter Ground Test

Several ground tests have been performed on the SRAD altimeter, in order to evaluate the algorithm's reliability and the circuitry robustness. During the ground tests on the SRAD altimeter, pressure data from different flights were collected using RocketPy, and the pressure curve was stored as an array in the internal memory of the microcontroller. This data served as input for the update routine of the altimeter's software, which is responsible for calculating the adaptive filter parameters and updating the system state accordingly. In addition to utilizing pressure data from RocketPy for updating the system state, further functionalities were evaluated. Once the system identified the hypothetical apogee (the peak altitude reached during flight), specific actions were triggered by the altimeter's software. Firstly, upon reaching the apogee, the altimeter activated the e-matches connected to the drogue connector. Additionally, the altimeter's software was programmed to activate the e-matches connected to the main connector when the code reached the disreefing altitude. A video for one of these tests can be found in this link.



Fig. 83 SRAD altimeter ground test. Moment of e-match activation

3. Ejection test

As mentioned in the Recovery Section, the CO2 cartridges are now on top of the parachute to ensure correct deployment. During the ejection test, the *SRAD* altimeter correctly triggered all events and monitored pressure. Then the e-matches were activated and the parachute was successfully ejected at apogee without causing major damage to the altimeters circuits. It is important to notice that no major pressure variation was detected inside the nosecone by the *SRAD* altimeter. This result points to a correct sealing between the CO2 cartridges and the Avionics Bay.

4. Battery drain test

The *SRAD* altimeter needs to run for a considerable amount of time, to ensure it is capable to wait for launch after being turned on. To perform this test, the board is powered by a fully charged Lithium-Ion battery and runs the code indefinitely, to simulate the rail conditions. During a whole work day at the project's lab, the voltage is measured at regular intervals. As seen in ??, the battery was comfortably capable of powering the *SRAD* altimeter for over 8 hour of operation. Thus, the test was considered successful.

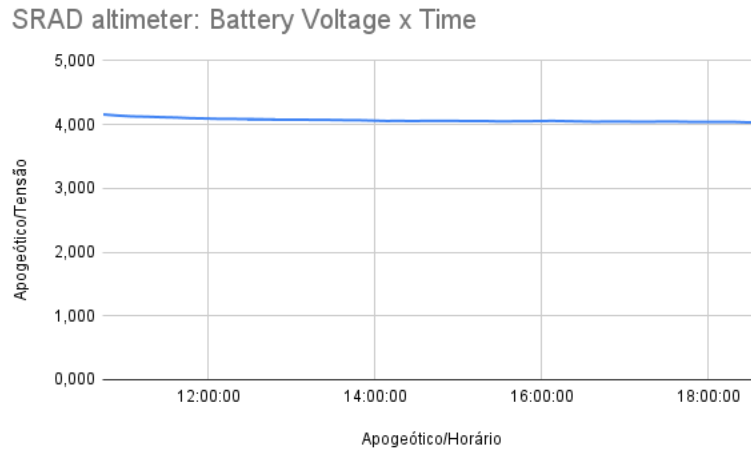


Fig. 84 SRAD altimeter battery test. Voltage was measured in 10 minute intervals.

II. SRAD Propulsion System Testing

A. Hydrostatic test

A hydrostatic test was carried out in order to guarantee that the casing was fit to stand pressures up to 2.0 times its maximum operating pressure of 640 psi. Therefore, the casing was successfully submitted to a pressure of 1300 psi.



Fig. 85 Hydrostatic test setup.

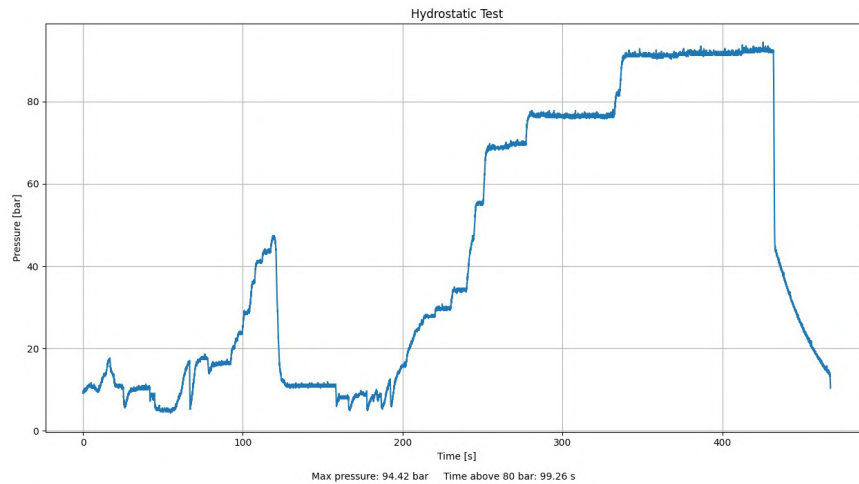


Fig. 86 Hydrostatic test data.

The motor resisted to the tested pressure and no leakage or permanent deformation of any parts were detected. This test was conducted with a hydrostatic test pump and the pressure data was obtained by means of a pressure transducer and an auxiliary manometer.

B. Static Fire Test

The motor "Mandioca" was submitted to a full scale static test following all safety measures. The test was conducted in a remote location with use of our specialized test stand while all of the team's members used the correct PPE and remained outside of the safety radius.



Fig. 87 Team with test stand.

For data acquisition, the instrumentation and telemetry system cited in II.A.4 was used. The static firing of the motor yielded the following results:

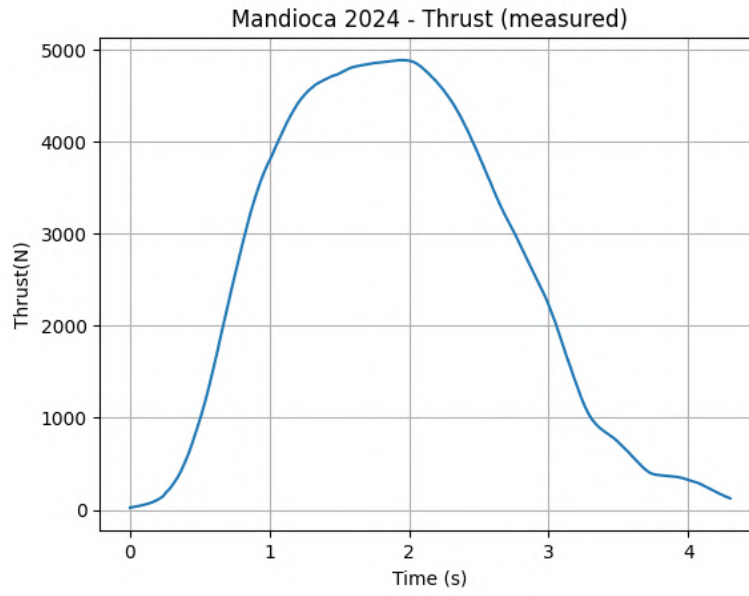


Fig. 88 Mandioca's real thrust curve.

Variable	Static Fire Test Value	Unit
Propellant Mass	8100	g
Total Impulse	10712.89	N.s
Specific Impulse	135	s
Total Burn Time	4.3	s
Maximum Thrust	4887	N
Average Thrust	2417.25	N

III. Aerodynamics & Structures system testing

A. Material Mechanical Tests

As part of the discipline PME-3596: Special Activities in Engineering II, members of Projeto Jupiter ran axial compression tests in carbon fiber tubes made through manual lamination by team members. Following general recommendations from technical standards [17], were run several tests enough for statistical evaluations of the results, with equal curing time for all samples, since material properties can vary depending on time. The chosen geometry of material samples were tubes with the same external and internal diameters as the ones used on our rockets back then, as shown in Fig. 89, with heights chosen with the objective to avoid buckling effects during tests.

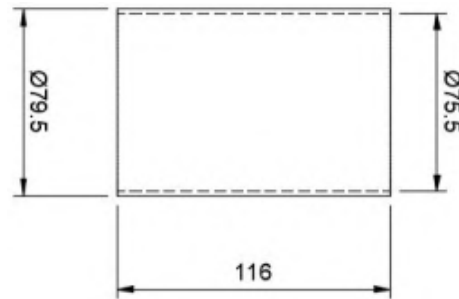


Fig. 89 Geometry characteristics of the samples used for tests, all dimensions in millimeters.

Tests were run in a KRATOS hydraulic press, with a maximum capacity of 10 000 kgf. It was adopted a load speed of 5mm/min and a pre-load of 98.07 N. For a better distribution of forces applied by the press, a soft material was positioned between the tube and equipment. In room temperature of 25° and air humidity of 50%, 6 samples were tested until the deformation seen was judged enough to compromise the structural integrity of a rockets tube. Figure 91 shows a chart of deformation (mm) in the function of the load applied (N) that was obtained from these tests. After statistical analysis of these data, material properties of team member made carbon fiber laminate were obtained, these are shown in Table 15. The equipment and setup used are shown in Fig. 90.

The results obtained for team manually made carbon fiber laminate were very different from default material properties of ANSYS, and were a valuable resource for more realistic structural simulations Pcífico's tubes.



Fig. 90 Equipment used in tests.

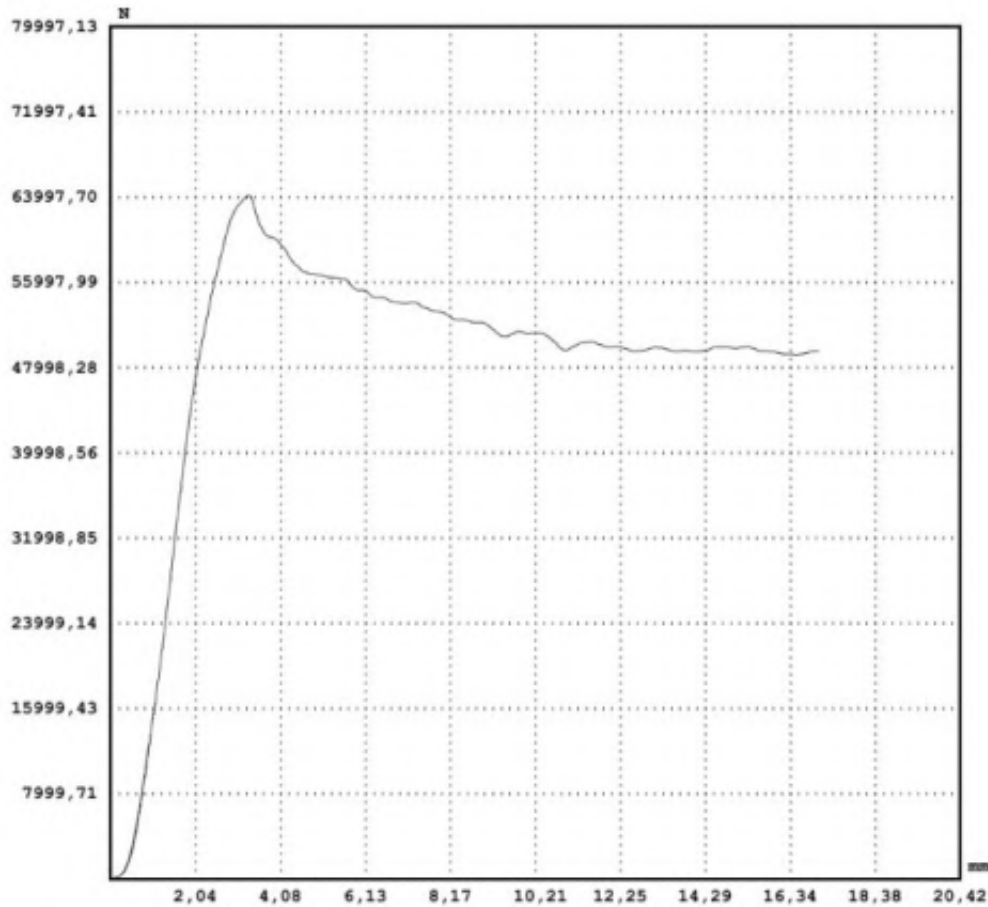


Fig. 91 Chart of deformation in function of load applied, obtained from test of one of the samples.

Table 15 Test results after statistical analysis.

Maximum Load (N)	42083.455
Area of Application (mm ²)	415.12
Maximum Strain (MPa)	102.52
Elasticity Modulus (MPa)	6195

B. Nosecone Manufacture Process

The nosecone is manufactured using an out-of-autoclave, wet-preg method. It is fabricated in two sections and joined using a co-cured stepped-lap technique. The layup schedule comprises 6 layers of 200gsm (6oz/sqyd) BID E-glass plies across the entire component, with an additional 2 plies on the straight extension of the nosecone (bottommost 150mm/6in). The plies are oriented in a quasi-isotropic manner, with odd plies at 45/-45 and even plies at 0/90 angles. Huntsman's LY1563/HY2963 system serves as the matrix material. The tip follows the same layup procedure, albeit with non-woven fiberglass plies totaling 900gsm (27oz/sqyd). This reinforcement was selected for its enhanced drapability compared to the BID fabric used elsewhere in the component. Its application is confined to the tip due to its lower glass/resin proportion of approximately 35%, contrasting with the 55% of the regular fabric. Consolidation of the plies is achieved using a vacuum bag method throughout the entire nosecone, except for the tip, where a silicone pressure bladder is employed to ensure improved compaction of the non-woven fiberglass.



Fig. 92 Fiberglass nosecone demolding after initial curing. Vacuum consumables are still inside the piece.

Two coats of primer are applied to enhance paint bondage to the nosecone. and then the surface is sanded to remove any texture. After sanding, layers of PU paint are applied to the surface, ensuring the structure is smooth and free of any additional roughness. This process is extremely important to reduce parasitic drag and ensure the most aerodynamic surface possible, and PU paint is an excellent material for this application, as it also offers UV light protection to the epoxy resin.

IV. SRAD GPS Testing

A. Telemetry Transmit and Receive Test

One requirement of the Telemetry Subsystem is to transmit and receive data reliably over relatively long distances, since this is essential to recover the rocket more easily after its landing. In order to assess the system performance in different scenarios, such as environments with trees and other obstacles and also open field environments, Transmit and Receive Tests are planned and performed. This kind of test gives an idea of the effectiveness of data transmission over extended distances, allowing for an evaluation of the system's reliability. It's important to notice that during the flight, the scenario closely resembles an open field environment. Another important consideration is that despite the team having a COTS Featherweight GPS, which serves as the Primary Tracker, the transmission of both SRAD and COTS data was tested (including geolocation). This was necessary, since both systems operate in similar frequencies and are located within the same module.

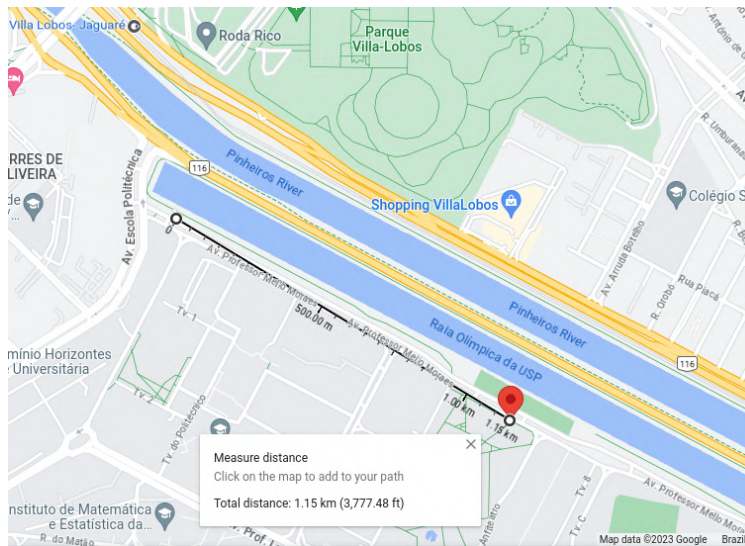


Fig. 93 Transmit and Receive Test distances between transmitter and receiver. Campus São Paulo.

The results showed that even at a distance of 1.1 kilometer and medium density of obstacles the data could be retrieved.

Furthermore, in a previous test conducted in our most recent successful launch at USP Campus Pirassununga, proved that the Telemetry system (with all its sensors and GPS) worked for at least 1.8km. At around 2km, we've lost connection to the B-L0722-LRWAN due to interference coming from the obstacles.

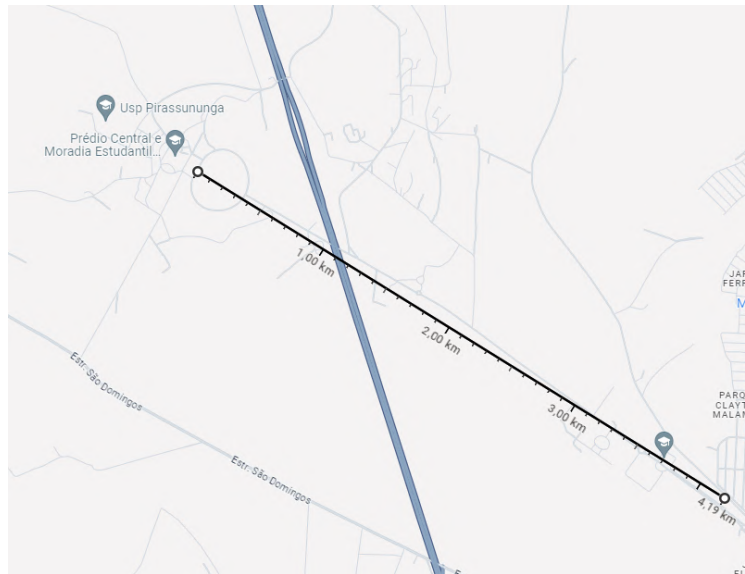


Fig. 94 Transmit and Receive Test distances between transmitter and receiver. Campus Pirassununga.

The Telemetry system was also tested in flight at mini Trix rocket, with had an Apogee of Approximately 860 m, in which it communicated for the most part of the flight, lost contacted at the moment of landing and informed a location close to the rocket landing

B. Telemetry Battery test

The Telemetry System is required to transmit and receive data reliably over a considerable period of time, so it is necessary to test about how long The Telemetry can be operated with high stability. In order to obtain this metric, the board is powered on with fully charged Li-Ion batteries, similarly to how it would be connected before the flight. Then, throughout a whole work day at the team's lab, the voltages of the system is measured at constant intervals. The data is then plotted in Voltage (V) x Time (s), which can be seen in Fig. 95.

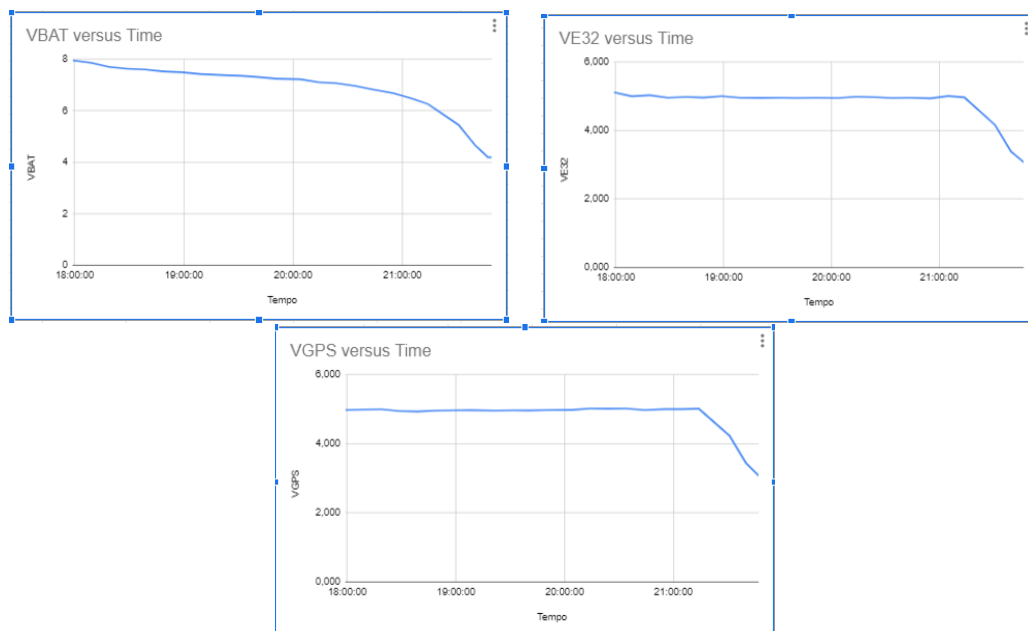


Fig. 95 SRAD Telemetry Receiver

The test shows that the *SRAD* Telemetry system works for about 3 hours and 50 minutes. After that, the data obtained is not considered reliable, since, upon observation of the graphics, the transmitter would not be receiving enough voltage to transmit the data at 20dBm after that time.

Appendix C

Hazard Analysis

Hazard Analysis				
Team	Rocket/Project Name	Date		
Escola Politécnica da USP	Pacifico / Projeto Jupiter	07 MAY 2023		
Hazard	Possible Causes	Risk of Mishap and Rationale	Mitigation Approach	Risk of Injury after Mitigation
Accidental solid-propellant igniter combustion.	Igniter is exposed to any favorable condition such as heat, flames or sparks so that it may cause an nonprogrammed ignition.	Low; The igniter is composed of mainly slow burning grains, without any ignition enhancer besides black powder.	Stock the igniters separately and inside a thermal bag.	Low
Accidental motor's ignition, causing potential explosions or injury to nearby personnel.	Igniter exposed to static electricity or other heat sources.	Medium; Pyrogen igniter is more sensitive to initiation.	Install the ignition line after all launch pad procedures have been done.	Low
Explosion of solid-propellant SRAD rocket motor with blast or flying debris causing injury.	Chunk of propellant grain breaking off and blocking nozzle's exit.	Medium; KNSB grains are vaporized inside the combustion chamber.	Inspect propellant's grain integrity during final assembly before launch.	Low
	Motor's end closures fail to hold.	Low; Parts and bolts are designed and tested for the required safety factors.	Launch crew 500 meters from rocket at launch, behind barrier.	
Rocket does not ignite when command is given ("hang fire"), but does ignite when team approaches to troubleshoot.	Ignition signal is still "on" when approaching launch pads.	Low; Ignition signal requires two action command.	Remove ignition jumper before approaching launch pads.	Low
Failure/Instability in rocket's communication during critical procedures when team approaches to troubleshoot.	Power outage.	Low; Batteries tested before the critical procedures.	Substitute batteries and check the stability in rocket's communication	Low
	Jammed signal.	Medium; Antenna lack of signal or troubles with geographic relief or interferences.	All connections will be re-established and checked.	
Rocket deviates from nominal flight path, comes in contact with personnel at high speed.	Failure on connection with launch platform.	Low; every component will be tested on manufacture process and during assembly to minimize unpredicted structural failures. A stall event simulation were made to estimate maximum wind velocities for a safe flight.	The rocket should be suspended in front of judges horizontally from a section of guide rail as a test.	Low
	Fins failure during flight.		Give the adhesive enough time to cure and ensure the component will not overcome flutter speed during flight.	
	Unstable flight.		Design of the structure of the fins based on aerodynamic models and simulations.	
	Excessive wind speed.		Use of safety coefficient of 1.5 for maximum side wind at launch.	
Black Powder accidental ignition.	Black Powder exposed to any favorable condition such as heat, flames or sparks so that it may cause an unprogrammed ignition.	Low; Ideally, none of these conditions are present in the team's work enviroment.	Stock the black powder in a sealed, non-shrapnel generating container away from any ignition source.	Low
Ejection system activation during assembly or pre-launch.	Failure on logic circuit to detect ejection situations.	Low; the COTS components are commercially tested. And the SRAD Circuit is tested for several hours to simulate this situations.	Data filtering methods to avoid wrong detections.	Low
	Accidental e-match ignition.	Low; The current needed to ignite an e-match can only be provided by batteries or faulty electronics.	Keep e-match leads shorted and verify electronics constantly.	Low
Lithium-ion battery short circuit.	Poor wire connections.	Low; each lithium-ion battery remains inside a rigid plastic case attached to the module's shelf with screws and clamps and all wire connections are properly tested .	Ensure the batteries are rigidly attached to the module and check wire connections through each phase of the module's assembly.	Low

Appendix D

Risk Assessment

RISK ASSESSMENT				
Team	Rocket/Project Name	Date		
Escola Politécnica da USP	Pacífico /Projeto Jupiter	07 MAY 2024		
Risk	Possible Causes	Risk of Mishap and Rationale	Mitigation Approach	Risk of Injury after Mitigation
Use of grains with different properties.	Non-standard and undocumented production.	Low; The production of grains is all documented and followed by who is responsible for this step.	Measure mass of each component during every step and mass and dimensions for the final result.	Low
Motor's structure failure.	Pressure in combustion chamber exceed their nominal value.	Low; Hydrostatic tests have been performed assuring that the combustion chamber resists the nominal pressure.	Use of safety coefficient near and higher than 2 for every component of the motor.	Low
	Excessive nozzle erosion due to high temperatures and high velocity gases.	Medium; Material properties have been specifically selected for its use.	Nozzle is replaced after each ignition. Cautious handling of the nozzle to prevent cracks.	Low
Improper motor's ignition.	Igniter not burning properly.	Low; Previous experience in KNSB solid propellant's fabrication and storage.	Igniter standardization for better control.	Low
	E-matches do not ignite due to poor contact.	Medium; The contact between cables are all made by hand and not tested beforehand.	Test wire continuity while assembling the system, the connections can be redone in case of failure.	Low
Ejection system completely or partially fails.	Recovery module is not properly sealed.	Low; Sealing method has been tested on ground and in multiple flights.	Do ground testing to ensure the best sealing material and method.	Low
	COTS or SRAD altimeter does not detect apogee or main launch point in the right moment.	Low; COTS system commercially tested and SRAD system successfully flown previously.	Ensure adequate operating conditions and several hours of ground tests executed.	Low
	E-matches fail to ignite.	Check e-match resistance and cables' continuity before assembling the rocket and verify that batteries are fully charged.	Low; No previous occurrence of failed ignition with the current system.	Low
	Accidental e-match ignition.	Low; The current needed to ignite an e-match can only be provided by batteries or faulty electronics.	Keep e-match leads shorted in storage and during assembly and verify electronics frequently.	Low
	Awl gets stuck in the CO ₂ cartridge due to low friction inside the ejector.	Medium; A tight fit is necessary to ensure proper operation and the O-ring can get caught in holes in the tube.	Checking for excessive friction during assembly and lubricating the O-ring.	Low
	Ejection gases' pressure is not enough to break shear pins and eject the parachute	Low; the shear pins have been broken in every ground test performed.	Test the system thoroughly to make sure that it is redundant.	Low
Reefing cutter system's early activation.	Accidental e-match ignition.	Low; The current needed to ignite an e-match can only be provided by batteries or faulty electronics.	Keep e-match leads shorted in storage and during assembly and verify electronics frequently.	Low
	COTS or SRAD Altimeter fails to detect main launch point at the right moment.	Low; COTS system commercially tested and SRAD system successfully flown previously.	System commercially tested. And the SRAD system already worked on flight test and several hours of ground tests.	Low
Recovery system partially deploys.	COTS or SRAD Altimeter does not detect apogee or main launch point in the right moment.	Low; COTS system commercially tested and SRAD system successfully flown previously.	System commercially tested. And the SRAD system already worked on flight test and several hours of ground tests.	Low
	Suspension lines winding in the parachute body.	Medium; Is agravated only in abnormal deployment conditions such as high winds.	Ensuring correct folding and packing of the canopy in the ejection module.	Low
	Main parachute rips apart due to the opening forces.	Low; In other flights, parachutes made with the same method and fabric have had no damages.	Test the the fabric's resistance and deploy the suspension lines first.	Low
	Pilot/Main parachute fails to inflate.	Low; In previous flights, when ejected, the parachute always inflated.	Use of deployment bag and adequate packing methods.	Low

RISK ASSESSMENT				
Risk	Possible Causes	Risk of Mishap and Rationale	Mitigation Approach	Risk of Injury after Mitigation
Fuselage's structure failure.	Coupling disks failure.	Low	Use of safety coefficient higher than 1.5 for every connection. Ensure all screws are properly bolted	Low
	Fins structural failure.	Low	Use of strict protocols to ensure uniformity during composites manufacture.	Low
	Tubes failure.	Low	Use of strict protocols to ensure uniformity during composites manufacture and use of a safety factor coefficient greater than 1.5 on all tubes.	Low

Appendix E
Assembly, Preflight, and Launch Checklists Appendix

I. Motor's Assembly Procedure

Table 16 Combustion Load Assembly

Step	Action	Components	Check
1	Allocate grains, separators, elevator, and string within liner	Liner, 5 grains, 4 separators, elevator, string	
2	Finalize liner alignment	Liner, 5 grains, 4 separators, elevator, string, tape	

Table 17 Combustion Chamber Assembly

Step	Action	Components	Check
1	Fit o'rings around bulkhead	2 o'rings, bulkhead	
2	Install bulkhead in combustion chamber	Bulkhead, combustion chamber, 12 M6 bolts	
3	Slide combustion chamber's load inside combustion chamber	combustion chamber's load, combustion chamber	
4	Fit o'rings around nozzle	2 o'rings, nozzle	
5	Install nozzle inside the combustion chamber	Combustion chamber, nozzle, 12 M6 bolts	

Table 18 Motor Module Assembly

Step	Action	Components	Check
1	Install fuselage on bulkhead	Bulkhead, fuselage, upper connector, 8 M5 bolts	
2	Place bottom connector to fix the fuselage to the combustion chamber	Combustion chamber, fuselage, bottom connector, 8 M5 bolts	
3	Install the lower rail button on the bottom connector	Rail button, bottom connector	

II. Motor's mission procedure

Table 19 Igniter activation sequence

Step	Action	Check
1	Seal the igniter with all the components	
2	Check if all the security methods are activated	
3	Connect igniter and ignition system	
4	Go / No Go for igniter procedure	
5	Slide igniter inside loaded combustion chamber. It should be attached to the top of the chamber	
6	Enable current flow through the circuit breaker	
7	Check launching system connection with the igniter	
8	Ready to receive permission to launch	
9	Go / No Go to launch	

Table 20 Launch abort

Step	Action	Check
1	Confirm launch abort	
2	Check launching system connection with the igniter	
3	Disable current flow through the circuit breaker	
4	Final status check	
5	Wait for green flag	
6	Begin personnel approach	
7	Remove the igniter of the combustion chamber	

III. Motor's static test procedure

Table 21 Static Fire test procedure

Step	Action	Check
1	Check launching system connection	
2	Disable current flow through the circuit breaker	
3	Personnel return to safety area	
4	Slide igniter inside loaded combustion chamber	
5	Igniter operator return to safety area	
6	Enable current flow through the circuit breaker	
7	Check launching system connection with the igniter	
8	Go / No Go for operation continuity	
9	Verify Load Cell and pressure sensor values	
11	Go / No Go for operation continuity	
12	Check data receipt status	
13	Check personnel evacuation	
14	Go / No Go to launch	

Table 22 Post static fire test procedure

Step	Action	Check
1	Check launching system connection	
2	Verify Load Cell values	
3	Disable current flow through the circuit breaker	
4	Wait for 5 min	
5	Begin Personnel approach	
6	Visual safety inspection at a safe distance	
7	Personnel approach	
8	Go / No Go for disassembly procedure	

IV. Recovery Module

Table 23 Ejection System Assembly

Step	Action	Check
1	Fix the cartridge base to the ejection base disk (2x)	
2	Insert the aluminum tube to the cartridge base (2x)	
3	Insert the awl to the tube (2x)	
4	Insert 2 ematches and add black powder to the black powder chamber (2x)	
5	Fix the black powder chamber to the aluminum tube (2x)	
6	Pass ematch through the ejection base disk (4x)	

Table 24 Reefing and Line-Cutter Assembly

Step	Action	Check
1	Thread the reefing line across the main parachute reefing rings and through the loop	
2	Pull the reefing line until its length is 8 in longer than suspension lines	
3	Fold the main parachute and store it into the deployment bag	
4	Thread the reefing line through the shock cord loops	
5	Insert 2 e-matches in the black powder chamber from the reefing cutter system (2x)	
6	Pass the reefing line through the black powder chamber (2x)	
7	Place the black powder chamber into the reefing-cutter support (2x)	
8	Add black powder to the chamber (2x)	
9	Screw black powder chamber to the support (2x)	
10	Fix the reefing line to the shock cord below the supports through a nut	
11	Pass wire through shock cord loops (4x)	
12	Crimp e-match to wire (4x)	
13	Crimp wire to the connector (4x)	

Table 25 Complete Disreefing System Assembly

Step	Action	Check
1	Pass shock cord through recovery tube	
2	Pass shock cord through the U-Bolt	
3	Attach U-Bolt to the ejection disk with four nuts	

Table 26 Recovery Module Assembly

Step	Action	Check
1	Pass the parachute shock cord through the piston	
2	Pass the parachute shock cord through the recovery module	
3	Pass parachute shock cord through U-bolt	
4	Attach U-bolt to the rocket base disk with four nuts	
5	Insert threaded bar (with counter nuts) to the ejection base disk and secure with three nuts	
6	Attach ejection bulkhead to nosecone coupler	
7	Insert the CO ₂ cartridge to the cartridge base (2x)	
8	Attach the avionics module to ejection bulkhead	
9	Divide e-matches between the positive and negative poles from the different ejection systems (2x)	
10	Attach nosecone	
11	Attach pilot chute to the deployment bag	
12	Put pilot and DB deployment bag inside the module	
13	Close the module	
14	Insert the shear pins (4x)	

Table 27 Recovery Module Disassembly

Step	Action	Check
1	Disconnect recovery module and nosecone	
2	Disconnect recovery and avionic modules	
3	Undo wire connections	
4	Remove shelf	
5	Remove CO ₂ cartridges	
6	Undo Wago connections	
7	Remove parachutes and reefing cutters from module	
7	Disconnect ejection disk from nosecone connection	

Table 28 Avionics Module Assembly

Step	Action	Check
1	Attach RRC3 altimeter to the first 3D-printed wall	
2	Attach SRAD altimeter to the second 3D-printed wall	
3	Attach Featherweight GPS to the third 3D-printed wall	
4	Attach battery holders to the fourth 3D-printed wall	
5	Check each battery's voltage	
6	Attach batteries to the battery holders and tightly fasten with zip ties	
7	Attach each threaded rod to the base disc and fasten with M5 nuts	
8	Attach each of the 3D-printed walls to the threaded rods	
9	Attach SRAD Telemetry Board to the 3D-printed upper wall	
10	Attach double battery holder to the back of the 3D-printed wall	
11	Check each battery's voltage	
12	Attach batteries to the double battery holder and tightly fasten with zip ties	
13	Attach each threaded rod to the middle disc and fasten with M5 nuts	
14	Attach the threaded rods to the middle disk and position the 3D-printed spacers	
15	Attach the 3D-printed Telemetry Wall to the middle disk, locking it with the upper disk	
16	Attach M5 nuts to the upper disk	
17	Crimp each key-switch's wires to the batteries of each system	
18	Connect Droque activation wire and GND to the RRC3 Sport Altimeter	
19	Connect Main activation wire to the RRC3 Sport Altimeter	
20	Connect switch wires to the RRC3 Sport Altimeter	
21	Connect RRC3 Sport Altimeter power supply wires	
22	Connect Droque activation wire and GND to the SRAD Altimeter	
23	Connect Main activation wire to the SRAD Altimeter	
24	Connect SRAD Altimeter supply wires	
25	Connect SRAD Telemetry Board supply wires	
26	Attach Avionics Module to the Recovery Module's threaded rods (Avionics Bay)	
27	Attach nose cone to Avionics Bay with screws	
28	Fix key-switches to the nose cone	
29	Check if key-switches are working as expected	

Table 29 Avionics Module Disassembly

Step	Action	Check
1	Disconnect the Avionics module from the Recovery's module	
2	Disconnect all the power supply wires	
3	Disconnect the key-switches wires	
4	Remove the structure's walls	
5	Remove batteries	

V. Payload Module

Table 30 Payload Module Assembly

Step	Action	Components	Check
1	Components attachment to respective shelves		
1.1	Shelf A		
1.1.1	Screw 1 4x18650 Battery Holder to Shelf Profile 1	1 4x18650 Battery Holder; 4 M2,5x8mm Phillips Head Screws; 4 M2,5mm Nuts; 1 Shelf Profile 1	
1.1.2	Fix 4 Li-Ion Batteries to the holder	4 18650 Li-Ion Batteries	
1.1.3	Secure the Holder and Batteries	2 Hellerman Tapes	
1.2	Shelf B		
1.2.1	Repeat steps 1.1.1 to 1.1.3	1 4x18650 Battery Holder; 4 M2,5x8mm Phillips Head Screws; 4 M2,5mm Nuts; 1 Shelf Profile 1; 4 18650 Li-Ion Batteries; 2 Hellerman Tapes	
1.3	PCB A		
1.3.1	Fix 4 Stepper Motor Drivers, 2 Raspberry Pi Pico and 1 Accelerometer to their respective pin sockets	4 A4988 Stepper Motor Drivers; 2 Raspberry Pi Pico; 1 MPU9250 Accelerometer	
1.4	Shelf C		
1.4.1	Align the double Raspberry Pi Zero Support Plate to the holes in Shelf Profile 2	1 Double Raspberry Pi Zero Support Plate; 1 Shelf Profile 2	
1.4.2	Screw 2 Raspberry Pi Zero 2W to support plate and Shelf Profile 2	2 Raspberry Pi Zero 2W; 8 2,5x12mm Phillips Head Screws	
1.5	PCB B	Pre-assembled PCB	
1.6	Shelf D		
1.6.1	Fix Pinion Gear to the Stepper Motor Axle	1 Pinion Gear; 1 NEMA 17 hs08-1004s	
1.6.2	Screw Stepper Motor to Shelf Profile 3	1 Shelf Profile 3; 2 M3x6mm Allen Head Screws	
1.7	Shelf E		
1.7.1	Repeat steps 1.6.1 and 1.6.2	1 Pinion Gear; 1 NEMA 17 hs08-1004s; 1 Shelf Profile 3; 2 M3x6mm Allen Head Screws	
1.8	Sliding Shelf 1		
1.8.1	Screw Stepper Motor to Sliding Shelf Profile	1 NEMA 17 hs08-1004s; 1 Sliding Shelf Profile 4 M3x6mm Allen Head Screws	
1.8.2	Screw the Camera to the Camera Adapter	4 M2x10mm Phillips Head Screws; 4 M2mm Nuts 1 Camera Adapter	
1.8.3	Fix Camera Adapter to the Stepper Motor Axle		
1.9	Sliding Shelf 2		
1.9.1	Repeat steps 1.8.1 to 1.8.3	1 NEMA 17 hs08-1004s; 1 Sliding Shelf Profile; 4 M3x6mm Allen Head Screws; 4 M2x10mm Phillips Head Screws; 4 M2mm Nuts 1 Camera Adapter	
2	Mechanism Assembly		
2.1	Fix the rack to Sliding Shelf 1 and Shelf D	1 Rack; 1 Shelf D; 1 Sliding Shelf 1; 2 M4x16mm; 2 M4 Locknuts	

2.2	Check if the Sliding Shelf 1 is not linearly constrained		
2.3	Repeat steps 2.1 and 2.2 with Sliding Shelf 2	1 Rack; 1 Shelf D; 1 Sliding Shelf 2; 2 M4x16mm; 2 M4 Locknuts	
2.4	Repeat steps 2.1 to 2.3 with Shelf E	2 Racks; 1 Shelf E; 4 M4x16mm; 4 M4 Locknuts	
2.5	Screw 25mm Standoffs through Shelf E to 65,3mm Standoffs	4 M3 1/4" 25mm Hex Standoffs; 4 M3 1/4" 65,3mm Hex Standoffs	
2.6	Screw Female Standoffs through Shelf D	4 M3 1/4" 40mm Female Hex Standoffs	
3	Inner Structure Assembly		
3.1	Screw 25mm Standoffs through PCB B to the Mechanism	Mechanism PCB B 4 M3 1/4" 25mm Hex Standoffs	
3.2	Screw 25mm Standoffs through Shelf C to the partly assembled module	4 M3 1/4" 25mm Hex Standoffs	
3.3	Screw 25mm Standoffs through PCB A to the partly assembled module	4 M3 1/4" 25mm Hex Standoffs	
3.4	Screw 25mm Standoffs through Shelf B to the partly assembled module	4 M3 1/4" 25mm Hex Standoffs	
3.5	Screw 25mm Standoffs through Shelf A to the partly assembled module	4 M3 1/4" 25mm Hex Standoffs	
3.6	Align the Boilerplate to the empty space between the Standoffs fixed onto Shelf A	1 Boilerplate	
4	Electrical Wiring		
4.1	Connect each camera's flat cable to their respective Raspberry Pi Zero	2 Flat Cables	
4.2	Wire the Stepper Motors to PCB A	4 JST Cable Sets	
4.3	Connect both Raspberry Pi Zeros to the batteries		
4.4	Connect PCB A to the batteries		
4.5	Connect PCB B to the batteries		
4.6	Screw both Key Switches to the respective Cubesat Acrylic Wall		
4.7	Connect one of the Key Switches to PCB A		
4.8	Connect the remaining Key Switch to PCB B		
4.9	Turn both Key Switches on to check nominal functioning. Do not forget to turn it off once tested		
5	Final Assembly		
5.1	Screw each Cubesat Base to one of the sides of the Inner Structure	Inner Structure; 2 Cubesat Bases; 8 M3x6mm Allen Head Screws	
5.2	Screw each Cubesat Wall to the Cubesat Bases	2 Cubesat Walls; 8 M4x10mm Allen Head Screws	
5.3	Screw each Cubesat Acrylic Wall to the Cubesat Bases	8 M3x6mm Allen Head Screws	
5.4	Measure every Payload dimension to check dimensional compliance		
5.5	Weigh Payload to check minimum weight compliance		
6	Rocket Integration and Payload Boot		

6.1	Screw each one of the 4 Cubesat Rails to the respective Rocket Coupler	4 M5x10mm Allen Head Screws;	
6.2	Turn both Key Switches on		

Table 31 Payload Module Disassembly

Step	Action	Check
1	Turn both Key Switches off	
2	Unscrew Cubesat from the Rocket Coupler	
3	Remove the Payload from the Tube	
4	Unscrew both Cubesat Acrylic Walls from the Cubesat Bases	
5	Disconnect both Key Switches wiring	
6	Proceed with the inverse order shown in Table 30	

Table 32 Telemetry Module Assembly

Step	Action	Check
1	Place Shelf I displaced at least 5cm from the table	
2	Screw four M4x12mm Allen Head Screws to Shelf I	
3	Insert two M4 1/4" x 120mm Hex Standoffs to upper shelf into the mounting holes closer to the antenna hole	
4	Screw the Shelf H into two M4 1/4" x 55mm Hex Standoffs	
5	Screw two M4 1/4" x 28mm Hex Female-Female Standoffs into Shelf H's screwed standoffs	
6	Slide camera into Shelf G's hole so that the lens stay upright	
7	Screw two M4 1/4" x 28mm Hex Male-Female Standoffs into Shelf G's bottom	
8	Telemetry Assembly	
9	Mount the X-NUCLEO-IKS01A2 shield to the B-L072-LRWAN1 board	
10	Place the B-L072-LRWAN1 board on top of the Telemetry Wall	
11	Mount SRAD Telemetry board on top of B-L072-LRWAN1's pinheaders	
12	Mount M3x10mm Phillips Head Screws to the upper B-L072-LRWAN1 board mounting holes and insert nuts	
13	Insert mounted Telemetry Wall into Shelf I's holes	
14	Featherweight Assembly	
15	Secure Featherweight COTS GPS transmitter to Featherweight Wall and separator with two M2.5x12mm Phillips Head Screws	
16	Screw Shelf F to the remaining mounted Standoffs	
17	Insert four M4 1/4" x 28mm Hex Standoffs into Shelf F	
18	Put 2 M2,5x8mm Phillips Head Screw into the Series Li-ion Battery container on Shelf E	
19	Put 1 M2,5x8mm Phillips Head Screw into the Single Li-ion Battery container to Shelf E	
20	Put 2 batteries in Series container checking with a multimeter its polarity	
21	Secure both containers with zip ties	
22	Screw Shelf E to the four M4 1/4" x 28mm Hex Standoffs present in Shelf F	
23	Connect key-switches to Telemetry module and Featherweight module	
24	Connect and crimp key switches to Telemetry batteries and Featherweight battery	
25	Assemble Telemetry module to the Payload Module	

Table 33 Telemetry Module Disassembly

Step	Action	Check
1	Disconnect all the power supply wires	
2	Disconnect the key-switches wires	
3	Disconnect the Telemetry module from the Payload module	
4	Remove the structure's shelves, electronic components and the camera	
5	Remove batteries	

VI. Rocket Assembly

Table 34 Nosecone and Recovery

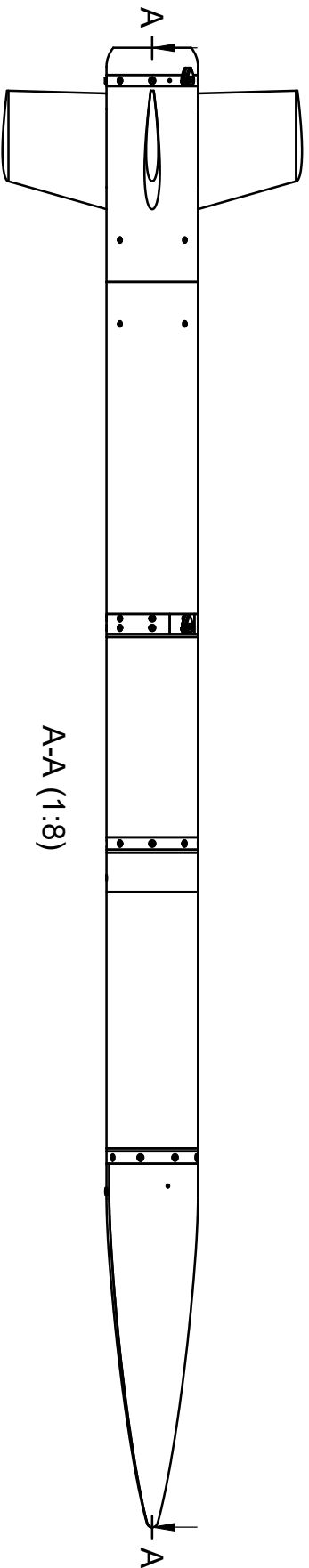
Step	Action	Check
1	Screw the male-female connection of the nosecone and coupling tube	
2	Check recovery module integrity after assemble	

Table 35 Avionics and Payload

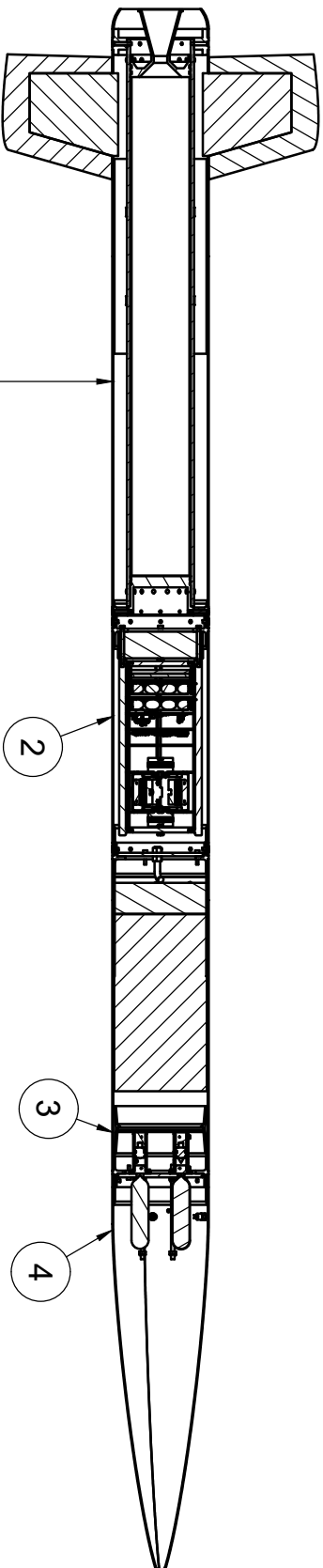
Step	Action	Check
1	Crimp the key-switches after assembling the system	
2	Screw the male-female connection of the Avionics module and the Recovery's module	
3	Check Avionics module integrity after assemble	

Appendix F

Engineering Drawings



A-A (1:8)



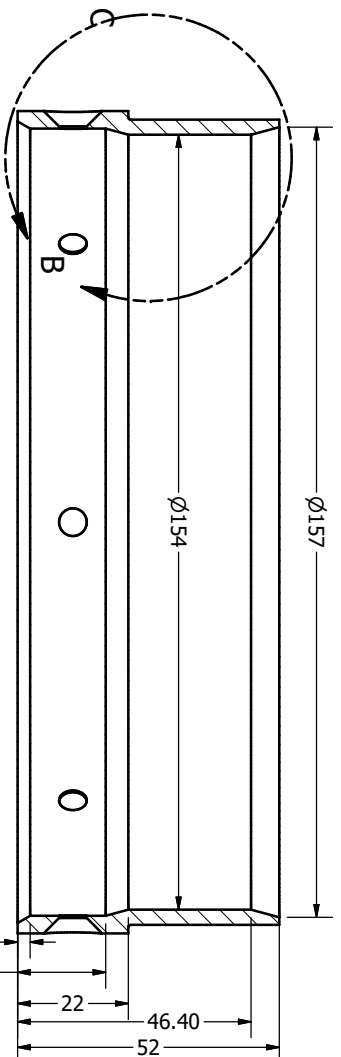
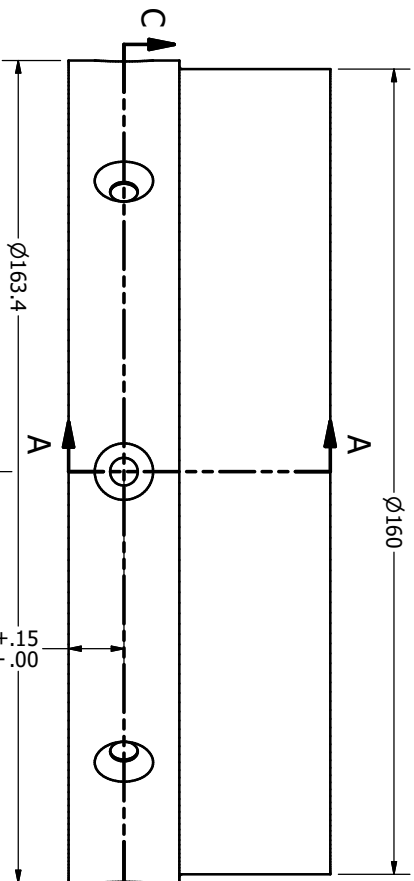
Components List

Item	Submodule
1	Motor
2	Payload
3	Avionics Ejection
4	Recovery + Avionics Disreefing

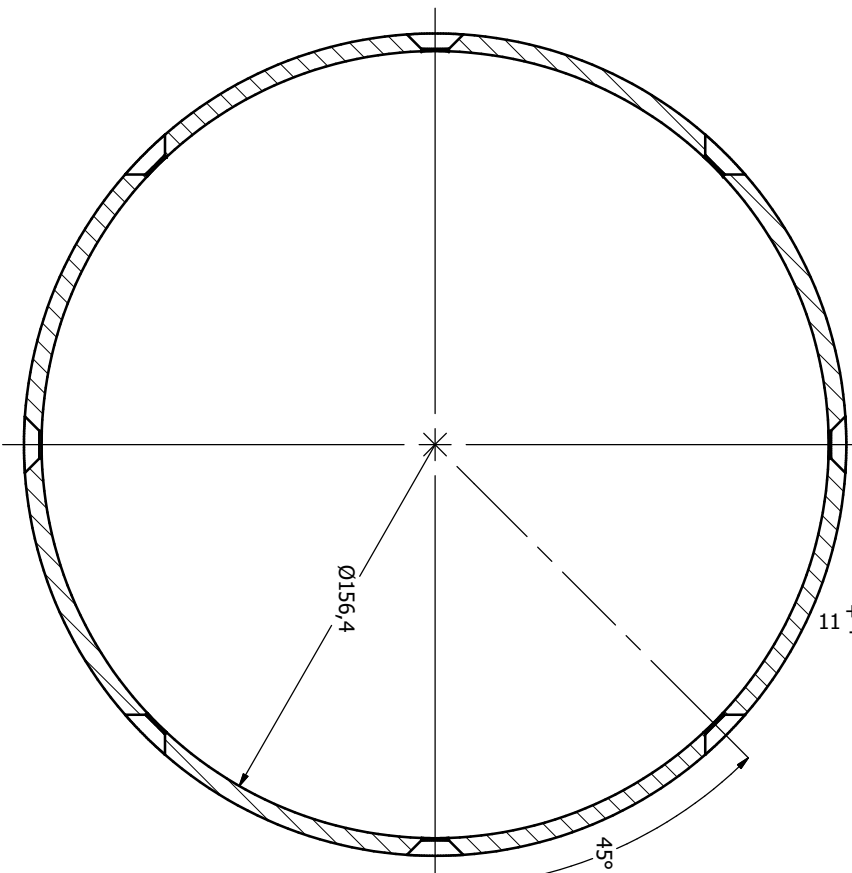
Dept.	Technical reference	Created by	Approved by
Projeto Jupiter	NBR 10067	Gustavo Martins	Felipe Fratti
		Document type	Document status
		Assembly Drawing	Approved
		Title	DWG No.
		Pacifico	1



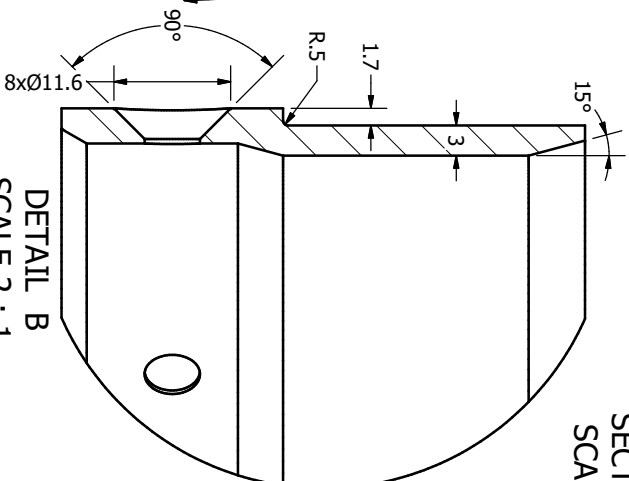
Rev.	Date of issue	Sheet
1	05/03/2024	1/1



SECTION A-A
SCALE 1 / 1



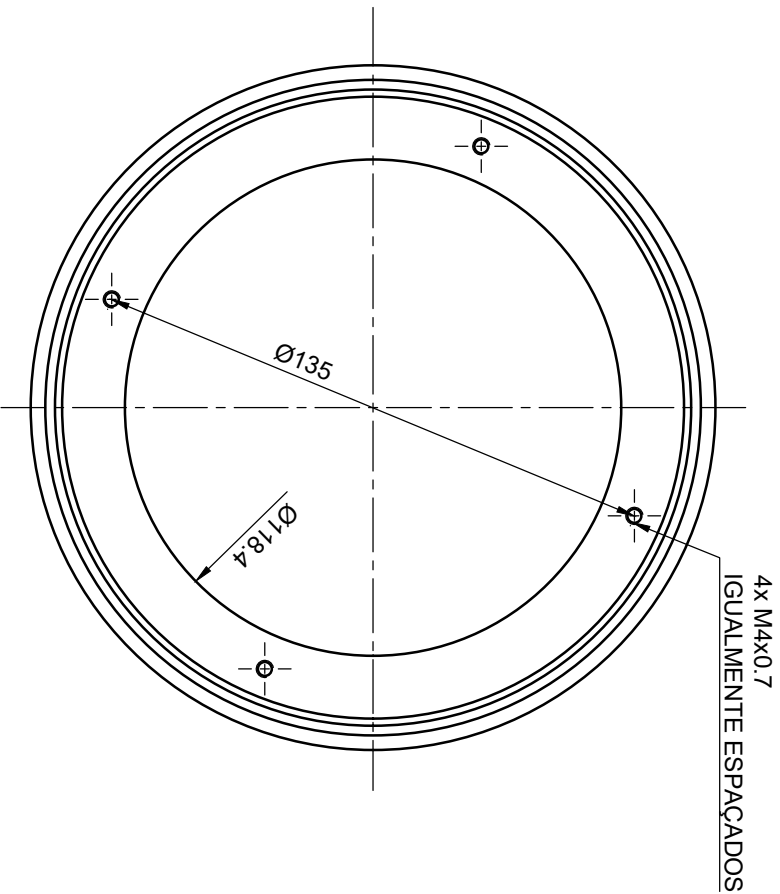
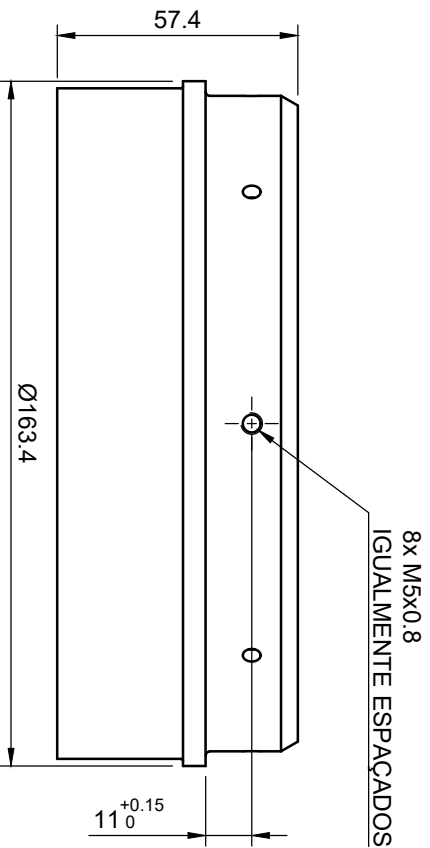
SECTION C-C
SCALE 1 / 1



DETAIL B
SCALE 2 : 1



DRAWN	Proj. Jupiter	18/03/2024	TITLE Fêmea Padrão 6" AI 6351-T6		
CHECKED					
QA					
MFG					
APPROVED			SIZE A3	DWG NO Fêmea Padrão 6in v19	REV
SCALE 1 / 1			SHEET 1 OF 1		

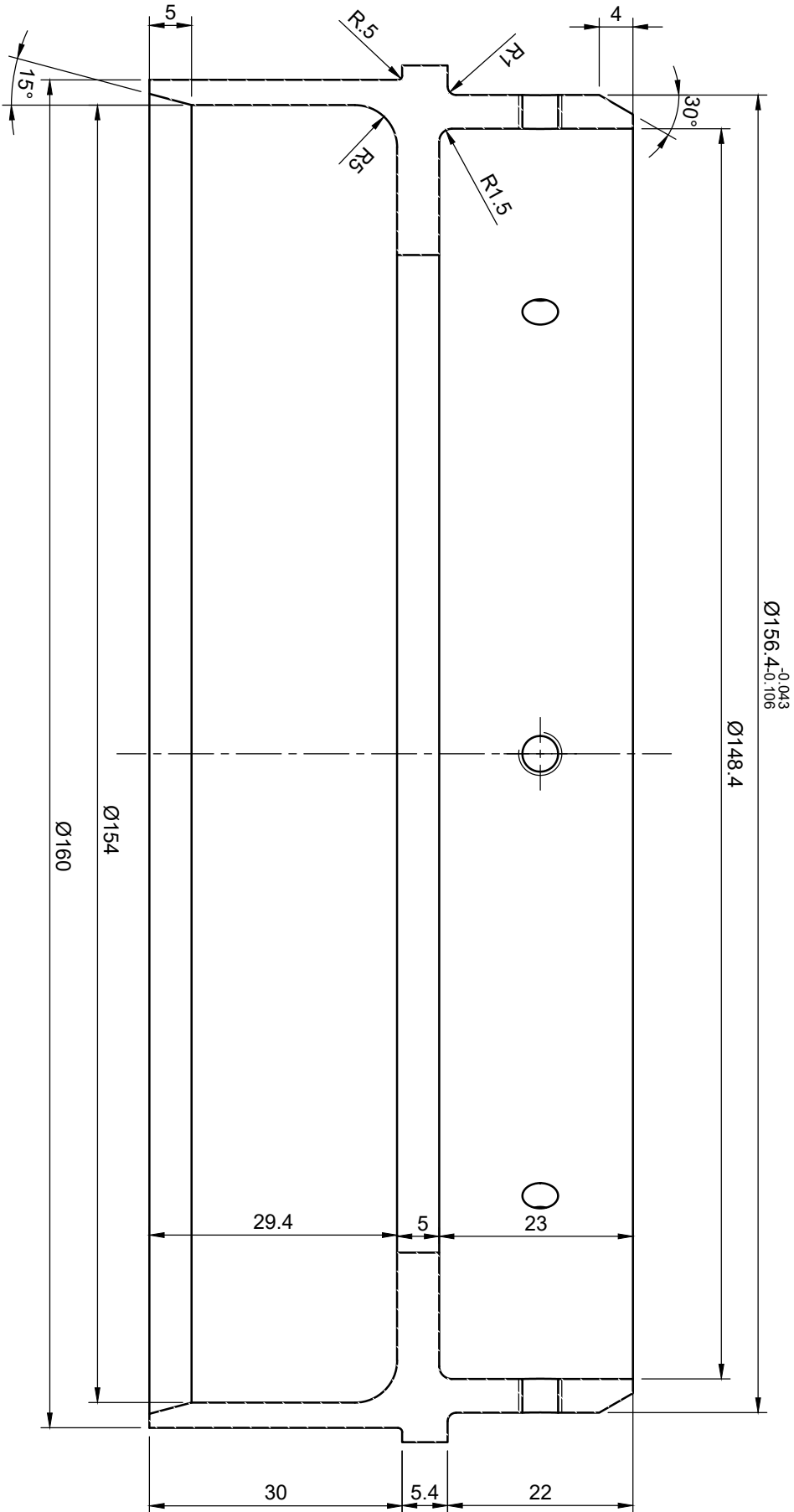


+

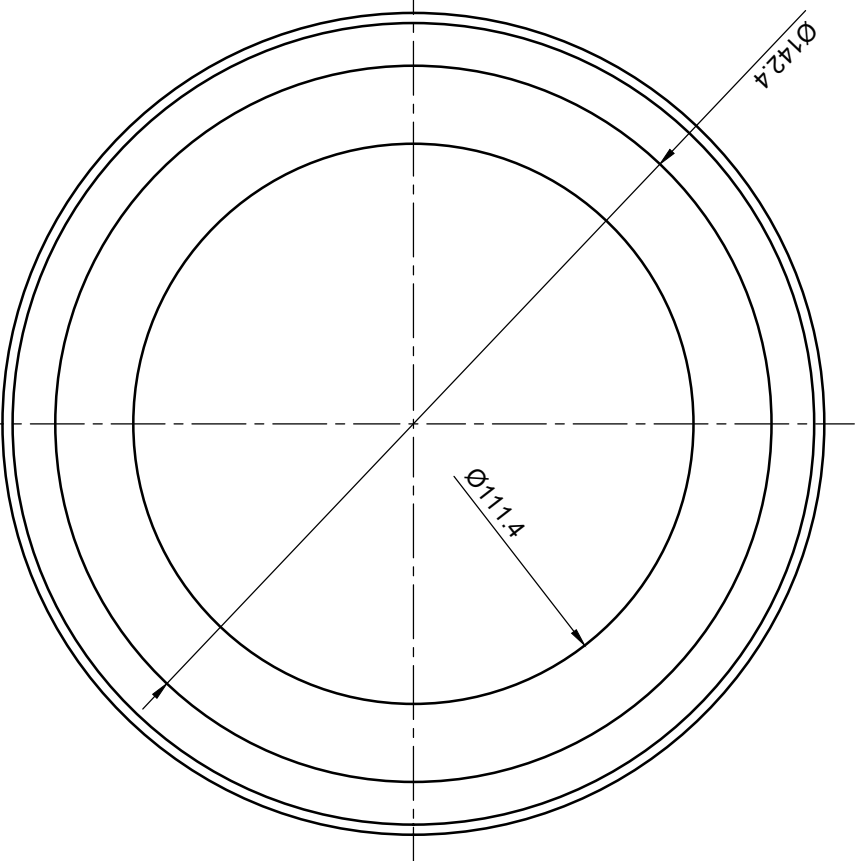
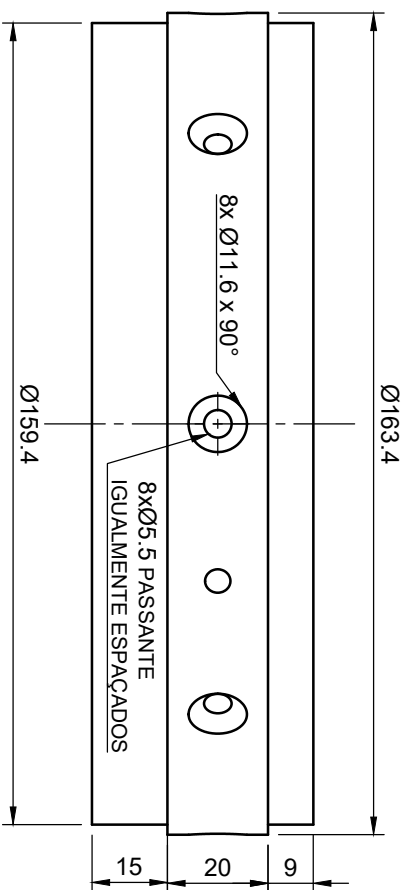
Dept.	Technical reference	Created by	Approved by
Proj. Jupiter	NBR6158 H8f8	Maria E. S. Silva 31/07/2023	
1:1	Document type		Document status
	Title	DWG No.	
	Macho Padrão 6"	A3	
	Rev.	Date of issue	Sheet
			1/2




VISTA AUXILIAR (2:1)

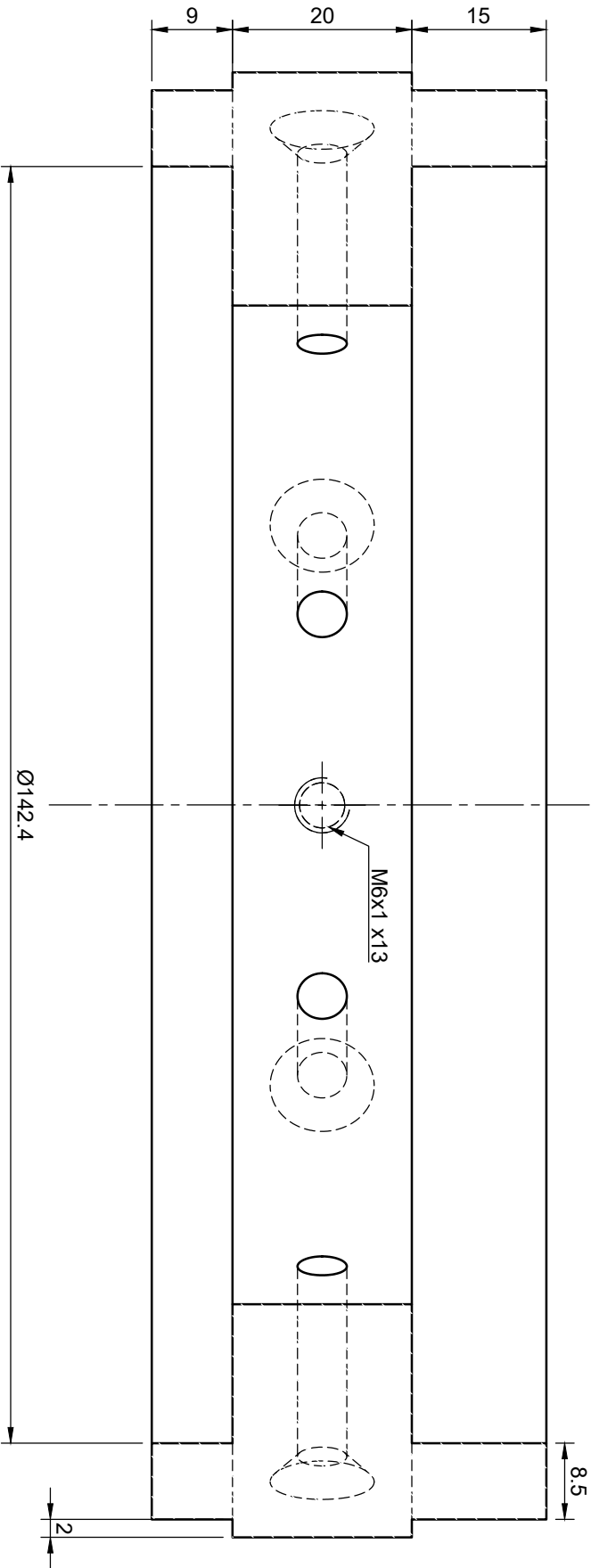


Dept.	Technical reference	Created by	Approved by
Proj. Jupiter	NBR6158 H8f8	Maria E. S. Silva 31/07/2023	Maria Clara Costa 18/03/2024
2:1	Document type	Title	DWG No.
		Macho Padrão 6"	A3
		Rev.	Date of issue
			Sheet
			2/2



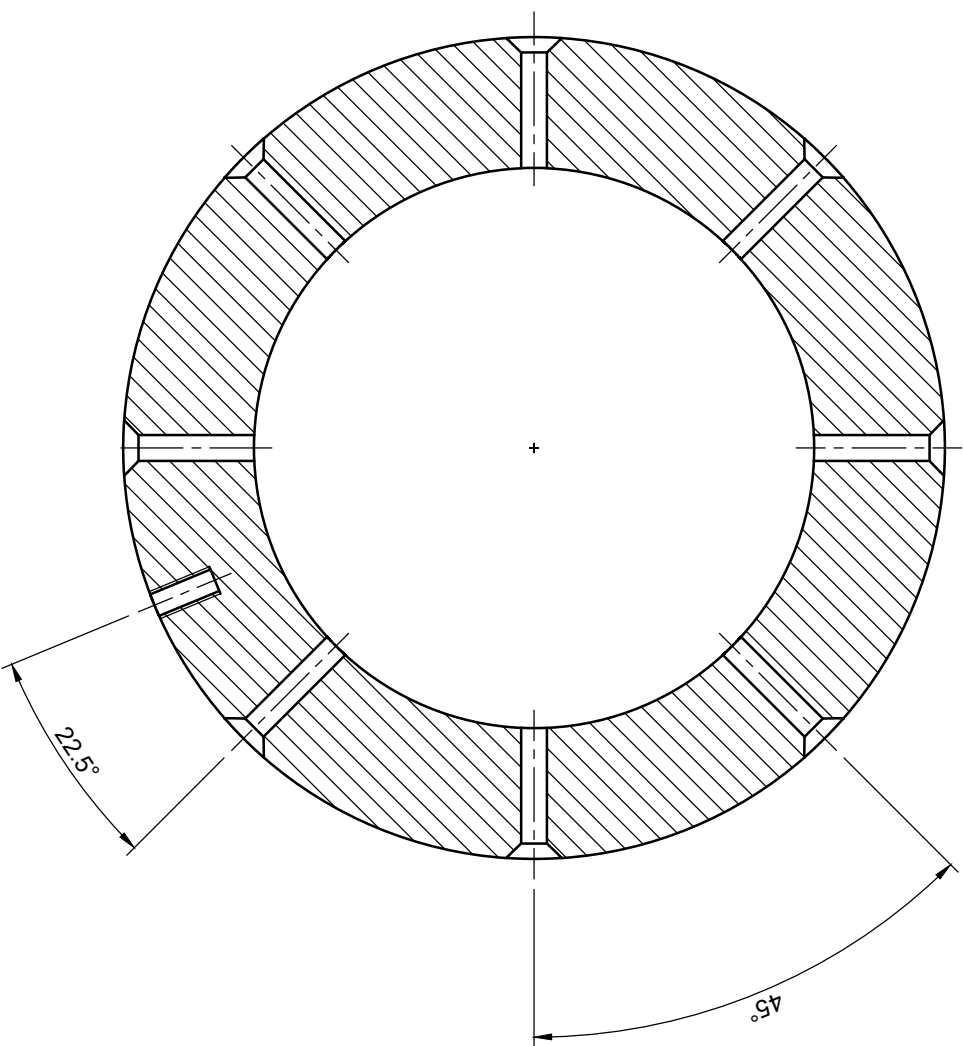
Dept.	Technical reference	Created by	Approved by		
Proj. Jupiter	NBR6158 H8f8	maria clara costa 08/05/2024			
		Document type	Document status		
Title		DWG No.			
Centralizador					
Rev.	Date of issue	Sheet			
		1/3			

A-A (2:1)



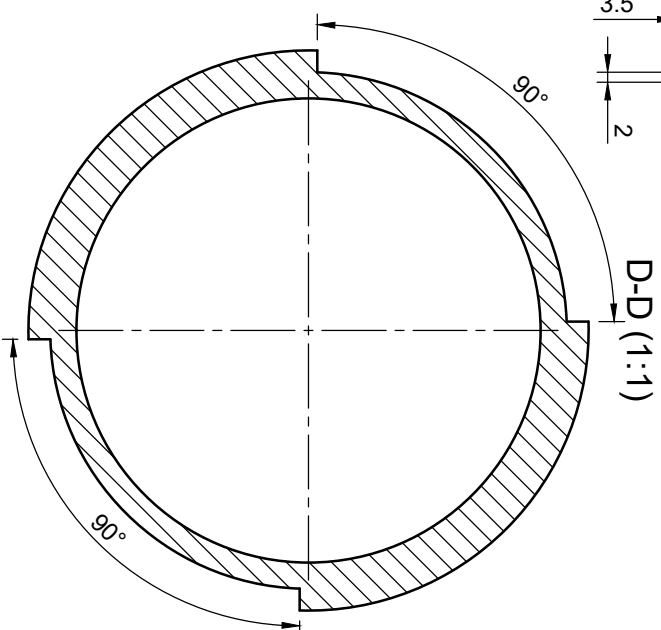
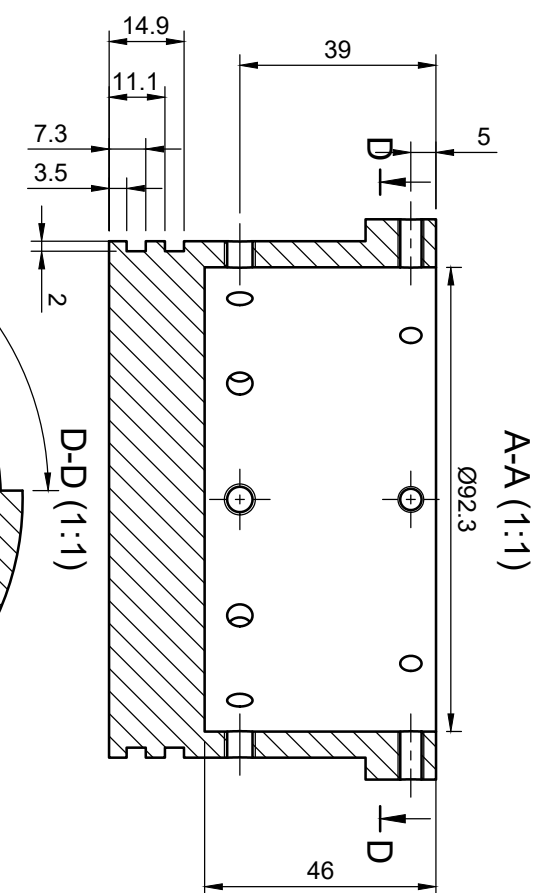
Dept.		Technical reference		Created by		Approved by	
Proj. Jupiter		NBR6158 H8f8		maria clara costa 08/05/2024			
		Document type		Title		DWG No.	
				Centralizador			
				Rev.		Date of issue	
						Sheet	
						2/3	


B-B (1:1)

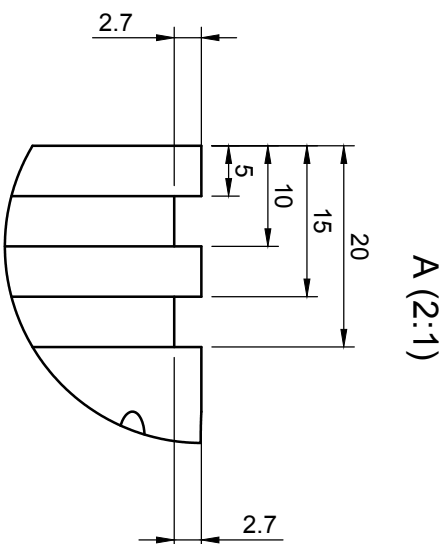
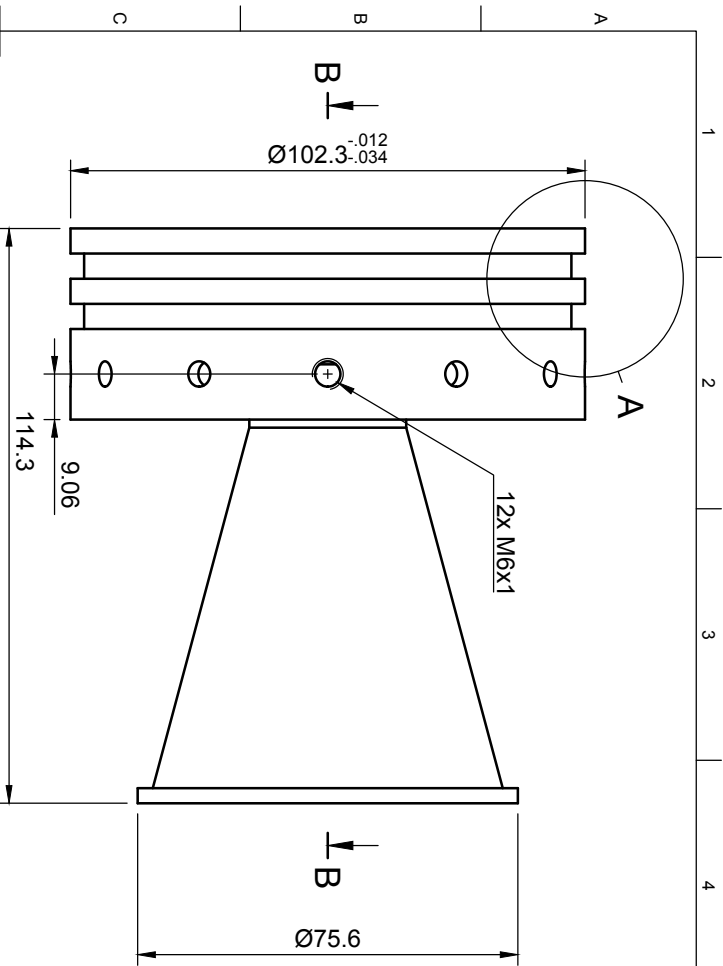


Dept.		Technical reference		Created by		Approved by	
Proj. Jupiter		NBR6158 H8f8		maria clara costa 08/05/2024			
				Document type		Document status	
				Title		DWG No.	
Centralizador							
Rev		Date of issue					
				Sheet		3/3	

width=!,height=!,pages=-,angle=270



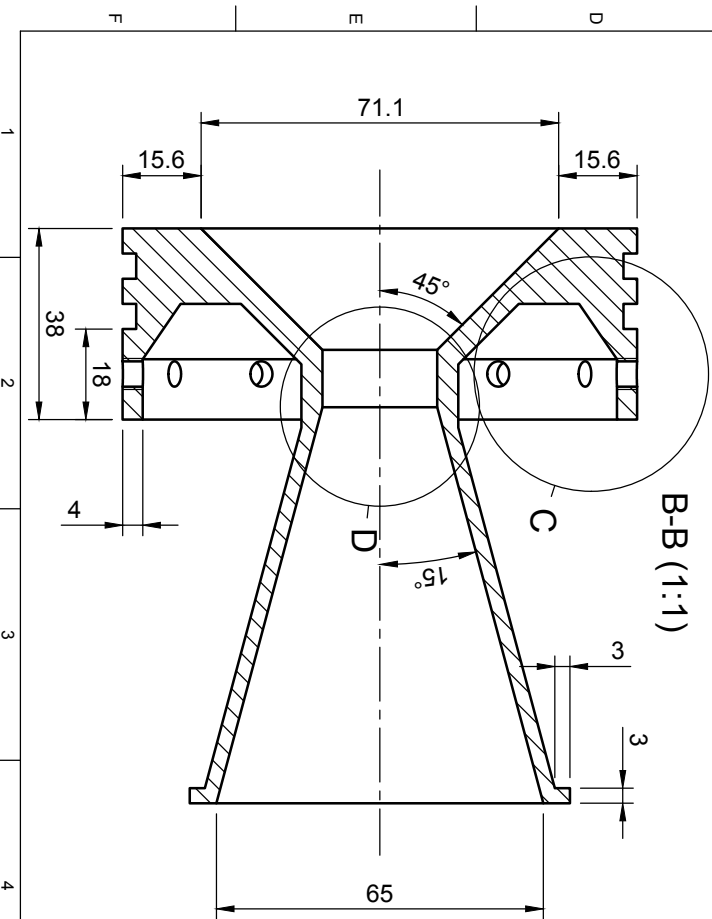
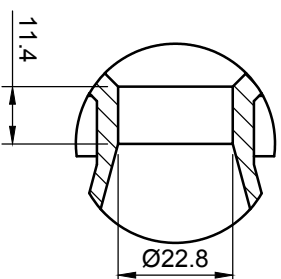
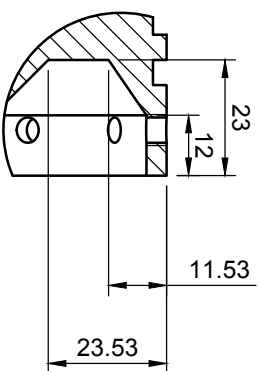
Dept.	Technical reference	Created by	Approved by	
Projeto Jupiter	NBR6158	Gabriel Ribeiro Silvério 04/04/2023		
		Document type	Document status	
		Desenho		
		Title	DWG No.	
Bulkhead Escala 1:1				
Rev.	Date of issue	Sheet		
		1/1		



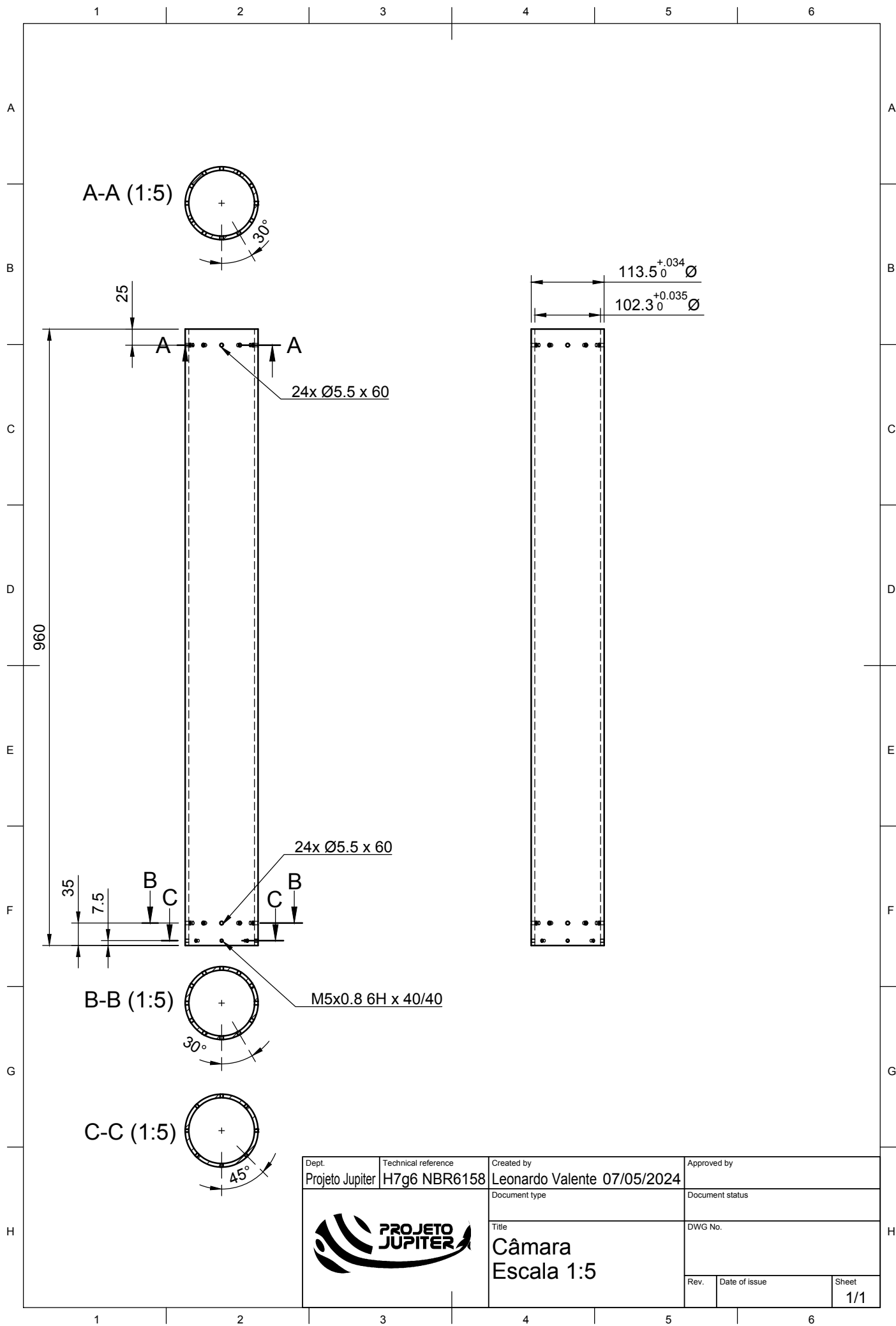
B-B (1:1)


C (1:1)

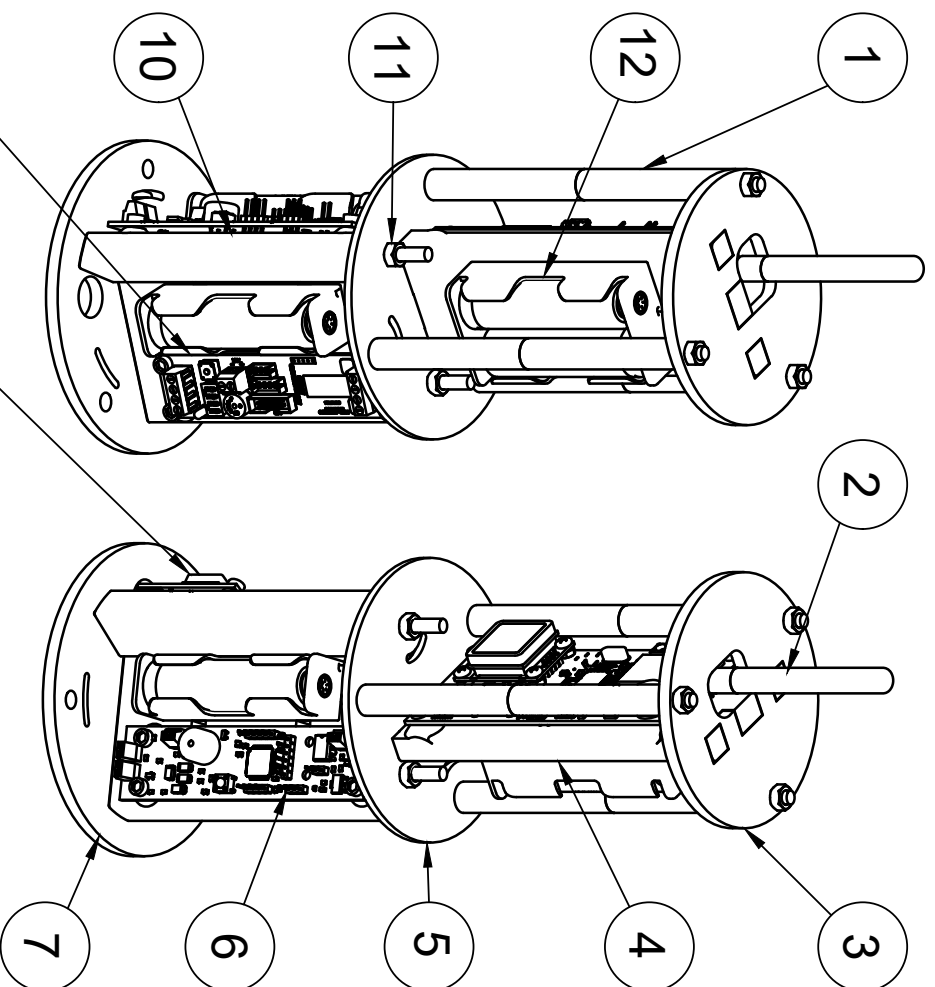
D (1:1)




Dept.	Technical reference	Created by	Approved by
Projeto Júpiter	H7g6 NBR6158	Leonardo Valente 27/03/2024	
	Document type	Document status	
	Title	DWG No.	
	Nozzle aço 1020		
	Aço 1020		
Rev.	Date of issue	Sheet	
		1/1	

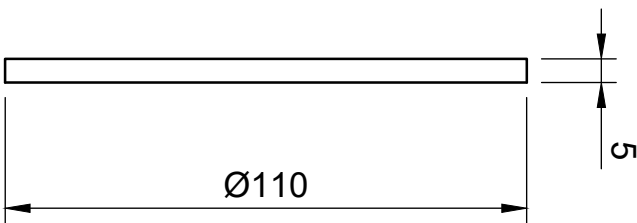
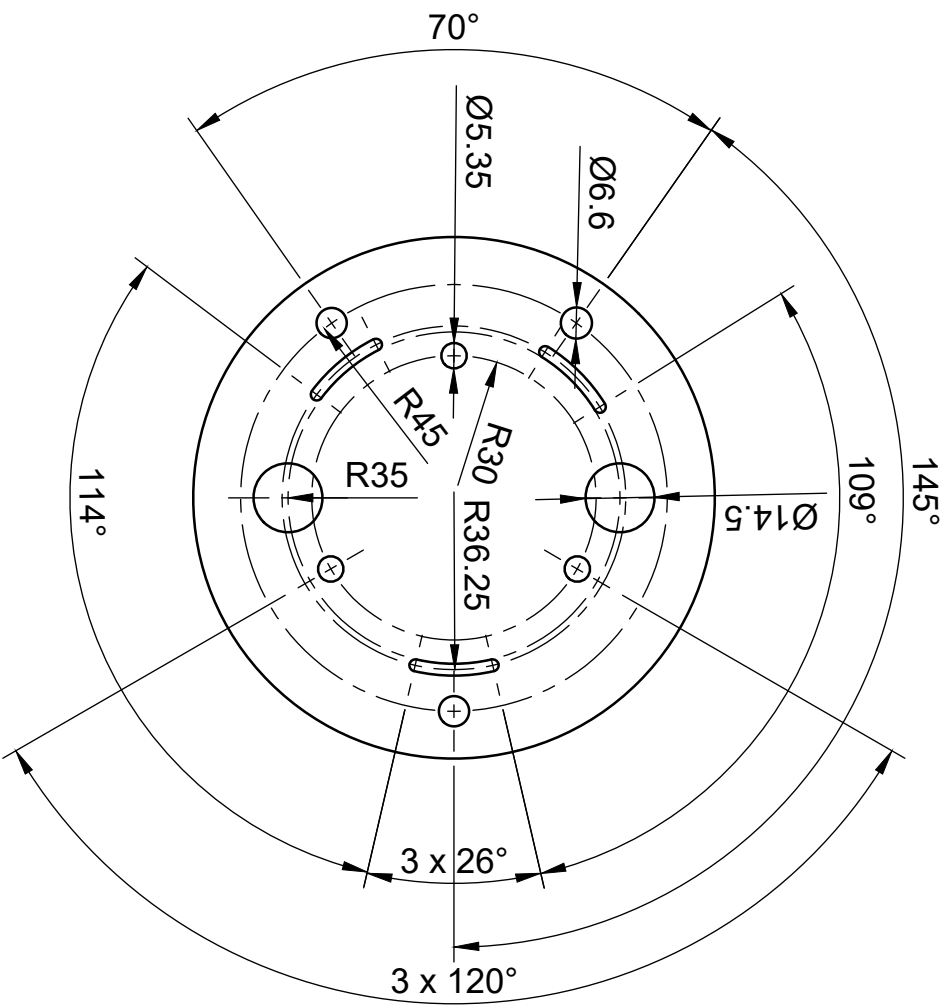


Dept. Projeto Jupiter	Technical reference H7g6 NBR6158	Created by Leonardo Valente 07/05/2024	Approved by
		Document type	Document status
		Title Câmara Escala 1:5	DWG No.
Rev.	Date of issue	Sheet 1/1	



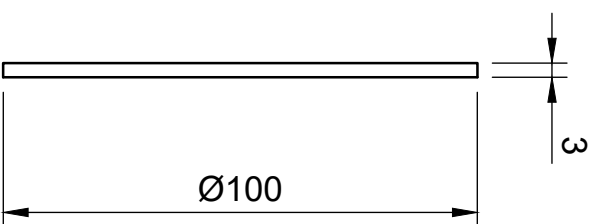
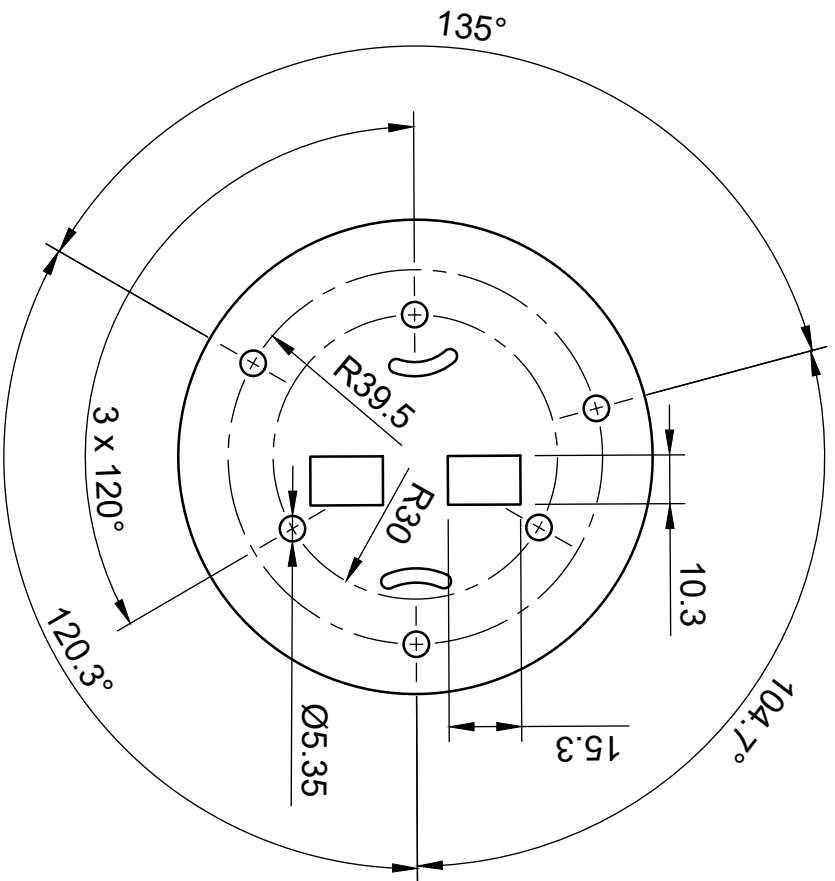
Parts List			
Item	Quantity	Part Namer	Material
1	6	Spacer	PETG
2	1	SRAD Telemetry	-
3	1	Telemetry Top Disk	PETG
4	1	Telemetry Wall	PETG
5	1	Telemetry Base Disk	Aluminum
6	1	SRAD Altimeter	-
7	1	Base Disk	Aluminum
8	1	Featherweight GPS	-
9	1	RRC3	-
10	3	Wall	PETG
11	6	M5x150 Threaded Rod	Steel
12	5	3.7V Li-Ion Battery	-

Dept.	Technical reference	Created by	Approved by
Projeto Jupiter		Soitiro Oura 03/05/2024	Luíza Trindade 08/05/2024
		Document type	Document status
		Drawing	Approved
		Title	DWG No.
Assembly Eletrônica		1	
Rev.	Date of issue	Sheet	
1	03/05/2024	1/1	



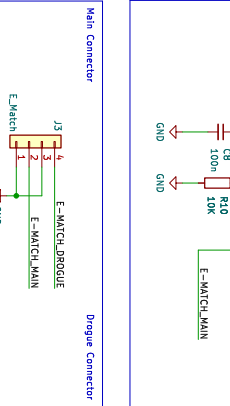
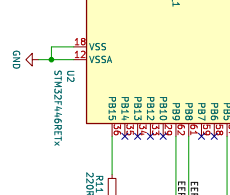
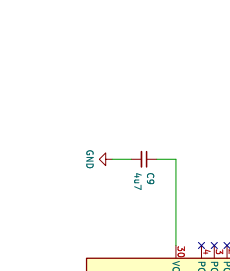
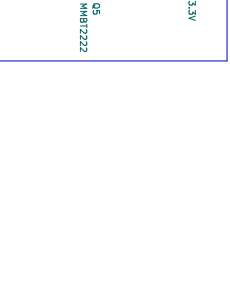
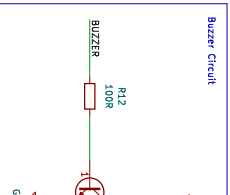
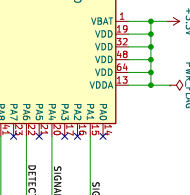
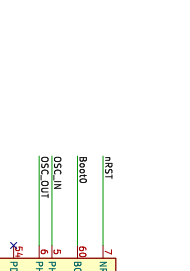
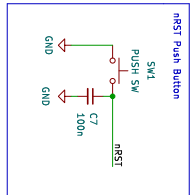
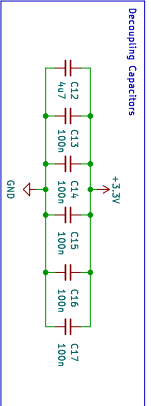
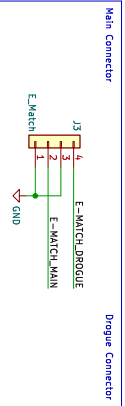
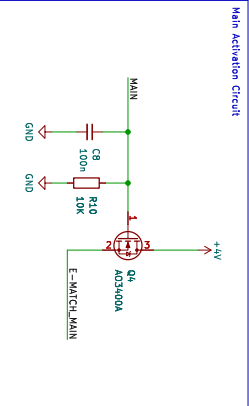
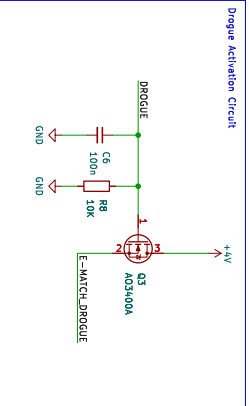
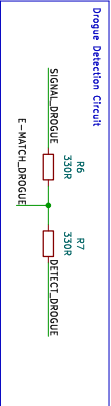
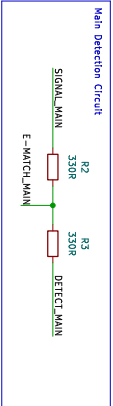
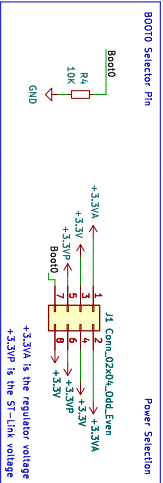
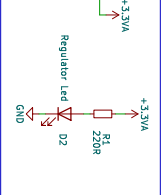
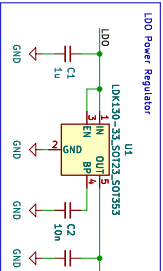
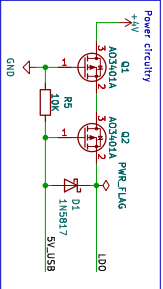
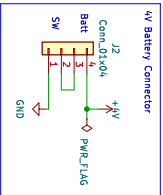
Dept.		Technical reference		Created by		Approved by	
Projeto Jupiter				Solteiro Oura		03/05/2024	
				Document type		Document status	
				Drawing		Under evaluation	
				Title		DWG No.	
				Avionics Bay Base Disk		1	
				Rev.		Date of issue	
				1		03/05/2024	
						Sheet	
						1/1	

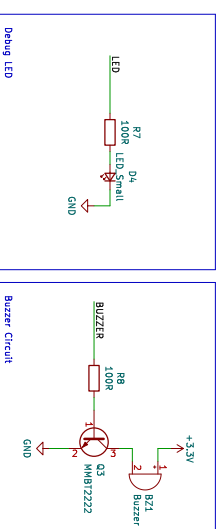
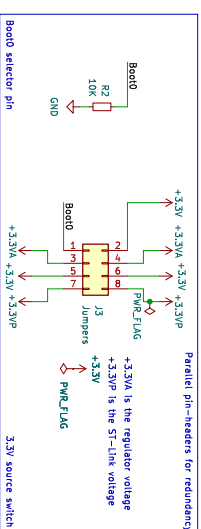
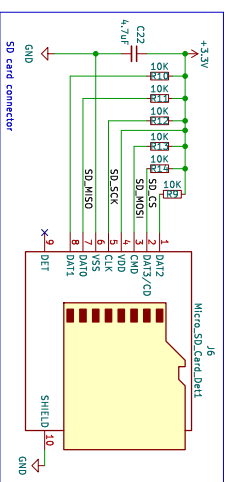
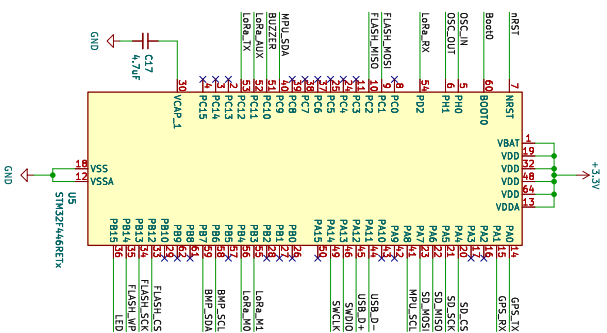
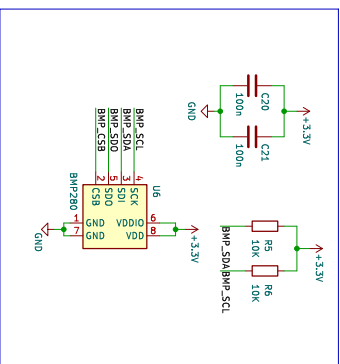
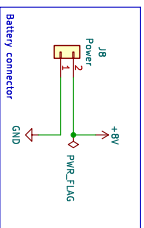
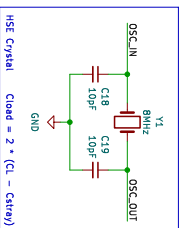
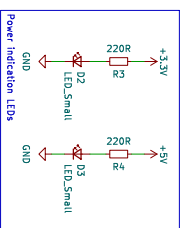
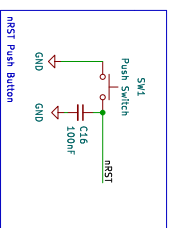
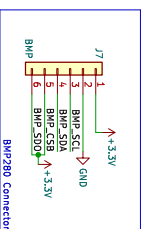
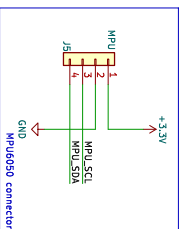
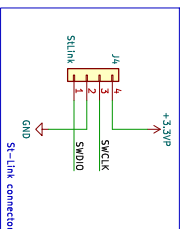
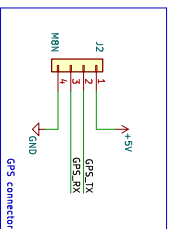
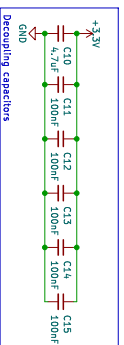
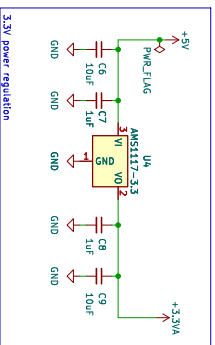
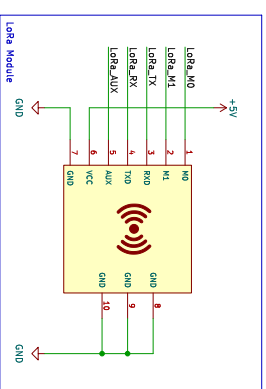
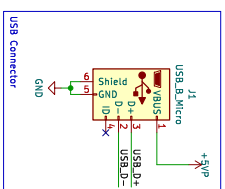
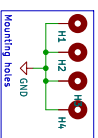
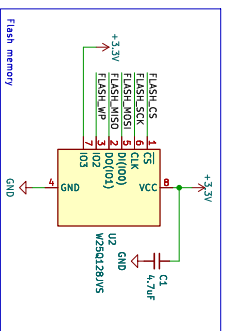
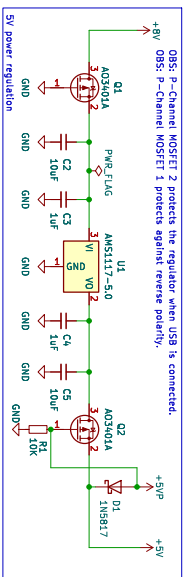


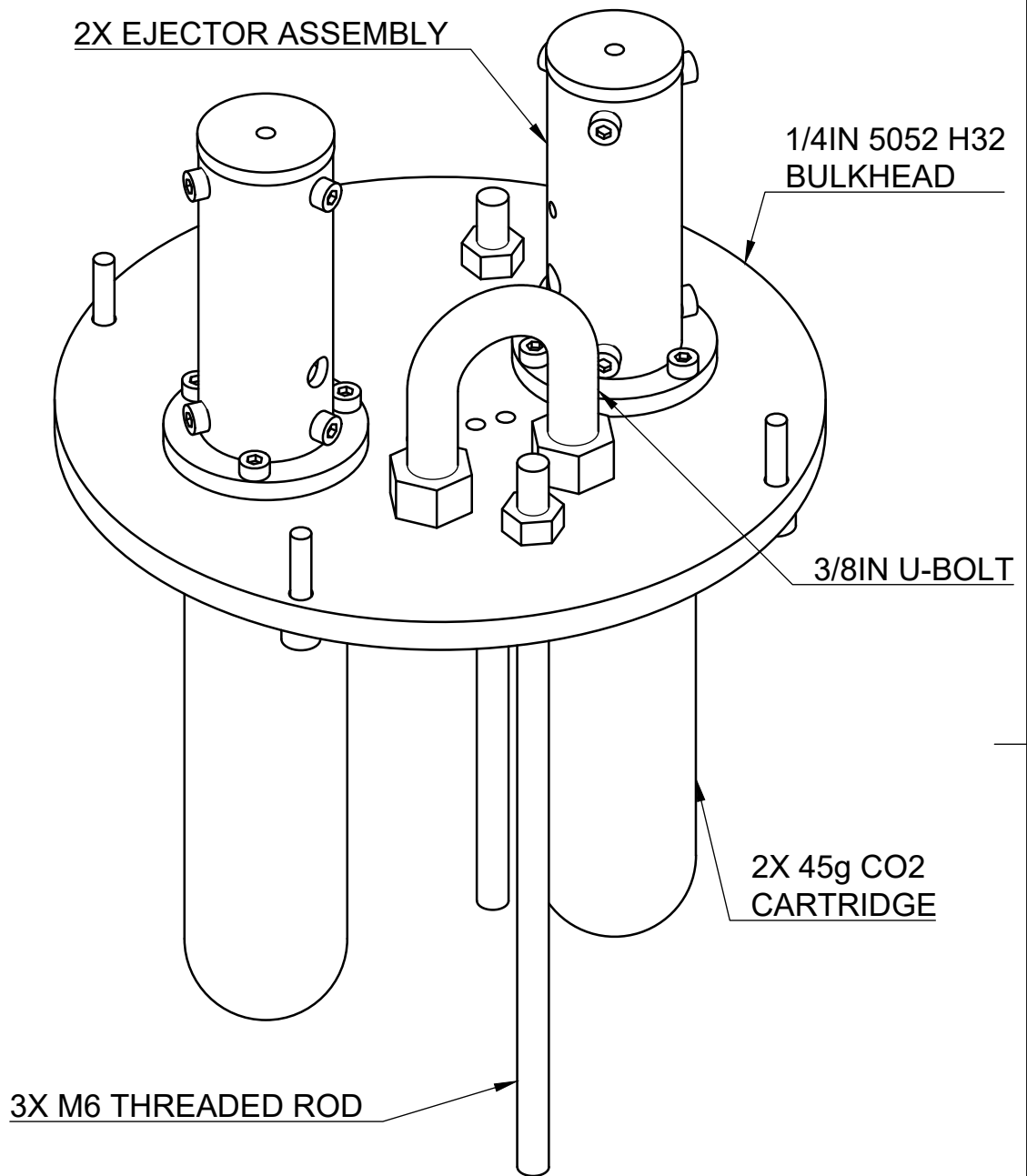


Dept.	Projeto Jupiter	Technical reference	Created by	Soitiro Oura	03/05/2024	Approved by	Arthur Salvador	03/05/2024
			Document type	Drawing		Document status	Under evaluation	
			Title	Disco Base Telemétrico		DWG No.	1	
			Rev.	1	Date of issue		Sheet	1/1

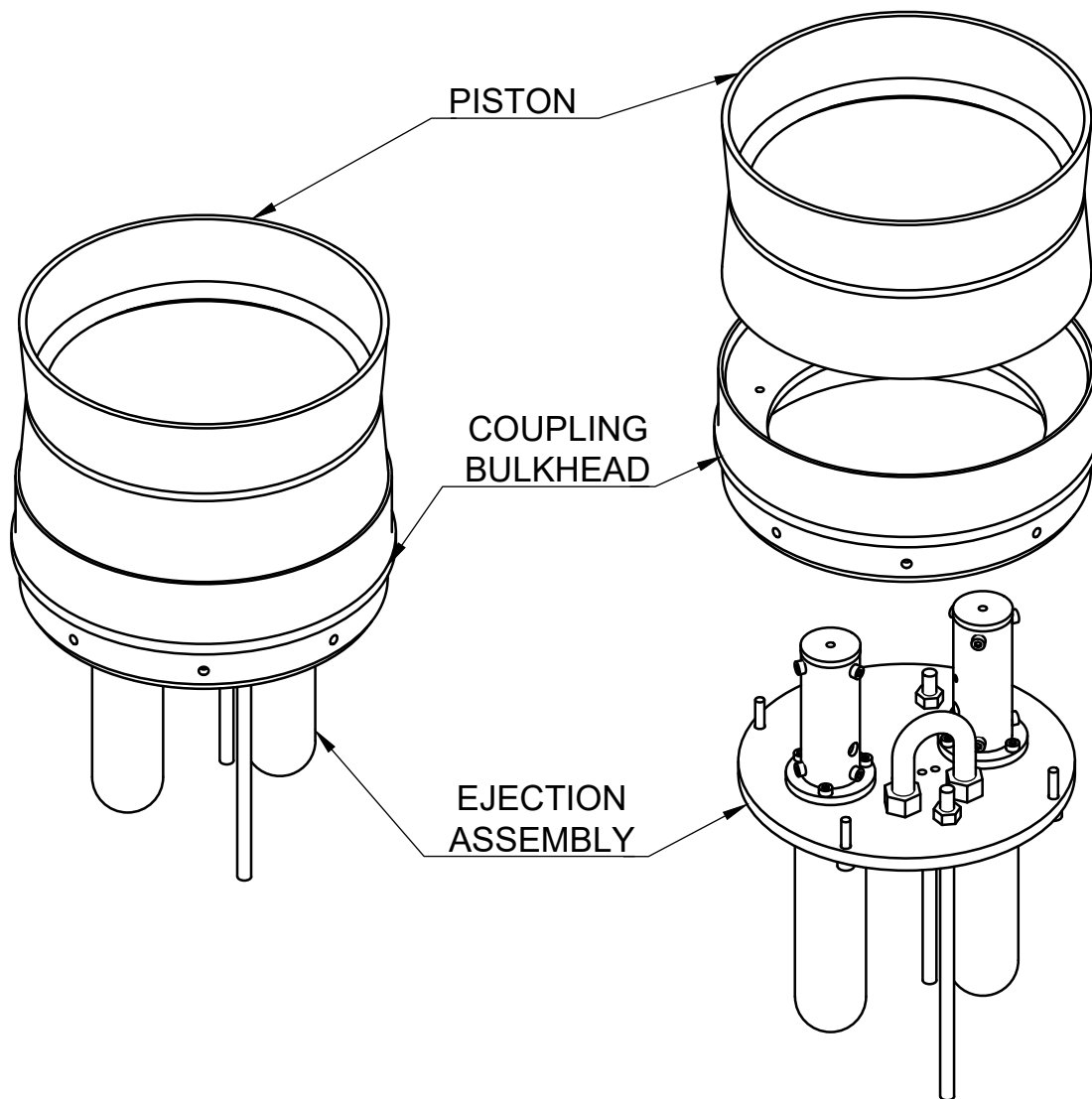




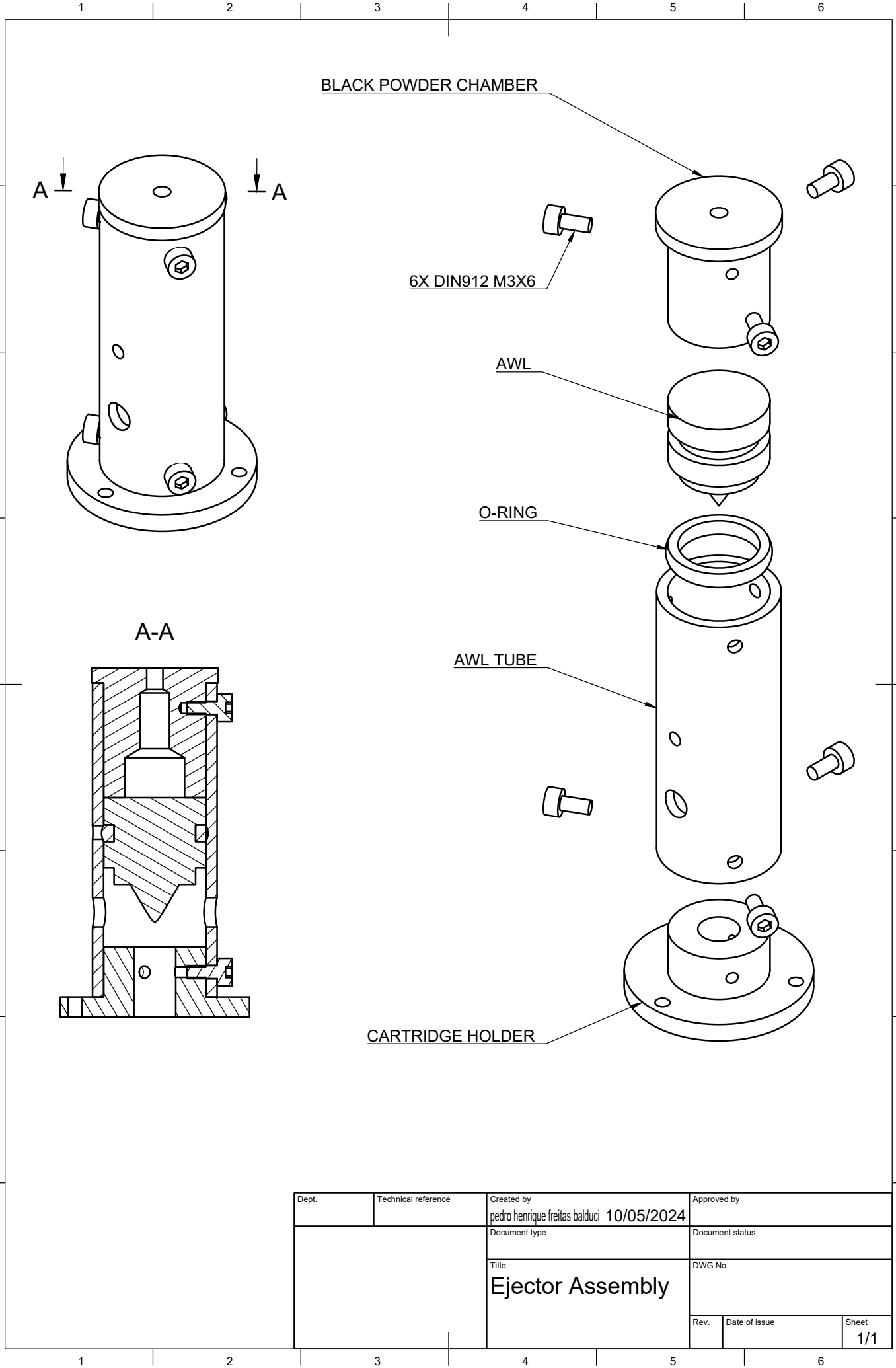




Dept.	Technical reference	Created by pedro henrique freitas balduci 10/05/2024	Approved by		
		Document type	Document status		
		Title Ejection Assembly	DWG No.		
			Rev.	Date of issue	Sheet 1/1



Dept.	Technical reference	Created by pedro henrique freitas balduci 10/05/2024	Approved by	
		Document type	Document status	
		Title Ejection Assembly	DWG No.	
			Rev.	Date of issue
			Sheet 1/1	



Dept.	Technical reference	Created by pedro henrique freitas balduci 10/05/2024	Approved by	
		Document type	Document status	
		Title Ejector Assembly	DWG No.	
			Rev.	Date of issue
			Sheet 1/1	

1 2 3 4 5 6

A A

B B

C C

D D

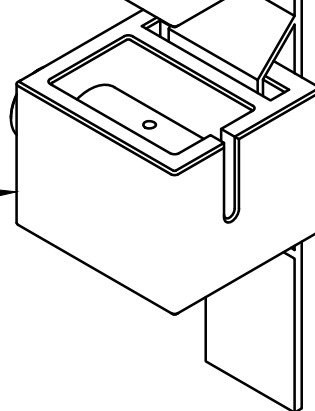
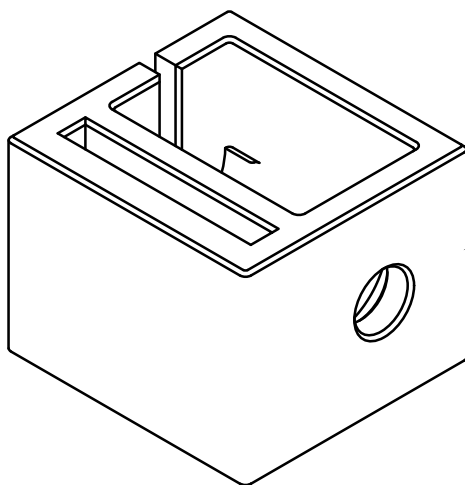
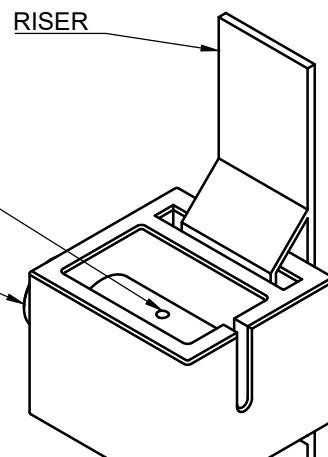
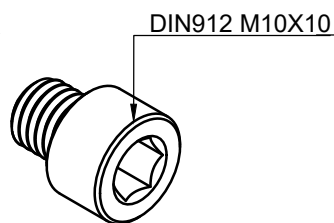
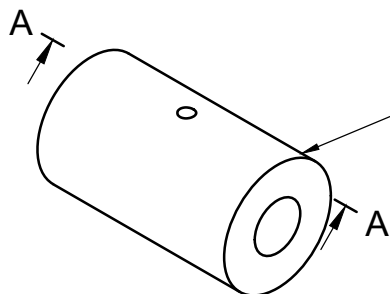
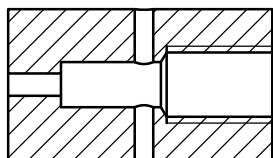
E E

F F

G G

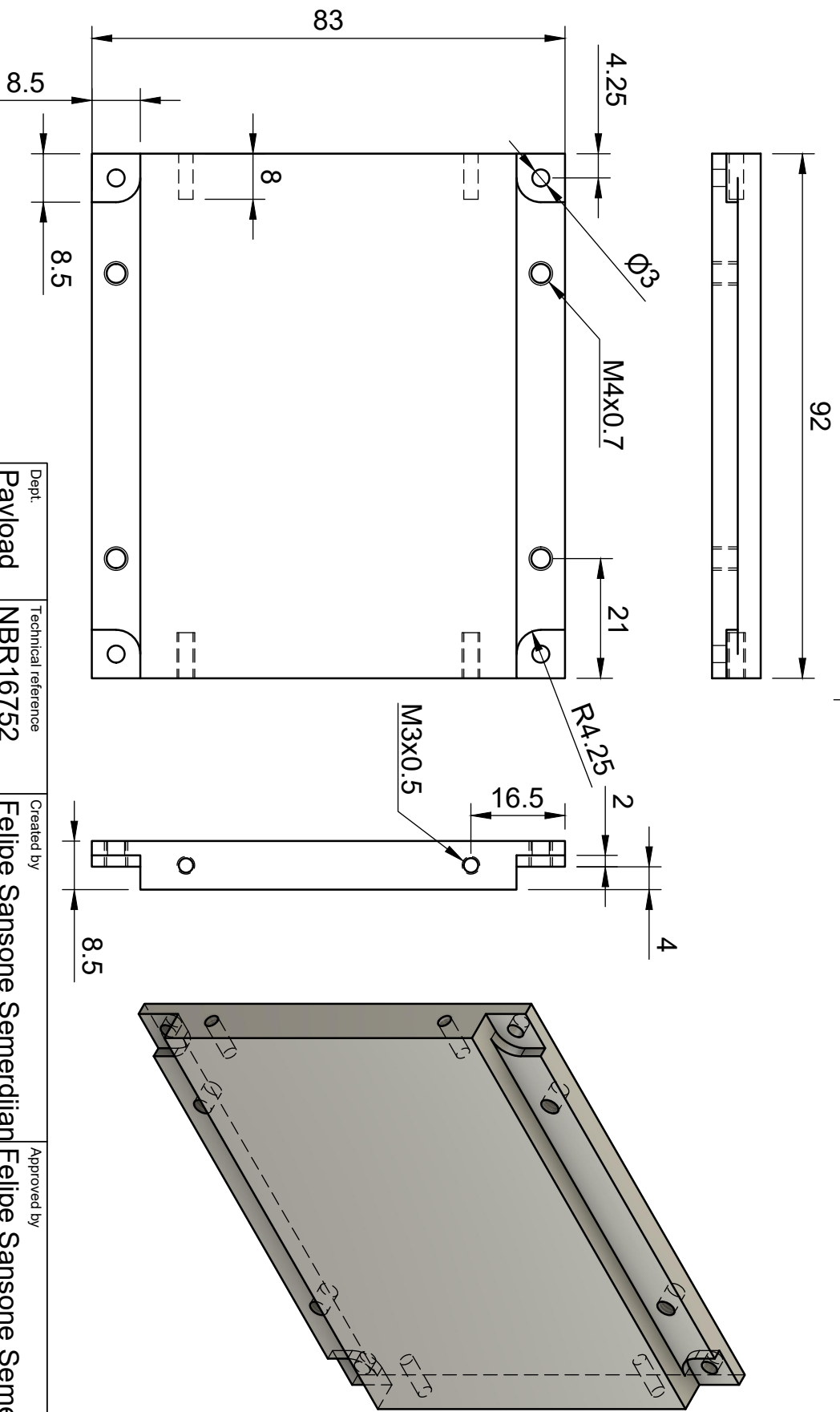
H H

A-A



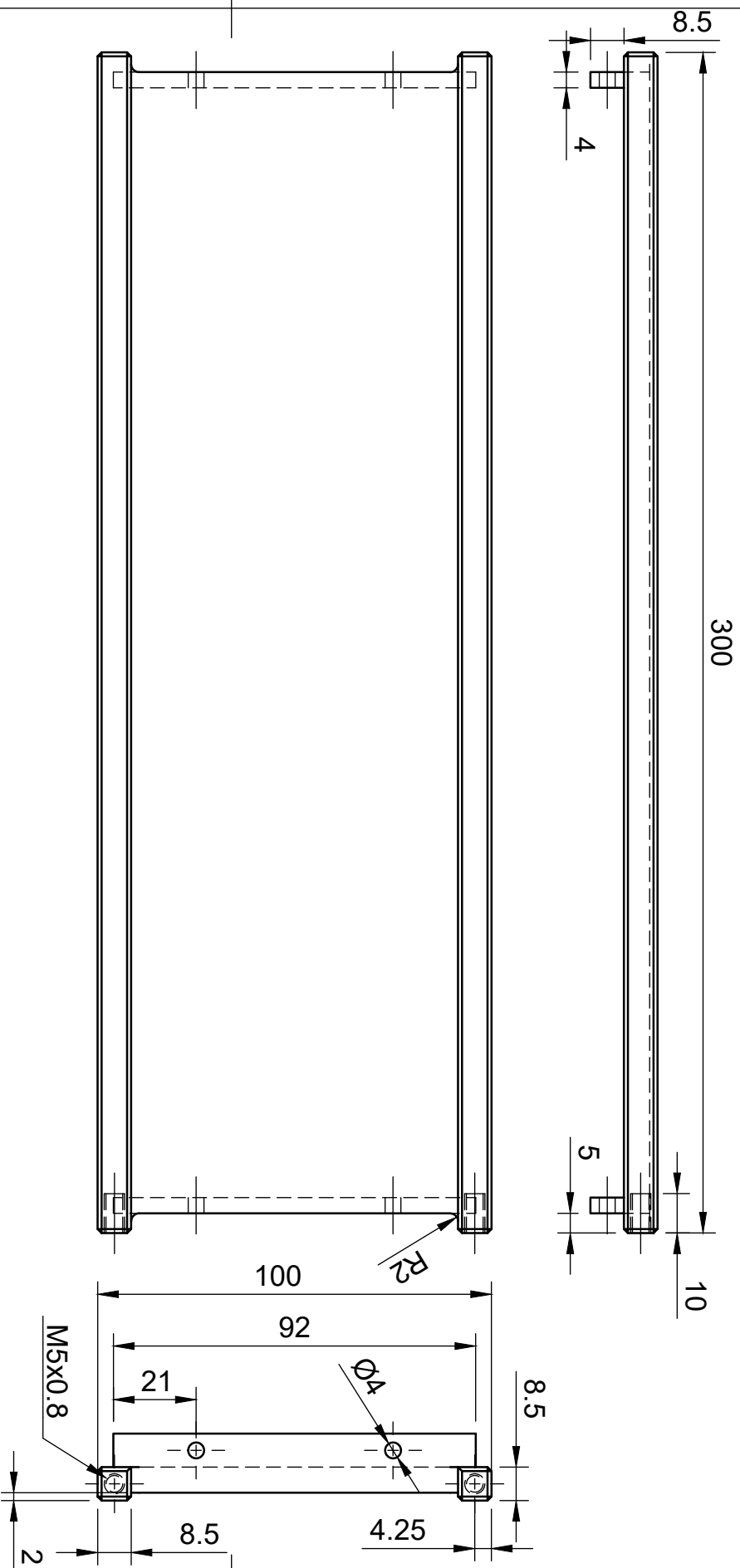
Dept.	Technical reference	Created by pedro henrique freitas balduci 10/05/2024	Approved by	
		Document type	Document status	
		Title Line Cutter	DWG No.	
		Rev.	Date of issue	Sheet 1/1

1 2 3 4 5 6



Dept.	Technical reference	Created by	Approved by
Payload	NBR16752	Felipe Sansone Semerdjian	Felipe Sansone Semerdjian
		Document type	Document status
		Detailed Drawing	Revised
		Title	DWG No.
		Cubesat Base	A4 1:1
		Rev.	Date of issue
		2	04/05/2024
		Sheet	1/1





Dept.	Technical reference	Created by	Approved by
Payload	NBR 16752	Felipe Sansone Semerdjian	Felipe Sansone Semerdjian
		Document type	Document status
		Detailed Drawing	Revised
		Title	DWG No.
		Cubesat Wall	A4 1:1.5
		Rev.	Date of Issue
		2	04/05/2024
		Sheet	1/1



Appendix G

Project Simulations Report

I. Computational Fluid Dynamics Simulations

1. Truncated airfoil

Airfoil profiles are a valuable design resource in fluid dynamics applications due to its capability of increasing the ratio between lift and drag when compared, for instance, to a flat aerodynamic [18]. In the rocket engineering scenario, airfoils are commonly used to enhance fin's [19]. However, the usually sharp trailing edge sets structural disadvantages, since the low thickness areas are more susceptible to chipping and other damages. Furthermore, when it comes to manufacturing, there are limitations of processes and materials that can properly and precisely create the desired airfoil profile. Recent research in the geometry of turbine's fan blades and bicycle frames show that, by cutting out determined portions of the chord – a technique also known as truncating –, the lift/drag ratio can be maintained or even increased within the specific restrictions of each case [5, 6]. Those studies shed light on the matter and have been contributing to applications in other fields of engineering. Even though existing data indicate better performance on truncated airfoils, further studies must be conducted in order to apply the same concept on rocket's fins. This necessity comes from the difference between boundary conditions and flow regimes described in the majority of contemporary documentation and sounding rockets' real flight characteristics. Turbine's fan blades, for example, have a tendency of using asymmetric airfoil designs and work in greater angles of attack; and bicycles are required to perform only in low Reynolds and low velocity conditions. On the other hand, sounding rockets, such as those developed by the team, experience Reynolds number above 1.5 Million, velocities close to Mach 1 and angles of attack below 8 degrees through the most part of its ascent. Therefore, to maximize lift whilst reducing drag and improve fin's performance and manufacturing, we studied the effect of truncating the trailing edge of a NACA0012 airfoil.

Although there is some research on the subject, the literature lacks specific guidelines about how or where to truncate the airfoil. Most studies were made by testing arbitrary chords and simulating its behavior with a CFD software. [6] suggests to change the overall shape of the airfoil in a way that the truncated version would have the same internal area as the original one. However, as this approach makes bigger changes on the design and profile characteristics, and was tested only for asymmetric airfoils, we decided to start the fin's optimization process with the simplest method, firstly expanding the basic knowledge on the matter in order to further develop this research in the future. Thus, for the purpose of this study, a standard e NACA0012 airfoil – as it is the profile used in our rocket – was truncated at 60%, 80% and 90% of the chord, following the most commonly used and documented procedure in the bibliography [6, 7].

Airfoils performance analysis was obtained with two-dimensional simulations in Ansys Fluent. We created a C shape, structured mesh with a geometry of 20 chords length and 20 chords height, on the rectangular section, and 20 chords diameter on the circular section in order to avoid domain's wall interference on the results. The mesh size varied between 250 thousand and 400 thousand elements according to the need for more or less cells to describe each airfoil's intricate parts and flow's turbulent regions. We also configured bias settings to have a denser mesh near the airfoil without increasing too much the computational cost.

The first step was to simulate a standard NACA0012 with variable angle of attack and compare the results with experimental data found in [20] for the purpose of validating our simulation model and understanding how well it matched real data. After testing different configurations, we established a k-omega optimal model operating at a compressible, subsonic and turbulent regime, as the rocket's real predicted flight conditions. The lift results proved to be reliable for angles of attack between 0 and 6 degrees, whereas, for drag, the results were accurate only from 0 to 2 degrees, since, in greater angles, limitations appear due to the low ability of steady state simulations to capture flow separation and recirculation [21].

Table 36 CFD model validation results.

NACA0012 (CFD)		Experimental data		Error	
Cd	Cl	Cd	Cl	Cd	Cl
0.0103	-0.0002	0.0102	0.0000	0.64%	–
0.0109	0.3289	0.0103	0.3300	6.23%	0.34%
0.0197	0.6203	0.0111	0.6520	77.46%	4.86%
0.0463	0.6838	0.0120	0.9730	285.59%	29.73%

The next step was to replicate the same simulation model on each truncated airfoil on the angle of attack interval aforementioned and compare the results with the standard NACA0012. The Lift Coefficient (Cl) and Drag Coefficient

(Cd) ratio was used as the main evaluation criteria, considering both parameters must be weighted to achieve stabilization and flight performance enhancement. For example, an increase in Cd alone is a setback to fin's geometry, but, when accompanied by an increase in Cl, it might show better overall results, given that proportionally smaller fins or even less fins can replicate the aerodynamic behavior of the original design.

The results showed that truncating the NACA0012 airfoil in the conditions proposed – compressible, subsonic, turbulent flow at low angles of attack –, would only increase the Cd and reduce the Cl, which may not be the ideal choice at a first analysis. Yet, the truncation at 90%, in which only the last 10% of the chord length was cut out of the body, can achieve the goals of being an easier to manufacture, sturdier and safer surface with a negligible aerodynamic penalty. Therefore, that was the best profile choice for the team's rocket fins airfoil, in order to avoid chipping and other damages that could have a worse and uneven aerodynamic impact. Following this research, our desire is to expand this evaluation using different criteria of truncating such as the one mentioned in [6]. It would also be interesting to test different airfoils and, most importantly, experimentally validate the results.

The following images show some of the results obtained. NACA0012 images are placed on the left and the 90% truncated airfoil on the right.

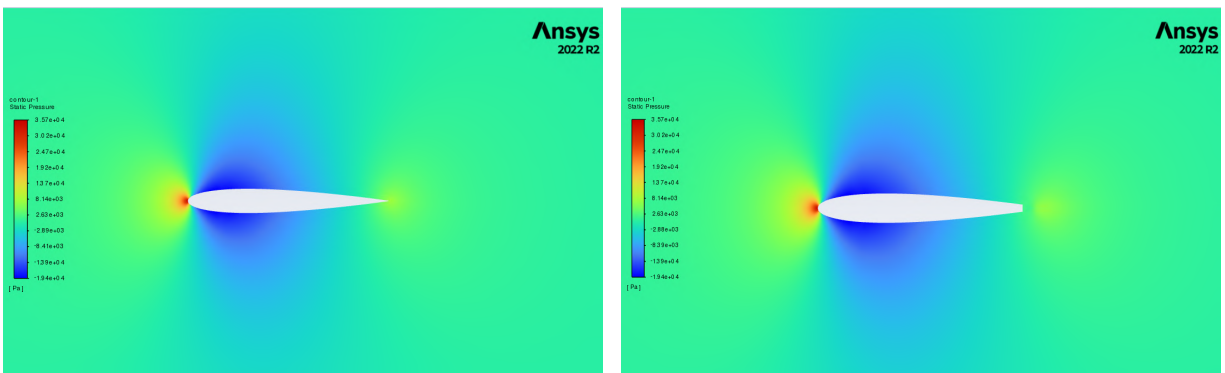


Fig. 96 Static pressure comparison at 0° angle of attack.

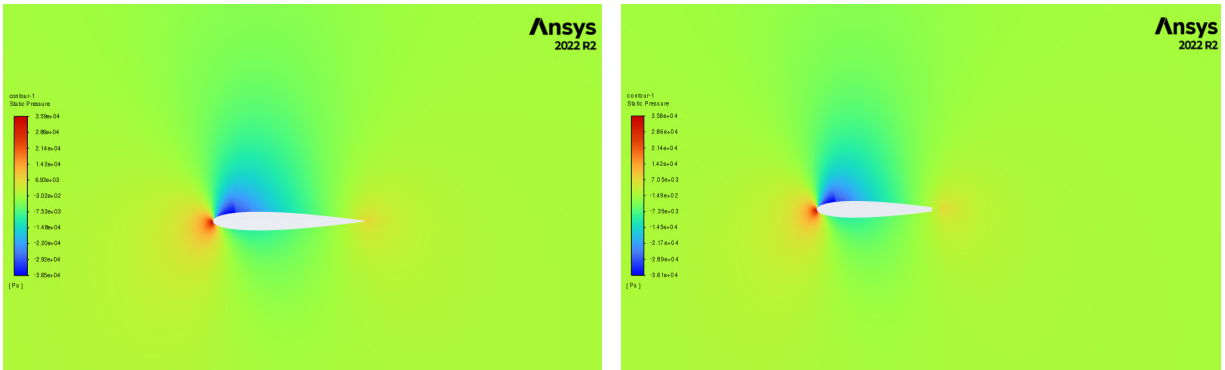


Fig. 97 Static pressure comparison at 2° angle of attack.

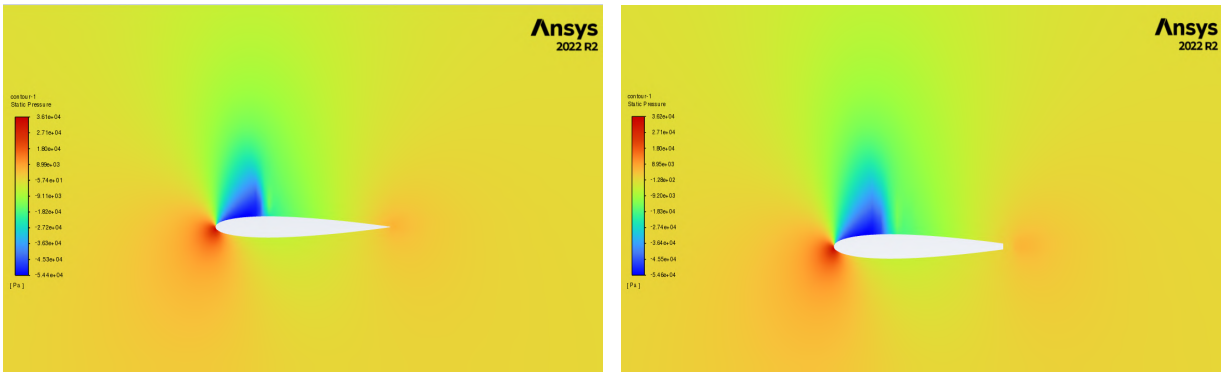


Fig. 98 Static pressure comparison at 4° angle of attack.

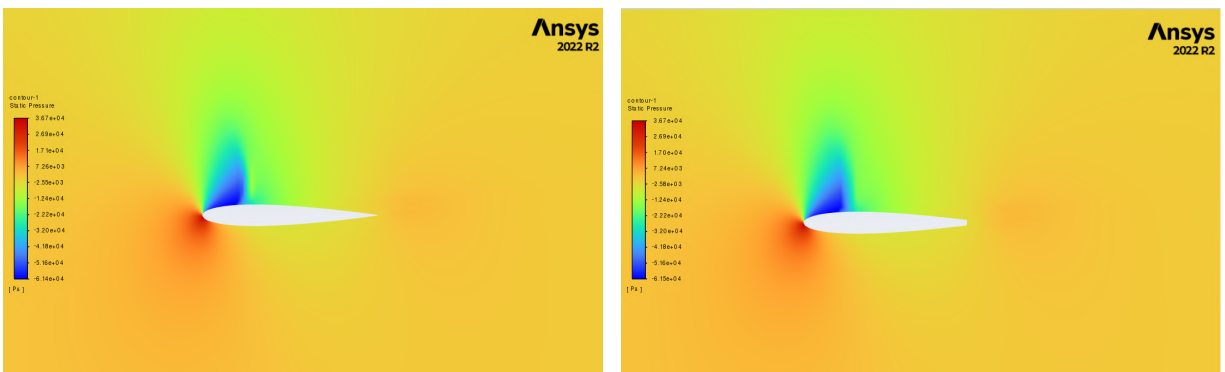


Fig. 99 Static pressure comparison at 6° angle of attack.

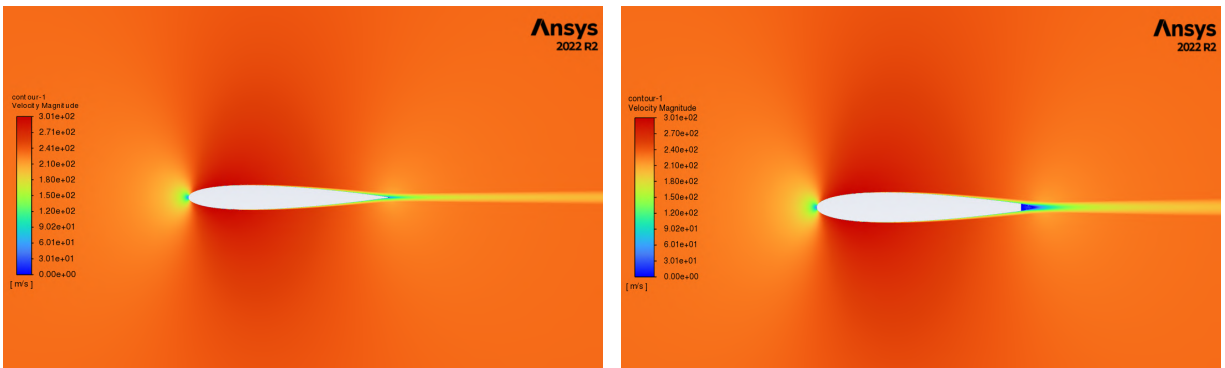


Fig. 100 Velocity comparison at 0° angle of attack.

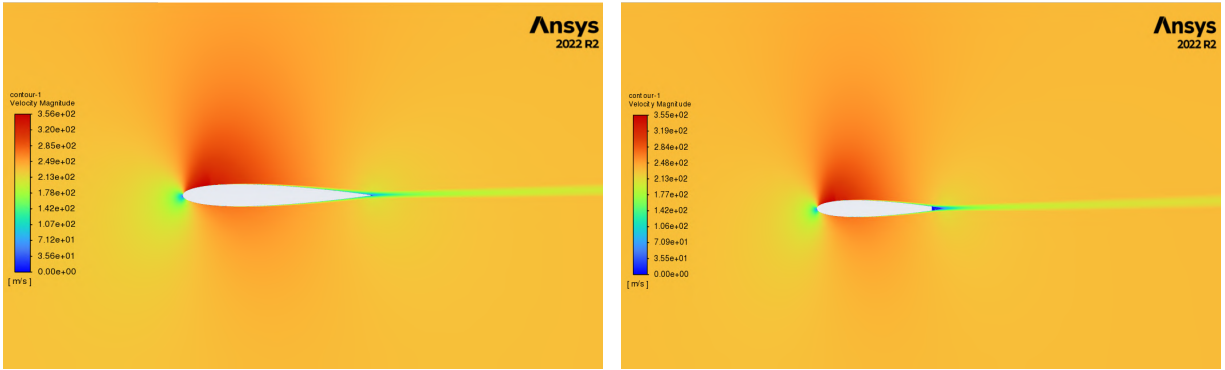


Fig. 101 Velocity comparison at 2° angle of attack.

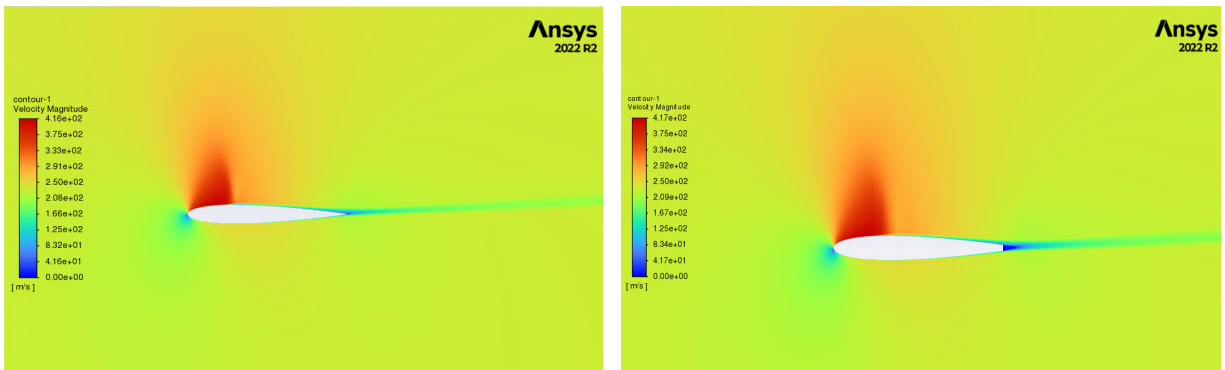


Fig. 102 Velocity comparison at 4° angle of attack.

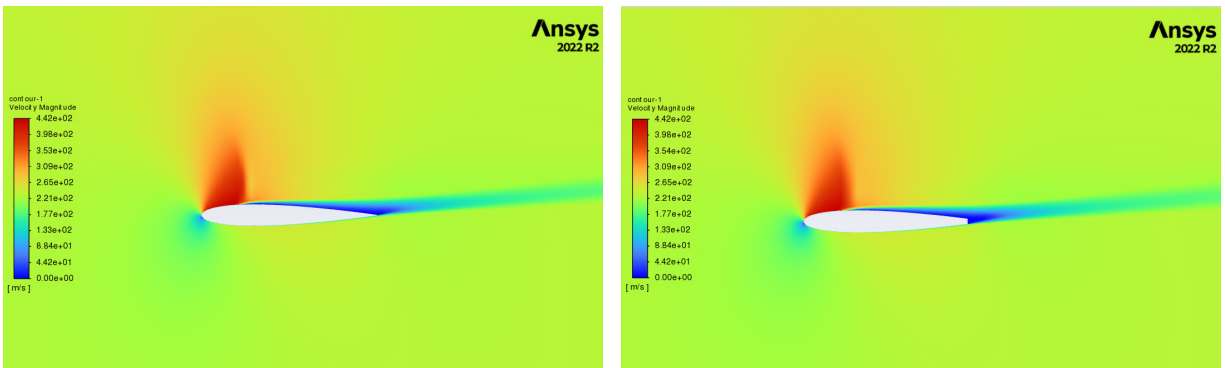


Fig. 103 Velocity comparison at 6° angle of attack.

II. Opening parachute force simulation

A. Structural Simulations

As explained in the ejection and section, the parachute is attached to the rocket through two risers attached to U-Bolts: one that is connected to the nosecone by the ejection system's bulkhead, and one that is connected to the rest of the rocket by another bulkhead, and to assure both disks will withstand the parachute's opening forces, the team made simulations using Ansys Static Structural. The team used the maximum forces calculated for each disk, as explained in

the parachute topic. Therefore, the value of forces used are: $2177N$ for the aft section's bulkhead and $894 N$ for the nosecone bulkhead. Each force was applied to the rounded U-Bolt surface. Its direction was perpendicular and opposite from the disks.

To ensure the simulation is more faithful to reality, the assembly contains in addition to the bulkhead and the u-bolt, the coupler of the recovery module and the nosecone, which is considered fixed for the simulation.

1. Fore Section Bulkhead

Simulations for the ejection disk using a $2177N$ force

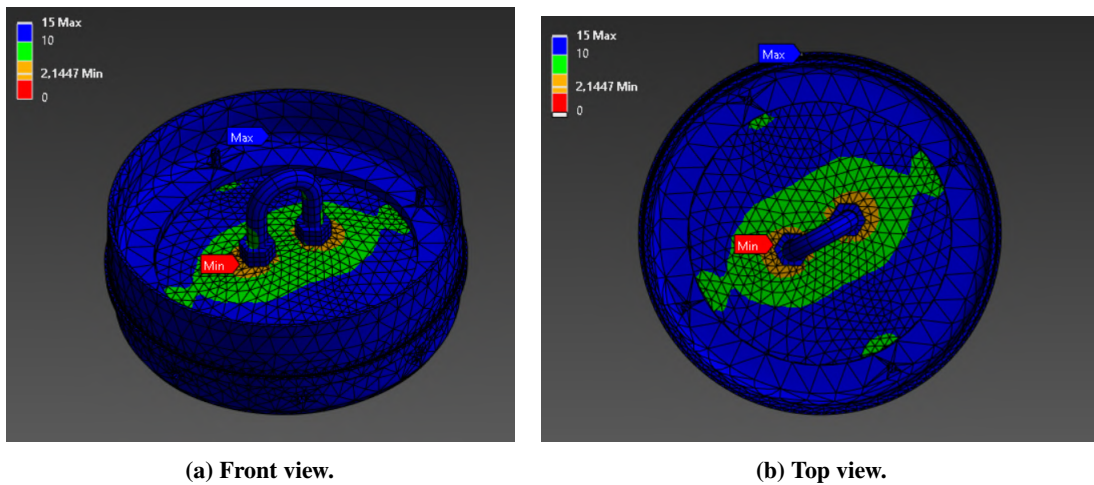


Fig. 104 Ejection disk simulations.

Minimum Safety Factor = 2.14

2. Aft Section Bulkhead

Simulations for the nosecone disk using a $849 N$ force

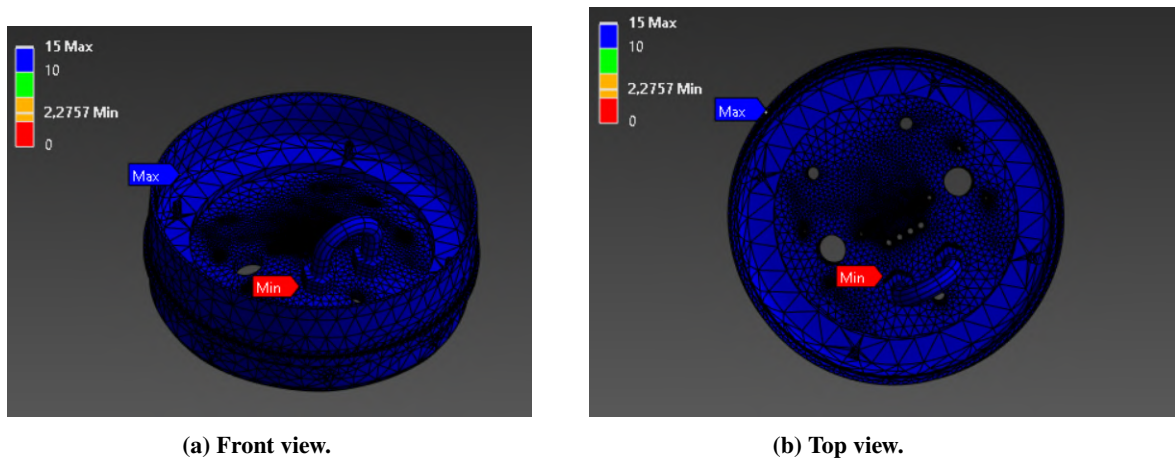


Fig. 105 Nosecone disk simulations.

Minimum Safety Factor = 2.27

Therefore, the team concludes that the bulkheads will withstand the forces without problems.

III. Apogee Detection Simulation

A. Simulation

To embed the *SRAD* altimeter algorithm as a viable detector of apogee, a flight simulation was executed using RocketPy and its pressure curve was used to simulate the performance of the detection algorithm. In order to simulate the sensor noise, Gaussian Correlated Noise was added to the original data, with parameters such as correlation and variance being measured in the real sensor (BMP280 barometer).

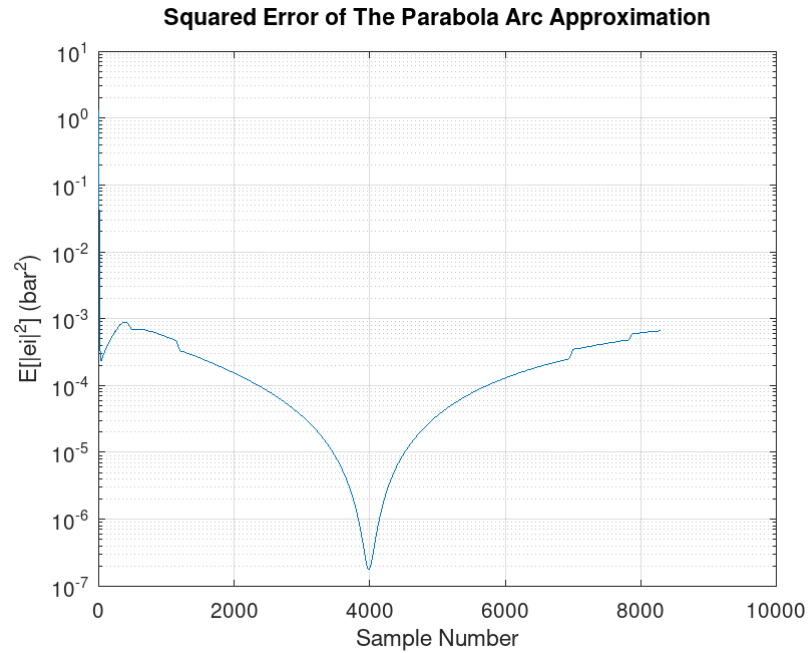


Fig. 106 Squared error of the parabola arc approximation.

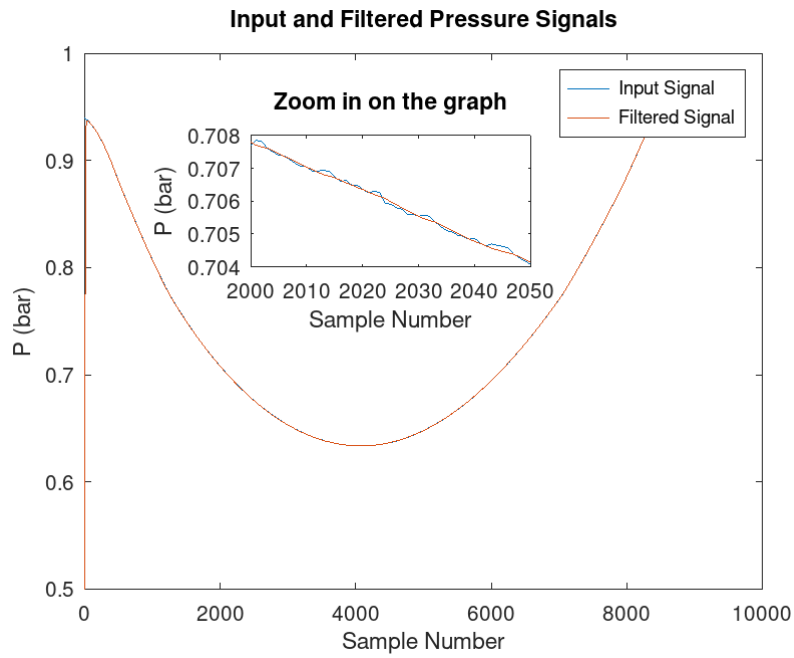


Fig. 107 Input and filtered pressure signals.

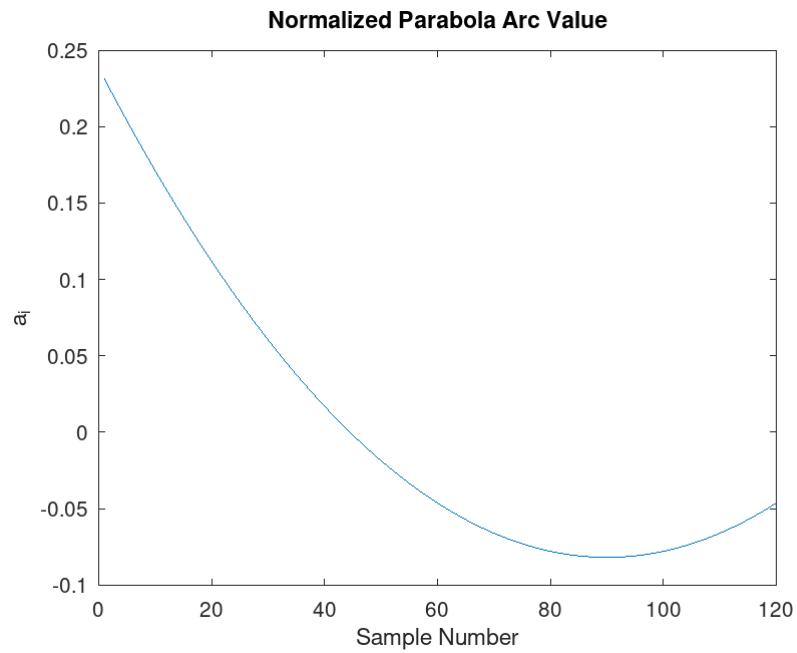


Fig. 108 Normalized parabola arc value.

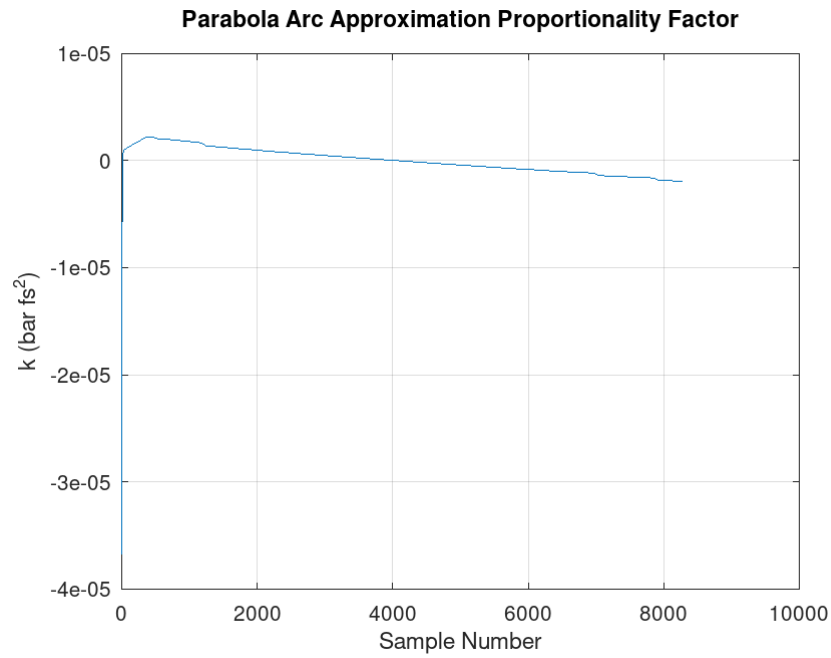


Fig. 109 Parabola arc approximation proportionality factor.

This simulation was performed with 10^3 pressure curves with different random noises and in every situation the apogee was correctly detected. Hence it is possible to conclude that the algorithm is a viable solution for detecting the Pacifico's apogee.

IV. 6DOF Flight Simulation with RocketPy

Pacifico Simulation

Setting Up a Simulation

Creating an Environment for Spaceport America

The `Environment` class is used to define the atmosphere, the winds, and the gravity models.

You can find more information about the `Environment` class in the [Environment Class Usage Docs](#).

```
env = Environment(latitude=32.990254, longitude=-106.974998,  
elevation=1400)
```

To get weather data from the GFS forecast, available online, we run the following lines.

First, we set tomorrow's date.

```
import datetime  
import inspect  
import traceback  
import warnings  
  
import matplotlib.pyplot as plt  
import numpy as np  
from scipy.integrate import solve_ivp  
  
tomorrow = datetime.date.today() + datetime.timedelta(days=1)  
  
env.set_date(  
    (2024, 5, 21, 12)  
) # Hour given in UTC time  
  
env.set_atmospheric_model(type="custom_atmosphere",  
    pressure=None, #Surface Pressure: 853.76 hPa  
    temperature=300,  
    wind_u=[(0,4.73), (5000,4.73)],  
    wind_v=[(0,-4.73), (5000,-4.73)],  
)  
  
#env.set_atmospheric_model(type="Forecast", file = "GFS")
```

Then, we tell env to use a GFS forecast to get the atmospheric conditions for flight.

Don't mind the warning, it just means that not all variables, such as wind speed or atmospheric temperature, are available at all altitudes given by the forecast.

We can see what the weather will look like by calling the info method!

```
env.all_info()
```

Gravity Details

Acceleration of gravity at surface level: 9.7913 m/s²
Acceleration of gravity at 5.000 km (ASL): 9.7802 m/s²

Launch Site Details

Launch Date: 2024-05-21 12:00:00 UTC
Launch Site Latitude: 32.99025°
Launch Site Longitude: -106.97500°
Reference Datum: SIRGAS2000
Launch Site UTM coordinates: 315468.64 W 3651938.65 N
Launch Site UTM zone: 13S
Launch Site Surface Elevation: 1400.0 m

Atmospheric Model Details

Atmospheric Model Type: custom_atmosphere
custom_atmosphere Maximum Height: 5.000 km

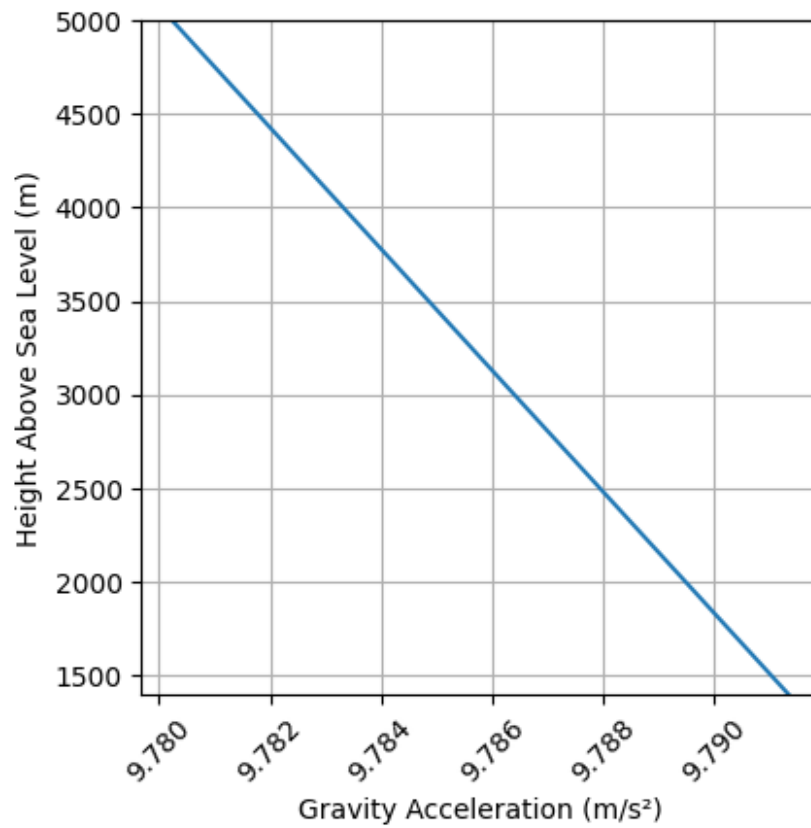
Surface Atmospheric Conditions

Surface Wind Speed: 6.69 m/s
Surface Wind Direction: 315.00°
Surface Wind Heading: 135.00°
Surface Pressure: 856.02 hPa
Surface Temperature: 300.00 K
Surface Air Density: 0.994 kg/m³
Surface Speed of Sound: 347.22 m/s

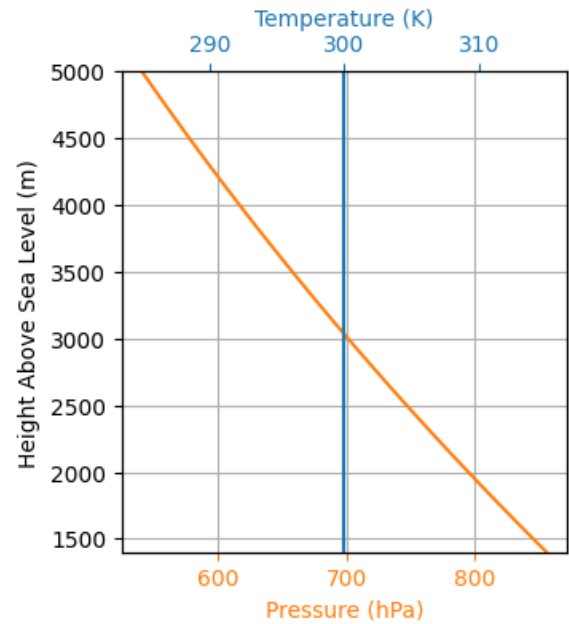
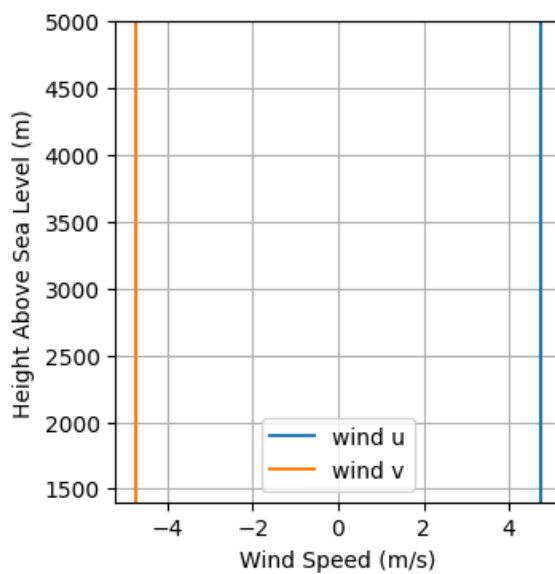
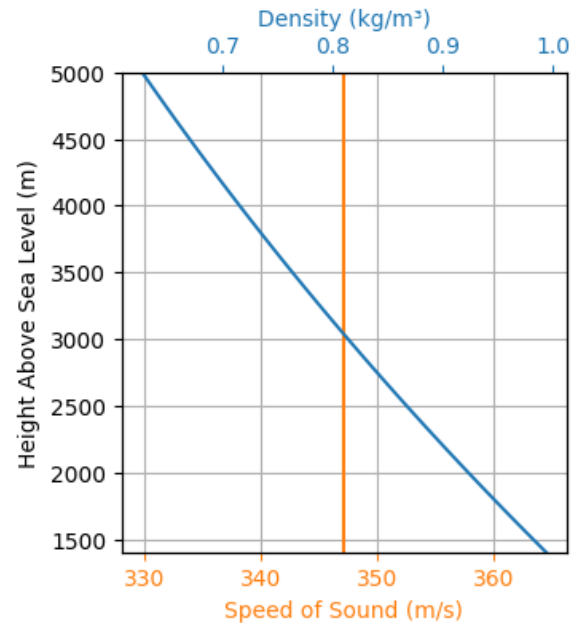
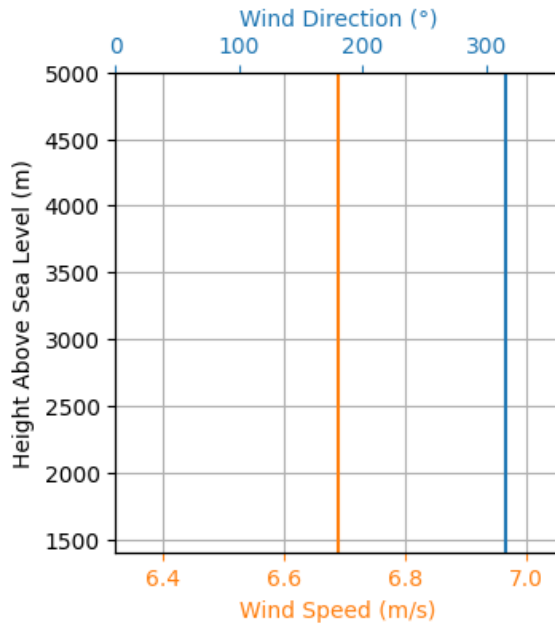
Earth Model Details

Earth Radius at Launch site: 6371.83 km
Semi-major Axis: 6378.14 km
Semi-minor Axis: 6356.75 km
Flattening: 0.0034

Gravity Model Plots



Atmospheric Model Plots



Creating a Motor

A solid rocket motor is used in this case. To create a motor, the SolidMotor class is used and the required arguments are given.

The SolidMotor class requires the user to have a thrust curve ready. This can come either from a .eng file for a commercial motor, such as below, or a .csv file from a static test measurement.

Besides the thrust curve, other parameters such as grain properties and nozzle dimensions must also be given.

See [Solid Motor Class Usage Docs](#) for more information.


```

Mandioca = SolidMotor(
    thrust_source='/gdrive/MyDrive/mandioca_2024.csv',
    dry_mass=0,
    dry_inertia=(0, 0, 0),
    nozzle_radius=65/2000,
    grain_number=5,
    grain_density=1691,
    grain_outer_radius=94/2000,
    grain_initial_inner_radius=32/2000,
    grain_initial_height=156/1000,
    grain_separation=9/1000,
    grains_center_of_mass_position=0.532,
    center_of_dry_mass_position=0,
    nozzle_position=0,
    burn_time=4.3,
    throat_radius=11.4/1000,
    coordinate_system_orientation="nozzle_to_combustion_chamber",
)

```

Pay special attention to *position* related parameters: More details on [Positions and Coordinate Systems](#)

To see what our thrust curve looks like, along with other import properties, we invoke the info method yet again. You may try the all_info method if you want more information all at once!

```
Mandioca.info()
```

Nozzle Details

Nozzle Radius: 0.0325 m

Nozzle Throat Radius: 0.0114 m

Grain Details

Number of Grains: 5

Grain Spacing: 0.009 m

Grain Density: 1691 kg/m³

Grain Outer Radius: 0.047 m

Grain Inner Radius: 0.016 m

Grain Height: 0.156 m

Grain Volume: 0.001 m³

Grain Mass: 1.619 kg

Motor Details

Total Burning Time: 4.3 s

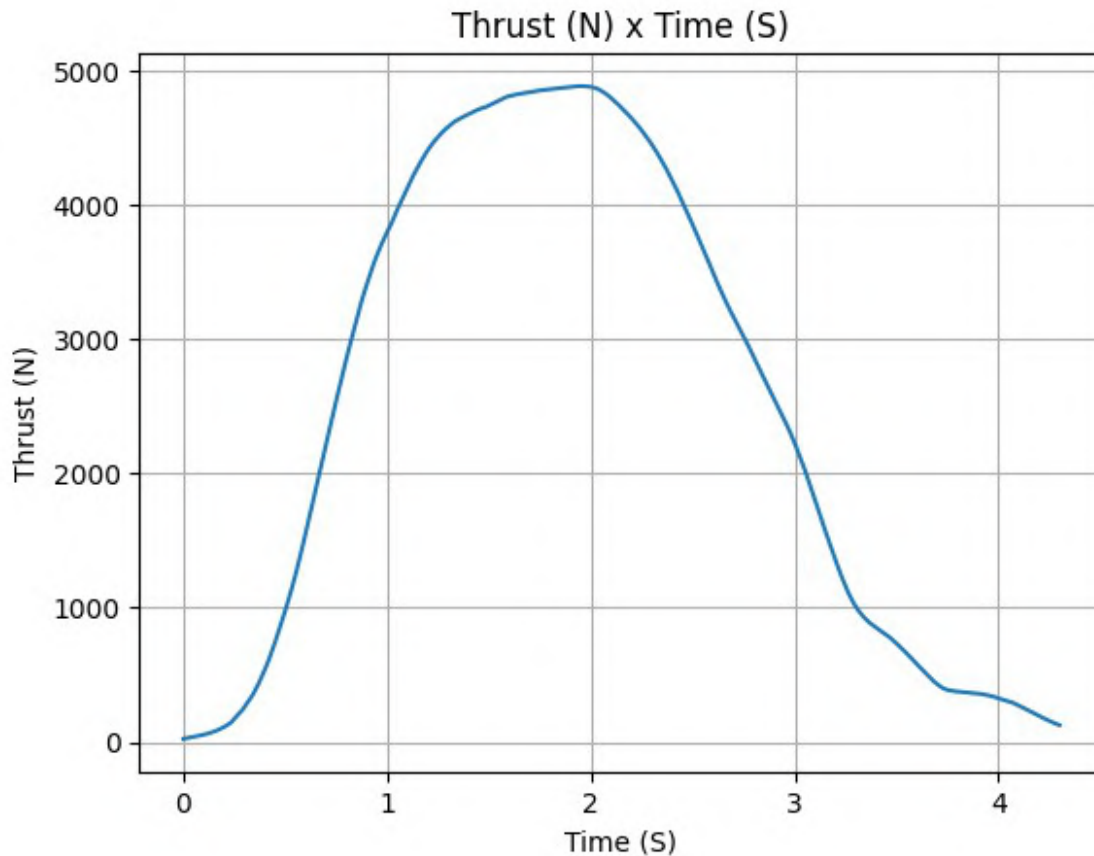
Total Propellant Mass: 8.093 kg

Average Propellant Exhaust Velocity: 1323.401 m/s

Average Thrust: 2490.654 N

Maximum Thrust: 4882.47264443292 N at 1.9550000000000018 s after ignition.

Total Impulse: 10709.812 Ns



Creating a Rocket

A rocket is composed of several components. Namely, we must have a motor (good thing we have the Pro75M1670 ready), a couple of aerodynamic surfaces (nose cone, fins and tail) and parachutes (if we are not launching a missile).

You can find more information about the `Rocket` class in the [Rocket Class Usage Docs](#).

Let's start by initializing our rocket, named Calisto, entering inertia properties, some dimensions and drag curves.

Pay special attention to *position* related parameters: More details on [Positions and Coordinate Systems](#)

```
Cd_RASAero = "/gdrive/MyDrive/SAC.csv"
Pacifico = Rocket(
    radius= 0.0817,
    mass=30.163,
    inertia=(11.487, 11.487, 0.137),
    power_off_drag= Cd_RASAero,
    power_on_drag= Cd_RASAero,
    center_of_mass_without_motor=1.028,
    coordinate_system_orientation="tail_to_nose",
```

```
)
rail_buttons = Pacifico.set_rail_buttons(
    upper_button_position=1.037,
    lower_button_position=0.059,
    angular_position=45,
)
```

To add the motor to our rocket we need only inform what motor we are adding (Pro75M1670) and inform the position, in meters, of the motor's nozzle exit area relative to the previously defined coordinate system.

```
# @title
Pacifico.add_motor(Mandioca, position=0)
```

Adding Aerodynamic Surfaces

Now we define the aerodynamic surfaces. They are really straight forward with special attention needed only for the position values. Here is a quick guide:

- The positions given **must** be relative to the same coordinate system as the rockets;
- Position of the Nosecone refers to the tip of the nose;
- Position of fins refers to the point belonging to the root chord which is highest in the rocket coordinate system;
- Position of the tail the point belonging to the tail which is highest in the rocket coordinate system.

See more details in [Positions and Coordinate Systems](#)

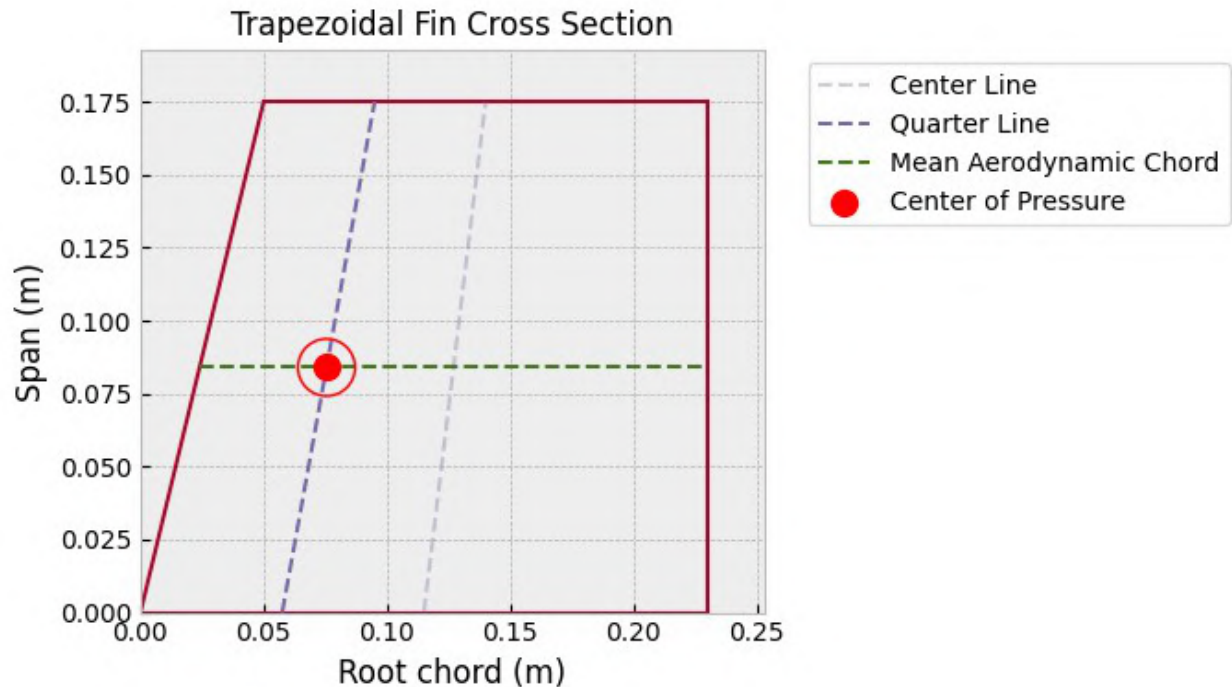
```
NACA0012_TRUNCADO =Function([[0,0.0002],[2,0.3320],[4,0.6335],
[6,0.6877]])

nose_cone = Pacifico.add_nose(
    length=0.650, kind="vonKarman", position=2.644
)

fin_set = Pacifico.add_trapezoidal_fins(
    n=4,
    root_chord=0.23,
    tip_chord=0.18,
    span=0.175,
    position=0.308,
    cant_angle=0.5,
    airfoil=(NACA0012_TRUNCADO, "degrees"),
    sweep_length=0.05,
)

tail = Pacifico.add_tail(
    top_radius=0.0817, bottom_radius=0.0695, length=0.035,
```

```
position=0.035
)
fin_set.draw()
```



To see all information regarding the rocket we just defined we run:

```
Pacifico.all_info()
```

Inertia Details

```
Rocket Mass: 30.163 kg (without motor)
Rocket Dry Mass: 30.163 kg (with unloaded motor)
Rocket Loaded Mass: 38.256 kg (with loaded motor)
Rocket Inertia (with unloaded motor) 11: 11.487 kg*m2
Rocket Inertia (with unloaded motor) 22: 11.487 kg*m2
Rocket Inertia (with unloaded motor) 33: 0.137 kg*m2
Rocket Inertia (with unloaded motor) 12: 0.000 kg*m2
Rocket Inertia (with unloaded motor) 13: 0.000 kg*m2
Rocket Inertia (with unloaded motor) 23: 0.000 kg*m2
```

Geometrical Parameters

```
Rocket Maximum Radius: 0.0817 m
Rocket Frontal Area: 0.020970 m2
```

Rocket Distances

Rocket Center of Dry Mass - Center of Mass without Motor: 0.000 m
Rocket Center of Dry Mass - Nozzle Exit: 1.028 m
Rocket Center of Dry Mass - Center of Propellant Mass: 0.496 m
Rocket Center of Mass - Rocket Loaded Center of Mass: 0.105 m

Aerodynamics Lift Coefficient Derivatives

Nose Cone Lift Coefficient Derivative: 2.000/rad
Fins Lift Coefficient Derivative: 11.247/rad
Tail Lift Coefficient Derivative: -0.553/rad

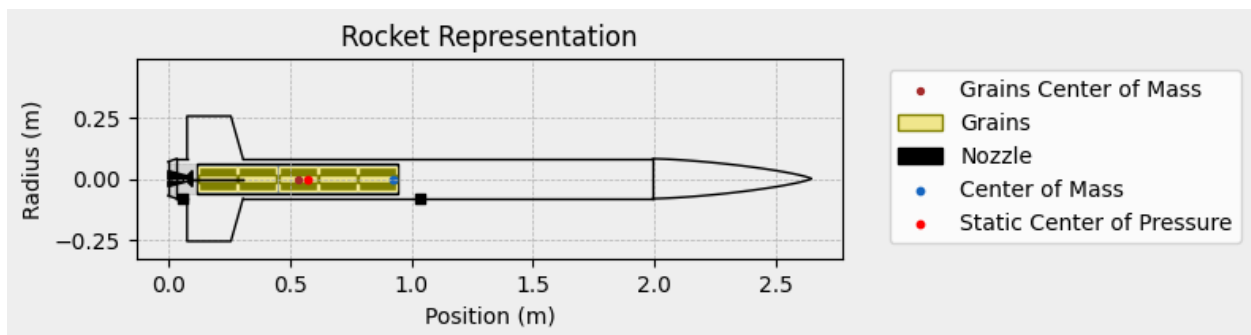
Center of Pressure

Nose Cone Center of Pressure position: 2.319 m
Fins Center of Pressure position: 0.233 m
Tail Center of Pressure position: 0.018 m

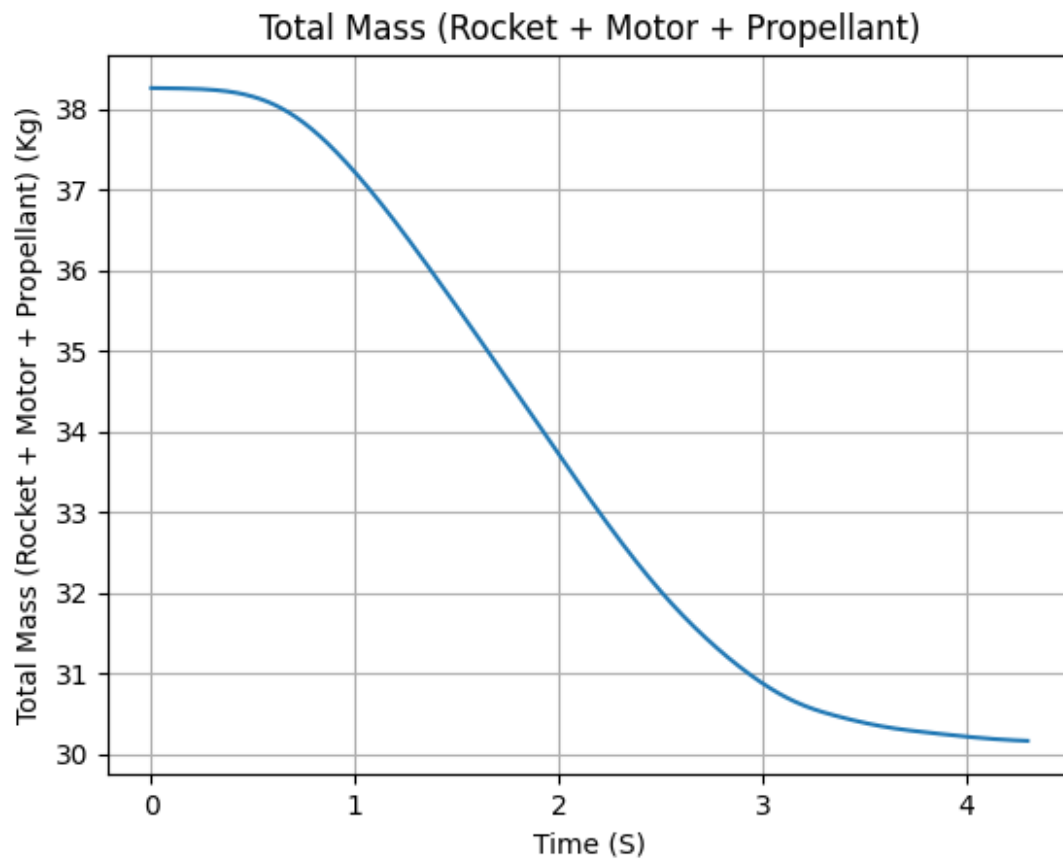
Stability

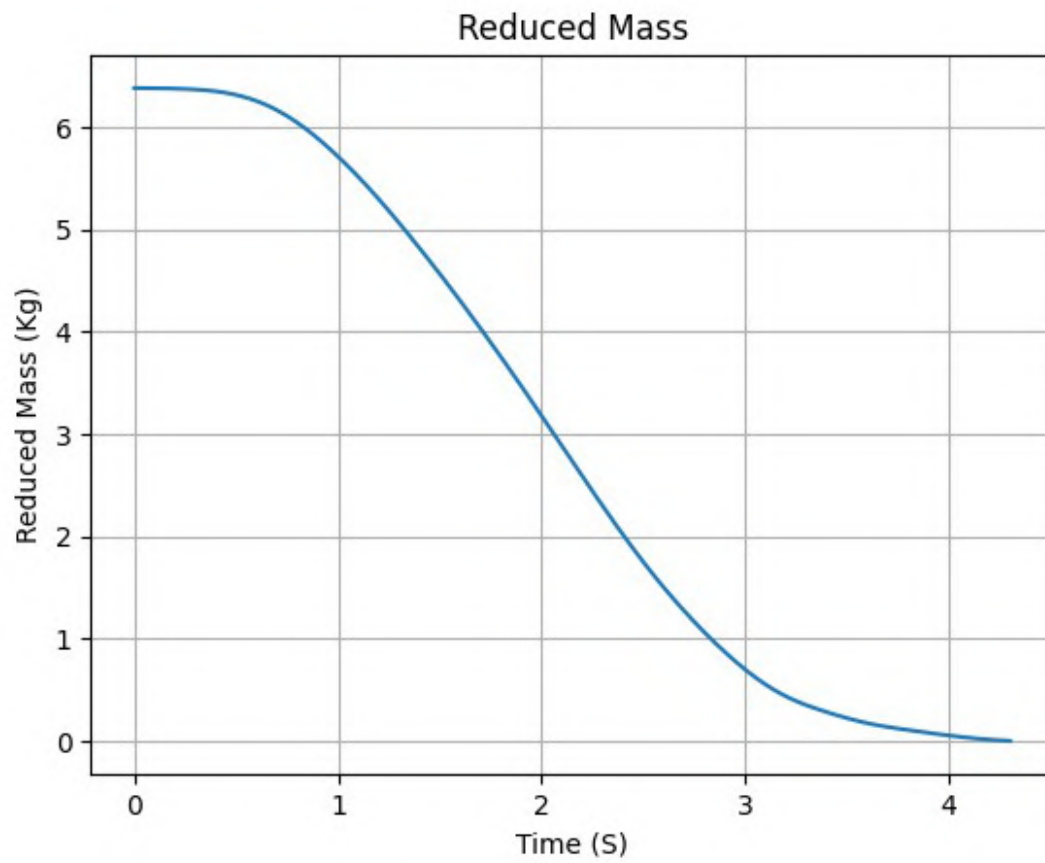
Center of Mass position (time=0): 0.923 m
Center of Pressure position (time=0): 0.571 m
Initial Static Margin (mach=0, time=0): 2.157 c
Final Static Margin (mach=0, time=burn_out): 2.799 c
Rocket Center of Mass (time=0) - Center of Pressure (mach=0): 0.353 m

Rocket Draw



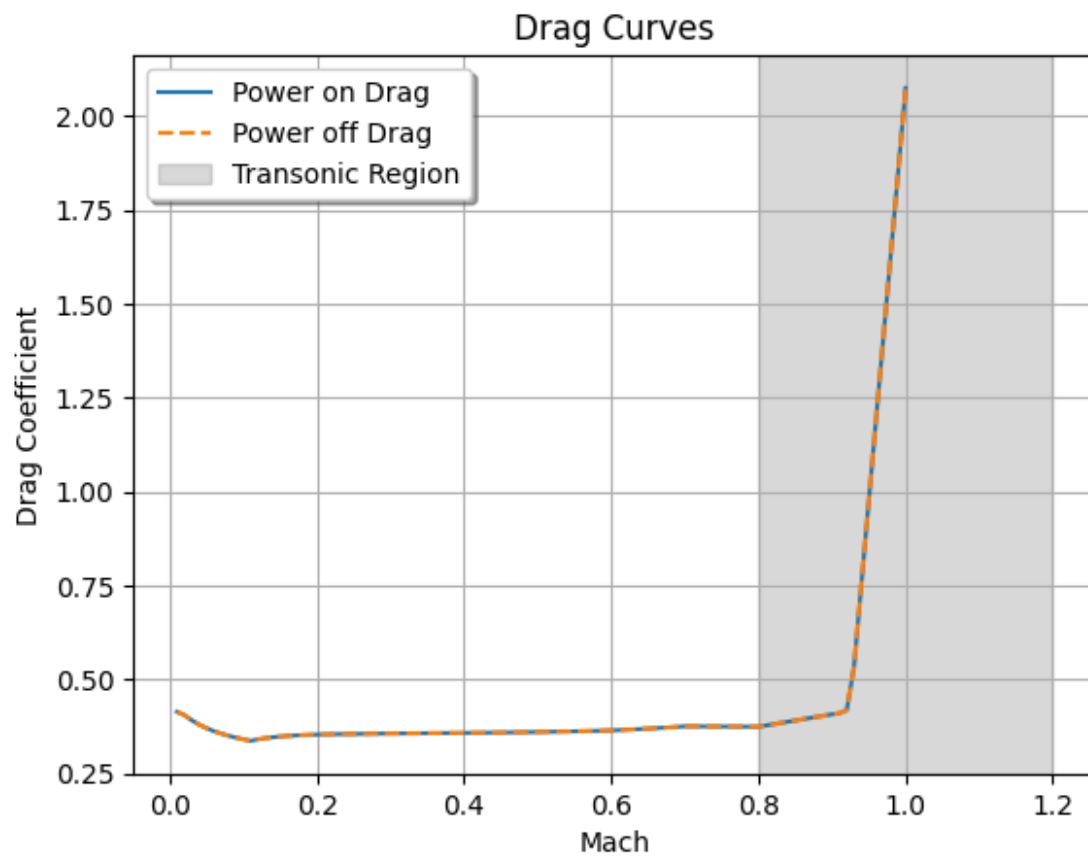
Mass Plots



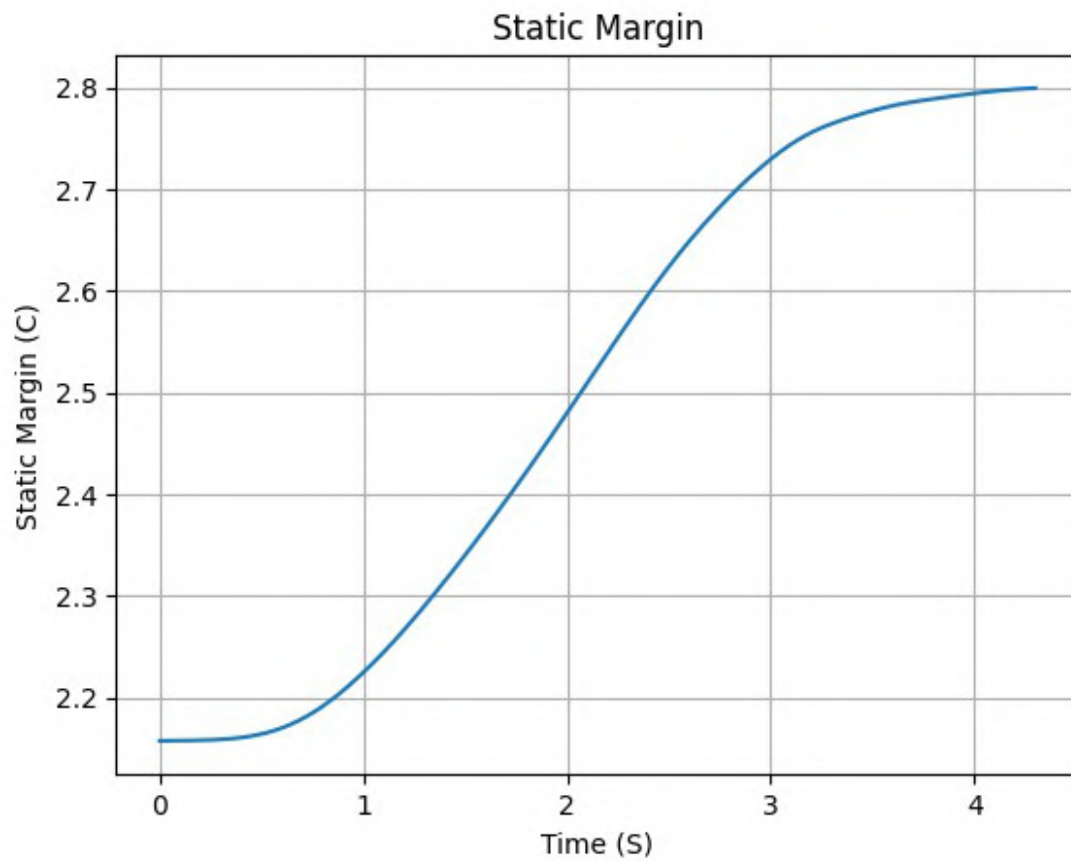


Aerodynamics Plots

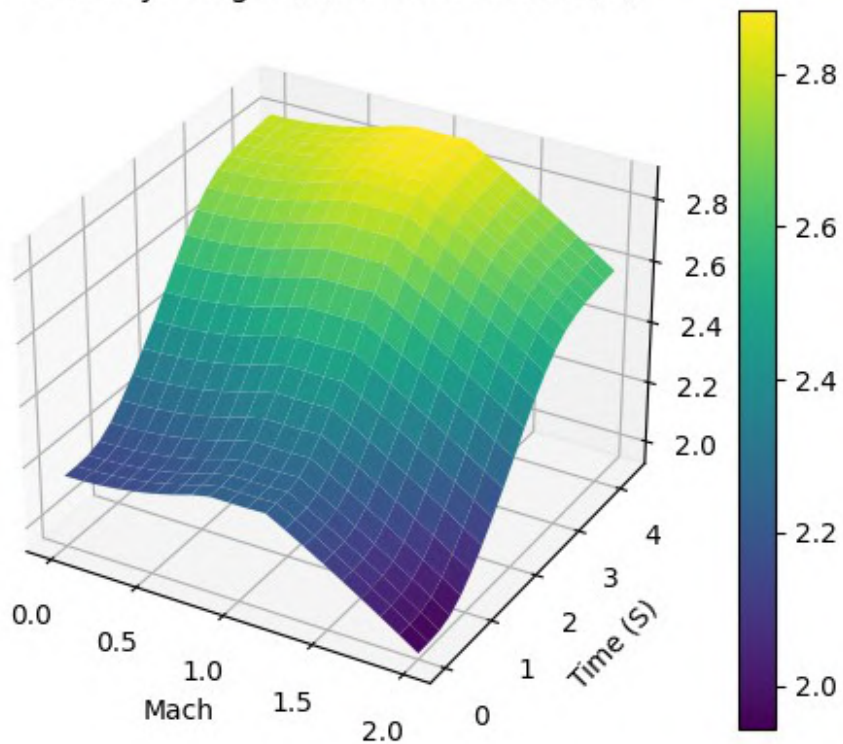
Drag Plots



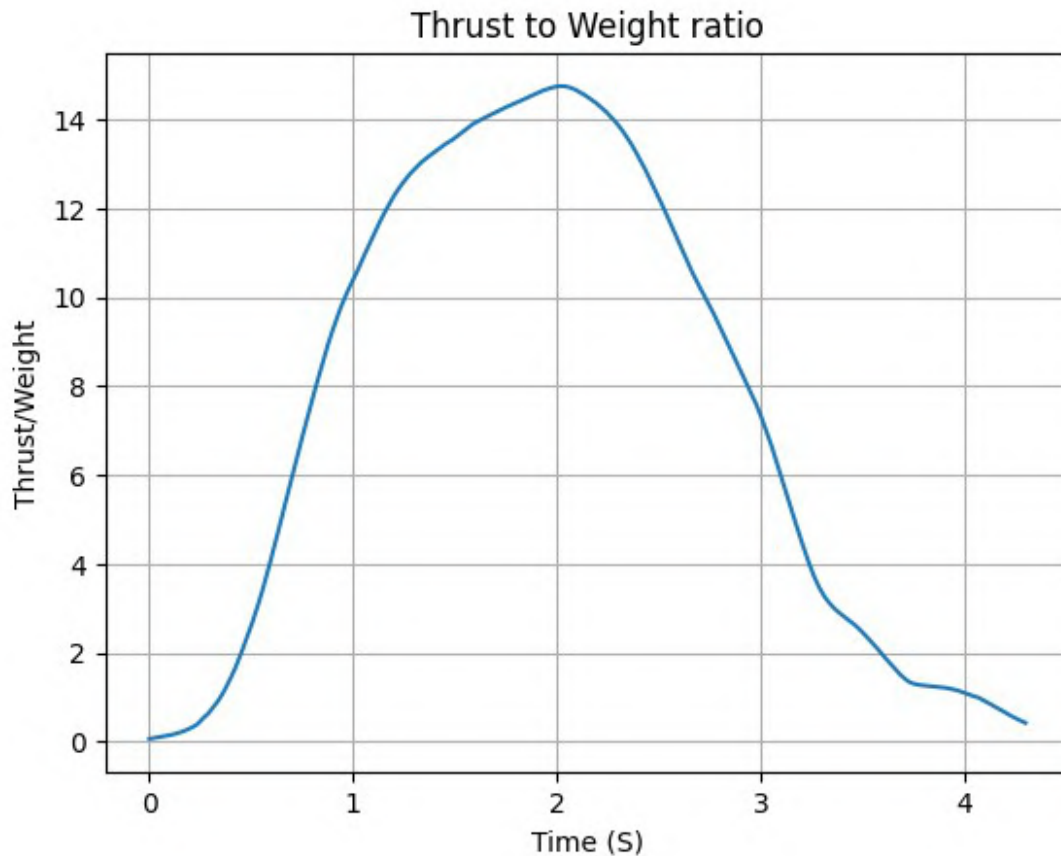
Stability Plots



Stability Margin (C) x Mach x Time (S)



Thrust-to-Weight Plot



Adding Parachutes

Finally, we have parachutes! Calisto will have two parachutes, Drogue and Main. The Drogue parachute will open at apogee while the Main parachute will open at 800m above ground level

For more details see [Adding Parachutes](#)

```
Main = Pacifico.add_parachute(  
    "Main",  
    cd_s=6.551,  
    trigger=426, #meters  
    sampling_rate=105,  
    lag=1.5,  
    noise=(0, 8.3, 0.5),  
)  
  
Drogue = Pacifico.add_parachute(  
    "Drogue",  
    cd_s=0.881,
```

```

trigger="apogee",
sampling_rate=105,
lag=1.5,
noise=(0, 8.3, 0.5),
)

```

Just be careful if you run this last cell multiple times! If you do so, your rocket will end up with lots of parachutes which activate together, which may cause problems during the flight simulation. We advise you to re-run all cells which define our rocket before running this, preventing unwanted old parachutes. Alternatively, you can run the following lines to remove parachutes.

```

Calisto.parachutes.remove(Drogue)
Calisto.parachutes.remove(Main)

```

Simulating a Flight

Simulating a flight trajectory is as simple as initializing a Flight class object given the rocket and environnement set up above as inputs. The launch rail inclination and heading are also given here.

```

test_flight = Flight(
    rocket=Pacifico, environment=env, rail_length=5.18,
    inclination=84, heading=0
)

```

Analyzing the Results

RocketPy gives you many plots, thats for sure! They are divided into sections to keep them organized. Alternatively, see the Flight class documentation to see how to get plots for specific variables only, instead of all of them at once.

```
test_flight.all_info()
```

Initial Conditions

```

Position - x: 0.00 m | y: 0.00 m | z: 1400.00 m
Velocity - Vx: 0.00 m/s | Vy: 0.00 m/s | Vz: 0.00 m/s
Attitude - e0: 0.999 | e1: -0.052 | e2: -0.000 | e3: 0.000
Euler Angles - Spin  $\phi$  : 0.00° | Nutation  $\theta$ : -6.00° | Precession  $\psi$ : 0.00°
Angular Velocity -  $\omega$ 1: 0.00 rad/s |  $\omega$ 2: 0.00 rad/s |  $\omega$ 3: 0.00 rad/s

```

Surface Wind Conditions

```
Frontal Surface Wind Speed: -4.73 m/s
```

Lateral Surface Wind Speed: -4.73 m/s

Launch Rail

Launch Rail Length: 5.18 m

Launch Rail Inclination: 84.00°

Launch Rail Heading: 0.00°

Rail Departure State

Rail Departure Time: 0.931 s

Rail Departure Velocity: 23.074 m/s

Rail Departure Stability Margin: 2.213 c

Rail Departure Angle of Attack: 15.804°

Rail Departure Thrust-Weight Ratio: 9.671

Rail Departure Reynolds Number: 2.154e+05

Burn out State

Burn out time: 4.300 s

Altitude at burn out: 621.809 m (AGL)

Rocket velocity at burn out: 257.964 m/s

Freestream velocity at burn out: 259.501 m/s

Mach Number at burn out: 0.747

Kinetic energy at burn out: 1.004e+06 J

Apogee State

Apogee Altitude: 4443.539 m (ASL) | 3043.539 m (AGL)

Apogee Time: 25.620 s

Apogee Freestream Speed: 50.506 m/s

Parachute Events

Drogue Ejection Triggered at: 25.629 s

Drogue Parachute Inflated at: 27.129 s

Drogue Parachute Inflated with Freestream Speed of: 52.295 m/s

Drogue Parachute Inflated at Height of: 3032.466 m (AGL)

Main Ejection Triggered at: 119.152 s

Main Parachute Inflated at: 120.652 s

Main Parachute Inflated with Freestream Speed of: 26.692 m/s

Main Parachute Inflated at Height of: 385.873 m (AGL)

Impact Conditions

X Impact: 77.192 m
Y Impact: 715.157 m
Latitude: 32.9966847°
Longitude: -106.9741704°
Time of Impact: 159.759 s
Velocity at Impact: -9.532 m/s

Stability Margin

Maximum Stability Margin: 2.869 c at 4.30 s
Minimum Stability Margin: 2.157 c at 0.00 s

Maximum Values

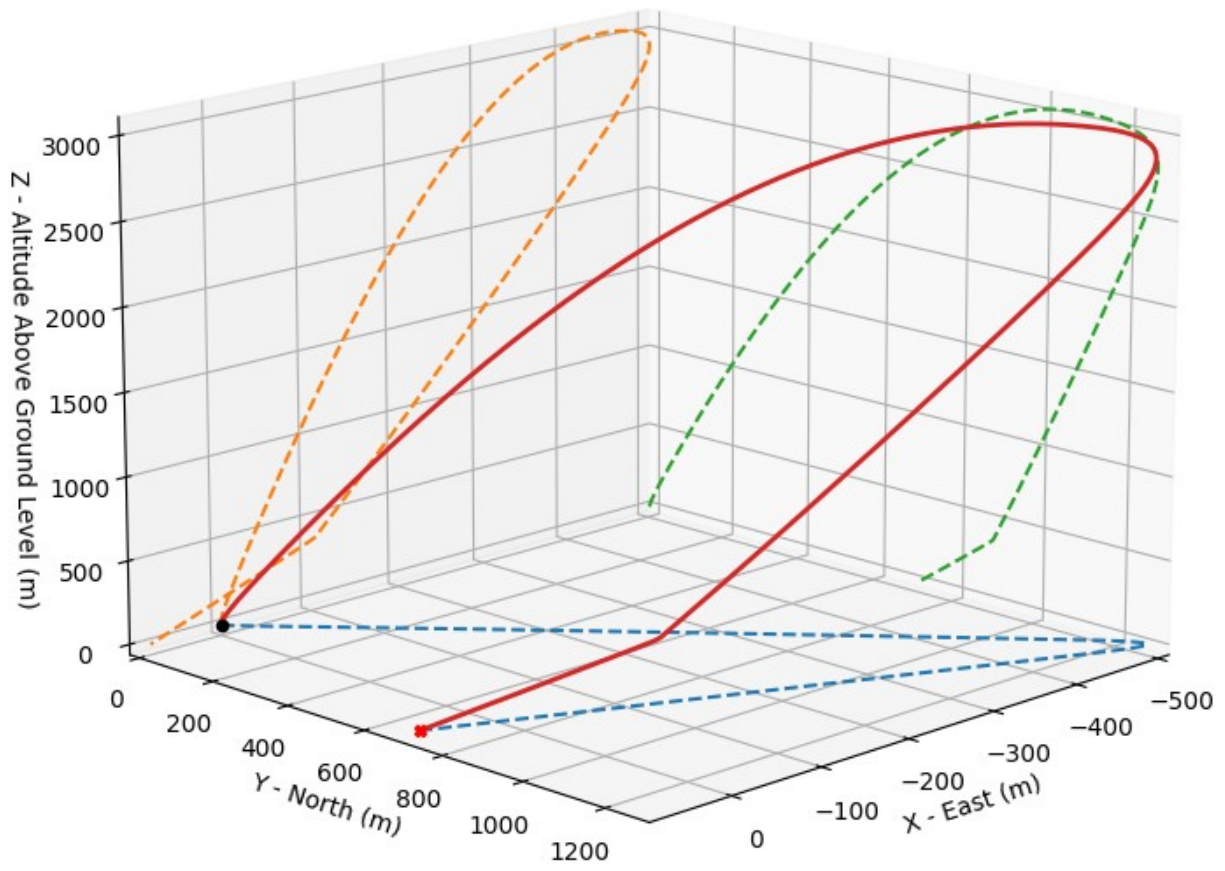
Maximum Speed: 262.891 m/s at 3.62 s
Maximum Mach Number: 0.761 Mach at 3.62 s
Maximum Reynolds Number: 2.207e+06 at 3.44 s
Maximum Dynamic Pressure: 3.292e+04 Pa at 3.54 s
Maximum Acceleration During Motor Burn: 132.588 m/s² at 2.02 s
Maximum Gs During Motor Burn: 13.520 g at 2.02 s
Maximum Acceleration After Motor Burn: 11.207 m/s² at 14.08 s
Maximum Gs After Motor Burn: 1.143 g at 14.08 s
Maximum Stability Margin: 2.869 c at 4.30 s
Maximum Upper Rail Button Normal Force: 0.038 N
Maximum Upper Rail Button Shear Force: 13.852 N
Maximum Lower Rail Button Normal Force: 0.022 N
Maximum Lower Rail Button Shear Force: 8.039 N

Numerical Integration Settings

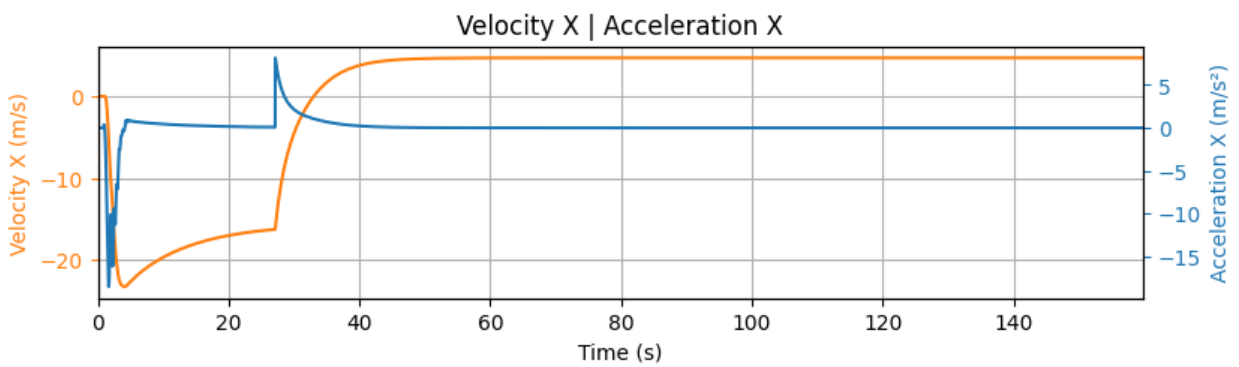
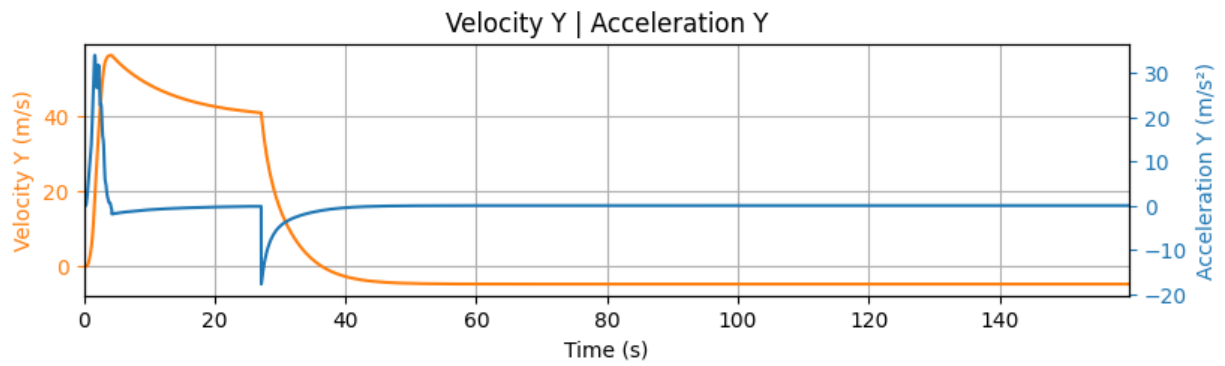
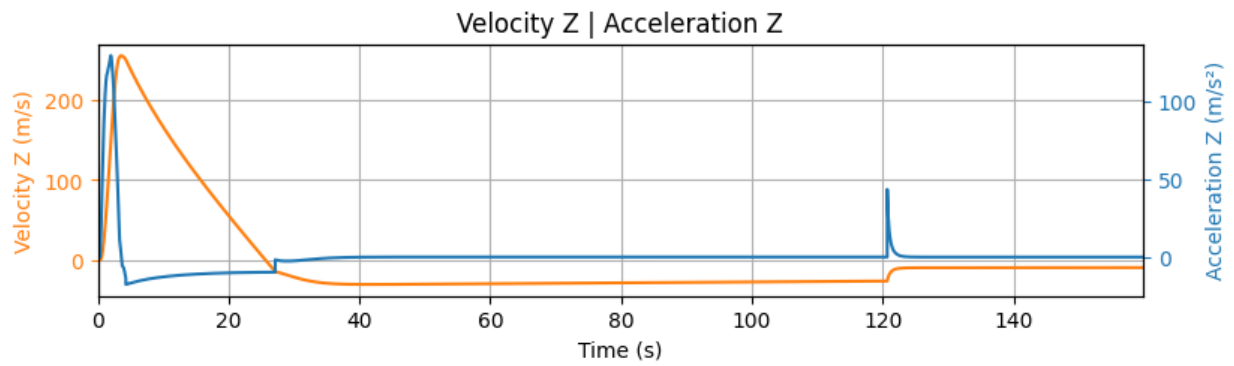
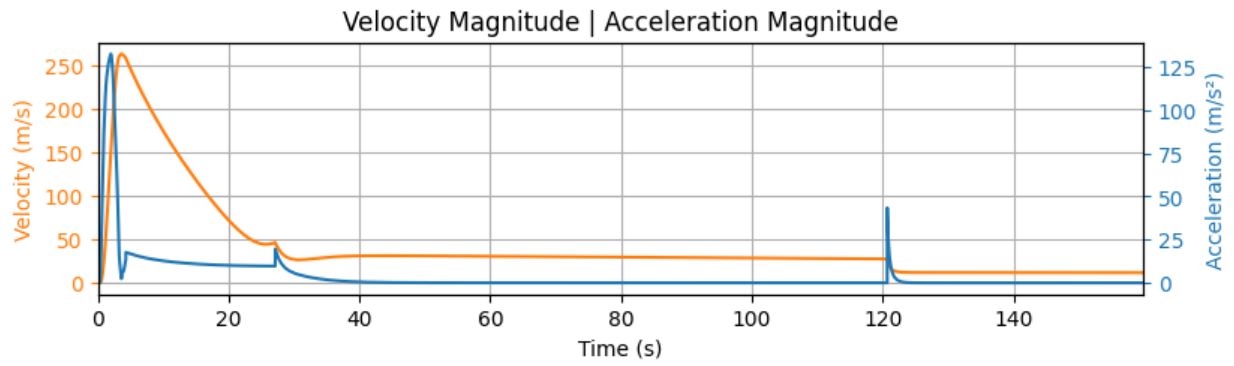
Maximum Allowed Flight Time: 600.000000 s
Maximum Allowed Time Step: inf s
Minimum Allowed Time Step: 0.000000e+00 s
Relative Error Tolerance: 1e-06
Absolute Error Tolerance: [0.001, 0.001, 0.001, 0.001, 0.001, 0.001, 1e-06, 1e-06, 1e-06, 1e-06, 0.001, 0.001, 0.001]
Allow Event Overshoot: True
Terminate Simulation on Apogee: False
Number of Time Steps Used: 779
Number of Derivative Functions Evaluation: 1627
Average Function Evaluations per Time Step: 2.088575

Trajectory 3d Plot

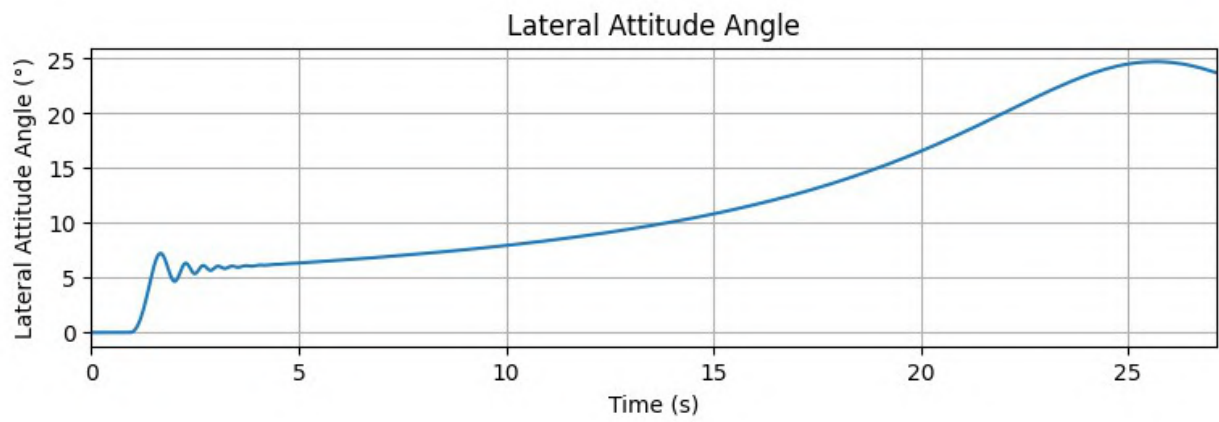
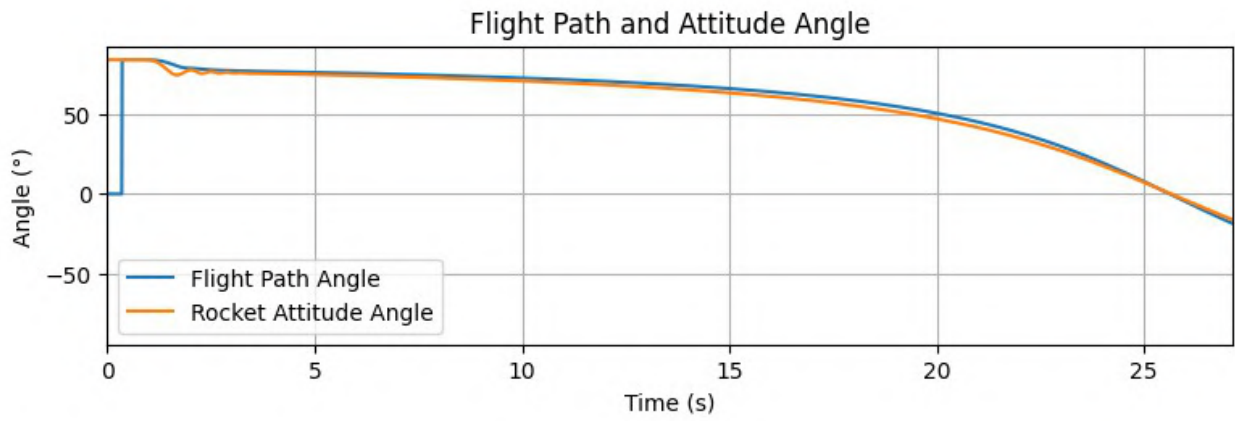
Flight Trajectory



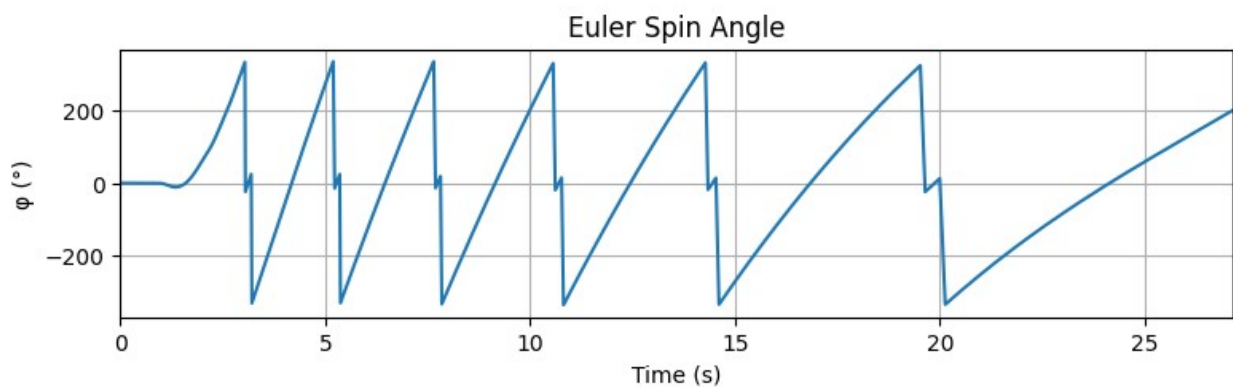
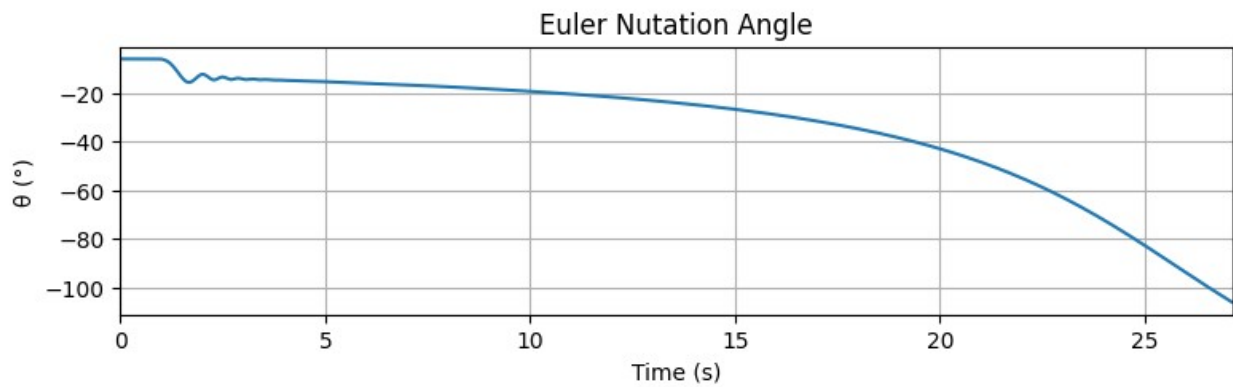
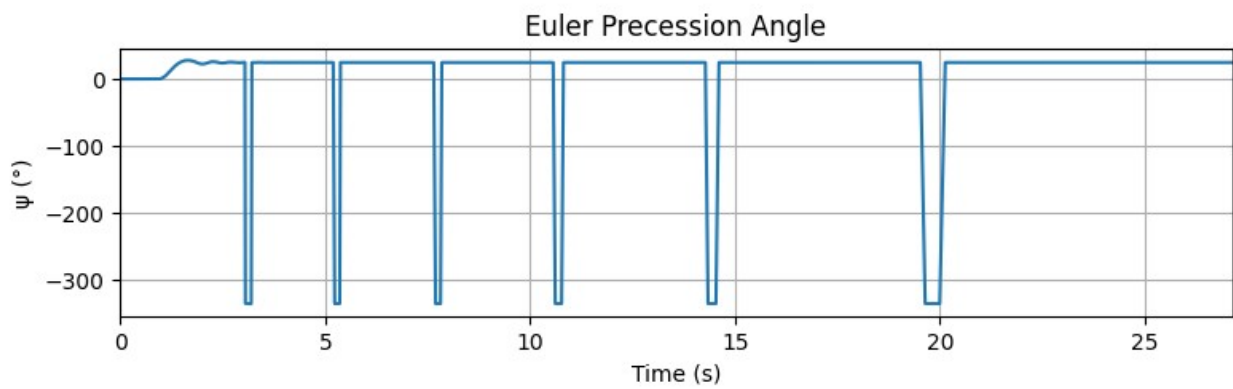
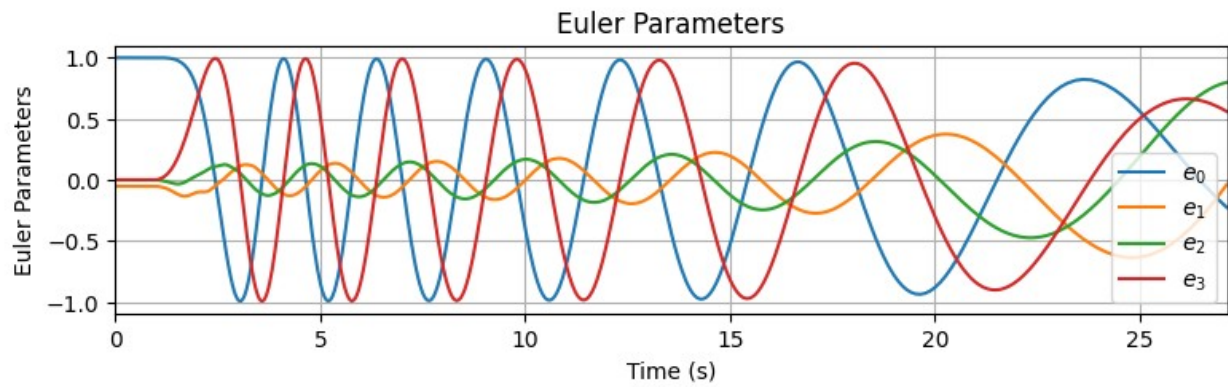
Trajectory Kinematic Plots



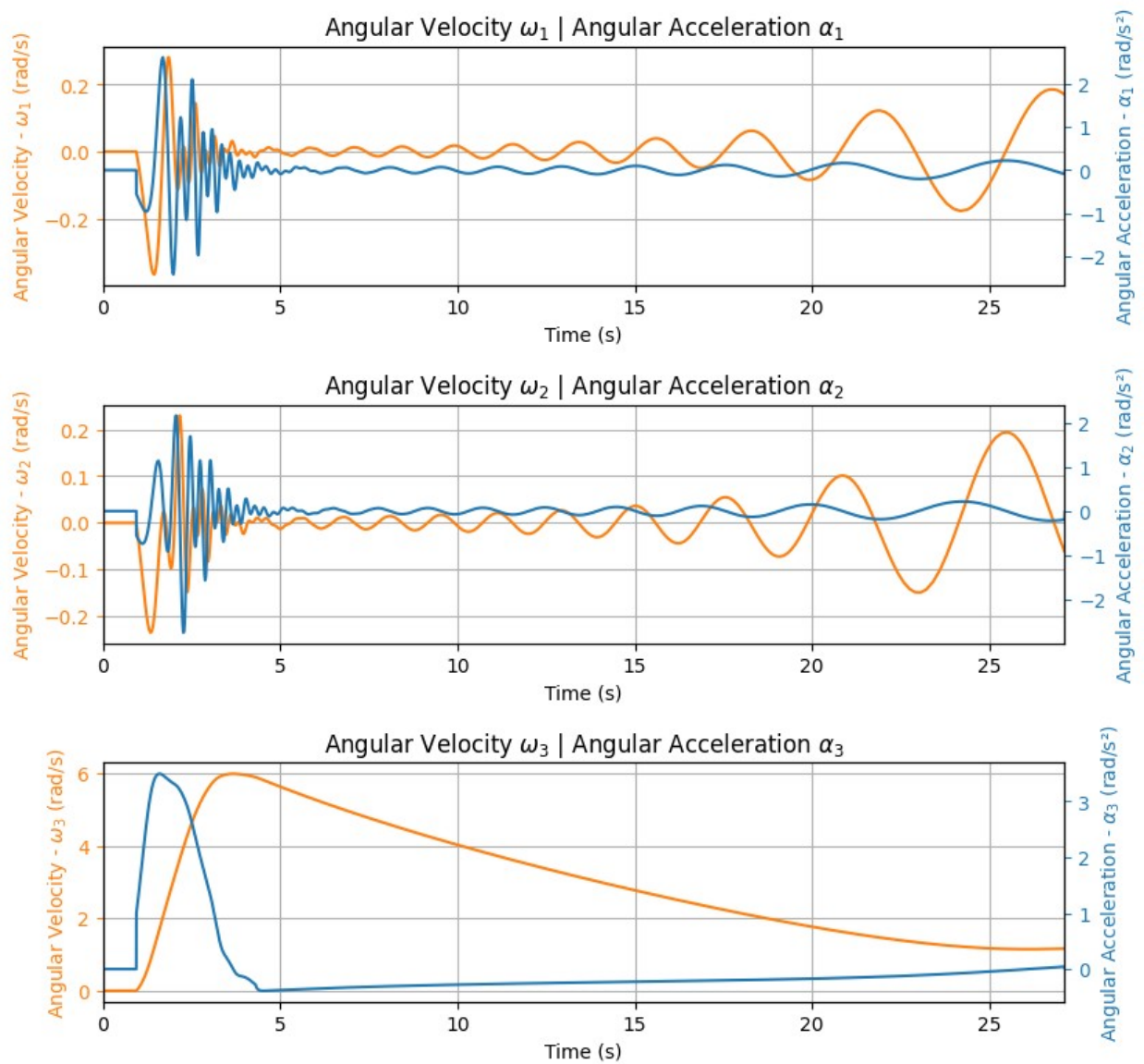
Angular Position Plots



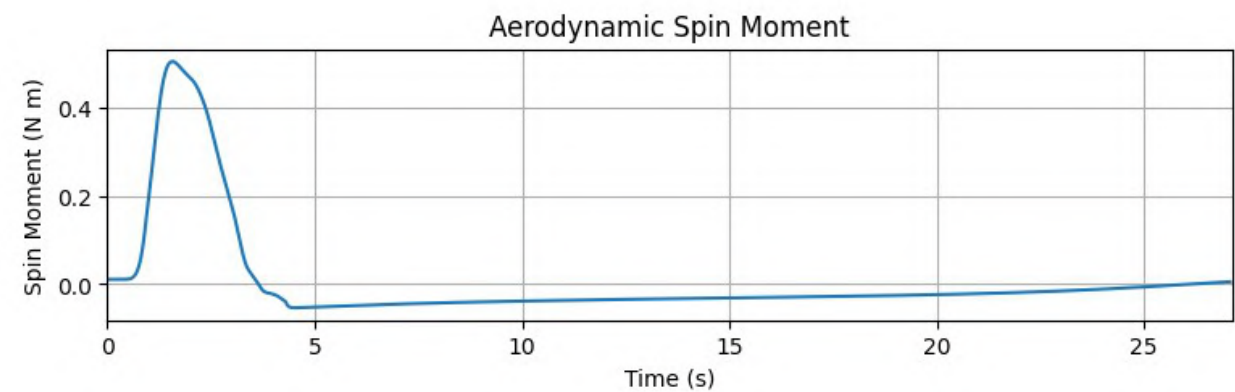
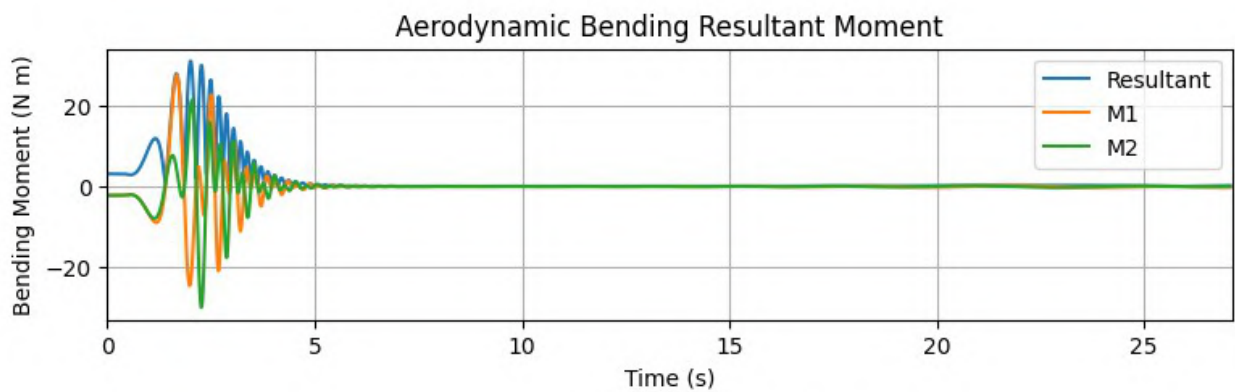
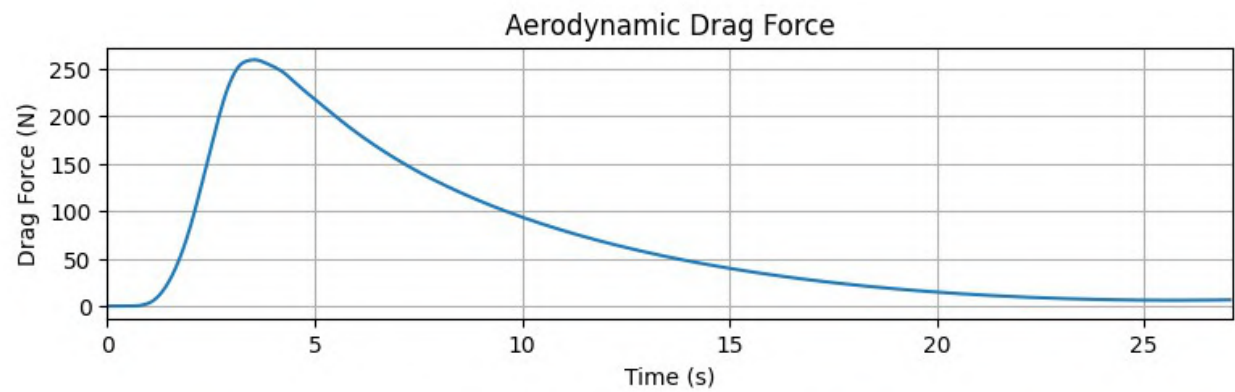
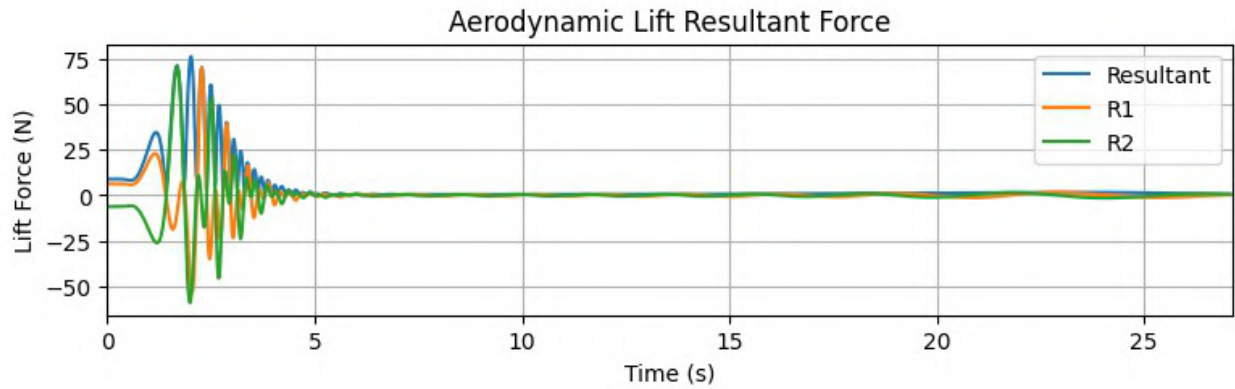
Path, Attitude and Lateral Attitude Angle plots



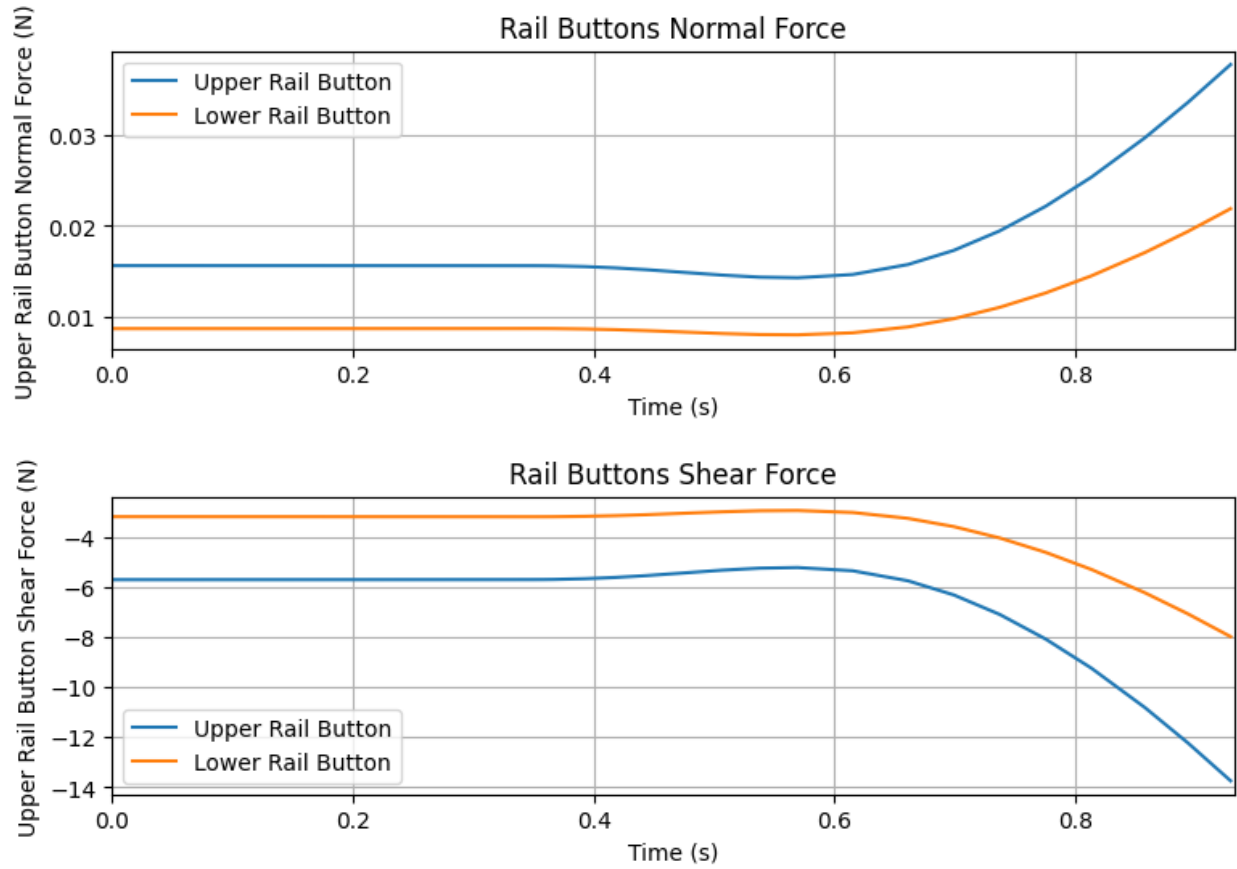
Trajectory Angular Velocity and Acceleration Plots



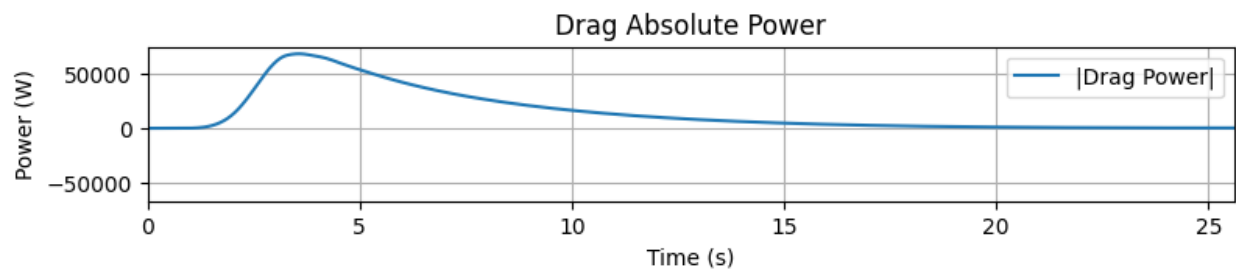
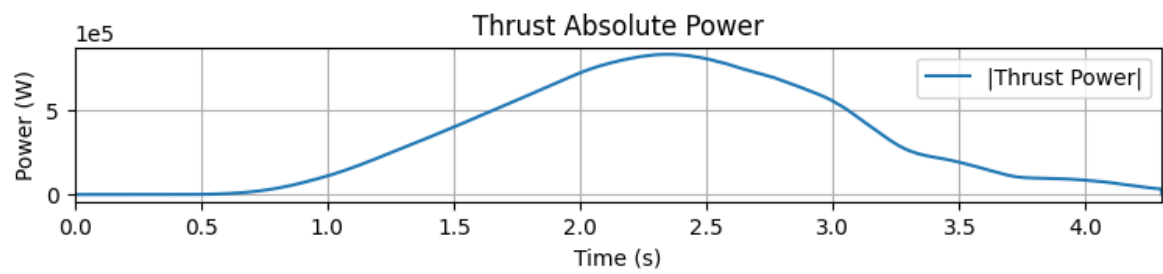
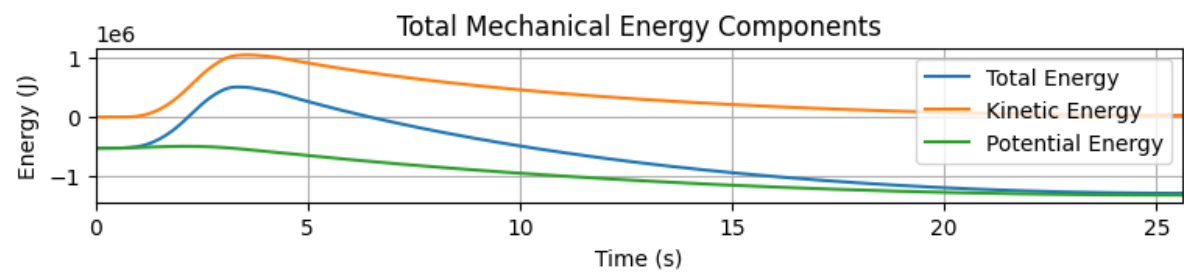
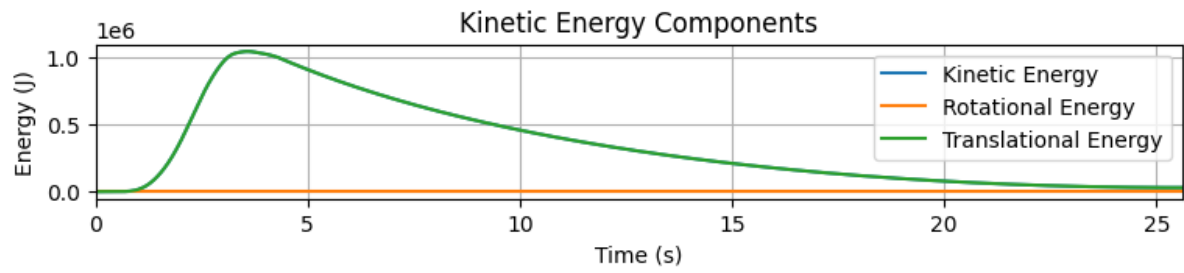
Aerodynamic Forces Plots



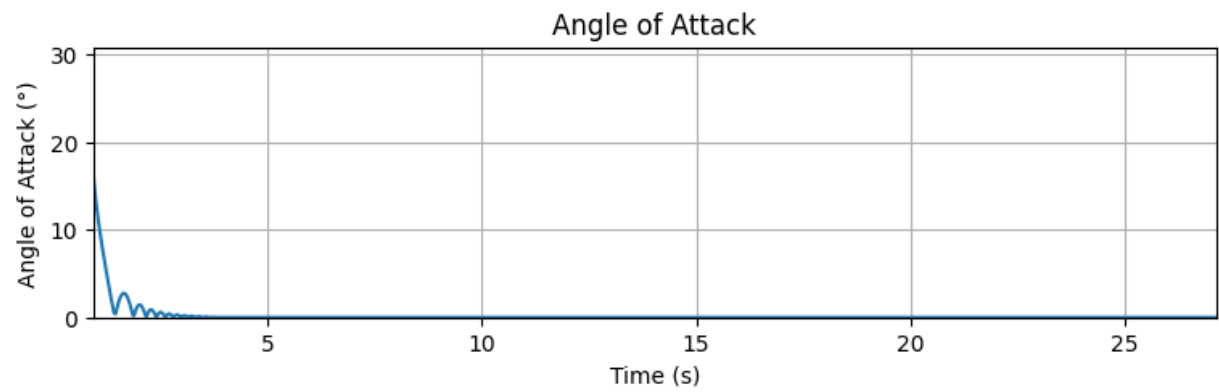
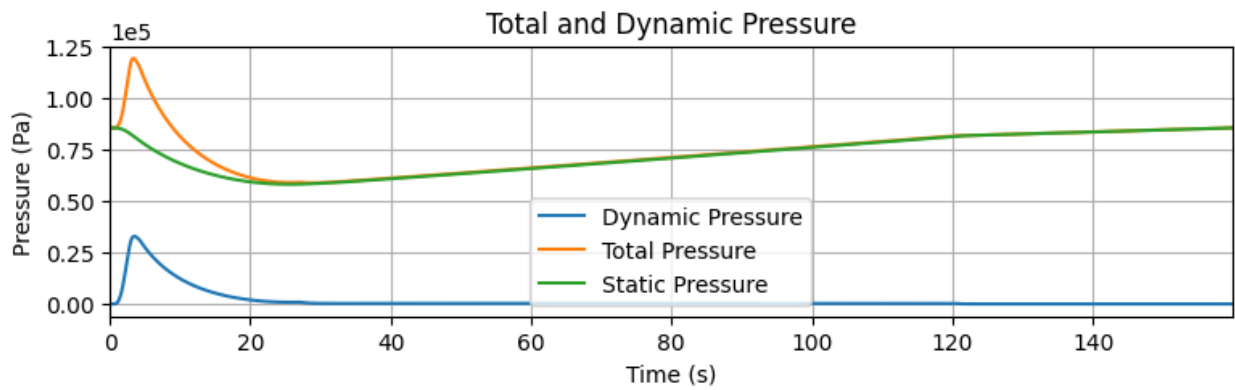
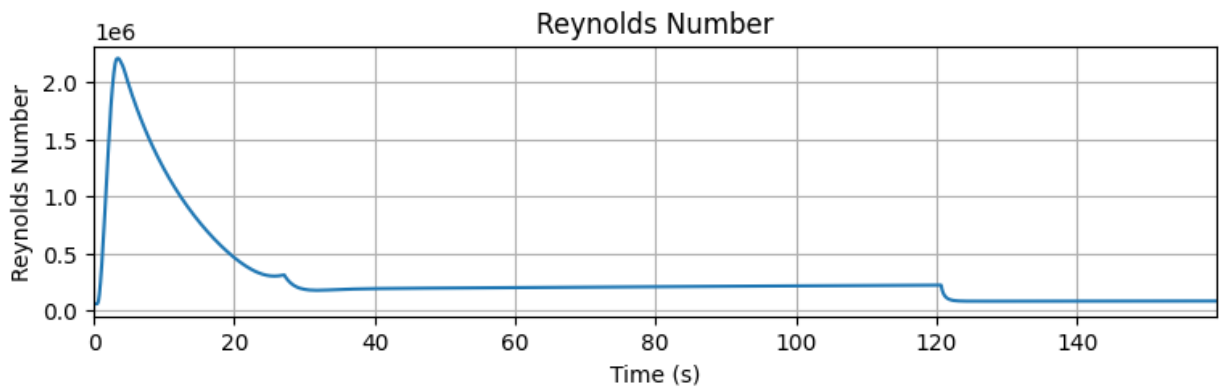
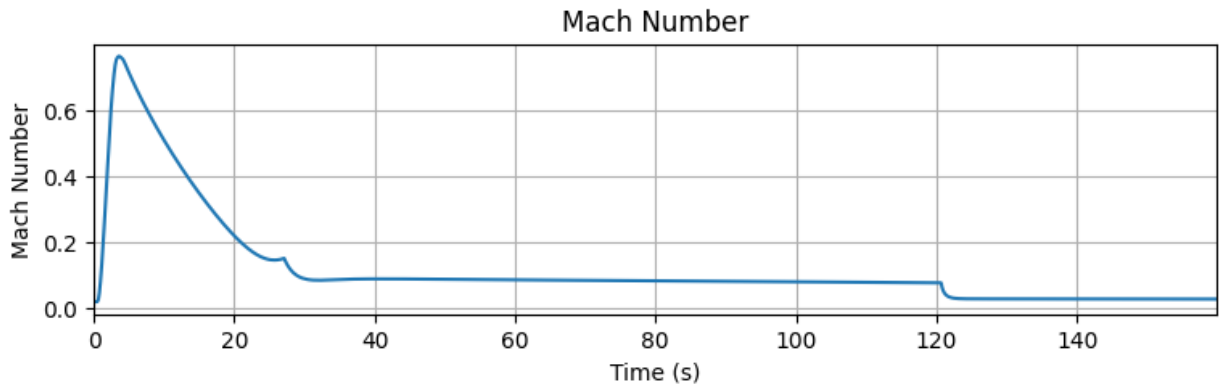
Rail Buttons Forces Plots



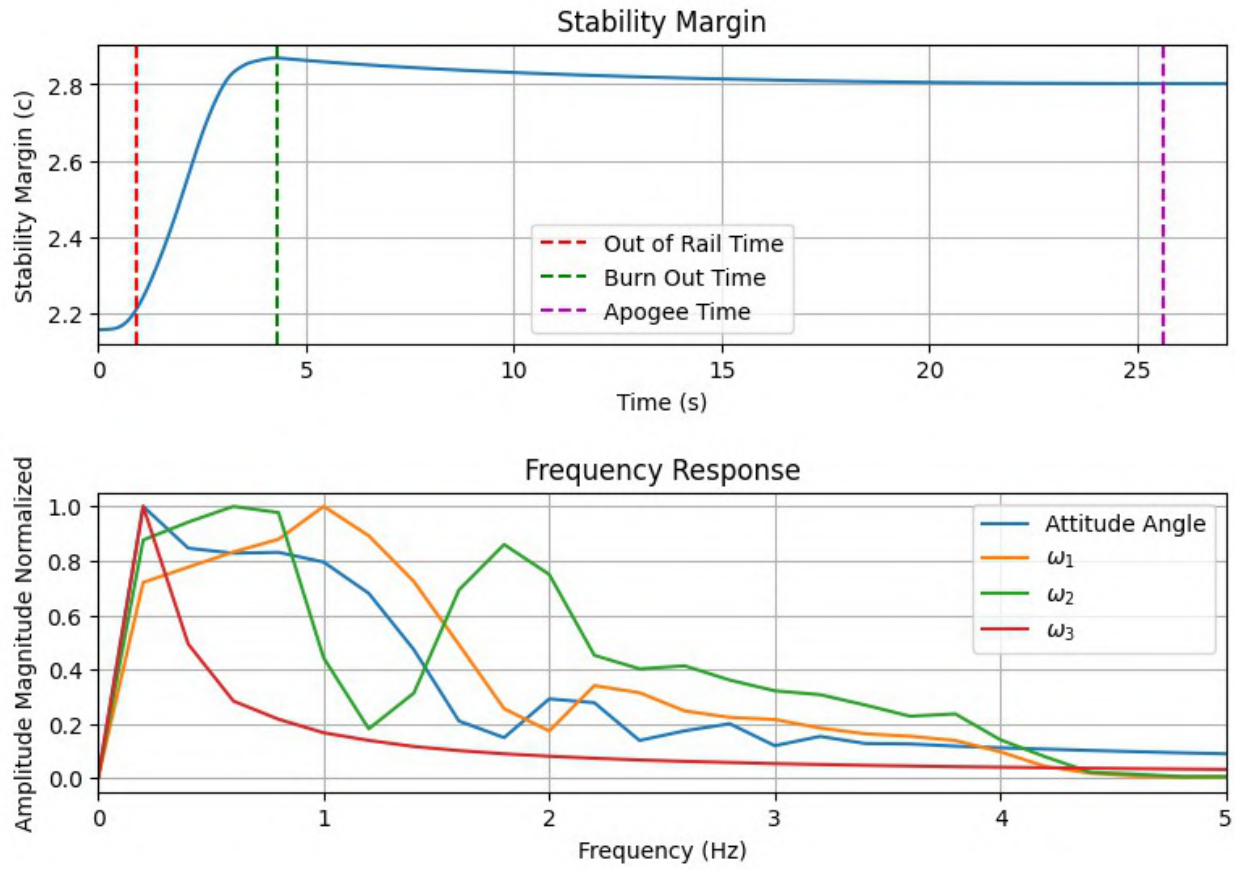
Trajectory Energy Plots



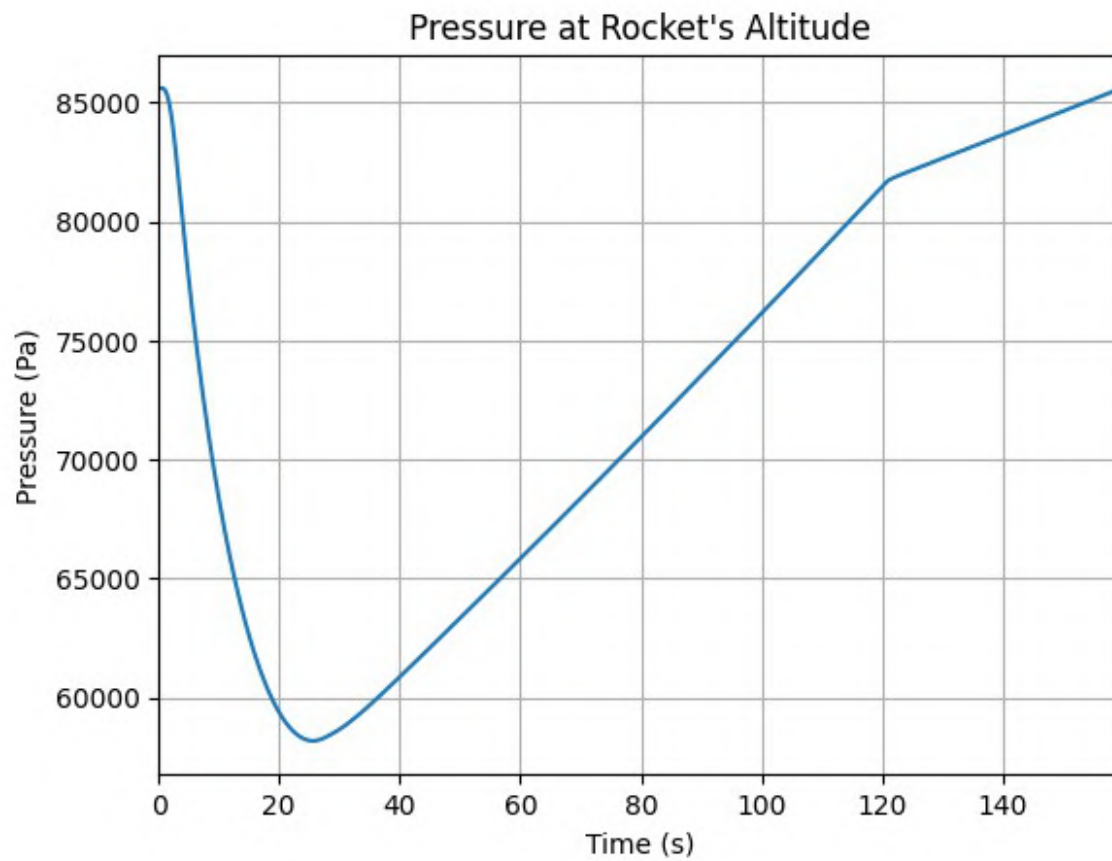
Trajectory Fluid Mechanics Plots



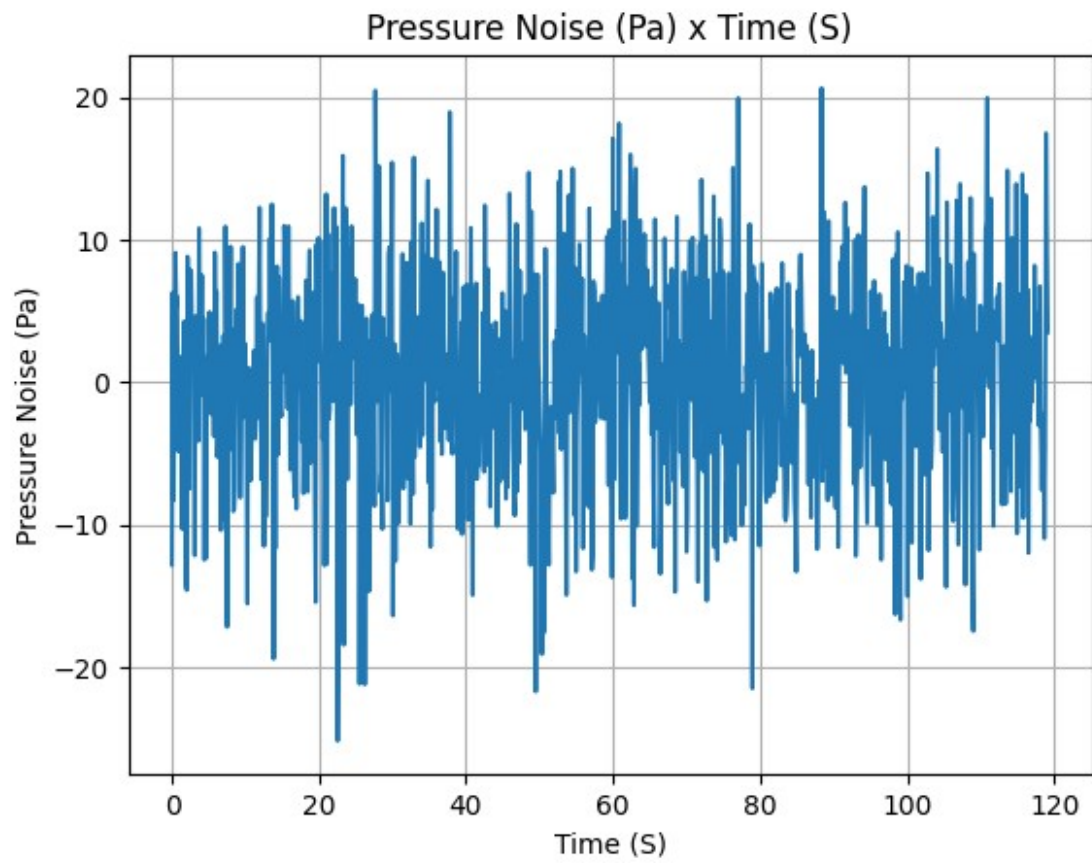
Trajectory Stability and Control Plots

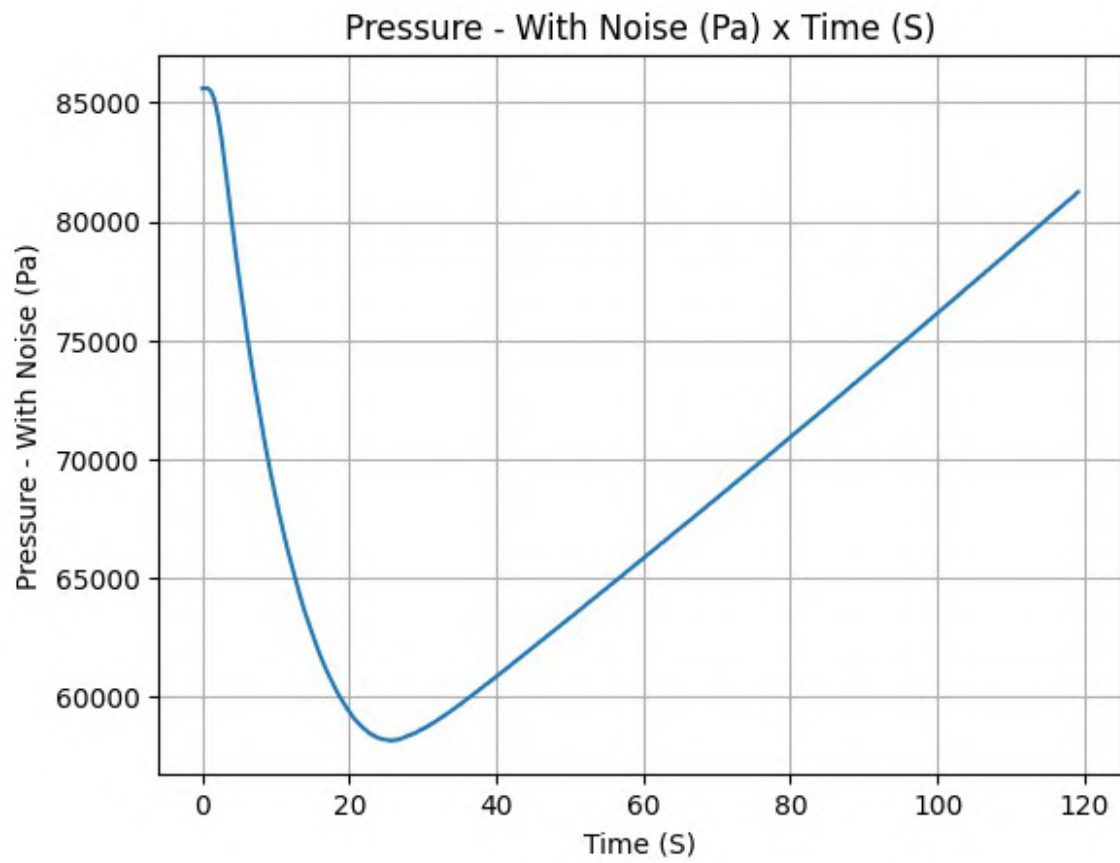


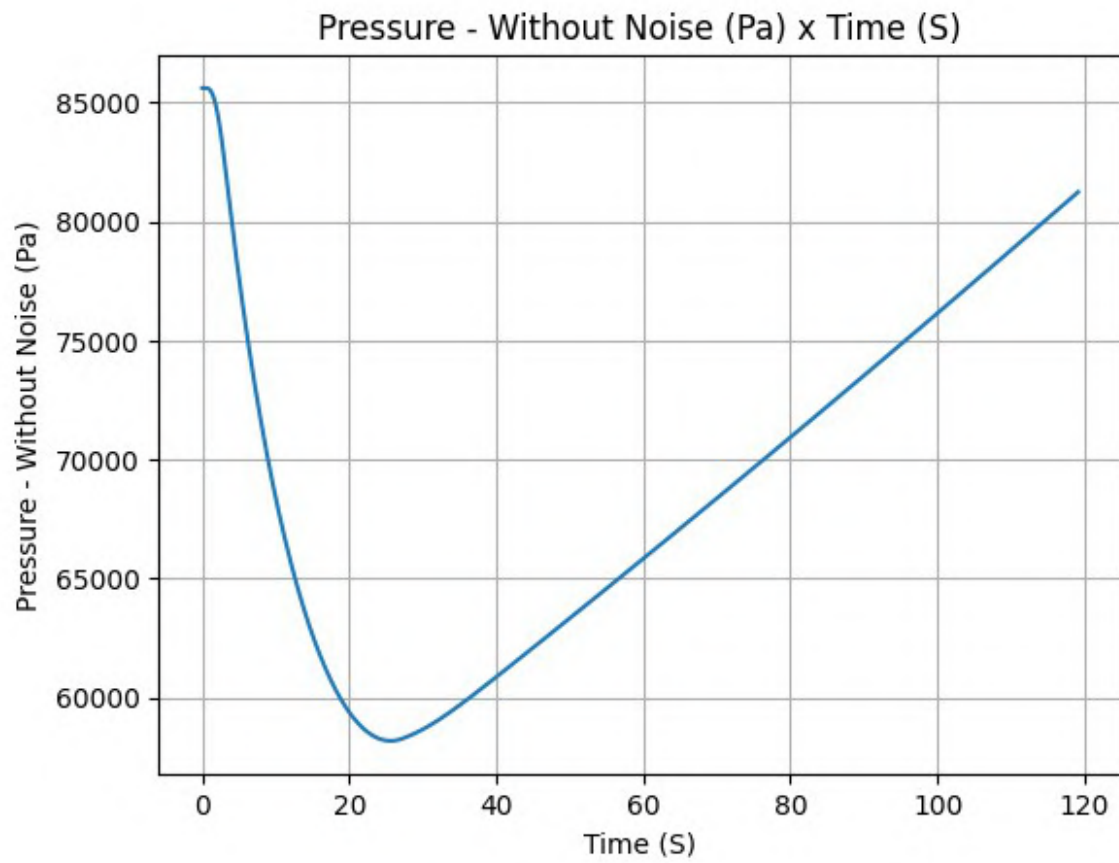
Rocket and Parachute Pressure Plots



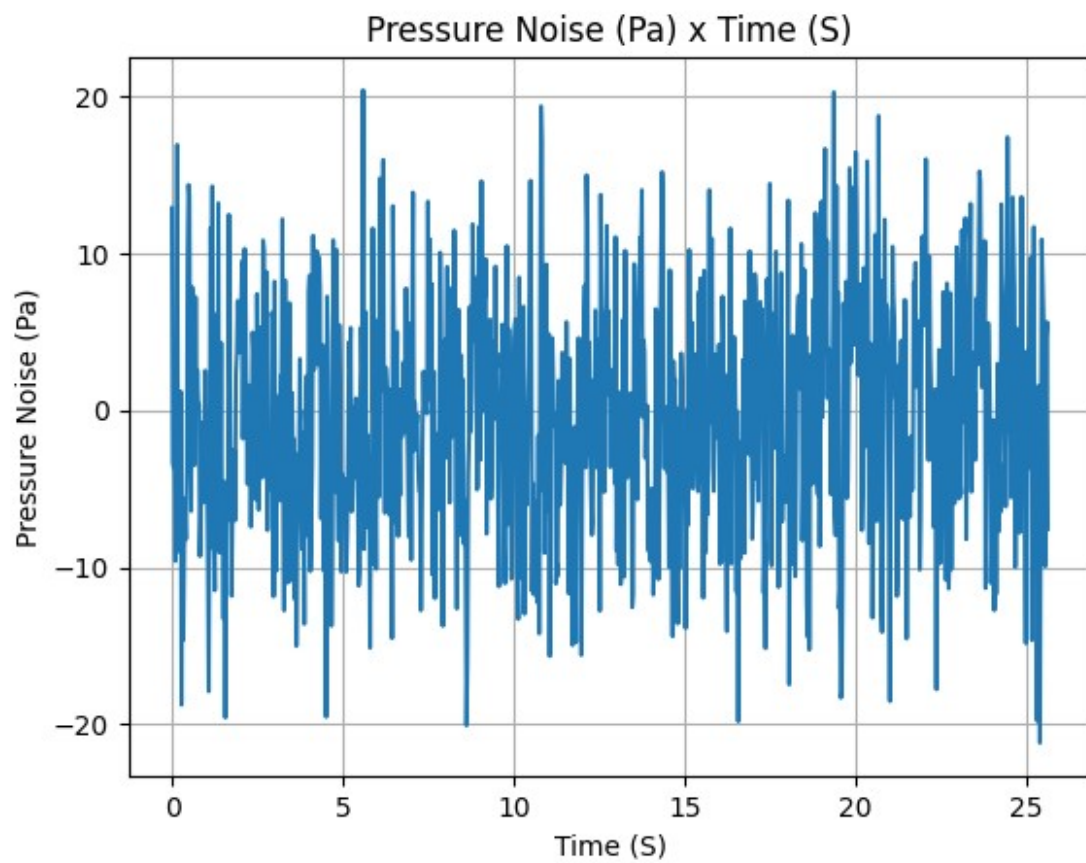
Parachute: Main

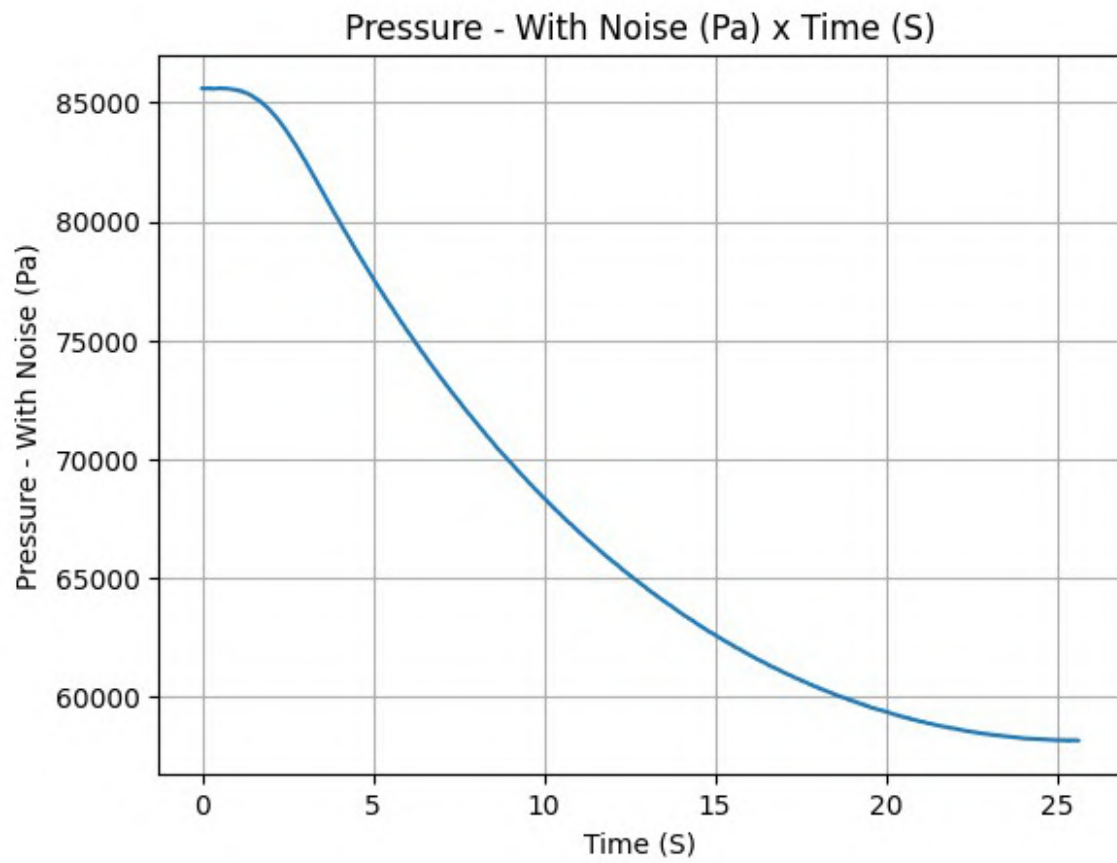


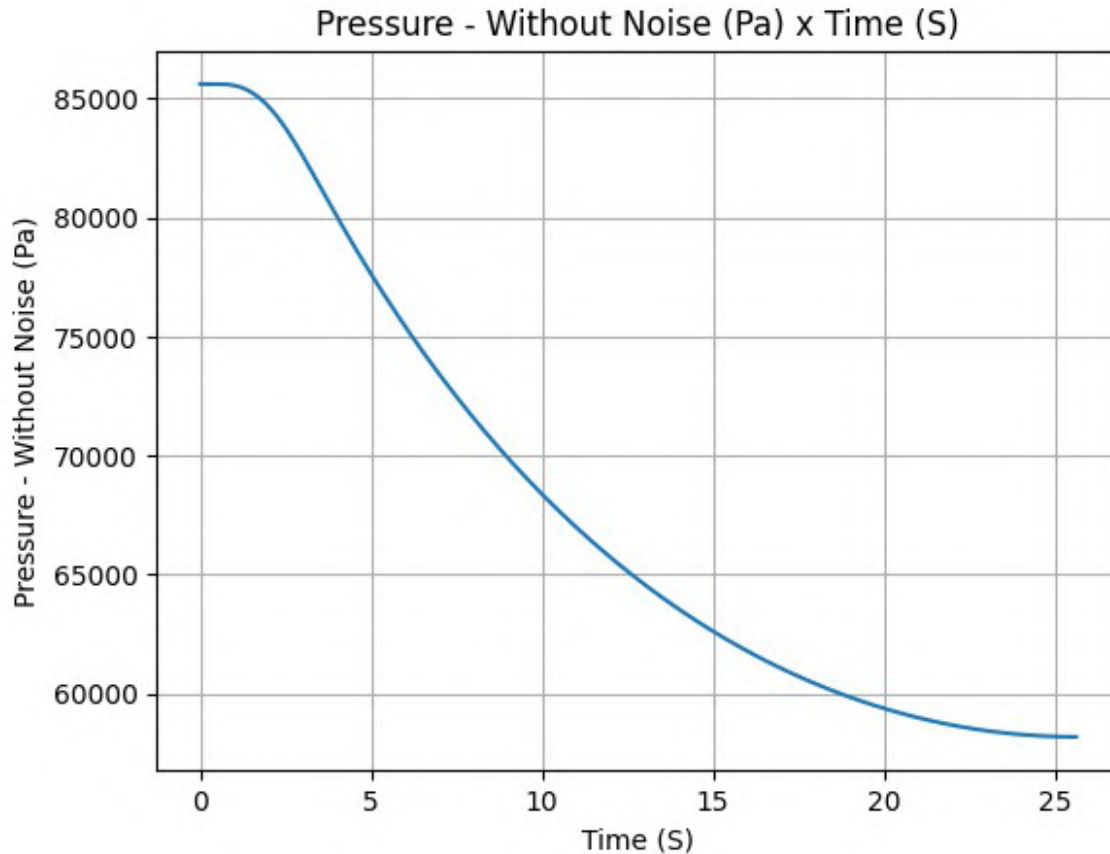




Parachute: Drogue







Export Flight Trajectory to a .kml file so it can be opened on Google Earth

```
test_flight.export_kml(
    file_name="trajectory.kml",
    extrude=True,
    altitude_mode="relative_to_ground",
)

File trajectory.kml saved with success!

def fin_flutter_analysis(
    fin_thickness, shear_modulus, flight, see_prints=True,
    see_graphs=True
):
    """Calculate and plot the Fin Flutter velocity using the pressure
    profile
    provided by the selected atmospheric model. It considers the
    Flutter
    Boundary Equation that published in NACA Technical Paper 4197.
    These results are only estimates of a real problem and may not be
    useful for
    fins made from non-isotropic materials.
    Currently, this function works if only a single set of fins is
```

```

added,
    otherwise it will use the last set of fins added to the rocket.

Parameters
-----
fin_thickness : float
    The fin thickness, in meters
shear_modulus : float
    Shear Modulus of fins' material, must be given in Pascal
flight : Flight
    Flight object containing the rocket's flight data
see_prints : boolean, optional
    True if you want to see the prints, False otherwise.
see_graphs : boolean, optional
    True if you want to see the graphs, False otherwise. If False,
the
    function will return the vectors containing the data for the
graphs.

Return
-----
None
"""
found_fin = False

# First, we need identify if there is at least one fin set in the
rocket
for aero_surface in flight.rocket.fins:
    if isinstance(aero_surface, TrapezoidalFins):
        # s: surface area; ar: aspect ratio; la: lambda
        root_chord = aero_surface.root_chord
        s = (aero_surface.tip_chord + root_chord) *
aero_surface.span / 2
        ar = aero_surface.span * aero_surface.span / s
        la = aero_surface.tip_chord / root_chord
        if not found_fin:
            found_fin = True
        else:
            warnings.warn("More than one fin set found. The last
one will be used.")
    if not found_fin:
        raise AttributeError(
            "There is no TrapezoidalFins in the rocket, can't run
Flutter Analysis."
        )

# Calculate variables
flutter_mach = _flutter_mach_number(
    fin_thickness, shear_modulus, flight, root_chord, ar, la
)

```

```

safety_factor = _flutter_safety_factor(flight, flutter_mach)

# Prints and plots
if see_prints:
    _flutter_prints(
        fin_thickness, shear_modulus, s, ar, la, flutter_mach,
        safety_factor, flight
    )
if see_graphs:
    _flutter_plots(flight, flutter_mach, safety_factor)
else:
    return flutter_mach, safety_factor

def _flutter_mach_number(fin_thickness, shear_modulus, flight,
    root_chord, ar, la):
    flutter_mach = (
        (shear_modulus * 2 * (ar + 2) * (fin_thickness / root_chord)
** 3)
        / (1.337 * (ar**3) * (la + 1) * flight.pressure)
    ) ** 0.5
    flutter_mach.set_title("Fin Flutter Mach Number")
    flutter_mach.set_outputs("Mach")
    return flutter_mach

def _flutter_safety_factor(flight, flutter_mach):
    """Calculates the safety factor for the fin flutter analysis.

Parameters
    -----
    flight : rocketpy.Flight
        Flight object containing the rocket's flight data
    flutter_mach : rocketpy.Function
        Mach Number at which the fin flutter occurs. See the
        `fin_flutter_analysis` function for more details.

Returns
    -----
    rocketpy.Function
        The safety factor for the fin flutter analysis.
    """
    safety_factor = flutter_mach / flight.mach_number
    safety_factor.set_title("Fin Flutter Safety Factor")
    safety_factor.set_outputs("Safety Factor")
    return safety_factor

def _flutter_plots(flight, flutter_mach, safety_factor):
    """Plot the Fin Flutter Mach Number and the Safety Factor for the

```


flutter.

Parameters

flight : rocketpy.Flight

Flight object containing the rocket's flight data

flutter_mach : rocketpy.Function

*Function containing the Fin Flutter Mach Number,
see fin_flutter_analysis for more details.*

safety_factor : rocketpy.Function

*Function containing the Safety Factor for the fin flutter.
See fin_flutter_analysis for more details.*

Returns

None

"""

TODO: move to rocketpy.plots submodule

_ = plt.figure(figsize=(6, 6))

ax1 = plt.subplot(211)

ax1.plot(
 flutter_mach[:, 0],
 flutter_mach[:, 1],
 label="Fin flutter Mach Number",
)

ax1.plot(
 flight.mach_number[:, 0],
 flight.mach_number[:, 1],
 label="Rocket Freestream Speed",
)

ax1.set_xlim(0, flight.apogee_time if flight.apogee_time != 0.0
else flight.tFinal)
ax1.set_title("Fin Flutter Mach Number x Time(s)")
ax1.set_xlabel("Time (s)")
ax1.set_ylabel("Mach")
ax1.legend()
ax1.grid()

ax2 = plt.subplot(212)
ax2.plot(safety_factor[:, 0], safety_factor[:, 1])
ax2.set_xlim(flight.out_of_rail_time, flight.apogee_time)
ax2.set_ylim(0, 6)
ax2.set_title("Fin Flutter Safety Factor")
ax2.set_xlabel("Time (s)")
ax2.set_ylabel("Safety Factor")
ax2.grid()

plt.subplots_adjust(hspace=0.5)
plt.show()

```

def _flutter_prints(
    fin_thickness,
    shear_modulus,
    s,
    ar,
    la,
    flutter_mach,
    safety_factor,
    flight,
):
    """Prints out the fin flutter analysis results. See
    fin_flutter_analysis for
    more details.

    Parameters
    -----
    fin_thickness : float
        The fin thickness, in meters
    shear_modulus : float
        Shear Modulus of fins' material, must be given in Pascal
    s : float
        Fin surface area, in squared meters
    ar : float
        Fin aspect ratio
    la : float
        Fin lambda, defined as the tip_chord / root_chord ratio
    flutter_mach : rocketpy.Function
        The Mach Number at which the fin flutter occurs, considering
the
        variation of the speed of sound with altitude. See
    fin_flutter_analysis
        for more details.
    safety_factor : rocketpy.Function
        The Safety Factor for the fin flutter. Defined as the Fin
Flutter Mach
        Number divided by the Freestream Mach Number.
    flight : rocketpy.Flight
        Flight object containing the rocket's flight data

    Returns
    -----
    None
    """
    # TODO: move to rocketpy.prints submodule
    time_index = np.argmin(flutter_mach[:, 1])
    time_min_mach = flutter_mach[time_index, 0]
    min_mach = flutter_mach[time_index, 1]
    min_vel = min_mach * flight.speed_of_sound(time_min_mach)

```

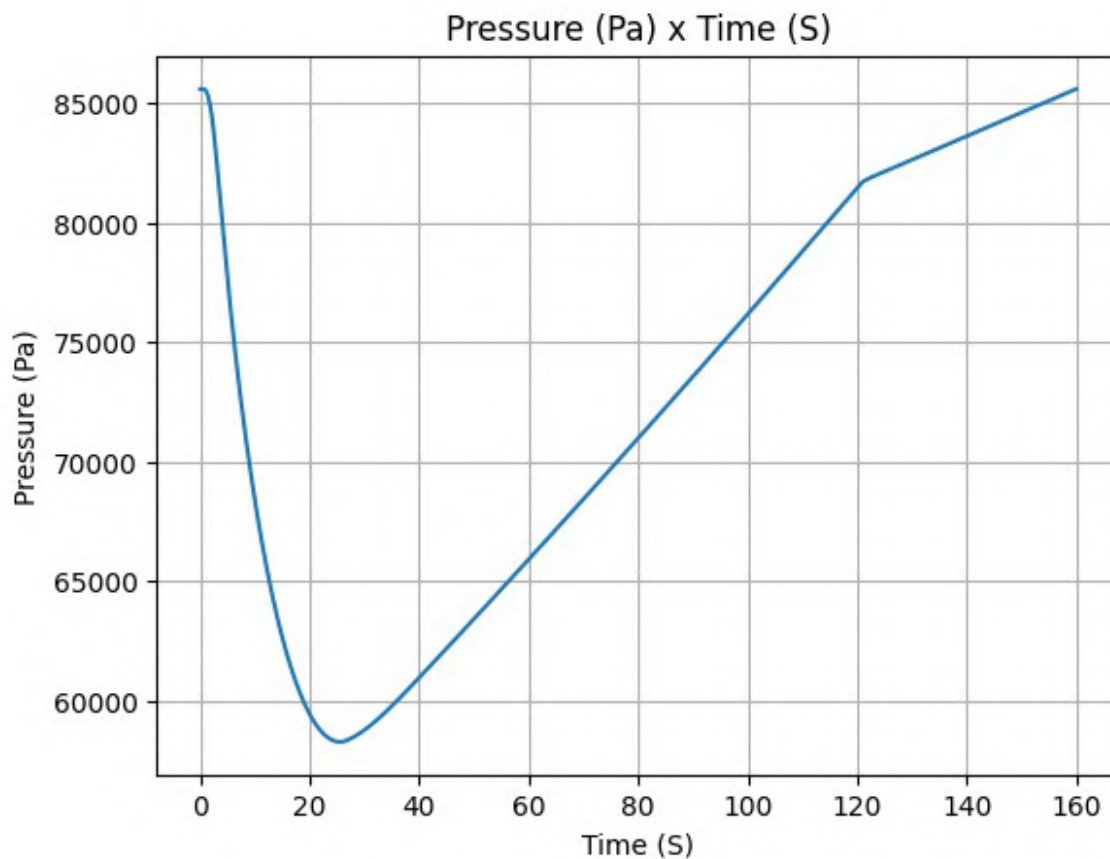
```

time_index = np.argmin(safety_factor[:, 1])
time_min_sf = safety_factor[time_index, 0]
min_sf = safety_factor[time_index, 1]
altitude_min_sf = flight.z(time_min_sf) - flight.env.elevation

print("\nFin's parameters")
print(f"Surface area (S): {s:.4f} m2")
print(f"Aspect ratio (AR): {ar:.3f}")
print(f"tip_chord/root_chord ratio = \u03BB = {la:.3f}")
print(f"Fin Thickness: {fin_thickness:.5f} m")
print(f"Shear Modulus (G): {shear_modulus:.3e} Pa")

print("\nFin Flutter Analysis")
print(f"Minimum Fin Flutter Velocity: {min_vel:.3f} m/s at
{time_min_mach:.2f} s")
print(f"Minimum Fin Flutter Mach Number: {min_mach:.3f} ")
print(f"Minimum Safety Factor: {min_sf:.3f} at {time_min_sf:.2f}
s")
print(f"Altitude of minimum Safety Factor: {altitude_min_sf:.3f} m
(AGL)\n")
test_flight.pressure()

```



```
fin_flutter_analysis((5)/1000, 10000000000, test_flight,  
see_prints=True, see_graphs=True)
```

Fin's parameters

Surface area (S): 0.0414 m²

Aspect ratio (AR): 1.035

tip_chord/root_chord ratio = λ = 0.600

Fin Thickness: 0.00500 m

Shear Modulus (G): 1.000e+10 Pa

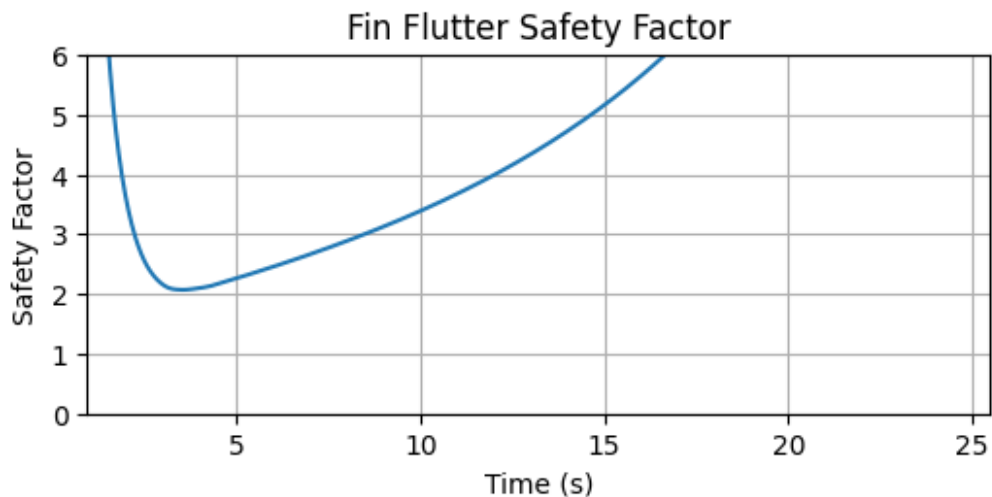
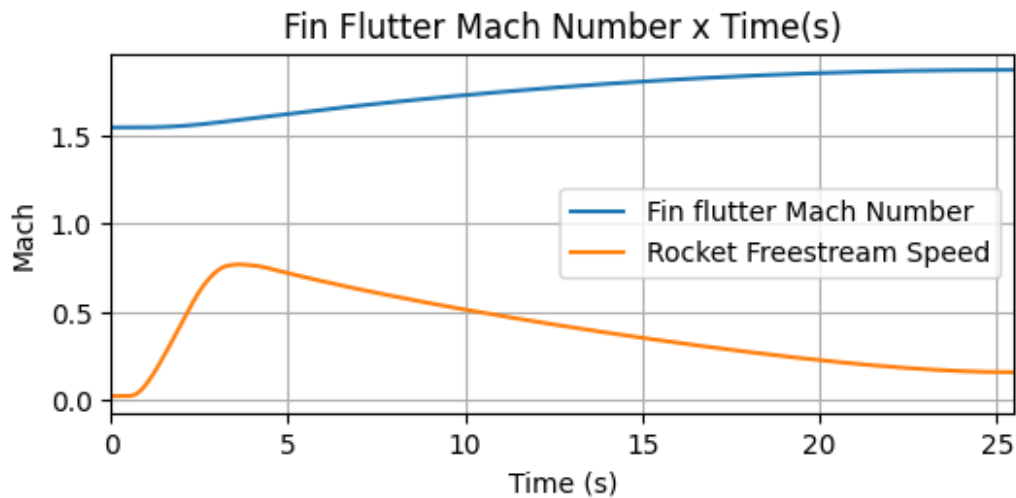
Fin Flutter Analysis

Minimum Fin Flutter Velocity: 536.991 m/s at 159.92 s

Minimum Fin Flutter Mach Number: 1.547

Minimum Safety Factor: 2.069 at 3.54 s

Altitude of minimum Safety Factor: 430.092 m (AGL)



```
fin_flutter_analysis((150*0.12)/1000, 10962664000, test_flight,  
see_prints=True, see_graphs=True)
```

Fin's parameters

Surface area (S): 0.0414 m²

Aspect ratio (AR): 1.035

tip_chord/root_chord ratio = λ = 0.600

Fin Thickness: 0.01800 m

Shear Modulus (G): 1.096e+10 Pa

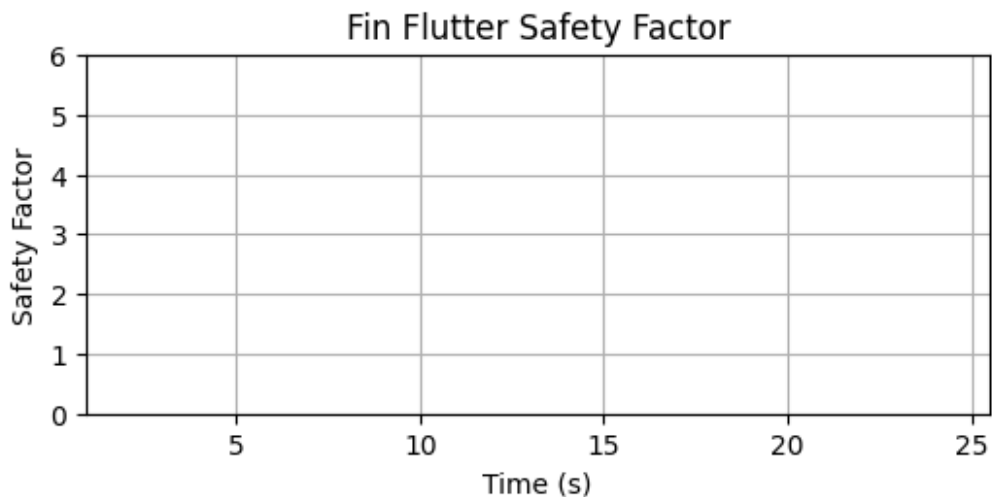
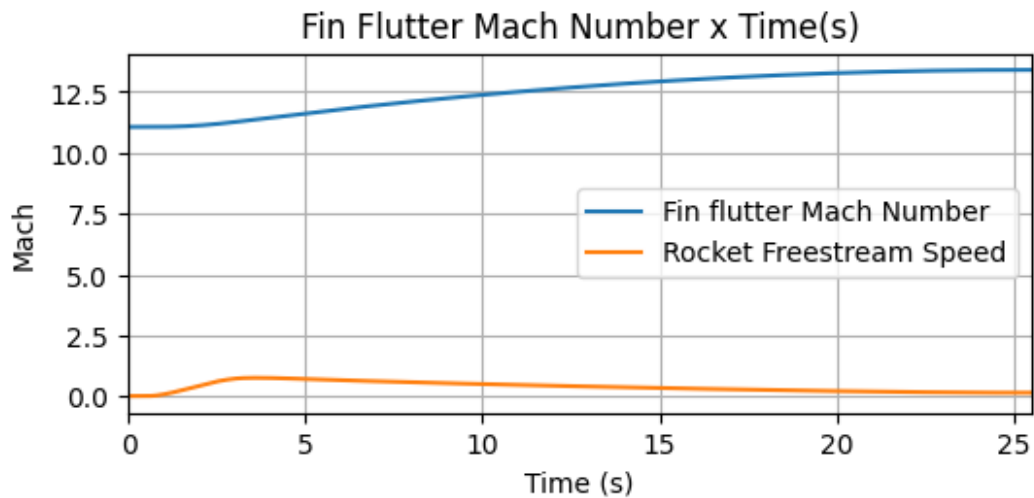
Fin Flutter Analysis

Minimum Fin Flutter Velocity: 3840.419 m/s at 159.92 s

Minimum Fin Flutter Mach Number: 11.060

Minimum Safety Factor: 14.800 at 3.54 s

Altitude of minimum Safety Factor: 430.092 m (AGL)



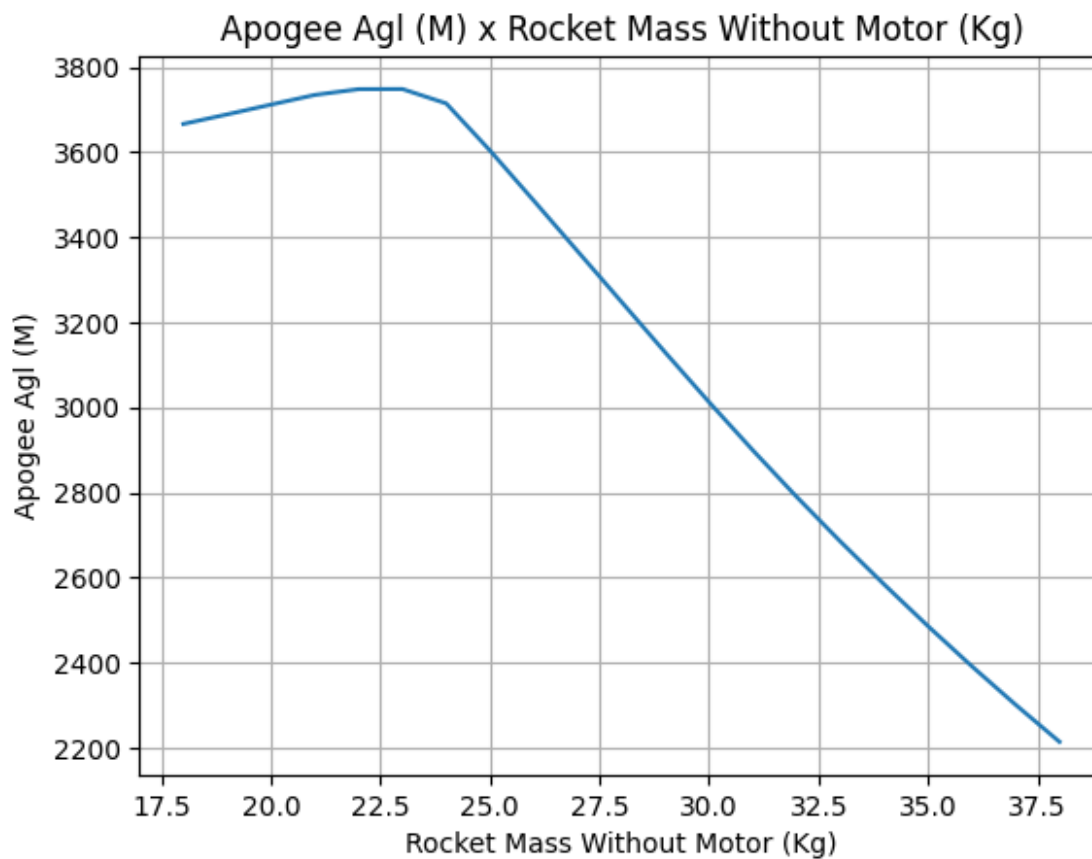
Using Simulation for Design

Here, we go through a couple of examples which make use of RocketPy in cool ways to help us design our rocket.

Apogee as a Function of Mass

This one is a classic one! We always need to know how much our rocket's apogee will change when our payload gets heavier.

```
from rocketpy.utilities import apogee_by_mass  
  
apogee_by_mass(flight=test_flight, min_mass=18, max_mass=38,  
points=21, plot=True)
```



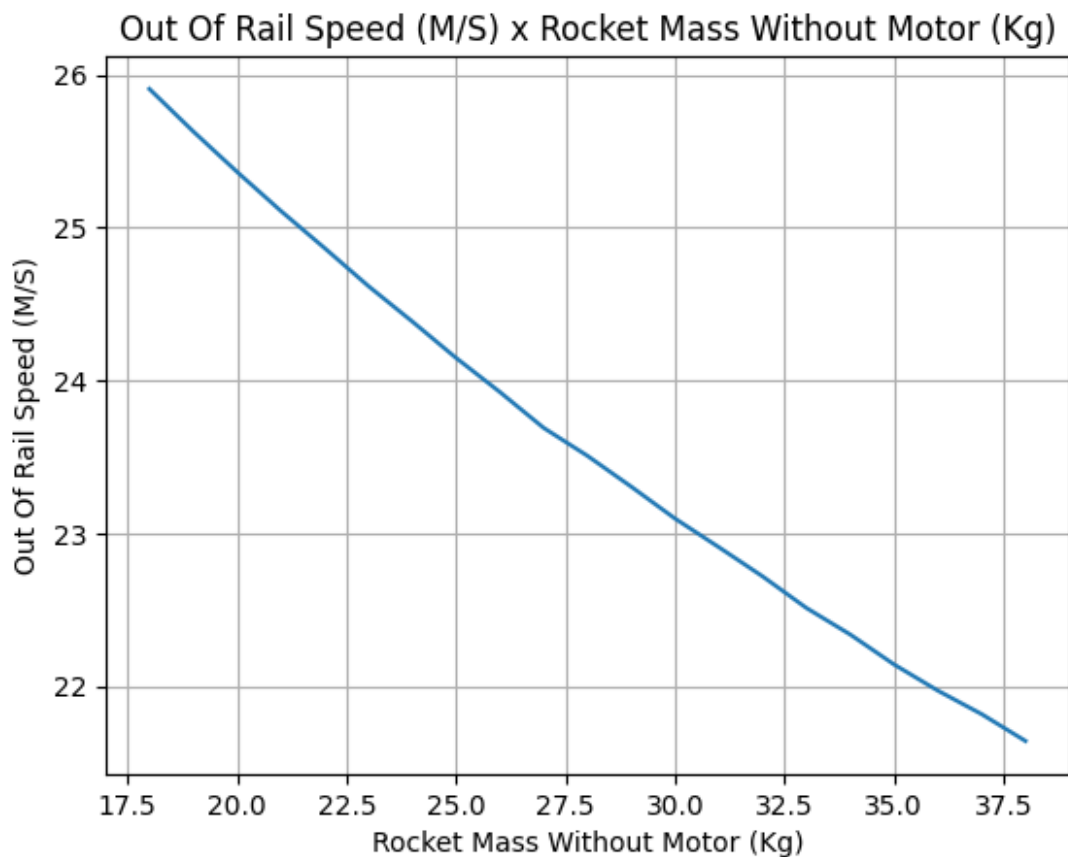
```
'Function from R1 to R1 : (Rocket Mass without motor (kg)) → (Apogee  
AGL (m))'
```

Out of Rail Speed as a Function of Mass

Lets make a really important plot. Out of rail speed is the speed our rocket has when it is leaving the launch rail. This is crucial to make sure it can fly safely after leaving the rail. A common rule

of thumb is that our rocket's out of rail speed should be 4 times the wind speed so that it does not stall and become unstable.

```
from rocketpy.utilities import liftoff_speed_by_mass  
liftoff_speed_by_mass(flight=test_flight, min_mass=18, max_mass=38,  
points=21, plot=True)
```



'Function from R1 to R1 : (Rocket Mass without motor (kg)) → (Out of Rail Speed (m/s))'

Appendix H

Parachutes dimensioning

1 - ROCKET DATA	
Main Terminal Velocity [fps]	30.4
Mass Aft of Coupler [lbs]	57.3
Mass Fore of Coupler [lbs]	11.9
Freestrem speed at drogue deployment [fps]	180.5
Reefed Terminal Velocity [fps]	72.2
Disreefing Altitude (AGL) [ft]	1401.0
Expected Apogee (AGL) [ft]	9967.7
Aft Section Lenght [ft]	5.1
Fore Section Lenght [ft]	3.8
Launch Site Altitude	Las Cruces
Nº of Gores	16

2 - TABLE DATA	
Cd0	0.92
Disreefed Cx	1.8
Reefed Cxr	1.1
Dp/Do	0.8269933431
$\eta(N)$ reefing	17
$\eta(N)$ disreefing	5
n disreefing	2
n reefing	0.5

3 - PHYSICAL CONSTANTS	
Gravity [m/s²]	9.807
Launch Site Altitude (AGL) [m]	1,189
Air Density at Ground Level [kg/m³]	1.09
Air Specific Mass at Disreefing Altitude[kg/m³]	0.9091
Air Specific Mass at apogee [kg/m³]	0.8191

4 - AUXILIARY VARIABLES	
Dynamic Pressure at drogue deployment [Pa]	1238.88875
Dynamic Pressure at disreefing [Pa]	253.5192
Dynamic Pressure at final descent [Pa]	46.8334305

5 - PARACHUTE ANALYSIS	
Supension Lines Lenght [ft]	11.4
Aft Shock Cord Lenght [ft]	14.1
Fore Shock Cord Lenght [ft]	7.7
DISREEFED PARACHUTE	
CdSo [ft²]	70.8
Nominal Area (So) [ft²]	76.9
Nominal Diameter (Do) [ft]	9.9
REEFED PARACHUTE	
CdSr [ft²]	13.1
Reefed Area (Sr) [ft²]	14.2
Reefed Diameter (Dr) [ft]	4.3

6 - OPENING FORCES	
DISREEFING	
Inflation time [s]	0.61903
Line Stretch Velocity [m/s]	25.74246
Ballistic Factor (Fore Section)	0.32282
X1 (Fore Section) using n = 2	0.29796
Opening force (Fore Section)	200.99522
Ballistic Factor (Aft Section) [lbf]	1.55432
X1 (Aft Section) using n = 2	0.72556
Opening force (Aft Section) [N]	489.44353
REEFING	
Inflation Time [s]	0.40075
Line Stretch Velocity [m/s]	126.92708
Ballistic Factor (Fore Section)	0.70018
X1 (Fore Section) using n = 1/2	0.43697
Opening force (Fore Section) [lbf]	162.61650
Ballistic Factor (Aft Section)	3.37123
X1 (Aft Section) using n = 1/2	0.72556
Opening force (Aft Section) [lbf]	270.01590

7 - REEFING LINE	
Skirt Diameter at 8 cm (Ds) [ft]	7.91014
Drag Area Ratio (ϵ)	0.18473
Diameter Ratio (τ)	0.42981
Dr	1.03622
Lr	3.25537
Reefing Line Lenght [m]	23.70341

8 - OUTPUTS	
Reefed CdS	13.1
Disreefed CdS	70.8
Supension Lines Lenght (le) [ft]	11.4
Supension Lines Manufacturing Lenght (Tsl) [ft]	23.4
Reefed Opening Force fore of Coupler(Fx) [lbf]	162.61650
Reefed Opening Force aft of Coupler(Fx) [lbf]	270.01590
Disreefing Force fore of Coupler (Fx) [lbf]	200.99522
Disreefing Force Aft of Coupler (Fx) [lbf]	489.44353
Reefed Diameter (Dr) [ft]	4.3
Constructed Diameter (Dc) [ft]	8.6
Reefing Line (Lr) [ft]	13.36425435
Bridle Lenght (Br) [ft]	2.812283925

Altitude (ASL) (m):	Air Specific Mass [kg/m³]
600	1.156
800	1.1336
1000	1.1116
1200	1.09
1400	1.0686
1600	1.0476
1800	1.0269
2000	1.0065
3000	0.9091
4000	0.8191

Altitudes (m):	
Las Cruces	1,189
Tatui	645
Pirassununga	627

Acknowledgments

We are enormously grateful for our team members, professors, researchers, technicians, and employees from the University of São Paulo. We are also thankful for the support of our sponsors, who make the project possible. Without the presence of each and every one of these contributions, we would not be what and where we are today.

All obtained sponsorship constitutes a vital part of the project: in the structure area, *Texiglass* and *Araldite/Huntsman*, that provide the materials for our rocket manufacturing. Besides that, we have the important support of *Ansys* and *ESSS*, who allows the obtainment of precise and fundamental data of rocket performance and optimization; in the electronics area, *STMicronics* and *Implastec* made it possible to design, build and test the rocket's electronics systems with high reliability; in the propulsion area, *Locfer* supplies the hydrostatic test pump, essential for conducting motor tests and verifying the integrity of the designed structures, *Yara* provides potassium nitrate, essential for the production of KNSB propellant, *AirLiquide* supplies the nitrous oxide used in developing our hybrid engine and *MalsNitro* provided valves for the development of our hybrid engine as well; in the recovery area, *SkyDive4Fun* has made it possible to conduct drop tests, enabling improved testing of the team's parachutes and data acquisition. *FDTE*, the foundation for the technological development of engineering in Brazil, who provides us considerable financial resources and services; *Alto da Serra*, *Guru Astral* and *WeVets* also provide us financial resources. *Poli-USP* and *PME*, who provide us space to work and support with the logistics of the trip, providing not only financial resources, but also material means. At last, we would like to especially thank the patrimony *Amigos da Poli*, which makes our project a reality, by providing 90% of our budget.

Projeto Jupiter is grateful for all the members who gave all their effort and energy to this project, wrote, studied and developed each area on this document. A heated greeting is sent to senior members of the team as they paved a way of excellence and dedication to Projeto Jupiter throughout our history, enabling us to reach incredible milestones such as Pacifico.

We would also like to thank the professors, who help the group a lot with academic and techniques questions. In particular, our late teacher Antonio Pacifico, who helped us with subjects and provided guidance on some of the team's projects and after whom the rocket is named. Also, our tutor professor PhD Bruno Souza Carmo, who supports the team during administrative and technical issues faced during the project and throughout the years. His dedication captivates us to be better professionals and persons as he provides a formidable example as a teacher, tutor, friend, and member of the team.

The team is deeply gratified to the SA Cup organization for promoting such an important annual event and developing the international aerospace scenario among students and enthusiasts. This opportunity was precious for our team and members since it allowed and pluralized an experience generally restricted to a few members in previous competitions. The effort made by the ESRA staff towards this 2023 Competition is splendid and admirable, and as an international team we are deeply grateful.

A special thanks are dedicated to USP - Campus "Fernando Costa" and *Academia da Força Aérea* (AFA), institutions that help the team's operations and rocket launches for testing purposes at Pirassununga - SP. Their goodwill in helping us and providing administrative, infrastructure and technical support motivates us to achieve higher standards of excellence and dedication.

Finally, we are grateful to all of our families and relatives, along with all the people who support us and admire our work. Such energy provides us motivation to work towards a more robust and competitive rocket. As a part of the team, enjoy the fantastic result that *Pacifico* is.

References

- [1] Nakka, R., “KNSB Propellant,” 2018. URL <https://www.nakka-rocketry.net/sorb.html>.
- [2] Jupiter, P., “Solid propellant rocket motor internal ballistics simulation tool,” 2022. URL <https://github.com/Projeto-Jupiter/SolidPy>.
- [3] Crowell Sr, G. A., *The descriptive geometry of nose cones*, 1996.
- [4] Hennin, B., “Why Should You Airfoil Your Fins?” *Peak of Flight: Newsletter, Apogee components*, Vol. 305, 2012-01-31.
- [5] Harder, P., Cusack, D., Matson, C., and M., L., “Airfoil Development for the Trek Speed Concept Triathlon Bicycle,” 2010.
- [6] Standish, K. J., and van Dam, C. P., “Aerodynamic Analysis of Blunt Trailing Edge Airfoils,” *Journal of Solar Energy Engineering*, 2003.
- [7] Gómez, A., and Pinilla, A., “Aerodynamic Characteristics of Airfoils with Blunt Trailing Edge,” *Revista de Ingeniería, No. 24*, 2006.
- [8] Van Milligan, T., “What is the best fin shape for a model rocket?” *Peak of Flight: Newsletter, Apogee components*, Vol. 442, May 2nd 2017.
- [9] Howard, Z., “How To Calculate Fin Flutter Speed,” *Peak of Flight: Newsletter, Apogee components*, Vol. 291, 2011.
- [10] Silhan, F. V., and James Jr, M., “Drag of Conical and Circular-Arc Boattail Afterbodies at Mach Numbers From 0.6 to 1.3,” Tech. rep., Lagley Aeronautical Laboratory, 1957.
- [11] Reubush, D. E., and Runckel, J. F., “Effect of fin ratio on boattail drag of circular-arc afterbodies having closure ratios of 0.50 with jet exhaust at mach numbers up to 1.30,” Tech. rep., NASA, 1973.
- [12] Shrewsbury, G. D., “Effect of boattail juncture shape on pressure drag coefficients of isolated afterbodies,” Tech. rep., Lewis Research Center, 1968.
- [13] Ewing, E. G., *RINGSAIL PARACHUTE DESIGN*, Wright-Patterson Air Force Base, Ohio: Air Force Flight Dynamics Laboratory, Air Force Systems Command, 1972.
- [14] Knacke, T. W., *Parachute Recovery Systems: Design Manual*, Para Pub., 1992.
- [15] *RRC3 — Rocket Recovery Controller 3 User Manual*, Missile Works Corporation, PO Box 1725, Lyons CO 80540, 2013. URL <https://www.apogeerockets.com/downloads/PDFs/RRC3-user-manual.pdf>.
- [16] Madgwick, S. O., “An efficient orientation filter for inertial and inertial/magnetic sensor arrays,” 2010. URL <https://forums.parallax.com/uploads/attachments/41167/106661.pdf>.
- [17] *Standard Test Method for Tensile Properties of Polymer Matrix Composite Materials*, 2017. https://doi.org/10.1520/D3039_D3039M-17, URL <http://www.astm.org/cgi-bin/resolver.cgi?D3039D3039M-17>.
- [18] White, F. M., “Fluid Mechanics, 7th ed,” 2011.
- [19] Abbott, I. H., and von Doenhoff, A. E., “Theory of Wing Sections,” *Dover Publications*, 1959.
- [20] Grelsson, B., Felsberg, M., and Isaksson, F., “NPL 9615 and NACA 0012, A Comparison of Aerodynamic Data,” *Aeronautical Research Council, C.P. No. 1261*, 1968.
- [21] Thomareisa, N., and Papadakis, G., “Effect of trailing edge shape on the separated flow characteristics around an airfoil at low Reynolds number: A numerical study,” *Physics of Fluids, AIP Publishing, Vol. 29, Issue 1*, 2017.